

**TOXICITY-ORIENTED CONTROL OF ADVANCED OXIDATION PROCESSES:
A CASE STUDY ON PHENOL DERIVATIVES**

by

Akın Karcı

BS. in Chem. Marmara University, 2005

M.Sc. in E.Sc. Boğaziçi University, 2008

**Submitted to the Institute of Environmental Sciences in partial fulfillment of
the requirements for the degree of
Doctor
of
Philosophy
in
Environmental Sciences**

Boğaziçi University

2013

**TOXICITY-ORIENTED CONTROL OF ADVANCED OXIDATION PROCESSES:
A CASE STUDY ON PHENOL DERIVATIVES**

APPROVED BY:

Prof. Dr. Miray Bekbölet.....
(Thesis Supervisor)

Prof. Dr. İdil Arslan-Alaton.....
(Thesis Co-Supervisor)

Assoc. Prof. Raşit Bilgin.....

Assist. Prof. Başak Güven.....

Prof. Dr. Nilsun İnce.....

Prof. Dr. İsmail Toröz.....

Prof. Dr. Orhan Yenigün.....

DATE OF APPROVAL.....

ACKNOWLEDGMENTS

I have thought that this will never end, but it is finally over. There are a lot of unforgettable people whom I am grateful to have met on this long journey. However, I am specially thankful to two people with whom I have blessed to work: Prof. Dr. Miray Bekbölet and Prof. Dr. İdil Arslan-Alaton. I would like to deeply appreciate my both supervisors for trusting me and giving me a huge amount of freedom during my PhD thesis. I should sincerely say that without their help I would not have been able to achieve all that I did. Very special thanks are extended to Prof. Dr. İdil Arslan-Alaton who kindly shared her theoretical and practical knowledge with me and provided laboratory facilities for me. Her guidance throughout the years of my PhD, even during her most busy times, had a paramount impact on the completion of this thesis. For this, I cannot thank her enough. I am forever grateful. Thank You Dr. Arslan-Alaton, You the most warm hearted person I have met in my life !

I would also like to express my best regards to my committee members Assist. Prof. Dr. Başak Güven, Prof. Dr. İsmail Toröz, Prof. Dr. Nilsun İnce, Prof. Dr. Orhan Yenigün and Assoc. Prof. Dr. Raşit Bilgin for their critical and supportive comments.

The financial support of the Scientific and Technological Research Council of Turkey (TÜBİTAK, Project No: 111Y145) is gratefully acknowledged. The study was conducted at the laboratory facilities of Istanbul Technical University, Environmental Engineering Department. Therefore, I kindly thank all faculty members, research assistants, technical personnels and secreterial staff for their hospitality and friendship. I would like to give my special thanks to Assoc. Prof. Dr. Tuğba Ölmez-Hancı for providing the chemicals and equipments necessary for my experimental work and for her valuable assistance during the first part of my studies. I am grateful to Res. Assist. Edip Avşar and Res. Assist. Çisem Ecer for their technical support during the GC-MS analysis, Res. Assist. Dr. Egemen Aydın for his technical support during the LC-MS analyses and Assist. Prof. Dr. Serdar Doğruel and Assist. Prof. Dr. Gülsüm Emel Zengin Balcı for the chloride measurements. I also thank Çisem for her help and assistance in the TOC analysis.

The *umu*-test was performed at Istanbul University, Department of Pharmaceutical Toxicology. I acknowledge Assoc. Prof. Dr. Gül Özhan and Prof. Dr. Buket Alpertunga for their technical support during the *umu*-test and for sharing their valuable feedback and suggestions during my thesis writing. I also deeply appreciate Prof. Dr. Gül den Omurtag (Marmara University, Department of Pharmaceutical Toxicology) for kindly directing me in finding a second toxicity bioassay. I am thankful to Prof. Dr. Zekiye Çınar (Yıldız Technical University, Department of Chemistry) for her courtesy of supplying the hydroquinone, benzoquinone, chlorohydroquinone and catechol standards.

Most of all, I would like to thank my family whose love, devotion and support through all my years of school have been indispensable to my success in reaching this point. Finally, a special thank goes to my cat Zeytin for always guiding me with his phosphorous eyes :)

ABSTRACT

Advanced oxidation processes are expected to be carefully operated and monitored based on their ecotoxicological impact because the partial oxidation of organic contaminants may result in the formation of intermediates more toxic than parent compounds. Toxicity tests in combination with the transformation product analyses could be an important tool for the control of advanced oxidation processes. Considering the commercial importance as well as toxicological properties of chlorophenol and nonylphenol polyethoxylate group phenolic compounds, degradation and detoxification of 2,4-dichlorophenol (2,4-DCP) and nonylphenol decaethoxylate (NP-10) in distilled water and synthetically prepared freshwater were investigated by applying the H₂O₂/UV-C, Fenton and photo-Fenton advanced oxidation processes that are well-known for their effectiveness in removing many organic pollutants from waste streams. Although not an advanced oxidation process, UV-C photolysis was also included in the study due to the fact that it is becoming an attractive technology in water treatment facilities due to several advantages. The marine photobacteria *Vibrio fischeri* were employed as the test organism to assess changes in acute inhibitory effect during the studied treatment processes, whereas the *umu*-test using *Salmonella typhimurium* TA1535/pSK1002 strain was selected as the genotoxicity assay. Toxicity results were complemented by transformation product analyses performed by means of high performance liquid chromatography, gas chromatography-mass spectrometry, liquid chromatography-mass spectrometry, colorimetry and ion chromatography in order to gain a deeper insight into acute toxicity and genotoxicity patterns during application of the studied treatment processes.

The H₂O₂/UV-C and photo-Fenton processes ensured complete 2,4-DCP removal and near-complete mineralization as well as effective abatement of UV_{280/254} absorbances. Hydroquinone, chlorohydroquinone, maleic and formic acids and aldehydes were identified as the common transformation products of the studied treatment processes. The most rapid decrease in the acute inhibitory effect was achieved by the H₂O₂/UV-C and photo-Fenton processes, however a re-increase in toxic effect was evidenced in the former advanced oxidation process when extending the treatment time beyond 30 min. The acute inhibitory effect ultimately measured in synthetic freshwater was higher than that recorded

in distilled water for UV-C photolysis and lower for the $\text{H}_2\text{O}_2/\text{UV-C}$ and Fenton processes, whereas the photo-Fenton process was not significantly affected by the inorganic constituents of synthetic freshwater based on acute toxicity test results. During application of the studied treatment processes in distilled water no significant genotoxic effect was observed with and without metabolic activation.

Complete NP-10 degradation that is very fast accompanied with high total organic carbon removal efficiencies were achieved by the $\text{H}_2\text{O}_2/\text{UV-C}$ and photo-Fenton processes, whereas the Fenton's reagent provided only poor NP-10 abatement and insignificant mineralization. Aliphatic carboxylic acids including formic, acetic and oxalic acids, aldehydes and polyethylene glycols containing 2-8 ethoxy units were all identified as the degradation products of NP-10 by the studied treatment processes. The photo-Fenton process appeared to be toxicologically safer both in distilled water and synthetic freshwater based on the acute toxicity tests since the inhibitory effect did not increase relative to the original NP-10 solution after treatment. The genotoxic effects obtained in distilled water both with and without metabolic activation followed the order; Fenton > $\text{H}_2\text{O}_2/\text{UV-C}$ > photo-Fenton > UV-C. Formation of weakly to moderately genotoxic transformation products was evidenced in the presence and absence of metabolic activation when the $\text{H}_2\text{O}_2/\text{UV-C}$ process was applied to synthetically prepared freshwater. The genotoxic effect levels were typically lower during photo-Fenton treatment of synthetic freshwater contaminated with NP-10 as compared to those achieved with the $\text{H}_2\text{O}_2/\text{UV-C}$ process both in the presence and absence of metabolic activation.

ÖZET

Organik kirleticilerin kısmi oksidasyonu sonucunda ana bileşiklerden daha toksik ara ürün oluşumu gerçekleşebileceğinden, ileri oksidasyon proseslerinin ekotoksikolojik etkilerine dayalı olarak dikkatle işletilmesi ve takip edilmesi beklenmektedir. Toksikite testleri parçalanma ürünü analizleri ile birlikte ileri oksidasyon proseslerinin kontrolü için önemli bir araç olabilmektedir. Klorofenol ve nonilfenol polietoksilat grubu fenolik bileşiklerin ticari önemi ve toksikolojik özellikleri göz önüne alınarak 2,4-diklorofenol (2,4-DCP) ve nonilfenol dekaetoksilatın (NP-10) distile su ve sentetik olarak hazırlanmış tatlısuda ayrışma ve detoksifikasyonları, pek çok organik kirleticinin atık akımlarından gideriminde etkili olduğu bilinen $H_2O_2/UV-C$, Fenton ve foto-Fenton ileri oksidasyon prosesleri uygulanarak araştırılmıştır. Bir ileri oksidasyon prosesi olmamasına karşın birkaç avantajından dolayı su arıtma tesislerinde cazip bir teknoloji haline gelen UV-C fotolizi de çalışmaya dahil edilmiştir. Araştırılan arıtma prosesleri süresince akut inhibisyon değişimlerinin belirlenmesi amacıyla test organizması olarak deniz fotobakterisi *Vibrio fischeri* kullanılırken, genotoksikite deneyi olarak da *Salmonella typhimurium* TA1535/pSK1002 suşunun kullanıldığı *umu*-testi seçilmiştir. Toksikite sonuçları yüksek performanslı sıvı kromatografisi, gaz kromatografisi-kütle spektrometrisi, sıvı kromatografisi-kütle spektrometrisi, kolorimetri ve iyon kromatografisi ile gerçekleştirilen parçalanma ürünü analizleriyle desteklenerek araştırılan arıtma proseslerinin uygulanması süresince gözlemlenen akut toksisite ve genotoksikite değişimlerine yönelik daha derin fikir sahibi olunması amaçlanmıştır.

$H_2O_2/UV-C$ ve foto-Fenton prosesleri tam 2,4-DCP giderimi, tama yakın mineralizasyon ve etkili $UV_{280/254}$ absorbans giderimi sağlamıştır. Hidrokinon, klorohidrokinon, maleik ve formik asitler ile aldehytler araştırılan arıtma proseslerinin ortak parçalanma ürünleri olarak tanımlanmıştır. En hızlı akut inhibisyon azalması $H_2O_2/UV-C$ ve foto-Fenton prosesleri ile elde edilmiş, ancak $H_2O_2/UV-C$ prosesinde arıtma süresinin 30 dakikanın ötesine taşınmasıyla toksik etkide yeniden artış kaydedilmiştir. Sentetik tatlısuda son durumda ölçülen akut inhibisyon UV-C fotolizi için distile suda kaydedilenden daha yüksek, $H_2O_2/UV-C$ ve Fenton prosesleri için ise daha düşük bulunurken, foto-Fenton prosesi akut toksisite testi sonuçlarına dayalı olarak

sentetik tatlısuyun inorganik bileşenlerinden önemli ölçüde etkilenmemiştir. Araştırılan arıtma proseslerinin distile suda uygulanması süresince metabolik aktivasyonlu ve aktivasyonsuz önemli seviyede genotoksik etki gözlemlenmemiştir.

$H_2O_2/UV-C$ ve foto-Fenton prosesleri ile tam ve çok hızlı NP-10 ayrışması ve yüksek toplam organik karbon giderim verimleri elde edilirken, Fenton reaktifi ancak düşük seviyede NP-10 giderimi ve önemsiz ölçüde mineralizasyon sağlamıştır. Formik, asetik ve okzalik asitleri kapsayan alifatik karboksilik asitler, aldehitler ve 2-8 etoksi birimi içeren polietilen glikollerin tamamı NP-10'un araştırılan arıtma prosesleri ile ayrışma ürünleri olarak tanımlanmıştır. Arıtma sonrası akut inhibisyonun orijinal NP-10 çözeltisine göre artış göstermemiş olması göz önünde bulundurularak foto-Fenton prosesi hem distile suda, hem de sentetik tatlısuda toksikolojik açıdan daha emniyetli bulunmuştur. Distile suda metabolik aktivasyonlu ve aktivasyonsuz elde edilen genotoksik etkiler, Fenton > $H_2O_2/UV-C$ > foto-Fenton > UV-C sırasını izlemiştir. $H_2O_2/UV-C$ prosesi sentetik olarak hazırlanmış tatlısuya uygulandığında, metabolik aktivasyon varlığında ve yokluğunda zayıf ve orta seviyede genotoksik etki gösteren parçalanma ürünleri oluşumu kaydedilmiştir. NP-10 ile kirletilmiş sentetik tatlısuyun foto-Fenton arıtımı süresince ölçülen genotoksik etki seviyeleri, metabolik aktivasyonlu ve aktivasyonsuz $H_2O_2/UV-C$ prosesi ile elde edilenlere kıyasla genelde daha düşük bulunmuştur.

TABLE OF CONTENTS

ACKNOWLEDGMENTS	iii
ABSTRACT	v
ÖZET	vii
LIST OF FIGURES	xiii
LIST OF TABLES	xxii
LIST OF SYMBOLS/ABBREVIATIONS	xxvi
1. INTRODUCTION	1
2. THEORETICAL BACKGROUND	5
2.1. Overview of Commercially Important Phenol Derivatives	5
2.1.1. Chlorophenols	5
2.1.2. Alkylphenol Polyethoxylates	6
2.2. Advanced Oxidation Processes	8
2.3. H ₂ O ₂ /UV, Fenton and Photo-Fenton Treatment of Chlorophenols	12
2.3.1. Transformation Products	13
2.3.2. Toxicity	23
2.3.3. Toxicity in Relation with Transformation Products	29
2.4. Photolysis and AOP Treatment of Alkylphenol Polyethoxylates	32
2.4.1. Transformation Products	33
2.4.2. Toxicity	39
3. MATERIALS AND METHODS	43
3.1. Materials	43
3.1.1. 2,4-Dichlorophenol (2,4-DCP)	43
3.1.2. Nonylphenol Decaethoxylate (NP-10)	44
3.1.3. Synthetic Freshwater (SFW) Sample	45
3.1.4. Other Chemicals and Reagents	45
3.2. Photoreactor and UV-C Light Source	46
3.3. Experimental Procedures	47
3.4. Analytical Procedures	48

3.4.1. HPLC Analyses	48
3.4.2. GC-MS Analyses	49
3.4.3. LC-MS Analyses	51
3.4.4. Aldehyde Analysis	52
3.4.5. Chloride Analysis	53
3.4.6. UV Absorbance Measurements	53
3.4.7. Other Procedures	53
3.5. Bioanalytical Procedures	54
3.5.1. Acute Toxicity Testing	54
3.5.2. Genotoxicity Testing	55
3.5.2.1. Preparation of the Bacterial Culture	56
3.5.2.2. Reincubation of the Bacteria	56
3.5.2.3. Exposure of Bacteria to Test Samples	56
3.5.2.4. Dilution Step and Second Incubation	57
3.5.2.5. Measurement of <i>umuC</i> Induction	57
3.5.2.6. Calculation	58
4. RESULTS AND DISCUSSION	59
4.1. Studies with 2,4-DCP	59
4.1.1. 2,4-DCP Baseline Experiments and Kinetics	59
4.1.1.1. Single H ₂ O ₂ and UV-C Photolysis Control Experiments	59
4.1.1.2. The H ₂ O ₂ /UV-C Experiments	62
4.1.1.3. The Fenton Experiments	73
4.1.1.4. The Photo-Fenton Experiments	75
4.1.1.5. Comparative Evaluation of Kinetics and Efficiencies of the Studied Treatment Processes	80
4.1.2. Evolution of Transformation Products	87
4.1.2.1. Chloride Release	87
4.1.2.2. Aromatic Transformation Products	89
4.1.2.3. Aliphatic Transformation Products	94
4.1.2.4. LC-MS Analyses	99
4.1.3. Toxicity Evolution During Transformation of 2,4-DCP	106
4.1.3.1. Acute Toxicity Evolution	106
4.1.3.2. Genotoxicity Evolution	114

4.1.4. 2,4-DCP Removal in Synthetic Freshwater	121
4.1.4.1. Treatment Performances and Kinetics	121
4.1.4.2. Chloride Release	127
4.1.4.3. Aromatic Transformation Products	129
4.1.4.4. Aliphatic Transformation Products	132
4.1.4.5. Acute Toxicity	134
4.1.4.6. Genotoxicity	138
4.2. Studies with NP-10	142
4.2.1. NP-10 Baseline Experiments and Kinetics	142
4.2.1.1. Single H ₂ O ₂ and UV-C Photolysis Control Experiments	142
4.2.1.2. The H ₂ O ₂ /UV-C Experiments	144
4.2.1.3. The Fenton Experiments	151
4.2.1.4. Photo-Fenton Experiments	152
4.2.1.5. Comparative Evaluation of Kinetics and Efficiencies of the Studied Treatment Processes	157
4.2.2. Evolution of Transformation Products	162
4.2.2.1. Aromatic Transformation Products	162
4.2.2.2. Aliphatic Transformation Products	163
4.2.2.3. GC-MS Analyses	168
4.2.3. Toxicity Evolution During Transformation of NP-10	172
4.2.3.1. Acute Toxicity Evolution	172
4.2.3.2. Genotoxicity Evolution	179
4.2.4. NP-10 Removal in Synthetic Freshwater	185
4.2.4.1. Treatment Performances and Kinetics	185
4.2.4.2. Oxidation Products	191
4.2.4.3. Toxicity Evolution	201
5. CONCLUSIONS	210
5.1. Studies with 2,4-DCP	210
5.2. Studies with NP-10	212
6. RECOMMENDATIONS	214
REFERENCES	215

APPENDIX A-Calibration Curves Being Established for the Target Compounds	250
APPENDIX B-96-Well Microplate Configuration in the <i>umu</i> -Test	254
APPENDIX C-UV Absorption Spectra Taken During Application of the Studied Treatment Processes	256
APPENDIX D-GC-MS Chromatogram and Mass Spectra of NP-10 Transformation Products	265

LIST OF FIGURES

Figure 2.1. Schematic representation of AOP being relatively well-established for treatment of industrial wastewaters.	9
Figure 2.2. Scientific studies covering toxicity during application of AOP with and without transformation products included.	12
Figure 3.1. Experimental set-up being used throughout the treatment runs.	47
Figure 3.2. The flow scheme representing experimental conditions and all analytical procedures involved in the study.	49
Figure 4.1. Normalized 2,4-DCP, TOC and H ₂ O ₂ decays during single H ₂ O ₂ oxidation of 2,4-DCP. Initial experimental conditions: 2,4-DCP = 25 mg L ⁻¹ (150 μM), H ₂ O ₂ = 40 mM, pH = 7.	60
Figure 4.2. Normalized 2,4-DCP and TOC removals as well as pH evolutions during direct UV-C photolysis of 2,4-DCP. Initial experimental conditions: 2,4-DCP = 25 mg L ⁻¹ (150 μM), pH = 7.	61
Figure 4.3. Effect of initial 2,4-DCP concentration on the decay of 2,4-DCP (a), TOC (b) and H ₂ O ₂ (c) as well as the pH evolution (d) during H ₂ O ₂ /UV-C treatment of 2,4-DCP. Initial experimental conditions: H ₂ O ₂ = 10 mM, pH = 7.	63
Figure 4.4. Effect of initial pH on the decay of 2,4-DCP (a), TOC (b) and H ₂ O ₂ (c) as well as the pH evolution (d) during H ₂ O ₂ /UV-C treatment of 2,4-DCP. Initial experimental conditions: 2,4-DCP = 25 mg L ⁻¹ (150 μM), H ₂ O ₂ = 10 mM.	67
Figure 4.5. Effect of initial H ₂ O ₂ concentration on the decay of 2,4-DCP (a), TOC (b) and H ₂ O ₂ (c) as well as the pH evolution (d) during H ₂ O ₂ /UV-C treatment of 2,4-DCP. Initial experimental conditions: 2,4-DCP = 25 mg L ⁻¹ (150 μM), pH = 7.	71
Figure 4.6. Effect of initial pH on the decay of 2,4-DCP (a), TOC (b) and H ₂ O ₂ (c) during photo-Fenton treatment of 2,4-DCP. Initial experimental conditions: 2,4-DCP = 25 mg L ⁻¹ (150 μM), H ₂ O ₂ = 10 mM, Fe ²⁺ = 200 μM.	77

- Figure 4.7. Effect of initial Fe^{2+} concentration on the decay of 2,4-DCP (a), TOC (b) and H_2O_2 (c) during photo-Fenton treatment of 2,4-DCP. Initial experimental conditions: 2,4-DCP = 25 mg L^{-1} (150 μM), H_2O_2 = 10 mM, pH = 3. 81
- Figure 4.8. Comparison of the decay of 2,4-DCP (a), TOC (b) and H_2O_2 (c) as well as pH change (d) during $\text{H}_2\text{O}_2/\text{UV-C}$, Fenton and photo-Fenton treatment as well as UV-C photolysis of 2,4-DCP. Initial experimental conditions: 2,4-DCP = 75 mg L^{-1} (460 μM), H_2O_2 = 10 mM, Fe^{2+} = 200 μM , pH = 7 for UV-C photolysis and the $\text{H}_2\text{O}_2/\text{UV-C}$ process and pH = 3 for the Fenton and photo-Fenton processes. 83
- Figure 4.9. Temporal evolution of the UV absorbances at $\lambda = 280$ nm (a) and $\lambda = 254$ nm (b) during UV-C, $\text{H}_2\text{O}_2/\text{UV-C}$, Fenton and photo-Fenton treatment of 2,4-DCP. Initial experimental conditions: 2,4-DCP = 75 mg L^{-1} (460 μM), H_2O_2 = 10 mM, Fe^{2+} = 200 μM , pH = 7 for UV-C photolysis and the $\text{H}_2\text{O}_2/\text{UV-C}$ process and pH = 3 for the Fenton and photo-Fenton processes. 86
- Figure 4.10. Cl^- release observed during UV-C, $\text{H}_2\text{O}_2/\text{UV-C}$, Fenton and photo-Fenton treatment of 2,4-DCP. Initial experimental conditions: 2,4-DCP = 75 mg L^{-1} (460 μM), H_2O_2 = 10 mM, Fe^{2+} = 200 μM , pH = 7 for UV-C and $\text{H}_2\text{O}_2/\text{UV-C}$ and pH = 3 for Fenton and photo-Fenton treatments. 88
- Figure 4.11. Temporal evolution of hydroquinone during UV-C, $\text{H}_2\text{O}_2/\text{UV-C}$, Fenton and photo-Fenton treatment of 2,4-DCP. Initial experimental conditions: 2,4-DCP = 75 mg L^{-1} (460 μM), H_2O_2 = 10 mM, Fe^{2+} = 200 μM , pH = 7 for UV-C and $\text{H}_2\text{O}_2/\text{UV-C}$ and pH = 3 for the Fenton and photo-Fenton treatments. 90
- Figure 4.12. A general scheme describing the degradation routes of 2,4-DCP by UV-C, $\text{H}_2\text{O}_2/\text{UV-C}$, Fenton and photo-Fenton treatments based on the GC-MS results. 93
- Figure 4.13. Temporal evolution of maleic and fumaric acids during $\text{H}_2\text{O}_2/\text{UV-C}$, Fenton and photo-Fenton treatment of 2,4-DCP. Initial experimental conditions: 2,4-DCP = 75 mg L^{-1} (460 μM), H_2O_2 = 10 mM, Fe^{2+} =

- 200 μM , pH = 7 for the $\text{H}_2\text{O}_2/\text{UV-C}$ and pH = 3 for the Fenton and photo-Fenton processes. 94
- Figure 4.14. Temporal evolution of acetic acid (a) and formic acid (b) during $\text{H}_2\text{O}_2/\text{UV-C}$, Fenton and photo-Fenton treatment of 2,4-DCP. Initial experimental conditions: 2,4-DCP = 75 mg L^{-1} (460 μM), H_2O_2 = 10 mM, Fe^{2+} = 200 μM , pH = 7 for the $\text{H}_2\text{O}_2/\text{UV-C}$ and pH = 3 for the Fenton and photo-Fenton processes. 97
- Figure 4.15. Temporal evolution of aldehydes during UV-C, $\text{H}_2\text{O}_2/\text{UV-C}$, Fenton and photo-Fenton treatment of 2,4-DCP. Initial experimental conditions: 2,4-DCP = 75 mg L^{-1} (460 μM), H_2O_2 = 10 mM, Fe^{2+} = 200 μM , pH = 7 for UV-C and $\text{H}_2\text{O}_2/\text{UV-C}$ and pH = 3 for Fenton and photo-Fenton treatments. 98
- Figure 4.16. Proposed pathway for UV-C photolysis of 2,4-DCP based on LC-MS data. 101
- Figure 4.17. Transformation products identified by means of LC-MS during degradation of 2,4-DCP via the $\text{H}_2\text{O}_2/\text{UV-C}$ process and proposed degradation pathway. 103
- Figure 4.18. Transformation products of 2,4-DCP identified by means of LC-MS during application of the Fenton process and proposed degradation pathway. 104
- Figure 4.19. Transformation products of 2,4-DCP identified by means of LC-MS during application of the photo-Fenton process and proposed degradation pathway. 105
- Figure 4.20. Changes in percent relative inhibition within the 2,4-DCP concentration range of 1.6-50 mg L^{-1} (9.8-307 μM). 107
- Figure 4.21. Temporal evolution of the acute inhibitory effect in relation with the identified 2,4-DCP transformation products whose signal intensities peaked after 10 (a), 20 (b), 30 (c) and 90 min (d) $\text{H}_2\text{O}_2/\text{UV-C}$ treatment. 110
- Figure 4.22. Temporal evolution of acute inhibitory effect in relation with unreacted 2,4-DCP concentration and the TOC originating from intermediates during photo-Fenton treatment of 2,4-DCP. Initial

- experimental conditions: 2,4-DCP = 75 mg L⁻¹ (460 μM), H₂O₂ = 10 mM, Fe²⁺ = 200 μM, pH = 3. 113
- Figure 4.23. Evolution of acute inhibitory effect with 2,4-DCP removal for UV-C, H₂O₂/UV-C, Fenton and photo-Fenton treatment processes. Initial experimental conditions: 2,4-DCP = 75 mg L⁻¹ (460 μM), H₂O₂ = 10 mM, Fe²⁺ = 200 μM, pH = 7 for UV-C and H₂O₂/UV-C and pH = 3 for Fenton and photo-Fenton treatment processes. 114
- Figure 4.24. The genotoxic effect versus 2,4-DCP concentration graph. 115
- Figure 4.25. Temporal evolution of genotoxic effect without S9 mix during H₂O₂/UV-C treatment of 2,4-DCP in relation with transformation products identified by LC-MS. 118
- Figure 4.26. Temporal evolution of genotoxic effect in the absence of S9 mix during photo-Fenton treatment of 2,4-DCP in relation with the identified 2-chloro-4-hydroxybenzaldehyde product. Initial experimental conditions: 2,4-DCP = 75 mg L⁻¹ (460 μM), H₂O₂ = 10 mM, Fe²⁺ = 200 μM, pH = 3. 120
- Figure 4.27. 2,4-DCP (a) and TOC removals (b) during UV-C, H₂O₂/UV-C, Fenton and photo-Fenton treatment of 2,4-DCP in SFW. Initial experimental conditions: 2,4-DCP = 75 mg L⁻¹ (460 μM), H₂O₂ = 10 mM, Fe²⁺ = 200 μM, pH = 7 for UV-C and H₂O₂/UV-C and pH = 3 for Fenton and photo-Fenton treatment. 122
- Figure 4.28. Evolution of UV₂₈₀ (a), (b) and UV₂₅₄ (c), (d) absorbances during UV-C, H₂O₂/UV-C (a), (c), Fenton and photo-Fenton (b), (d) treatment of 2,4-DCP in DW and SFW. Initial experimental conditions: 2,4-DCP = 75 mg L⁻¹ (460 μM), H₂O₂ = 10 mM, Fe²⁺ = 200 μM, pH = 7 for UV-C and H₂O₂/UV-C and pH = 3 for Fenton and photo-Fenton treatment processes. 126
- Figure 4.29. Cl⁻ releases during UV-C, H₂O₂/UV-C (a), Fenton and photo-Fenton (b) treatment of 2,4-DCP in DW and SFW. Initial experimental conditions: 2,4-DCP = 75 mg L⁻¹ (460 μM), H₂O₂ = 10 mM, Fe²⁺ = 200 μM, pH = 7 for UV-C and H₂O₂/UV-C and pH = 3 for Fenton and photo-Fenton treatment. 128

- Figure 4.30. Hydroquinone formation during UV-C, H₂O₂/UV-C (a), Fenton and photo-Fenton (b) treatment of 2,4-DCP in DW and SFW. Initial experimental conditions: 2,4-DCP = 75 mg L⁻¹ (460 μM), H₂O₂ = 10 mM, Fe²⁺ = 200 μM, pH = 7 for UV-C and H₂O₂/UV-C and pH = 3 for Fenton and photo-Fenton treatment. 130
- Figure 4.31. Evolution of maleic (a), (b) and formic (c), (d) acid products during UV-C, H₂O₂/UV-C (a), (c), Fenton and photo-Fenton (b), (d) treatment of 2,4-DCP in DW and SFW. Initial experimental conditions: 2,4-DCP = 75 mg L⁻¹ (460 μM), H₂O₂ = 10 mM, Fe²⁺ = 200 μM, pH = 7 for UV-C and H₂O₂/UV-C and pH = 3 for Fenton and photo-Fenton treatment processes. 133
- Figure 4.32. Aldehyde formation during UV-C, H₂O₂/UV-C (a), Fenton and photo-Fenton (b) treatment of 2,4-DCP in DW and SFW. Initial experimental conditions: 2,4-DCP = 75 mg L⁻¹ (460 μM), H₂O₂ = 10 mM, Fe²⁺ = 200 μM, pH = 7 for UV-C and H₂O₂/UV-C and pH = 3 for Fenton and photo-Fenton treatment. 135
- Figure 4.33. Temporal evolution of acute inhibitory effect during UV-C, H₂O₂/UV-C (a), Fenton and photo-Fenton (b) treatment of 2,4-DCP in DW and SFW. Initial experimental conditions: 2,4-DCP = 75 mg L⁻¹ (460 μM), H₂O₂ = 10 mM, Fe²⁺ = 200 μM, pH = 7 for UV-C and H₂O₂/UV-C and pH = 3 for Fenton and photo-Fenton treatment. 136
- Figure 4.34. Temporal evolution of the genotoxic effect in the absence (a), (b) and presence of metabolic activation (c), (d) during UV-C, H₂O₂/UV-C (a), (c), Fenton and photo-Fenton (b), (d) treatment of 2,4-DCP in DW and SFW. Initial experimental conditions: 2,4-DCP = 75 mg L⁻¹ (460 μM), H₂O₂ = 10 mM, Fe²⁺ = 200 μM, pH = 7 for UV-C and H₂O₂/UV-C and pH = 3 for Fenton and photo-Fenton treatment. 139
- Figure 4.35. Changes in NP-10, TOC and H₂O₂ concentrations during treatment of NP-10 by H₂O₂ alone. Initial experimental conditions: NP-10 = 50 mg L⁻¹ (76 μM), H₂O₂ = 10 mM, pH = 7. 143

- Figure 4.36. Changes in NP-10 concentration and TOC as well as pH during UV-C photolysis of NP-10. Initial experimental conditions: NP-10 = 50 mg L⁻¹ (76 μM), pH = 7. 143
- Figure 4.37. Effect of initial NP-10 concentration on the decay of NP-10 (a), TOC (b) and H₂O₂ (c) as well as the pH evolution (d) during H₂O₂/UV-C treatment of NP-10. Initial experimental conditions: H₂O₂ = 1 mM, pH = 7. 145
- Figure 4.38. Effect of initial pH on the decay of NP-10 (a), TOC (b) and H₂O₂ (c) as well as the pH evolution (d) during H₂O₂/UV-C treatment of NP-10. Initial experimental conditions: NP-10 = 50 mg L⁻¹ (76 μM), H₂O₂ = 5 mM. 147
- Figure 4.39. Effect of initial H₂O₂ concentration on the decay of NP-10 (a), TOC (b) and H₂O₂ (c) as well as the pH evolution (d) during H₂O₂/UV-C treatment of NP-10. Initial experimental conditions: NP-10 = 50 mg L⁻¹ (76 μM), pH = 7. 150
- Figure 4.40. Effect of initial pH on the decay of NP-10 (a), TOC (b) and H₂O₂ (c) during photo-Fenton treatment of NP-10. Initial experimental conditions: NP-10 = 50 mg L⁻¹ (76 μM), H₂O₂ = 5 mM, Fe²⁺ = 100 μM. 153
- Figure 4.41. Effect of initial Fe²⁺ concentration on the decay of NP-10 (a), TOC (b) and H₂O₂ (c) during photo-Fenton treatment of NP-10. Initial experimental conditions: NP-10 = 50 mg L⁻¹ (76 μM), H₂O₂ = 5 mM, pH = 3. 156
- Figure 4.42. Comparison of NP-10 (a) and TOC (b) abatements, H₂O₂ consumptions (c) and pH changes (d) during UV-C, H₂O₂/UV-C, Fenton and photo-Fenton treatment of NP-10. Initial experimental conditions: NP-10 = 100 mg L⁻¹ (150 μM), H₂O₂ = 10 mM, Fe²⁺ = 200 μM, pH = 7 for UV-C and H₂O₂/UV-C and pH = 3 for Fenton and photo-Fenton treatment. 158
- Figure 4.43. Temporal evolution of the UV absorbances at λ = 280 nm (a) and λ = 254 nm (b) during UV-C, H₂O₂/UV-C, Fenton and photo-Fenton treatment of NP-10. Initial experimental conditions: NP-10 = 100 mg

- L^{-1} (150 μ M), $H_2O_2 = 10$ mM, $Fe^{2+} = 200$ μ M, pH = 7 for UV-C and $H_2O_2/UV-C$ and pH = 3 for Fenton and photo-Fenton treatment. 161
- Figure 4.44. Temporal evolution of oxalic (a), acetic (b) and formic (c) acids during UV-C, $H_2O_2/UV-C$, Fenton and photo-Fenton treatment of NP-10. Initial experimental conditions: NP-10 = 100 mg L^{-1} (150 μ M), $H_2O_2 = 10$ mM, $Fe^{2+} = 200$ μ M, pH = 7 for UV-C and $H_2O_2/UV-C$ and pH = 3 for Fenton and photo-Fenton treatment. 165
- Figure 4.45. Temporal evolution of aldehydes during UV-C, $H_2O_2/UV-C$, Fenton and photo-Fenton treatment of NP-10. Initial experimental conditions: NP-10 = 100 mg L^{-1} (150 μ M), $H_2O_2 = 10$ mM, $Fe^{2+} = 200$ μ M, pH = 7 for UV-C and $H_2O_2/UV-C$ and pH = 3 for Fenton and photo-Fenton treatment. 167
- Figure 4.46. Temporal evolution of PEG during UV-C, $H_2O_2/UV-C$, Fenton and photo-Fenton treatment of NP-10. Initial experimental conditions: NP-10 = 100 mg L^{-1} (150 μ M), $H_2O_2 = 10$ mM, $Fe^{2+} = 200$ μ M, pH = 7 for UV-C and $H_2O_2/UV-C$ and pH = 3 for Fenton and photo-Fenton treatment. 171
- Figure 4.47. Changes in percent relative inhibition within the NP-10 concentration range of 3.9-250 mg L^{-1} (5.8-375 μ M). 172
- Figure 4.48. Temporal evolution of the acute inhibitory effect in relation with the identified transformation products during UV-C photolysis of NP-10. Initial experimental conditions: NP-10 = 100 mg L^{-1} (150 μ M), pH = 7. 174
- Figure 4.49. Temporal evolution of the acute inhibitory effect in relation with the identified transformation products during Fenton treatment of NP-10. Initial experimental conditions: NP-10 = 100 mg L^{-1} (150 μ M), $H_2O_2 = 10$ mM, $Fe^{2+} = 200$ μ M, pH = 3. 174
- Figure 4.50. Temporal evolution of the acute inhibitory effect in relation with the identified transformation products during $H_2O_2/UV-C$ (a) and photo-Fenton (b) treatment of NP-10. Initial experimental conditions: NP-10 = 100 mg L^{-1} (150 μ M), $H_2O_2 = 10$ mM, $Fe^{2+} = 200$ μ M, pH = 7 and 3 for the $H_2O_2/UV-C$ and photo-Fenton processes, respectively. 176

- Figure 4.51. Evolution of acute toxicity in synthetic samples and reaction samples treated by the H₂O₂/UV-C (a) and photo-Fenton (b) processes. Initial experimental conditions for the reaction samples: NP-10 = 100 mg L⁻¹ (150 μM), H₂O₂ = 10 mM, Fe²⁺ = 200 μM, pH = 7 for the H₂O₂/UV-C and pH = 3 for the photo-Fenton processes. 178
- Figure 4.52. The genotoxic effect versus NP-10 concentration graph. 179
- Figure 4.53. Temporal evolution of genotoxic effect without S9 mix during UV-C photolysis of NP-10 in relation with transformation products identified by GC-MS. Initial experimental conditions: NP-10 = 100 mg L⁻¹ (150 μM), pH = 7. 182
- Figure 4.54. Temporal evolution of genotoxic effect without S9 mix during H₂O₂/UV-C treatment of NP-10 in relation with the identified transformation products. Initial experimental conditions: NP-10 = 100 mg L⁻¹ (150 μM), H₂O₂ = 10 mM, pH = 7. 183
- Figure 4.55. NP-10 (a) and TOC removals (b) during UV-C, H₂O₂/UV-C, Fenton and photo-Fenton treatment of NP-10 in SFW. Initial experimental conditions: NP-10 = 100 mg L⁻¹ (150 μM), H₂O₂ = 10 mM, Fe²⁺ = 200 μM, pH = 7 for UV-C and H₂O₂/UV-C and pH = 3 for Fenton and photo-Fenton treatment. 186
- Figure 4.56. Evolution of UV₂₈₀ (a) and UV₂₅₄ (b) absorbances during H₂O₂/UV-C, Fenton and photo-Fenton treatment as well as UV-C photolysis of NP-10 in SFW. Initial experimental conditions: NP-10 = 100 mg L⁻¹ (150 μM), H₂O₂ = 10 mM, Fe²⁺ = 200 μM, pH = 7 for UV-C and H₂O₂/UV-C and pH = 3 for Fenton and photo-Fenton treatment. 190
- Figure 4.57. Evolution of formic acid (a), acetic acid (b) and oxalic acid (c) during H₂O₂/UV-C, Fenton and photo-Fenton treatment as well as UV-C photolysis of NP-10 in SFW. Initial experimental conditions: NP-10 = 100 mg L⁻¹ (150 μM), H₂O₂ = 10 mM, Fe²⁺ = 200 μM, pH = 7 for UV-C and H₂O₂/UV-C and pH = 3 for Fenton and photo-Fenton treatment. 192
- Figure 4.58. Evolution of aldehydes during H₂O₂/UV-C, Fenton and photo-Fenton treatment as well as UV-C photolysis of NP-10 in SFW. Initial

experimental conditions: NP-10 = 100 mg L⁻¹ (150 μM), H₂O₂ = 10 mM, Fe²⁺ = 200 μM, pH = 7 for UV-C and H₂O₂/UV-C and pH = 3 for Fenton and photo-Fenton treatment.

194

Figure 4.59. Temporal evolution of the intensities of individual nonylphenol polyethoxylate homologues during UV-C (a), H₂O₂/UV-C (b), Fenton (c) and photo-Fenton (d) treatment of NP-10 in SFW. Initial experimental conditions: NP-10 = 100 mg L⁻¹ (150 μM), H₂O₂ = 10 mM, Fe²⁺ = 200 μM, pH = 7 for UV-C and H₂O₂/UV-C and pH = 3 for Fenton and photo-Fenton treatment.

198

Figure 4.60. Proposed pathways for the transformation of NP-10 in SFW via the H₂O₂/UV-C and photo-Fenton processes based on LC-MS results.

200

Figure 4.61. Comparative evolution of formic acid and the acute inhibitory effect during H₂O₂/UV-C treatment of NP-10 in DW and SFW. Initial experimental conditions: NP-10 = 100 mg L⁻¹ (150 μM), H₂O₂ = 10 mM, pH = 7.

203

Figure 4.62. Comparative evolution of formic acid and the acute inhibitory effect during photo-Fenton treatment of NP-10 in DW and SFW. Initial experimental conditions: NP-10 = 100 mg L⁻¹ (150 μM), H₂O₂ = 10 mM, Fe²⁺ = 200 μM, pH = 3.

205

Figure 4.63. Box and whisker plots comparing genotoxic effects being observed during H₂O₂/UV-C, Fenton and photo-Fenton treatment as well as UV-C photolysis of NP-10 in DW and SFW in the presence of metabolic activation. Initial experimental conditions: NP-10 = 100 mg L⁻¹ (150 μM), H₂O₂ = 10 mM, Fe²⁺ = 200 μM, pH = 7 for UV-C and H₂O₂/UV-C and pH = 3 for Fenton and photo-Fenton treatment.

208

LIST OF TABLES

Table 2.1. Recent studies on transformation products of chlorophenols being generated during application of the H ₂ O ₂ /UV, Fenton and photo-Fenton processes.	14
Table 2.2. Recent studies on toxicity changes during H ₂ O ₂ /UV, Fenton and photo-Fenton treatment of chlorophenols.	24
Table 2.3. Relationships between transformation products and toxicity being drawn from the recent studies regarding the H ₂ O ₂ /UV, Fenton and photo-Fenton treatment of chlorophenols.	30
Table 2.4. Reported transformation products of alkylphenol polyethoxylates being generated during photolysis and AOP as well as their molecular ions/fragments.	34
Table 2.5. Scientific studies documenting the toxicity changes during photolysis and chemical oxidation of alkylphenol polyethoxylates.	40
Table 3.1. Structural formula and selected physicochemical properties of 2,4-DCP.	43
Table 3.2. Structural formula and selected physicochemical properties of NP-10.	44
Table 3.3. Final composition and quality of SFW.	45
Table 3.4. HPLC operating conditions.	50
Table 4.1. The pseudo-first-order rate coefficients and removal percentages for 2,4-DCP, TOC and H ₂ O ₂ decays by the H ₂ O ₂ /UV-C process as a function of initial 2,4-DCP concentration.	64
Table 4.2. The pseudo-first-order rate coefficients and removal percentages for 2,4-DCP, TOC and H ₂ O ₂ decays by the H ₂ O ₂ /UV-C process as a function of initial pH.	66
Table 4.3. The pseudo-first-order rate coefficients and removal percentages for 2,4-DCP, TOC and H ₂ O ₂ decays by the H ₂ O ₂ /UV-C process as a function of initial H ₂ O ₂ concentration.	70
Table 4.4. The pseudo-first-order rate coefficients and removal percentages for 2,4-DCP, TOC and H ₂ O ₂ decays by the Fenton process as a function of H ₂ O ₂ :Fe ²⁺ molar ratio.	74

Table 4.5. The pseudo-first-order rate coefficients and removal percentages for 2,4-DCP, TOC and H ₂ O ₂ decays by the photo-Fenton process as a function of initial reaction pH.	75
Table 4.6. The pseudo-first-order rate coefficients and removal percentages for 2,4-DCP, TOC and H ₂ O ₂ decays by the photo-Fenton process as a function of initial Fe ²⁺ concentration.	80
Table 4.7. The pseudo-first-order rate coefficients and removal percentages for 2,4-DCP, TOC and H ₂ O ₂ decays by the studied treatment processes.	84
Table 4.8. Transformation products identified by GC-MS during UV-C, H ₂ O ₂ /UV-C, Fenton and photo-Fenton treatment of 2,4-DCP.	92
Table 4.9. Proposed identities of transformation products formed during UV-C, H ₂ O ₂ /UV-C, Fenton and photo-Fenton treatment of 2,4-DCP.	99
Table 4.10. Acute toxic effects observed during UV-C, H ₂ O ₂ /UV-C, Fenton and photo-Fenton treatment of 2,4-DCP.	108
Table 4.11. Genotoxic effects observed at different stages of 2,4-DCP degradation by UV-C, H ₂ O ₂ /UV-C, Fenton and photo-Fenton treatment processes.	117
Table 4.12. Pseudo-first-order abatement rate coefficients and percent removal efficiencies obtained for degradation of 2,4-DCP by UV-C, H ₂ O ₂ /UV-C, Fenton and photo-Fenton treatment processes in DW and SFW.	121
Table 4.13. Pseudo-first-order abatement rate coefficients and percent consumptions obtained for H ₂ O ₂ during H ₂ O ₂ /UV-C, Fenton and photo-Fenton treatment of 2,4-DCP in DW and SFW.	123
Table 4.14. Pseudo-first-order abatement rate coefficients and percent removal efficiencies obtained for TOC removal by UV-C, H ₂ O ₂ /UV-C, Fenton and photo-Fenton treatment of 2,4-DCP in DW and SFW.	125
Table 4.15. Pseudo-first-order abatement rate coefficients and percent removal efficiencies obtained for NP-10, TOC and H ₂ O ₂ by the H ₂ O ₂ /UV-C process as a function of initial NP-10 concentration.	144
Table 4.16. Pseudo-first-order abatement rate coefficients and percent removal efficiencies obtained for NP-10, TOC and H ₂ O ₂ by the H ₂ O ₂ /UV-C process as a function of initial pH.	146

Table 4.17. Pseudo-first-order abatement rate coefficients and percent removal efficiencies obtained for NP-10, TOC and H ₂ O ₂ by the H ₂ O ₂ /UV-C process as a function of initial H ₂ O ₂ concentration.	149
Table 4.18. Pseudo-first-order abatement rate coefficients and percent removal efficiencies obtained for NP-10, TOC and H ₂ O ₂ by the Fenton process as a function of H ₂ O ₂ :Fe ²⁺ molar ratio.	152
Table 4.19. Pseudo-first-order abatement rate coefficients and percent removal efficiencies for NP-10, TOC and H ₂ O ₂ during photo-Fenton process as a function of initial pH.	154
Table 4.20. Pseudo-first-order abatement rate coefficients and percent removal efficiencies for NP-10, TOC and H ₂ O ₂ during photo-Fenton process as a function of initial Fe ²⁺ concentration.	155
Table 4.21. Pseudo-first-order abatement rate coefficients and percent removal efficiencies obtained for NP-10, TOC and H ₂ O ₂ by applying UV-C, H ₂ O ₂ /UV-C, Fenton and photo-Fenton treatments.	159
Table 4.22. Transformation products identified by GC-MS during UV-C, H ₂ O ₂ /UV-C, Fenton and photo-Fenton treatment of NP-10.	169
Table 4.23. Comparison of the initial and final acute inhibitory effects for H ₂ O ₂ /UV-C, Fenton and photo-Fenton treatment as well as UV-C photolysis of NP-10.	177
Table 4.24. Genotoxic effects observed at different stages of NP-10 degradation by UV-C, H ₂ O ₂ /UV-C, Fenton and photo-Fenton treatment processes.	181
Table 4.25. Pseudo-first-order abatement rate coefficients and percent removal efficiencies obtained for degradation of NP-10 by UV-C, H ₂ O ₂ /UV-C, Fenton and photo-Fenton treatment processes in DW and SFW.	185
Table 4.26. Pseudo-first-order abatement rate coefficients and percent removal efficiencies obtained for TOC removal by UV-C, H ₂ O ₂ /UV-C, Fenton and photo-Fenton treatment processes in DW and SFW.	188
Table 4.27. Pseudo-first-order abatement rate coefficients and percent consumptions obtained for H ₂ O ₂ during H ₂ O ₂ /UV-C, Fenton and photo-Fenton treatment of NP-10 in DW and SFW.	188

Table 4.28. Transformation products identified via the GC-MS during H ₂ O ₂ /UV-C and photo-Fenton treatment as well as UV-C photolysis of NP-10 in SFW.	195
Table 4.29. Evolution of acute inhibitory effects during the H ₂ O ₂ /UV-C, Fenton and photo-Fenton treatment as well as UV-C photolysis of NP-10 in SFW.	201
Table 4.30. Genotoxic effects observed at different stages of NP-10 degradation by UV-C, H ₂ O ₂ /UV-C, Fenton and photo-Fenton treatment processes in SFW.	206

LIST OF SYMBOLS/ABBREVIATIONS

Symbol	Explanation	Units used
2,4-DCP	2,4-Dichlorophenol	
2,4-DCP/2,4-DCP ₀	Normalized 2,4-DCP concentration	–
AOP	Advanced Oxidation Processes	
C	Concentration after a given treatment time	(mg L ⁻¹)
C ₀	Concentration of the original solution	(mg L ⁻¹)
Cl [•]	Chlorine radical	
COD	Chemical Oxygen Demans	
DAD	Diode Array Detection	
DW	Distilled Water	
EC ₂₀	Effective concentration causing 20% bioluminescence inhibition	(mg L ⁻¹)
EC ₅₀	Effective concentration causing 50% bioluminescence inhibition	(mg L ⁻¹)
GC-MS	Gas Chromatography-Mass Spectrometry	
H ₂ O ₂ /H ₂ O _{2,0}	Normalized H ₂ O ₂ concentration	–
HO [•]	Hydroxyl radical	
HPLC	High Performance Liquid Chromatography	
IC	Ion Chromatography	
k _{2,4-DCP}	Pseudo-first-order 2,4-DCP removal rate coefficient	(min ⁻¹)
k _{H₂O₂}	Pseudo-first-order H ₂ O ₂ consumption rate coefficient	(min ⁻¹)
k _{NP-10}	Pseudo-first-order NP-10 removal rate coefficient	(min ⁻¹)
k _{TOC}	Pseudo-first-order TOC removal rate coefficient	(min ⁻¹)
LC-MS	Liquid Chromatography-Mass Spectrometry	
n	Ethoxylate unit number	–

Symbol	Explanation	Units used
NP-10	Nonylphenol decaethoxylate	
NP-10/NP-10 ₀	Normalized NP-10 concentration	–
PEG	Polyethylene Glycols	
p <i>K</i> _a	Dissociation constant	–
<i>R</i> ²	Regression coefficient	
- S9	Without metabolic activation	
+ S9	With metabolic activation	
SFW	Synthetic Freshwater	
TOC	Total Organic Carbon	(mg L ⁻¹)
TOC/TOC ₀	Normalized total organic carbon removal	–
UV ₂₅₄	UV absorbance at 254 nm	(cm ⁻¹)
UV ₂₈₀	UV absorbance at 280 nm	(cm ⁻¹)
λ	Wavelength	(nm)

1. INTRODUCTION

Phenol derivatives comprise one of the major families of industrially important chemicals, representing a diverse group of compounds with different physical and chemical properties. Among them, chlorophenols and alkylphenol polyethoxylates deserve special attention due to their high production and consumption rates. Chlorophenols and alkylphenol polyethoxylates have been widely used in the preparation of detergents, wood preservatives and polymeric materials for household and industrial applications (Chiu et al., 2010; Olaniran and Igbinosa, 2011). Therefore, it is not uncommon to detect both of these compound classes in process waters and effluents originated from specific industries including pulp and paper (Lacorte et al., 2003) and textile industries (Rutherford et al., 2003). As a result, both of these ubiquitous substances are frequently being discharged into municipal as well as industrial wastewater treatment plants or released directly into receiving water bodies. Most chlorophenols are well known for their toxicity to microorganisms including activated sludge bacteria (Ricco et al., 2004). Moreover, their biodegradability is rather poor (Pera-Titus et al., 2004). Alkylphenol polyethoxylates on the other hand, although readily biodegradable in conventional activated sludge processes, are rather slowly biotransformed into alkylphenols, alkylphenol monoethoxylates and alkylphenol diethoxylates, which are recognized as potential endocrine disruptors (Andreu et al., 2007; Karahan et al., 2010). Because of these properties, chlorophenols have been listed as priority toxic substances by the US EPA in the Clean Water Act (Keith and Telliard, 1979) and by the European Decision 2455/2001/EC (2001), and nonylphenol and its polyethoxylates have been designated as priority hazardous substances in the Water Framework Directive (Directive 2000/60/EC, 2000).

Considering the abovementioned issues, the efficient treatment of chlorophenols and alkylphenol polyethoxylates is a challenging task to protect human health and the environment. Being widely recognized as highly efficient for the treatment of a wide array of aqueous wastes containing different classes of organic pollutants (Tünay et al., 2010; O'Shea and Dionysiou, 2012; Wang and Xu, 2012), advanced oxidation processes (AOP) are destruction technologies alternative to conventional treatment methods. These methods are based on the formation of reactive species including hydroxyl radicals (HO^\bullet) which are

capable of degrading even the most recalcitrant molecules within a reasonable time span. Major limitations of their full-scale application, however, have not been overcome yet; their capital and operating costs are still relatively high, and in some cases the oxidation products are more toxic than the parent pollutants (Suarez-Ojeda et al., 2007; Oturan et al., 2008; Radjenović et al., 2009; Rizzo, 2011). Consequently, the control and optimization of AOP remains a serious challenge, in particular for industrial wastewater treatment applications. In light of this, chlorophenols and alkylphenol polyethoxylates acting as model pollutants found in different kinds of industrial effluents, seem to be very good candidates to examine the correlation between the type of oxidation products and their toxicity evolution.

The $\text{H}_2\text{O}_2/\text{UV}$, Fenton ($\text{Fe}^{2+}/\text{H}_2\text{O}_2$) and photo-Fenton ($\text{Fe}^{2+}/\text{H}_2\text{O}_2/\text{UV}$) processes are among the most investigated AOP which have been proved to be highly successful in extensively degrading organic contaminants in a variety of wastewater streams (Ikehata and El-Din, 2006; Pignatello et al., 2006; Stasinakis, 2008). Former treatability studies have already demonstrated that the $\text{H}_2\text{O}_2/\text{UV}$, Fenton and photo-Fenton processes could be used to successfully degrade aqueous chlorophenols and alkylphenol polyethoxylates (Arslan-Alaton, 2007; Pagano et al., 2008; Arslan-Alaton et al., 2012a, 2012b). However, these treatability studies rather focused on process efficiency evaluated by means of monitoring the changes in parent pollutant concentration, as well as collective environmental parameters such as chemical oxygen demand (COD) and total organic carbon (TOC). In most cases, AOP did not achieve total mineralization of chlorophenols and alkylphenol polyethoxylates, and hence the toxicity of transformation products should be a critical point when establishing the benefits of any applied technology. Until now, the effect of different AOP types including $\text{H}_2\text{O}_2/\text{UV}$, Fenton and photo-Fenton processes, on the changes in toxicity of chlorophenols has been scarcely documented in the scientific literature (Essam et al., 2007; Pérez-Moya et al., 2007; Munoz et al., 2012a). Furthermore, the scientific literature concerning the toxicity of alkylphenol polyethoxylates subjected to AOP is restricted to two research papers describing toxicity changes during ozonation (Lenz et al., 2004; Ledakowicz et al., 2005). This information has to be established to transform pollutants to more biodegradable, less toxic degradation products during application of AOP. A more important point is that for both chlorophenols and alkylphenol polyethoxylates relationships between transformation products and toxicity during AOP

treatment are relatively unknown and have not been studied in depth up to date. The assessment of possible relationships between advanced oxidation products and toxicity could be a valuable tool in the estimation of ecological risks created by the discharge of xenobiotic industrial pollutants including chlorophenols and alkylphenol polyethoxylates.

The present research was planned, considering that advanced oxidation products of chlorophenols and alkylphenol polyethoxylates might affect seriously public health and the environment due to their potential of toxicity and/or low rates of biodegradability. The innovative aspect of the study is the elucidation of toxicity patterns derived from the advanced oxidation of a chlorophenol and an alkylphenol polyethoxylate compound, namely 2,4-dichlorophenol (2,4-DCP) and nonylphenol decaethoxylate (NP-10), respectively, in relation with identified transformation products. Main motivation of the present study was to propose the oxidation products and toxicity as a potential criterion for the selection of an AOP as an alternative for cost effective treatment of problematic substances including chlorophenols and alkylphenol polyethoxylates. The H₂O₂/UV-C, Fenton and photo-Fenton AOP were investigated as potential treatment processes for 2,4-DCP and NP-10 due to their well-known reaction kinetics and mechanism. Although not an AOP, UV-C photolysis was also included in the study due to the availability of UV based systems in many water utilities and potential effectiveness of such UV systems for treatment of chemical contaminants. In the first part of the study baseline experiments were conducted to determine the most appropriate reaction conditions for effective treatment of aqueous 2,4-DCP and NP-10 and to comparatively elucidate degradation (parent pollutant, TOC removal) and dearomatization (UV₂₈₀ and UV₂₅₄ abatement) during application of different treatment processes. In the second part, dechlorination and transformation of 2,4-DCP and NP-10 into aromatic and aliphatic transformation products were investigated under selected treatment conditions. In the third part, acute toxicity changes were monitored for the same treatment processes by using the marine photobacterium *Vibrio fischeri* that has been the test organism most often employed in toxicity assays because of its high sensitivity towards a wide range of pollutants (Rizzo, 2011). In addition, the genotoxicity profiles during the studied treatment processes were investigated by means of the *umu*-test which is a simple, sensitive and rapid bacterial colorimetric assay to determine genotoxic potential of environmental waters influenced by anthropogenic input (Özhan et al., 2008). In the fourth and final part of the study experiments were replicated in

synthetically prepared freshwater containing a mixture of inorganic salts at typical concentrations encountered in moderately hard freshwaters to elucidate overall efficiency of the studied treatment processes under conditions relevant to natural waters.

2. THEORETICAL BACKGROUND

2.1. Overview of Commercially Important Phenol Derivatives

Among numerous phenol derivatives used in industrial processes, chlorophenols have received special scientific and public interest due to their high toxicity and low biodegradability. A large majority of the research related to alkylphenol polyethoxylate destruction in the water environment, however, has focused on nonylphenols rather than nonylphenol polyethoxylates. The common feature of chlorophenols and alkylphenol polyethoxylates is that they are produced and consumed in massive quantities, and a substantial fraction is released into the wastewater streams or directly into receiving water bodies. It is also not uncommon to detect both of these compound classes in process waters and effluents originated from specific industries including pulp and paper (Lacorte et al., 2003) and textile industries (Rutherford et al., 2003).

2.1.1. Chlorophenols

Chlorophenols are chlorinated aromatic ring structures consisting of the benzene ring, –OH group and atom(s) of chlorine. Together with the 19 main compounds, chloroderivatives of methyl- and ethylphenols are also considered as chlorophenols (Czaplicka, 2004). All chlorophenols are solids at room temperature except 2-chlorophenol, which is a liquid. In general, these compounds dissolve weakly in water, but in reactions with alkaline metals (sodium, potassium) in the aquatic environment, they yield salts highly soluble in water (Czaplicka, 2004). The partition coefficients of chlorophenols increase, but their dissociation constants (as pK_a) decrease as the number of chlorine substituents increases (Kishino and Kobayashi, 1994). *Ortho* chlorophenols are more stable and acidic than other isomers as a result of intramolecular hydrogen bonding and large inductive effect of chlorine on the –OH group in close proximity (Han et al., 2004).

Chlorophenols are being employed as disinfectants and preservatives in wood, dyes, vegetable fibers and leather due to their broad-spectrum antimicrobial properties. They

constitute an important group of aromatic chemicals having an annual world market share of about 100 kilotons most of which (~ 60 kilotons) are constituted by mono-, di- and trichlorophenols (Pera-Titus et al., 2004). The large scale production and heavy consumption of chlorophenols and their derivatives generate wastewaters that contain these substances at high concentrations. In addition to their intentional use, chlorophenols may also be generated during waste incineration, bleaching of pulp with chlorine and water disinfection by chlorination (Ahlborg and Thunberg, 1980). Most chlorophenols are highly toxic to microorganisms including activated sludge bacteria and their removal with biological treatment processes is rather problematic due to their inhibitory properties and resistance to biodegradation, making the efficient removal of these substances from wastewaters in a conventional wastewater treatment plant very difficult if not impossible (Sharma et al., 2013). When wastewaters containing chlorophenols are being discharged into natural water bodies they may cause serious environmental as well as ecotoxicological problems since many of them are highly toxic to a number of environmental organisms, produce sharp odor, rather persistent in the environment, are suspected of being carcinogenic and mutagenic, and have a high potential to bioaccumulate in organisms (Araki et al., 2000; Ucisik and Trapp, 2008). Because of the abovementioned issues, chlorophenols have been listed as priority toxic substances by the US EPA in the Clean Water Act (Keith and Telliard, 1979) as well as by the European Decision 2455/2001/EC (2001).

2.1.2. Alkylphenol Polyethoxylates

Alkylphenol polyethoxylates are synthesized by the reaction of alkylphenols with ethylene oxide to produce alkylphenol molecules with a single chain polyethoxylate moiety. The alkylphenol parts of the molecule are mostly branched chained nonyl- and octylphenols, and the polyethoxylate chain lengths can extend to 100 units (Staples et al., 2008). Nonylphenol polyethoxylates bearing an average of 1.5 to 9 ethoxy units are liquids at ambient temperatures, whereas higher nonylphenol polyethoxylates (ethoxy unit number > 12) are solids at ambient temperatures. Lower alkylphenol polyethoxylate oligomers (ethoxy unit number < 5) are usually described as “water-insoluble” or lipophilic, with log K_{ow} (the octanol-water partition coefficient) values of about 4, whereas the higher oligomers are described as “water-soluble” or hydrophilic (Ying et al., 2002). The

adsorption coefficients (K_d) for nonylphenol polyethoxylates onto organic sediments increase with decreasing degree of ethoxylation (John et al., 2000). The logarithm of the critical micelle concentration, the concentration at which micelles first appear in the solution, increases with an increase in the polyethoxylate chain length (Huibers et al., 1996).

Alkylphenol polyethoxylates are applied to a number of industrial, institutional, commercial and household uses such as detergents, emulsifiers, wetting and dispersing agents, antistatic agents, demulsifiers and solubilizers (Soares et al., 2008). They are the second largest class of nonionic surfactants in use today comprising approximately 6% of the total surfactant production in the world (Ning et al., 2007). The worldwide production of alkylphenol polyethoxylates has been reported as 500 kilotons in 1997, of which 80% were nonylphenol polyethoxylates and 20% were octylphenol polyethoxylates (Chiu et al., 2010). Alkylphenol polyethoxylates are generally treatable in conventional wastewater treatment plants (Ahel et al., 1994), whereas inhibitory effects on biomass growth, and in turn, on hydrolysis process in a non-acclimated activated sludge system have also been reported (Karahan et al., 2010). Under anaerobic conditions such as those found in biotreatment operations at wastewater treatment plants, alkylphenols (mostly nonylphenol and octylphenol) are generated, whereas mono- and diethoxylated metabolites as well as their carboxylated derivatives, namely alkylphenol ethoxycarboxylates, are predominantly formed under aerobic conditions (Montgomery-Brown and Reinhard, 2003). Although alkylphenol polyethoxylates being often characterized by their low acute toxicity tend to be degraded via the biological processes, the metabolites of alkylphenol polyethoxylates including alkylphenols, alkylphenol monoethoxylates and alkylphenol diethoxylates being more toxic, lipophilic and biorecalcitrant than the mother pollutant accumulate during conventional biological treatment (González et al., 2007a; Céspedes et al., 2008; Janex-Habibi et al., 2009). These degradation products are also recognized as endocrine disruptors (Petrovic et al., 2003). As a result, the contamination of natural water resources by alkylphenol polyethoxylate metabolites at ng L^{-1} to $\mu\text{g L}^{-1}$ levels has been widely reported from all around the world (Ying et al., 2002). Accordingly, nonylphenol and its polyethoxylates have been designated as priority hazardous substances in the Water Framework Directive (Directive 2000/60/EC, 2000).

2.2. Advanced Oxidation Processes

Water scarcity as well as health and hygienic problems related to water pollution are two important issues which are expected even to grow in the coming decades (Bauer et al., 1999). To tackle these problems, development of effective new water treatment processes seems to be the key, without further stressing the environment or endangering human health by the treatment itself. In fact, number of scientific studies on this research field is continuously increasing in parallel with the rigorous pollution control and legislation in many countries (Andreozzi et al., 1999). Although conventional biological and chemical methods of water treatment can address many of these problems, these processes have some drawbacks such as the requirement of a long residence time for microorganisms to degrade toxic and/or biorefractory pollutants and transfer of pollution problem only from one phase to another (Pera-Titus et al., 2004).

Among the chemical oxidation processes being largely studied as an efficient alternative to conventional treatment technologies, advanced oxidation processes (AOP) which have the ability to nearly completely remove a number of organic compounds present in aqueous and solid environmental matrices without the need for extreme process conditions present challenges (Bekbolet et al., 2009; Lee et al., 2009; Arslan-Alaton et al., 2010). These processes take advantage of using hydroxyl radicals (HO^\bullet) with an oxidation potential of 2.8 V as the major oxidant which react nonselectively at diffusion-limited reaction rates (Legrini et al., 1993). Although the high cost of AOP is the most important factor limiting their applicability in full-scale wastewater treatment plants, significant cost reductions can be achieved by applying these processes as a pre- or post-treatment stage, whose main role is the partial oxidation of the biologically persistent part to produce biodegradable reaction intermediates (Oller et al., 2011).

AOP can be categorized in various means, but mainly depending on the source for the generation of HO^\bullet (Figure 2.1). The conventional oxidants H_2O_2 and O_3 mostly constitute the source for the generation of HO^\bullet , although in recent years other alternative oxidants such as persulfate ($\text{S}_2\text{O}_8^{2-}$) have been reported to be used for the radicalic oxidation of organic pollutants (Liang et al., 2009). While H_2O_2 alone is inefficient for the destruction of high concentrations of refractory organic pollutants in most cases, the introduction of

transition metal salts such as Fe^{2+} , O_3 and/or UV irradiation into the system greatly improves the oxidation and mineralization rates due to the generation of HO^\bullet (Neyens and Baeyens, 2003). Similarly, UV photolysis alone has also been reported to ensure decomposition of most organic molecules at very slow rates (Goi and Trapido, 2002), although efficient destruction of strongly UV-absorbing compounds can be achieved via direct UV photolysis (Sanches et al., 2010).

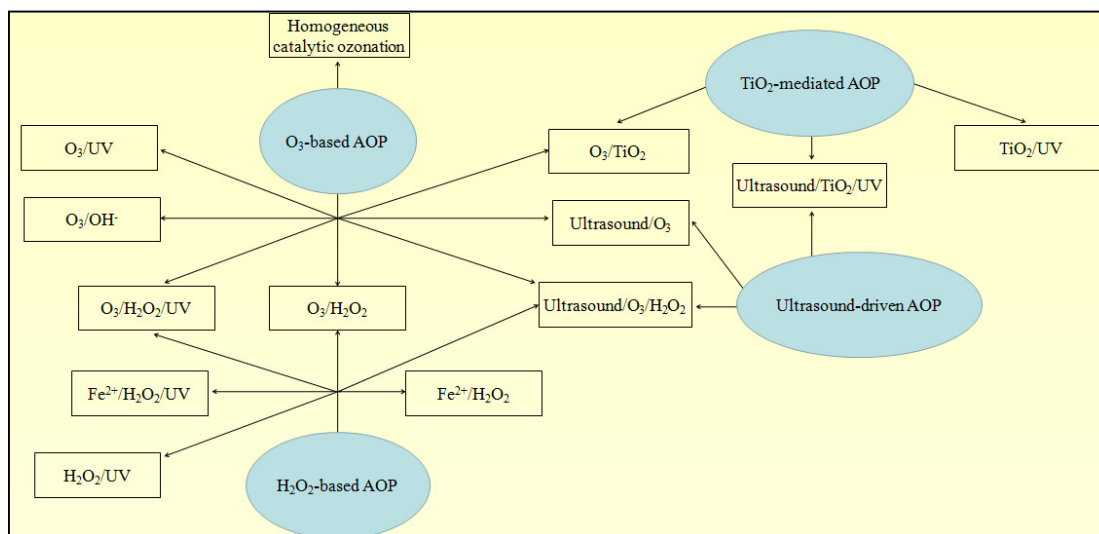


Figure 2.1. Schematic representation of AOP being relatively well-established for treatment of industrial wastewaters.

Among the single oxidants, O_3 generally appears to be the most effective one for the oxidation of refractory pollutants due to its high oxidation potential (+ 2.07 V) (Benitez et al., 2000a; Contreras et al., 2003). Single ozonation of organic pollutants proceeds via mechanistic pathways of both molecular O_3 attack and indirect oxidation with free radicals that are formed during O_3 decomposition, the latter being much more effective at alkaline pH (Beltrán, 2005). The combinations of O_3 with H_2O_2 , UV irradiation, homogeneous catalysts such as transition metals and heterogeneous catalysts such as metal oxides, clays and activated carbon can further enhance the production of HO^\bullet (Abe and Tanaka, 1997; Ormad et al., 1997; Kasprzyk-Hordern et al., 2003).

Being a heterogeneous photochemical process, TiO_2 photocatalysis is by far the most commonly used AOP which is based on the suggested mechanism of the oxidation of

pollutants directly by the photogenerated holes in the valence band of the semiconductor or indirectly by HO^\bullet resulting from the reaction of adsorbed H_2O , HO^- or surface titanol groups with the holes (Hoffmann et al., 1995; Mills and Le Hunte, 1997). The recombination of valence band hole and conduction band electrons can be prevented by the addition of several electron acceptors such as O_2 , H_2O_2 and O_3 , producing additional reactive oxygen species and improving the process efficiency (Fox and Dulay, 1993; Pengyi et al., 2003; Pekakis et al., 2006). Although its application as a wastewater treatment process is more recent compared to TiO_2 photocatalysis, the homogeneous photocatalytic process photo-Fenton ($\text{Fe}^{2+}/\text{H}_2\text{O}_2/\text{UV}$) is among the most applied AOP, as evidenced by the significant increase in number of publications treating this process (Malato et al., 2009). TiO_2 photocatalysis and photo-Fenton processes can also be applied under the solar irradiation which eliminates the operational cost involving the use of artificial UV light sources (Malato et al., 2002), and their application at solar pilot plant scale have been already shown for a range of pollutants/wastewaters (Gernjak et al., 2004; Maldonado et al., 2007). This is most probably the main reason of increased interest to these two AOP particularly in recent years.

Other AOP such as wet air oxidation, supercritical water oxidation and those based on the use of power ultrasound has been demonstrated to be effective for the treatment of wastewaters containing refractory pollutants (Bermejo and Cocero, 2006; Levec and Pintar, 2007; Joseph et al., 2009). On the other hand, the high pressure and temperature conditions required by wet air oxidation and supercritical water oxidation processes make these treatment techniques a non-viable option in point of economical view. Similarly, ultrasonic irradiation which is based on the formation, growth and subsequent collapse of microbubbles or cavities occurring in extremely small intervals of time and releasing large amount of energy upon high-intensity acoustic irradiation of liquids (Gogate and Pandit, 2004), has the shortcoming of inefficient conversion of energy in producing ultrasonic cavitation which hinders its scale-up to industrial applications. Although the relatively well-established chemical and photochemical AOP as well as relationships between them are schematized in Figure 2.1, it should be stated that the AOP researched and developed in the scientific literature are not limited to these. For instance, γ -radiolysis (Wu et al., 2002), the electrochemical anodic oxidation and electro-Fenton processes (Brillas et al.,

2000) and the Fe^{3+} -induced photolysis (Brand et al., 1998) have also been revealed to be the potential sources of HO^\bullet for the destruction of organic pollutants.

Although AOP has the ability to efficiently improve the degradation and mineralization rates of pollutants due to the radicalic pathways involved in these processes, they have specific drawbacks limiting their full scale application. For instance, the main limitation of Fe-based AOP is the necessity to work at acidic pH range (pH 2-4) due to the precipitation of Fe as their hydroxides at higher pH (Shemer et al., 2006). Separation and proper disposal of Fe sludge after the processes are complete, are also a problem in terms of the practical application of the relevant AOP. The major drawbacks of AOP in which heterogeneous catalysts are used, are the separation of the catalyst when used in suspension and the potential leaching of metal ions if present. However, the most important and common drawback of all AOP is that they have the inherent risk of producing toxic transformation products during their application. Accordingly, the collective environmental parameters such as chemical oxygen demand (COD) and total organic carbon (TOC) remain insufficient for the evaluation of the biocompatibility of AOP-treated effluents before they can be safely discharged into receiving water bodies or transferred to a biological treatment. A number of scientific studies have already revealed that the partial mineralization of organic contaminants by different AOP resulted in a toxicity increase at the end of treatment compared to the untreated water/wastewater (Neamtu et al., 2004; Micó et al., 2010; Olmez-Hanci et al., 2010). This major drawback makes the careful operation and monitoring of AOP by means of toxicity bioassays necessary in order to evaluate the detoxification level achieved after an AOP. Toxicity screening is also useful for deciding on samples in which the inhibitory effect has changed enough to make performing biodegradability tests (Oller et al., 2007). The literature review using the keywords “Advanced Oxidation Processes” and “Toxicity” revealed that the number of publications (whose full texts were accessible via Web of Science) in which the evolution of toxicity during the application of AOP has been dealt presented a substantial increase between 2006-2011 as evident from Figure 2.2. It is even more worthwhile to conclude from Figure 2.2 that the scientific literature increasingly took into account the assessment of the ecotoxicological impact of AOP in relation with the identified transformation products between the years 2008-2011. Although it is clear that such a simple search

underestimates the real number of relevant publications, it still serves to prove the general trend of an increasing interest of the scientific community.

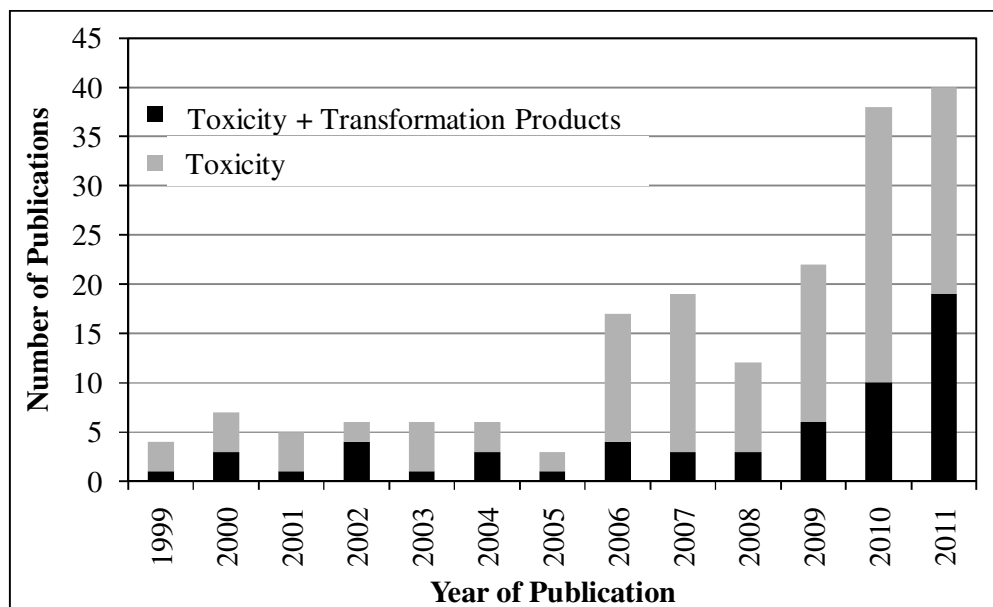


Figure 2.2. Scientific studies covering toxicity during application of AOP with and without transformation products included.

2.3. H₂O₂/UV, Fenton and Photo-Fenton Treatment of Chlorophenols

Among the AOP, the H₂O₂/UV, Fenton and photo-Fenton processes have been extensively studied in the scientific literature for the degradation of chlorophenols due to the efficient elimination of these substances during application of these processes. Several review papers have combined the results being drawn from such studies (Pera-Titus et al., 2004; Sharma et al., 2013), but none of them have focused on description of the formed transformation products and more importantly the toxicity changes. This section will cover the findings regarding the transformation product and inhibitory effect changes during application of the H₂O₂/UV, Fenton and photo-Fenton processes for the removal of aqueous chlorophenols.

2.3.1. Transformation Products

The studies aiming at identifying and monitoring of transformation products during H₂O₂/UV, Fenton and photo-Fenton treatment of aqueous chlorophenols are presented in Table 2.1. As is evident from Table 2.1, monochlorinated phenols have been extensively selected as the model pollutants in the transformation product studies, 4-chlorophenol being the prototype of this group of compounds. The Fenton process has been by far the most commonly studied AOP with regard to the identification of transformation products of chlorophenols. One plausible reason for this could be that the Fenton's reagent was relatively ineffective in the mineralization of chlorophenols as compared to the H₂O₂/UV and photo-Fenton processes, rendering the monitoring strategies of transformation products much more vital for the Fenton process. In most of the cases, the initial pollutant concentrations have been established as > 100 mg L⁻¹ being significantly higher than the environmental concentrations of chlorophenols. Although this was necessary to improve the analytical sensitivity, it should be kept in mind that use of high experimental conditions may shift the degradation mechanism of chlorophenols to bimolecular coupling reactions (Hirvonen et al., 2000) and hinder scale up of the results to real applications.

According to Table 2.1, the breakdown pathways and the type of transformation products were largely independent of the type of treatment, since the processes are driven by the same reactive species, which are mainly HO[•]. In each processes, the direct addition of HO[•] onto the aromatic ring of the respective chlorophenols resulted in the generation of mono- and polyhydroxylated chlorophenolic transformation products. Transformation of 4-chlorophenol into 4-chlororesorcinol, 4-chlorocatechol and chlorinated benzenetriols could be attributed to this transformation pathway (Du et al., 2006, 2007; Arsene et al., 2010; Kralik et al., 2010; Catrinescu et al., 2011; Gomez et al., 2012a; Murcia et al., 2012; Peternel et al., 2012). On the other hand, HO[•] could also preferentially attack onto the C atom being occupied by the —Cl group and substitute chlorine, resulting in the release of organically bound Cl in the form of free Cl⁻ (Basu and Wei, 1998; Ghaly et al., 2001). Generation of hydroquinone and catechol being originated from the HO[•]-mediated transformation of 4-chlorophenol and 2-chlorophenol has been ascribed to this mechanistic pathway (Kang et al., 2002; Bertelli and Selli, 2006). HO[•] have also been reported to be

Table 2.1. Recent studies on transformation products of chlorophenols being generated during application of the H₂O₂/UV, Fenton and photo-Fenton processes.

Compound	Initial Experimental Conditions	Transformation Product	Reference
	<i>H₂O₂/UV</i>		
4-Chlorophenol	4-Chlorophenol = 130 mg L ⁻¹ (1 mM) H ₂ O ₂ = 30 mM pH = 7 Irradiation source = UV-C lamp	Hydroquinone Benzoquinone 4-Chlorocatechol Phenol 4-Chlorocatechol Hydroquinone Benzoquinone	Peternel et al., 2012
4-Chlorophenol	4-Chlorophenol = 100 and 250 mg L ⁻¹ (0.78 and 1.95 mM) H ₂ O ₂ = 0.78-39 mM Irradiation source = KrCl excimer lamp	1,2,4-Trihydroxybenzene Resorcinol Chlorohydroquinone 4-Chlororesorcinol Phenol	Murcia et al., 2012
	4-Chlorophenol = 100 mg L ⁻¹ H ₂ O ₂ = 12-23 mM Irradiation source = KrCl excimer lamp	The above eight photoproducts + catechol	Gomez et al., 2012a
4-Chlorophenol	4-Chlorophenol = 64 and 128 mg L ⁻¹ (0.5 and 1.0 mM) H ₂ O ₂ = 50-150 mM pH = 5-9 Irradiation source = UV-C lamp	4-Chlorocatechol Hydroquinone Maleic acid Fumaric acid Malonic acid Oxalic acid Formic acid	Kralik et al., 2010
2,4-Dichlorophenol	2,4-Dichlorophenol = 30 mg L ⁻¹ H ₂ O ₂ = 0.18-1.1 mM pH = 3 Irradiation source = Low pressure Hg lamp (15 W)	4,6-Dichlorocatechol 2,5-Dichlorohydroquinone 4-Chloro-1-naphthalenole 1-Chloro-2,6-dimethoxynaphthalene	Kucharska and Naumczyk, 2009

Table 2.1. *Continued*

Compound	Initial Experimental Conditions	Transformation Product	Reference
<i>H₂O₂/UV</i>			
2-Chlorophenol	2-Chlorophenol = 1500 mg L ⁻¹ H ₂ O ₂ = 15-303 mM Irradiation source = UV-C lamp	Formic acid Acetic acid	Poulopoulos et al., 2008
2-Chlorophenol	2-Chlorophenol = 128 mg L ⁻¹ (1 mM) H ₂ O ₂ = 4.5-18 mM pH = 5.2-6.3 Irradiation source = UV-C lamp	Catechol Chlorohydroquinone 1,2,4-Trihydroxybenzene	Bertelli and Selli, 2006
<i>Fenton</i>			
4-Chlorophenol	4-Chlorophenol = 1000 mg L ⁻¹ H ₂ O ₂ = 21 mM Fe source = Al/Fe pillared montmorillonite (8.2% Fe ₂ O ₃ , 1 g L ⁻¹) pH = 3.5	2,4-Dichlorophenol 4-Chlorocatechol Hydroquinone Chlorohydroquinone Dichlorocatechol 5-Chloro-1,2,4-benzenetriol Chlorinated hydroxylated biphenyls Chlorinated hydroxylated diphenyl ethers Chlorinated hydroxylated dibenzo- <i>p</i> -dioxins	Catrinescu et al., 2011
Pentachlorophenol	Pentachlorophenol = 14 mg L ⁻¹ H ₂ O ₂ = 0.22 and 0.37 mM Fe ²⁺ = 0.20 mM Fe ²⁺ source = FeSO ₄ ·7H ₂ O pH = 3.5	Tetrachlorohydroquinone Dichloromaleic acid	Zimbron and Reardon, 2011

Table 2.1. *Continued*

Compound	Initial Experimental Conditions	Transformation Product	Reference
	<i>Fenton</i>		
2,4-Dichlorophenol	2,4-Dichlorophenol = 1000 mg L ⁻¹ H ₂ O ₂ ≅ 49 mM Fe ²⁺ ≅ 2.0 mM Fe ²⁺ source = FeSO ₄ pH = 3	Hydroxylated 2,4-dichlorophenol Chlorohydroquinone Maleic anhydride Chloroacetic acid 3-Chloropropynal 3-Chloro-2-propenal Chloromaleic anhydride Chlorinated hydroxylated biphenyls Chlorinated hydroxylated diphenyl ethers Hydroxylated diphenyl ethers 4,6-Dichlororesorcinol 2,5-Dichlorohydroquinone 5,6-Dichloro-3-hydroxyhydroquinone Phenol 2-Chlorophenol 4-Chlorocatechol 5-Chloro-1,2,4-benzenetriol	Cravotto et al., 2010
4-Chlorophenol	Fe source = Fe-exchanged montmorillonite pH = 3.5	Hydroquinone 1,2,4-Benzenetriol 3-Chloromuconic acid Benzoquinone	Arsene et al., 2010
Pentachlorophenol	Pentachlorophenol = 14 mg L ⁻¹ (55 μM) H ₂ O ₂ = 0.028-0.39 mM Fe ²⁺ = 0.20 mM Fe ²⁺ source = FeSO ₄ ·7H ₂ O pH = 3.5	Tetrachlorohydroquinone Dichloromaleic acid	Zimbron and Reardon, 2009

Table 2.1. *Continued*

Compound	Initial Experimental Conditions	Transformation Product	Reference
	<i>Fenton</i>		
2-Chlorophenol	2-Chlorophenol = 500 mg L ⁻¹ (3.9 mM) H ₂ O ₂ = 4.0-88 mM Fe ²⁺ = 1.1 mM Fe ²⁺ source = FeSO ₄ ·7H ₂ O pH = 3.0	Chlorinated benzenetriol 3-Chlorocatechol Chlorohydroquinone 2-Chlororesorcinol Oxalic acid Acetic acid Muconic acid Chlorinated hydroxylated biphenyls Chlorinated hydroxylated diphenyl ethers Chlorinated hydroxylated dibenzofurans Hydroxylated biphenyls Hydroxylated dibenzofurans Phenol	Poerschmann et al., 2009
4-Chloroguaiacol	4-Chloroguaiacol = 1590 mg L ⁻¹ (10 mM) H ₂ O ₂ = 16 mM Fe ²⁺ = 16 mM Fe ²⁺ source = FeSO ₄ ·7H ₂ O pH = 3 (same conditions under solar irradiation)	5-Chloro-3-methoxycatechol Methoxyhydroquinone 4-Chlorocatechol	Samet et al., 2009
4-Chlorophenol	4-Chlorophenol = 128 mg L ⁻¹ (1.0 mM) H ₂ O ₂ = 2.5 mM Fe ²⁺ = 0.12 mM Fe ²⁺ source = FeSO ₄ ·7H ₂ O pH = 3.0	4-Chlorocatechol Hydroquinone Catechol Oxalic acid Acetic acid Maleic acid Fumaric acid Benzoquinone	Du et al., 2007

Table 2.1. *Continued*

Compound	Initial Experimental Conditions	Transformation Product	Reference
<i>Fenton</i>			
4-Chlorophenol	4-Chlorophenol = 128 mg L ⁻¹ (1.0 mM) H ₂ O ₂ = 2.5 mM Fe ³⁺ = 0.12 mM Fe ³⁺ source = Fe ₂ (SO ₄) ₃ pH = 3.0	4-Chlorocatechol Hydroquinone Catechol	Du et al., 2006
2,4-Dichlorophenol	2,4-Dichlorophenol = 375 mg L ⁻¹ (2.3 mM) Fe ²⁺ = 0.1 mM Fe ²⁺ source = FeSO ₄ ·7H ₂ O	Chloroacetic acid Formic acid Oxalic acid Acetic acid Glycolic acid Malonic acid Tartaric acid Fumaric acid Dichloroacetic acid Tentatively identified 13 other organic acids	Mascolo et al., 2005
2,4-Dichlorophenol	2,4-Dichlorophenol = 375 mg L ⁻¹ (2.3 mM) H ₂ O ₂ = 138 mM (gradual addition) Fe ²⁺ = 0.1 mM Fe ²⁺ source = FeSO ₄ ·7H ₂ O pH = 3	Hydroxylated 2,4-dichlorophenol Chloroacetic acid Formic acid Oxalic acid Acetic acid Glycolic acid Malonic acid Tartaric acid Chlorinated hydroxylated diphenyl ethers	Detomaso et al., 2003
4-Chlorophenol	4-Chlorophenol = 256 mg L ⁻¹ (2 mM) H ₂ O ₂ = 6 mM Fe ²⁺ = 0.3 mM Fe ²⁺ source = FeSO ₄ pH = 3.0	Hydroquinone Benzoquinone	Kang et al., 2002

Table 2.1. *Continued*

Compound	Initial Experimental Conditions	Transformation Product	Reference
<i>Photo-Fenton</i>			
4-Chlorophenol	4-Chlorophenol = 50-150 mg L ⁻¹ H ₂ O ₂ = 20 mM Fe ²⁺ = 0.018-0.12 mM Fe ²⁺ source = FeSO ₄ Irradiation source = KrCl lamp	1,2,4-Trihydroxybenzene Hydroquinone Resorcinol Chlorohydroquinone Benzoquinone Catechol 4-Chlororesorcinol Phenol 4-Chlorocatechol	Gomez et al., 2012a
2-Chlorophenol	2-Chlorophenol = 50 mg L ⁻¹ (0.39 mM) H ₂ O ₂ ≅ 5.1 mM (20 mM for goethite) Iron source = Zero valent iron nanoparticles (6-45 mg L ⁻¹ total Fe) and goethite (500 mg L ⁻¹ Fe) pH = 3 and 6.3 Irradiation wavelength = 340-410 nm range	Chlorobenzoquinone Chlorohydroquinone	Ortiz de la Plata et al., 2012
2-Chlorophenol	2-Chlorophenol = 1500 mg L ⁻¹ H ₂ O ₂ = 152 mM Fe ³⁺ = 0.11-2.0 mM Fe ³⁺ source = FeCl ₃ ·6H ₂ O Irradiation source = UV-C lamp	Formic acid Acetic acid	Poulopoulos et al., 2008
2,4-Dichlorophenol	2,4-Dichlorophenol = 163 mg L ⁻¹ (1.0 mM) H ₂ O ₂ = 1.2 mM Fe ³⁺ = 0.4 mM Fe ³⁺ source = Fe ₂ (SO ₄) ₃ ·H ₂ O pH = 3.0 Irradiation source = UV-C lamp	Chlorohydroquinone 4-Chlorocatechol Chlorobenzoquinone 3,5-Dichloro-2-hydroxy- <i>p</i> -benzoquinone 3,5-Dichlorocatechol 2,4-Dichlororesorcinol 4,6-Dichlororesorcinol	Chu et al., 2005

capable of substituting groups other than —Cl including —OCH₃ group during Fenton and photo-Fenton treatment of chlorophenols (Samet et al., 2009). Previous studies have already revealed that in phenols, owing to the strong electron-donating resonance effect of the —OH group, the major points of attack for HO• are at the *ortho* and *para* positions (Moza et al., 1988), as could also be drawn from Table 2.1. Table 2.1 also indicates that in addition to the pathways where HO• take part, dechlorination could also proceed via a reductive pathway during application of the H₂O₂/UV, Fenton and photo-Fenton processes, as could be drawn from the generation of phenol being originated from the transformation of 4-chlorophenol and 2,4-dichlorophenol (Cravotto et al., 2010; Gomez et al., 2012a). A number of studies have also indicated that the position of —Cl group on the aromatic ring changed or an additional —Cl group was introduced into the structure during the course of the H₂O₂/UV, Fenton and photo-Fenton processes, suggesting the participation of the generated chlorine radicals (Cl•) in the free radical-mediated pathway (Catrinescu et al., 2011; Gomez et al., 2012a). However, at this point, it should be underlined that the experimental findings being reported by the studies given in Table 2.1 largely relied on mass spectral library matching and/or comparison of the chromatographic peaks with authentic standards, and hence, more reliable assessments or techniques are needed to differentiate isomeric species.

Benzoquinone and to a lesser extent chlorinated and hydroxylated benzoquinones have been reported in the H₂O₂/UV, Fenton and photo-Fenton treated samples together with their hydroquinone counterparts (Table 2.1), since benzoquinone and hydroquinone are known as an active redox couple in equilibrium in an aqueous solution (Li et al., 2005). However, when the medium is strongly oxidizing, hydroquinone could be quickly oxidized to benzoquinone (Pimentel et al., 2008). The formation of hydroquinone- and quinone-like intermediates during Fenton and photo-Fenton treatment of chlorophenols has important implications for the reaction kinetics and efficiencies. The formation of the hydroquinone-like intermediates promotes the generation of Fe²⁺, thus the degradation of chlorophenols changing the Fenton-like reaction into the Fenton reaction (Du et al., 2006). Quinone intermediates shuttle electrons from the HO• adduct of the starting aromatic compound to Fe³⁺, and in light, they serve as photosensitizers via their conversion to semiquinone, which reduces Fe³⁺, and HO• (Chen and Pignatello, 1997). All these reactions can facilitate

the decomposition of starting chlorophenolic pollutant via the Fenton and photo-Fenton processes.

The non-photochemical Fenton process has been often reported to differ from the photochemical H₂O₂/UV-C and photo-Fenton processes in that condensation products arising from the coupling reactions of resonance-stabilized chlorophenol radicals could be formed in the Fenton system (Detomaso et al., 2003; Poerschmann et al., 2009; Cravotto et al., 2010; Catrinescu et al., 2011). These condensation products include chlorinated hydroxylated biphenyls, hydroxylated biphenyls, chlorinated hydroxylated diphenyl ethers, hydroxylated diphenyl ethers, chlorinated hydroxylated dibenzo-*p*-dioxins, chlorinated hydroxylated dibenzofurans and hydroxylated dibenzofurans. The extent of the formation of such products has been demonstrated to strongly depend on the applied H₂O₂:pollutant molar ratio. For instance, Poerschmann and co-workers have reported that use of the H₂O₂:chlorophenol substoichiometric molar ratios 4 and 16 did not result in the formation of condensation products, whereas when using the H₂O₂:chlorophenol substoichiometric molar ratios of ≤ 2.2 , condensation products were generated (Poerschmann et al., 2009). In addition to the dimeric condensation products, the generation of trimers, tetramers, pentamers, etc. has been suggested being originated from the addition of organoradicals onto neutral analyte molecules with biphenyl-, diphenyl ether or dibenzofuran backbone. Formation of such polymeric species has also been reported during transformation of phenol via the Fenton process and was evidenced by the visual observation of a dark brown precipitate followed by the elemental analysis of air-dried residue (Zazo et al., 2007; Poerschmann and Trommler, 2009). This type of condensation products have been less frequently detected during H₂O₂/UV and photo-Fenton treatment of chlorophenols (Hirvonen et al., 2000; Fukushima and Tatsumi, 2001), suggesting a mechanistic difference between dark and photo-assisted H₂O₂-driven AOP. For the identification of soluble condensation products arising from the AOP treatment of chlorophenols, more direct and sensitive methods including LC-MS-MS are recommended rather than gas chromatography-mass spectrometry (GC-MS) combined with derivatization techniques.

Up to now, hydroxylated and chlorinated polycyclic aromatic hydrocarbon (PAH)-type transformation products have been largely overlooked most probably due to the lack of an appropriate analytical protocol, although generation of such products during

H₂O₂/UV treatment of 2,4-dichlorophenol (Kucharska and Naumczyk, 2009) and Fenton treatment of phenol (Poerschmann and Trommler, 2009) have been already reported. Polychlorinated naphthalenes have also been identified along with dibenzo-*p*-dioxin and dibenzofuran products in the slow combustion of dichlorophenols at 600 °C, and a mechanism involving an intermediate formed by *ortho-ortho* carbon coupling of phenoxy radicals has been proposed for their generation (Kim et al., 2007).

Aliphatic carboxylic acids being originated from the cleavage of aromatic ring have generally been reported as the final organic degradation products prior to mineralization of chlorophenols during the application of AOP (Abe and Tanaka, 1997; Androulaki et al., 2000). Accordingly, these transformation products have also been detected during application of the H₂O₂/UV, Fenton and photo-Fenton processes for aqueous chlorophenol removal (Table 2.1). The most common carboxylic acids generated in the H₂O₂/UV, Fenton and photo-Fenton transformation of chlorophenols have been identified as the simplest structured non-chlorinated carboxylic acids acetic, oxalic and formic acids (Poulopoulos et al., 2008; Kralik et al., 2010). On the other hand, chlorinated aliphatic carboxylic acids including dichloromaleic acid, chloroacetic acid, 3-chloromuconic acid and dichloroacetic acid have also been identified during Fenton treatment of chlorophenols (Detomaso et al., 2003; Zimbron and Reardon, 2009; Arsene et al., 2010; Cravotto et al., 2010; Zimbron and Reardon, 2011). In addition to largely reported carboxylic acids being detected by comparison with authentic standards, Mascolo and co-workers have tentatively identified 13 other organic acids being generated during Fenton treatment of 2,4-dichlorophenol by using the capabilities of ion chromatography-electrospray mass spectrometry (IC-ESI-MS) technique (Mascolo et al., 2005).

Other potential ring cleavage products including acid anhydrides, aldehydes and ketones as well as non-oxygenated aliphatic saturated and unsaturated hydrocarbons have been nearly completely overlooked up to now in studies regarding AOP treatment of chlorophenols. For instance, Cravotto and co-workers have identified maleic anhydride, chloromaleic anhydride, 3-chloropropynal and 3-chloro-2-propenal upon Fenton transformation of 2,4-dichlorophenol by using GC-MS without derivatization (Cravotto et al., 2010). In a former study, formaldehyde and small quantity of acetone have been reported to be generated during O₃/UV treatment of 2,4,6-trichlorophenol (Abe and

Tanaka, 1997). The formation of such products could also be anticipated during photochemical treatment of chlorophenols via other AOP including H₂O₂/UV and photo-Fenton processes.

2.3.2. Toxicity

Table 2.2 presents studies concerning the ecotoxicological characterization of the H₂O₂/UV, Fenton and photo-Fenton processes for the removal of aqueous chlorophenols reported during the period 2004 – 2012. In published studies, toxicity was generally taken as the overall toxicity of the solution (i.e. mixture of transformation products and possibly parent chlorophenols) towards the bacterial species, the marine photobacterium *Vibrio fischeri* (formerly known as *Photobacterium phosphoreum*) being by far the most preferred one (Table 2.2). The bioassay is based on the measurement of the bioluminescence of bacteria which decreases as a consequence of the inhibition of bacterial luciferase when exposed to toxic substances (Radjenović et al., 2009). It measures the non-specific toxicity and has been widely used for acute toxicity estimation due to the rapid response of *V. fischeri* to toxicants which requires only 5 to 30 min for toxicity prediction (Parvez et al., 2006).

Liou and co-workers have measured the inhibitory effect (expressed as EC_{50} which refers to the concentration causing 50% reduction in bioluminescence intensity) of aqueous solutions of pentachlorophenol towards *V. fischeri* during modified Fenton treatment by Fe³⁺-resin catalyst (Liou et al., 2004). The study results indicated that when pentachlorophenol being originally toxic ($EC_{50} = 14\text{-}15\%$, w/v) was oxidized by Fe³⁺-resin/H₂O₂ after 2 h, their 5 min- and 15 min- EC_{50} values were greater than 100%, indicating that the intermediates produced from Fe³⁺-resin/H₂O₂ system were not toxic. Lapertot and co-workers also employed *V. fischeri* to evaluate whether the evolution of biocompatibility of the water solution contaminated with six separate pesticides including pentachlorophenol during application of the solar photo-Fenton treatment can be predicted from the acute inhibitory effect (Lapertot et al., 2008). In this study, overall toxicity (expressed as toxicity units, TU = 100/ EC_{50}) of the pentachlorophenol ($EC_{50} = 1 (\pm 0.1)$ mg L⁻¹)-contaminated water increased at the first steps of oxidation process, but decreased regularly thereafter in parallel to mineralization. At the point where pentachlorophenol was

Table 2.2. Recent studies on toxicity changes during H₂O₂/UV, Fenton and photo-Fenton treatment of chlorophenols.

Compound	Initial Experimental Conditions	Evaluation of Toxic Effect	Reference
<i>H₂O₂/UV-C</i>			
4-Chlorophenol	4-Chlorophenol = 100 and 250 mg L ⁻¹ (0.78 and 1.95 mM) H ₂ O ₂ = 20 and 49 mM Irradiation source = KrCl UV-C lamp	<i>Vibrio fischeri</i> <i>Pseudomonas putida</i>	Murcia et al., 2009
Mixtures of 4-chlorophenol, 2,4-dichlorophenol, 2,4,6- trichlorophenol and pentachlorophenol	Individual chlorophenols = 50 and 100 mg L ⁻¹ H ₂ O ₂ = 50 mM pH ≅ 7 Irradiation source = UV blue-lamps (~ 30% UV-A – 5% UV-B)	<i>Lipedium sativum</i>	Essam et al., 2007
<i>Fenton</i>			
Triclosan	Triclosan = 10 mg L ⁻¹ H ₂ O ₂ = 0.15-0.74 mM Fe ³⁺ = 18 μM Fe ³⁺ source = Fe(NO ₃) ₃ ·9H ₂ O pH = 3.0	<i>Vibrio fischeri</i>	Munoz et al., 2012a
4-Chlorophenol	4-Chlorophenol = 500 mg L ⁻¹ H ₂ O ₂ = 11-47 mM Fe ²⁺ = 13 μM Fe ²⁺ source = (NH ₄) ₂ Fe(SO ₄) ₂ ·6H ₂ O pH = 3.5	<i>Vibrio fischeri</i>	Arsene et al., 2011
4-Chlorophenol	4-Chlorophenol = 100 and 250 mg L ⁻¹ H ₂ O ₂ = 20 and 49 mM Fe ²⁺ = 6.6-130 μM Fe ²⁺ source = FeSO ₄	<i>Vibrio fischeri</i> <i>Pseudomonas putida</i>	Murcia et al., 2009
Triclosan	Triclosan = 500 mg L ⁻¹ H ₂ O ₂ = 20 mM Fe ²⁺ = 5 mM Fe ²⁺ source = FeSO ₄ ·7H ₂ O pH = 3 Irradiation source = UV-A lamp (for the photo-Fenton runs)	<i>Daphnia magna</i>	Arslan-Alaton, 2007

Table 2.2. *Continued*

Compound	Initial Experimental Conditions	Evaluation of Toxic Effect	Reference
<i>Fenton</i>			
Pentachlorophenol	Pentachlorophenol = 100 mg L ⁻¹ H ₂ O ₂ = 100 mM Fe ³⁺ source = Fe ³⁺ -resin (Fe ³⁺ content = 10 mmol g ⁻¹ , 0.5% Fe ³⁺ -resin w/v)	<i>Vibrio fischeri</i>	Liou et al., 2004
<i>Photo-Fenton</i>			
4-Chlorophenol	4-Chlorophenol = 130 mg L ⁻¹ (1 mM) H ₂ O ₂ = 100 mM Fe ²⁺ = 1.0 mM Fe ²⁺ source = FeSO ₄ ·7H ₂ O pH = 3 Irradiation source = UV-C lamp	<i>Daphnia magna</i>	Peternel et al., 2012
Pentachlorophenol	Pentachlorophenol < 50 mg L ⁻¹ Fe ²⁺ = 36 μM Fe ²⁺ source = FeSO ₄ ·7H ₂ O pH ≅ 2.7-2.8 Irradiation source = Sunlight	<i>Vibrio fischeri</i>	Lapertot et al., 2008; Hincapié et al., 2005
2-Chlorophenol	2-Chlorophenol = 128 mg L ⁻¹ (1 mM) H ₂ O ₂ = 5.9 and 21 mM Fe ²⁺ = 0.36 and 1.2 mM Fe ²⁺ source = FeSO ₄ ·7H ₂ O pH ≅ 2.5 Irradiation source = Sunlight lamp	<i>Escherichia coli</i>	Pérez-Moya et al., 2007
2,4-Dichlorophenol	2,4-Dichlorophenol = 100 mg L ⁻¹ H ₂ O ₂ = 0.59-1.5 mM Fe ²⁺ source = FeSO ₄ ·7H ₂ O pH = 4.5 (± 0.5) Irradiation source = UV-A lamp	<i>Vibrio fischeri</i>	Al Momani, 2006

completely degraded, toxicity was close to the initial value, whereas the treated solution was positive in Zahn-Wellens test, suggesting that toxicity and biodegradability should be considered separately. However, the authors concluded that the Microtox® assay can help for selecting samples to be tested by the Zahn-Wellens biodegradability assessment method. Very similar results on the evolution of acute inhibitory effect towards *V. fischeri* during solar photo-Fenton treatment of pentachlorophenol and its relationship with mineralization could be drawn from another study of the same research group (Hincapié et al., 2005). This latter study additionally concluded that evolution of Cl^- could be a key parameter for predicting toxicity during degradation of chlorinated compounds. Toxicological consequences of the photo-Fenton treatment of aqueous 2,4-dichlorophenol as assessed by employing *V. fischeri* photobacteria have been considered in the study by Al Momani (2006). The results of this study indicated that the acute inhibitory effect (expressed as TU) regularly decreased during the course of the photo-Fenton treatment from an initial TU of 17 down to $\text{TU} \cong 5$ after 40 min treatment. Another finding being not mentioned by the author in the text was that the residual acute inhibitory effect remaining after treatment was inversely correlated with the applied initial H_2O_2 concentration in the range 20-50 mg L^{-1} (0.59-1.5 mM) H_2O_2 , thus signifying the role of optimizing treatment conditions in the detoxification efficiency. Munoz and co-workers examined the evolution of ecotoxicity towards *V. fischeri* upon Fenton-like oxidation of triclosan (2,4,4'-trichloro-2'-hydroxydiphenyl ether) at H_2O_2 doses ranging from 0.15 to 0.74 mM (Munoz et al., 2012a). Ecotoxicity being expressed as TU decreased to values $< 5\%$ of the initial ($\text{TU} = 40$) after 15 min reaction with the stoichiometric dose of H_2O_2 at 35 °C. The authors related the evolution of ecotoxicity intimately to the disappearance of the parent compound. Similar findings have been reported in the study by Arsene and co-workers where the toxicity of aqueous 4-chlorophenol being expressed as the percent luminescence inhibition and lower ineffective dilution (the dilution of the aqueous sample causing $< 20\%$ luminescence inhibition) decreased significantly by increasing the H_2O_2 dose, the same trend as for removal efficiency expressed by 4-chlorophenol, COD and TOC, during application of the Fenton process (Arsene et al., 2011).

Use of photoluminescent bacteria other than *V. fischeri* has also been attempted in the scientific literature for the purpose of examining the acute inhibitory effect before and after AOP treatment of chlorophenols. For instance, Murcia and co-workers determined EC_{50}

values of a 4-chlorophenol solution before and after 5 min H₂O₂/UV-C and Fenton processes by using the bacteria *Pseudomonas putida* being engineered to emit light and compared the results with those obtained by using *V. fischeri* (Murcia et al., 2009). *V. fischeri* was found to be more sensitive towards the untreated and treated samples as compared to *P. putida* presumably due to the acclimatized nature of the latter bacterial species being isolated from an activated sludge plant.

In addition to inhibition of the bioluminescence being emitted from the photobacteria, inhibition of the growth of gram-negative *Escherichia coli* bacteria was also employed to evaluate inhibitory effects being observed during simulated solar photo-Fenton treatment of 2-chlorophenol (Pérez-Moya et al., 2007). In this study, when the initial Fe²⁺ and H₂O₂ concentrations were decreased from 70 mg L⁻¹ (= 1.2 mM) and 700 mg L⁻¹ (= 21 mM) to 20 mg L⁻¹ (= 0.36 mM) and 200 mg L⁻¹ (= 5.9 mM), respectively, the velocity of exponential growth of *E. coli* being recorded after 30 min of photo-Fenton treatment significantly decreased from 0.032 h⁻¹ to 0.006 h⁻¹ after 24 h incubation, suggesting the governing role of the initial Fe²⁺ and H₂O₂ concentrations in the inhibitory effect pattern. From the optical density values at 600 nm representing the growth status of the bacteria, the authors concluded, however, that transformation products obtained in the partial degradation of the samples have revealed toxicity levels similar to 2-chlorophenol. The authors also concluded that even 93% TOC removal rates were insufficient for ensuring an acceptable shortage of toxicity of the system. This latter statement has practical importance and indicates that the ecotoxicological safety of an advanced oxidatively treated water could not solely be evaluated using TOC parameter.

Besides the bacterial toxicity bioassays, a short term assay using the invertebrate *Daphnia magna* has also been applied for determination of acute toxicity. The bioassay using *D. magna* is based on the principle that certain acute inhibitory conditions result in certain percentages of *D. magna* being no longer capable of swimming after 24 or 48 h incubation, thus losing its mobility. Arslan-Alaton compared acute inhibitory effect patterns towards *D. magna* during Fenton and photo-Fenton treatment of a commercial biocide solution whose active ingredient was 90%, w/w triclosan (Arslan-Alaton, 2007). The author reported that complete detoxification was achieved after 30 min photo-Fenton treatment, whereas the detoxification was not complete via the Fenton's reagent under

otherwise identical conditions, the LC_{50} (percent test toxicant dilution causing 50% death or immobilization of *D. magna*) value increasing from 8% to 55%, v/v after 30 min Fenton treatment. An important conclusion being drawn from this study was that the evolution of UV absorbance of the treated solution at 280 nm was closely linked with the disappearance of toxicity, suggesting a positive relationship between dearomatization and detoxification efficiencies. In another study, Peternel and co-workers evaluated the efficiency of photo-Fenton treatment of 4-chlorophenol in terms of acute inhibitory effect towards *D. magna* being expressed as the EC_{50} (Peternel et al., 2012). The authors reported that 92% TOC removal was accompanied by 75% reduction in EC_{50} after 60 min photo-Fenton treatment, delineating the capability of this treatment process in detoxifying aqueous chlorophenols.

Toxicity profiles of aqueous chlorophenols towards organisms being higher than invertebrates during photochemical treatment have also been reported in the scientific literature. Phytotoxic (= being toxic for plant growth) impact of the H_2O_2/UV treated chlorophenolic solutions towards the *Lepidium sativum* (garden cress) has been reported in Essam et al. (2007). In this study, mixtures of 4-chlorophenol, 2,4-dichlorophenol, 2,4,6-trichlorophenol and pentachlorophenol have been photochemically treated, and the photochemical treatments have been conducted in mineral salt medium to simulate the potential matrix effects from compounds present in wastewater. The phytotoxicity (expressed as the ratio (%) of the average stem length of the test seeds by the average stem length of the control seeds) of the 10-fold diluted mixtures being originally 41% and 94% for the mixtures containing each individual chlorophenol compound at 50 and 100 mg L⁻¹, respectively, was completely eliminated after the H_2O_2/UV treatment. On the other hand, when phytotoxicity assays were conducted on undiluted reaction samples, the phytotoxic effect decreased only by 23% and 7% for the mixtures initially containing 50 mg L⁻¹ and 100 mg L⁻¹ of the individual chlorophenols, respectively, referring to the limited capability of the H_2O_2/UV treatment alone in reducing the phytotoxic effect under the studied experimental conditions.

From the studies presented above it is clear that the number of studies dealing with the ecotoxicological impact of the H_2O_2/UV , Fenton and photo-Fenton processes for the treatment of aqueous chlorophenols is still limited. However, there are no data available on chronic, sublethal effects of the H_2O_2/UV , Fenton and photo-Fenton treated chlorophenolic

waters, although it is generally unlikely that non-target organisms would be exposed to concentrations causing acute toxicity in environmental aqueous matrices. In addition, more specific toxicity types including genotoxicity and estrogenicity should be taken into account in such studies in order to be able to make a more comprehensive risk evaluation of the H₂O₂/UV, Fenton and photo-Fenton treated chlorophenolic waters. Since the organic and inorganic constituents being present in natural waters might affect the kinetics of parent compounds and transformation products as well as the identity of transformation products (Postigo et al., 2011a; Michael et al., 2012), it is not unlikely that different ecotoxicological consequences may arise from the oxidative treatment of natural waters being contaminated with chlorophenols and should be further investigated.

2.3.3. Toxicity in Relation with Transformation Products

The relatively high inhibitory effects being observed after AOP treatment of chlorophenols and fluctuations in inhibitory effect including the most frequently reported “initial toxicity increases” during application of AOP encouraged some researchers to investigate the possible relationships between the identified (and also unidentified) transformation products and the observed toxicity evolution. The most relevant investigations on this issue published during the last three years which cover the H₂O₂/UV, Fenton and photo-Fenton treatment of aqueous chlorophenols are listed in Table 2.3.

As a first remark, *V. fischeri* photobacteria were the toxicity test species of choice in a majority of cases most possibly due to its high sensitivity towards a wide range of pollutants (Rizzo, 2011). Different approaches were adopted by the studies being listed in Table 2.3 to evaluate the possible relationships between the transformation products and toxicity. The most comprehensive assessment was made in the study by Krebel and co-workers where three principal routes were followed: (1) testing the toxicity of the mixture of transformation products and differentiation of identified transformation products at the point where the toxicity of the mixture is most significantly increased compared to the parent compound and at the end of treatment, (2) simulating the reaction samples by preparing synthetic samples containing the same concentrations of the identified transformation products as the reaction samples and comparing their toxicity, and (3) performing a statistical bivariate correlation analysis for the individually identified

Table 2.3. Relationships between transformation products and toxicity being drawn from the recent studies regarding the H₂O₂/UV, Fenton and photo-Fenton treatment of chlorophenols.

Compound	Treatment Process	Bioassay Organism	Suspected Relationship with By-products	Reference
2,4-Dichlorophenol 2,6-Dichlorophenol 3,5-Dichlorophenol 2,4,5-Trichlorophenol 2,4,6-Trichlorophenol	Fenton	<i>Vibrio fischeri</i>	The chlorine-containing aromatic byproducts, including chlorobenzenediols and condensation compounds	Munoz et al., 2012b
2,4-Dichlorophenol	H ₂ O ₂ /UV-C Fenton Photo-Fenton	<i>Vibrio fischeri</i>	Non-chlorinated ring opening products including carboxylic acids (for the Fenton process) Dechlorination (for the H ₂ O ₂ /UV-C and photo-Fenton processes)	Karci et al., 2012
4-Chlorophenol	H ₂ O ₂ /UV-C Fenton Photo-Fenton	<i>Pseudomonas putida</i>	1,2,4-Trihydroxybenzene and hydroquinone (for the Fenton and photo-Fenton processes)	Gómez et al., 2012b
2-Chlorophenol 3-Chlorophenol 4-Chlorophenol	Fenton	<i>Vibrio fischeri</i>	The chlorinated condensation by-products	Munoz et al., 2011
4-Chlorophenol	H ₂ O ₂ /UV-C	<i>Vibrio fischeri</i>	<i>Initial toxicity increase:</i> Hydroquinone and unidentified aromatics (presumably three or more substituted hydroxy- and phenoxy-derivates of phenols) <i>Final toxicity:</i> Identified non-chlorinated carboxylic acids (most possibly maleic acid) and unidentified chlorinated aliphatic by-products	Krebel et al., 2011
4-Chlorophenol	H ₂ O ₂ /UV-C	<i>Pseudomonas putida</i>	Hydroquinone, benzoquinone, resorcinol, chlorohydroquinone, 4-chlororesorcinol, phenol and 1,2,4-trihydroxybenzene depending on the initial pollutant concentration and the studied H ₂ O ₂ :pollutant molar ratio	Gomez et al., 2010

transformation products and toxicity (Krebel et al., 2011). By means of a combination of these approaches, the authors concluded that the increase in acute inhibitory effect being observed at the initial stages of the H₂O₂/UV-C treatment of 4-chlorophenol was largely contributed by hydroquinone being identified by high performance liquid chromatography (HPLC) and unidentified aromatics (presumably three or more substituted hydroxy- and phenoxy-derivates of phenols). On the other hand, the final acute inhibitory effect being still higher than the initial toxicity related to the parent 4-chlorophenol pollutant was attributed to the identified non-chlorinated carboxylic acids (most possibly maleic acid) and unidentified chlorinated aliphatic by-products.

Gómez and co-workers intended to estimate the final toxicity of the AOP treated aqueous 4-chlorophenol towards the photoluminescent bacteria *P. putida* by determining the non-effect concentrations (concentrations causing 0.1% photoluminescence inhibition) for all the transformation products being monitored during the treatment processes using the pure compounds and by comparing the values with the product concentrations remaining after treatment (Gómez et al., 2010, 2012b). The identified aromatic transformation products including hydroquinone, benzoquinone, resorcinol, chlorohydroquinone, 4-chlororesorcinol, phenol and 1,2,4-trihydroxybenzene were suspected for causing the acute inhibitory effect after treatment depending on their measured concentrations in the treated samples. However, it should be stated here that this approach has the drawback of overlooking potential synergistic and antagonistic effects of the transformation products when present in mixtures.

Certain analytical parameters have been used as an indirect measure of the unidentified transformation products and their relationship with the observed inhibitory effect. For instance, Karci and co-workers indicated that the difference in the rates of dechlorination being observed between the H₂O₂/UV-C, Fenton and photo-Fenton processes was the indicator of the difference in the transformation rate of chlorinated oxidation intermediates remained largely unidentified, and in turn, the acute inhibitory effect towards *V. fischeri* during the studied AOP (Karci et al., 2012).

Munoz and co-workers in their studies very tentatively attributed the high residual acute inhibitory effect being observed after Fenton-like oxidation of a series of mono-, di-

and trichlorophenols at substoichiometric concentrations of H₂O₂ mainly to the chlorinated condensation products, since this type of transformation products was predominant under substoichiometric H₂O₂ doses and the remaining organic acids were assumed to represent no relevant acute inhibitory effect towards *V. fischeri* (Munoz et al., 2011, 2012b). The evolution of short- and long-term toxicity levels in relation with the condensation products should be more extensively studied, however, to decide whether Fenton-based treatment of aqueous chlorophenols under economically feasible conditions could be ecotoxicologically safe.

Overall, concerning the ecotoxicological effects of transformation products, as already known for the parent chlorophenols, there is still a lot to be done. As Escher and Fenner have recently underlined, the bioluminescent bacterium *V. fischeri* being used in the majority of studies (Table 2.3) does not reflect the specific mode of toxic action of the transformation products and at least should be supported with another bioassay (Escher and Fenner, 2011).

2.4. Photolysis and AOP Treatment of Alkylphenol Polyethoxylates

Unlike the case for chlorophenols, transformation of alkylphenol polyethoxylates via advanced chemical treatment processes, including AOP, has been scarcely investigated in the scientific literature. Most of the studies concerning the chemical oxidation of alkylphenol polyethoxylates have focused on ozonation being overviewed in several relevant review papers (Delanghe et al., 1991; Ikehata and El-Din, 2004; Ning et al., 2007). Nevertheless, the reaction pathways and generation of transformation products arising from photolysis and AOP treatment of alkylphenol polyethoxylates have been poorly understood up to date. More importantly, significant data gap still exists regarding the impact of such treatment processes on overall solution toxicity despite the established knowledge that the biotransformation products of alkylphenol polyethoxylates may be more inhibitory than the parent molecules. The present section aimed at distilling existing literature on transformation products and inhibitory effects arising from photolysis and AOP treatment of alkylphenol polyethoxylates into a general framework that will hopefully stimulate future, more systematic studies.

2.4.1. Transformation Products

It is essential, first, to gain an understanding of composition of commercial alkylphenol polyethoxylate mixtures in order to be able to account for the limited effort in the scientific literature regarding the identification of transformation products of alkylphenol polyethoxylates. Commercial alkylphenol polyethoxylate nonionic surfactants comprise a mixture of various polyethoxylate chain lengths and free polyethylene glycols (PEG) as well as unreacted ethylene oxide and alkylphenols (Brand et al., 1998). As a consequence, the formation of transformation products of a wide array of chemical structures is the anticipated outcome when alkylphenol polyethoxylates are degraded in the environment or via different treatment processes, which necessitates reliable protocols for their identification. The low volatility of alkylphenol polyethoxylates as well as most of their transformation products hinders the application of GC-MS for their analysis unless a derivatization step is applied, which could however result in loss of sample during the additional manipulation (González et al., 2007b). This drawback of GC-MS methodologies for the analysis of alkylphenol polyethoxylates and their transformation products can be solved by liquid chromatography-mass spectrometry (LC-MS), particularly liquid chromatography-tandem mass spectrometry, LC-MS-MS (Vega-Morales et al., 2010).

Considering the above-mentioned facts, the existing scientific literature on photolysis and AOP treatment of aqueous alkylphenol polyethoxylates largely reported the application of LC-MS(-MS) methodologies for the purpose of identification of their transformation products, as listed in Table 2.4. Electrospray ionization (ESI) under positive ionization has in general been the ionization system of choice for the identification of alkylphenol polyethoxylates as well as their transformation products as their Na^+ , NH_4^+ and H^+ adducts depending on ions from the buffer, the sample and/or the introduction system, whereas the use of atmospheric pressure chemical ionization has also been reported (Castillo et al., 2001).

A polyethoxylated alkylphenol possesses three principal units being susceptible to HO^\bullet attack as well as UV irradiation, namely, the polyethoxylate chain, the aromatic ring and the alkyl chain. Transformation of alkylphenol polyethoxylates via AOP has in general been suggested to proceed preferentially via fragmentation of the polyethoxylate chain

Table 2.4. Reported transformation products of alkylphenol polyethoxylates being generated during photolysis and AOP as well as their molecular ions/fragments.

Compound	Molecular weight (g mol ⁻¹)	Ionization mode	Reference
OP6-OP14	470-822	[M+H ₂ O] (m/z = 488-840) (Δ m/z 44)	Liu et al., 2010
Dealkylation and subsequent hydroxylation	327-635	[M+H] ⁺ (m/z = 328-636) (Δ m/z 44)	
	302-522	[M+H] ⁺ (m/z = 303-523) (Δ m/z 44)	
Hydroxylation	222-530	[M+H ₂ O] (m/z = 240-548) (Δ m/z 44)	
Dealkylation	418-682	[M+H] ⁺ (m/z = 419-683) (Δ m/z 44)	
Formyl ethoxylates	410-762	[M+H] ⁺ (m/z = 411-763) (Δ m/z 44)	
PEG4-PEG11	194-502	[M+Na] ⁺ (m/z = 217-525) (Δ m/z 44)	Kong and Lemley, 2007
OP2-OP7	294-514	[M+Na] ⁺ (m/z = 317-537) (Δ m/z 44)	
Dicarboxylated PEG5- PEG10	354-574	[M+Na] ⁺ (m/z = 377-597) (Δ m/z 44)	
Monocarboxylated PEG8-PEG11	428-560	[M+Na] ⁺ (m/z = 451-583) (Δ m/z 44)	
OP4-OP7	382-514	[M+H] ⁺ (m/z = 383-515) (Δ m/z 44)	
Aldehydic compounds	424	[M+Na] ⁺ (m/z = 447)	Chen et al., 2007a
	468	[M+Na] ⁺ (m/z = 491)	
	512	[M+Na] ⁺ (m/z = 535)	
	266	[M+Na] ⁺ (m/z = 289)	
	310	[M+Na] ⁺ (m/z = 333)	
	354	[M+Na] ⁺ (m/z = 377)	
Carboxylic compounds	238	[M+Na] ⁺ (m/z = 261)	
	282	[M+Na] ⁺ (m/z = 305)	
	326	[M+Na] ⁺ (m/z = 349)	
	370	[M+Na] ⁺ (m/z = 393)	
Cyclohexanyl compounds	216	[M+Na] ⁺ (m/z = 239)	
	244	[M+Na] ⁺ (m/z = 267)	
	349	[M+Na] ⁺ (m/z = 372)	
	363	[M+Na] ⁺ (m/z = 386)	
	450	[M+Na] ⁺ (m/z = 473)	
	464	[M+Na] ⁺ (m/z = 487)	

Table 2.4. *Continued*

Compound	Molecular weight (g mol ⁻¹)	Ionization mode	Reference
NP-5, NP-6, ..., NP-16	440, 484, ..., 924	[M+Na] ⁺ (<i>m/z</i> = 463, 507, ..., 947) (Δ <i>m/z</i> 44)	Chen et al., 2007a
Cyclohexanylic aldehydes	288-420 418	[M+H] ⁺ (<i>m/z</i> = 289-421) (Δ <i>m/z</i> 44) [M+H] ⁺ (<i>m/z</i> = 419)	Chen et al., 2007b
Aromatic aldehydes	473 487 385	[M+H] ⁺ (<i>m/z</i> = 474) [M+H] ⁺ (<i>m/z</i> = 488) [M+H] ⁺ (<i>m/z</i> = 386)	
Nonylphenol polyethoxycarboxylates	238-458	[M+NH ₄] ⁺ (<i>m/z</i> = 256-476) (Δ <i>m/z</i> 44)	
NP1-NP15	264-880	[M+Na] ⁺ (<i>m/z</i> = 287-903) (Δ <i>m/z</i> 44)	Petrovic et al., 2007
OP1-OP15	250-910	[M+Na] ⁺ (<i>m/z</i> = 273-933) (Δ <i>m/z</i> 44)	
PEG3-PEG10	150-458	[M+Na] ⁺ (<i>m/z</i> = 173-481) (Δ <i>m/z</i> 44)	
Monocarboxylated PEG2-PEG5	164-296	[M+Na] ⁺ (<i>m/z</i> = 187-319) (Δ <i>m/z</i> 44)	
NP1 – NP15	264-880	[M+Na] ⁺ (<i>m/z</i> = 287-903) (Δ <i>m/z</i> 44)	Petrovic et al., 2004
PEG2 – PEG8	106-370	[M+Na] ⁺ (<i>m/z</i> = 129-393) (Δ <i>m/z</i> 44)	
Tetraethylene glycol	194	[HO(C ₂ H ₄ O) ₂ CH ₂ CH ₂] ⁺ (<i>m/z</i> = 133) [M+H] ⁺ (<i>m/z</i> = 195)	Castillo et al., 2001
NP-2	308	[M+H] ⁺ (<i>m/z</i> = 309) [M+H-C ₉ H ₁₈] ⁺ (<i>m/z</i> = 187) [C ₉ H ₁₉] ⁺ (<i>m/z</i> = 127)	
Nonylphenol diethoxycarboxylate	322	[M+H] ⁺ (<i>m/z</i> = 323) [A ₁ PE ₂ C+H] ⁺ (<i>m/z</i> = 211) [A ₁ PE ₂ C+H-COOH] ⁺ (<i>m/z</i> = 165)	
Phenol diethoxycarboxylate	196	[M+H] ⁺ (<i>m/z</i> = 197)	

Table 2.4. *Continued*

Compound	Molecular weight (g mol ⁻¹)	Ionization mode	Reference
Methylphenol ethoxycarboxylate	210	[M+H] ⁺ (<i>m/z</i> = 211) [M+H-COOH] ⁺ (<i>m/z</i> = 166)	Castillo et al., 2001
Ethoxyphenyl heptanoic acid	280	[M+H] ⁺ (<i>m/z</i> = 281) [M-COOH] ⁺ (<i>m/z</i> = 236 and 235) (<i>m/z</i> = 209)	
NP-6	484	[M+H] ⁺ (<i>m/z</i> = 485)	
Phenol tetraethoxylate	270	[M+H] ⁺ (<i>m/z</i> = 271)	
NP-5	440	[M+H] ⁺ (<i>m/z</i> = 441)	
NP-9	616	[M+H] ⁺ (<i>m/z</i> = 617)	
OP-5, ..., OP-10	426, ..., 646	[M+H ₂ O] (<i>m/z</i> = 444, ..., 664) ($\Delta m/z$ 44) [M+H] ⁺ (<i>m/z</i> = 427, ..., 647) ($\Delta m/z$ 44) [M+Na] ⁺ (<i>m/z</i> = 449, ..., 669) ($\Delta m/z$ 44) [M+K] ⁺ (<i>m/z</i> = 465, ..., 685) ($\Delta m/z$ 44)	Destailats et al., 2000
Dealkylation products	372, ..., 593	[M _{PC} -54] (<i>m/z</i> = 372, ..., 593) ($\Delta m/z$ 44)	
	344, ..., 653	[M _{PC} -38] (<i>m/z</i> = 344, ..., 653) ($\Delta m/z$ 44)	
	242, ..., 507	[M _{PC} -96+H ₃ O] ⁺ (<i>m/z</i> = 261, ..., 526) ($\Delta m/z$ 44)	
	88	[M+H] ⁺ (<i>m/z</i> = 89)	
Deethoxylation products	238, ..., 370	[OH(CH ₂ CH ₂ O) _n H + H] ⁺ (<i>m/z</i> = 239, ..., 371) ($\Delta m/z$ 44)	
	89, ..., 177	[(CH ₂ CH ₂ O) _n H] (<i>m/z</i> = 89, ..., 177) ($\Delta m/z$ 44)	
Hydroxylation products	427, ..., 647	[M _{PC} +16+H ₂ O] (<i>m/z</i> = 461, ..., 681) ($\Delta m/z$ 44)	
Formate ethoxylates	366, ..., 631	[M _{PC} -(n-m)44-16+H ₂ O] (<i>m/z</i> = 384, ..., 649) ($\Delta m/z$ 44)	

length due to high specific rate constants of HO^\bullet toward ethylene oxide subunits (Pelizzetti et al., 1989) producing shorter chain alkylphenol ethoxylates. Nagarnaik and Boulanger recently reported in their study the formation of OP-2 (octylphenol diethoxylate) as well as NP-2 (nonylphenol diethoxylate) and NP-3 (nonylphenol triethoxylate) being not present in the initial spiked solution during $\text{H}_2\text{O}_2/\text{UV-C}$ treatment of Triton-X 100 (OP-10, octylphenol decaethoxylate) and Tergitol 15 (NP-15, nonylphenol pentadecaethoxylate), respectively (Nagarnaik and Boulanger, 2011). Although rarely reported during AOP treatment of alkylphenol polyethoxylates, complete fragmentation of the polyethoxylate chain may give rise to the generation of alkylphenols, as could be exemplified by the formation of octylphenol during Fe^{3+} -photoinduced degradation of Igepal CA 520, an octylphenol polyethoxylate with an average five ethoxy units (Brand et al., 1998). The fragmentation of polyethoxylate chain could also be indirectly realized from the generation of PEG during the course of the reaction (Castillo et al., 2001; Petrovic et al., 2004; Kong and Lemley, 2007; Petrovic et al., 2007). The attack of HO^\bullet on the polyethoxylate chain can alternatively result in the formation of formate ethoxylates and aldehyde ethoxylates (Brand et al., 1998; Destailats et al., 2000; Liu et al., 2010) depending on the site of radical attack. According to Brand and co-workers, the attack of HO^\bullet on the methylene group next to the $\text{CH}_2\text{—O—}$ group of an ethoxy unit leads to the formate ethoxylates, whereas the attack of HO^\bullet on the methylene group next to the terminal —OH group of an ethoxy unit gives rise to the aldehyde ethoxylates (Brand et al., 1998). The formed formate ethoxylates and aldehyde ethoxylates could be the precursors of carboxyalkylphenol polyethoxylates and alkylphenol polyethoxycarboxylates (APEC), respectively. APEC have been reported during UV-A-induced photodegradation of NP-10, the nonylphenol polyethoxylate with an average ethoxy units of 10 (Chen et al., 2007a, 2007b) and NP-9 (nonylphenol nonaethoxylate) as well as photo-Fenton-like treatment of NP-9 (Castillo et al., 2001). The fragmentation of APEC via a central fission pathway could account for the generation of mono- and dicarboxylated PEG having previously been identified from the anodic Fenton treatment of Triton X-100 (Kong and Lemley, 2007) and radiolytic decomposition of a series of octyl- and nonylphenol polyethoxylates as well as their polyethoxycarboxylates in sewage treatment plant effluent (Petrovic et al., 2007).

In addition to the polyethoxylate side chain, the hydrophobic alkyl chain could also act as the site of attack for HO^\bullet . The study of Castillo and co-workers reported

transformation of NP-9 into phenol diethoxycarboxylate, methylphenol ethoxycarboxylate and phenol tetraethoxylate, suggesting a degradation mechanism proceeding via the fragmentation of alkyl chain (Castillo et al., 2001). However, the most widely accepted mechanisms accounting for the interaction of alkyl chain with HO• are: (1) the cleavage in the bond linking the alkyl chain to the aromatic ring yielding a polyethoxylated phenol and (2) HO• attack on the tertiary carbon of the alkyl chain yielding tertiary alcohols (Destailats et al., 2000; Liu et al., 2010). The oxidation of the terminal —CH₃ group of the alkyl group to aldehyde and carboxyl groups has also been reported in combination with fragmentation of alkyl chain in several cases (Castillo et al., 2001; Chen et al., 2007a, 2007b). This mechanism is nearly identical to that accounting for the generation of carboxyalkylphenoxy carboxylates (CAPEC) and carboxyalkyl polyethoxylates during biotransformation of alkylphenol polyethoxylates (Chiu et al., 2010) and alkyl polyethoxylates (Schröder, 2001), respectively.

According to the available scientific literature, direct addition of HO• to the aromatic ring is also possible (Destailats et al., 2000; Liu et al., 2010). Pelizzetti and co-workers have already indicated that less than 10% of HO• abstract hydrogen from methylated benzenes, methoxylated benzenes and phenylacetic acid, whereas the remaining HO• add to the aromatic ring, emphasizing the specific reactivity of HO• towards the aromatic ring (Pelizzetti et al., 1989). Besides the HO• attack, Chen and co-workers proposed a photodegradation mechanism proceeding via the hydrogenation of aromatic ring and formation of cyclohexanyl structures (Chen et al., 2007a, 2007b).

Formation of simple structured aliphatic transformation products during AOP treatment of alkylphenol polyethoxylates has been documented in the scientific literature. For instance, de la Fuente and co-workers followed quantitatively the evolution of aldehydes during transformation of NP-9 via the H₂O₂/UV-C, TiO₂ photocatalysis and photo-Fenton processes (de la Fuente et al., 2010). In another study, Horikoshi and co-workers reported the formation of formic and acetic acids from the TiO₂ photocatalytic degradation of NP-9 (Horikoshi et al., 2002). It should be underlined here that the formation of such aliphatic species can be originated from a number of reaction sites on alkylphenol polyethoxylate molecules including the aromatic ring, aldehydic and

carboxylic terminal groups on the oxidized alkyl and polyethoxylate chains as well as PEG.

2.4.2. Toxicity

As outlined in Section 2.4.1, identification of the transformation products of alkylphenol polyethoxylates is a challenging task due to structural complexity and unique physical-chemical properties of these compounds. An alternative approach is to focus on the impact of treatment processes on overall toxicity of aqueous alkylphenol polyethoxylates. The most relevant investigations being extracted from the scientific literature are listed in Table 2.5. As a first remark, it should be stated that the existing studies have been devoted to UV irradiation, ozonation and the H₂O₂/UV-C process being already applicable in practical scale which clearly indicates the significant lack of data relating to ecotoxicological impact of AOP for the removal of aqueous alkylphenol polyethoxylates.

Temporal evolution of the non-specific toxicity towards *V. fischeri* arising from the photochemical treatment as well as ozonation of alkylphenol polyethoxylates has been treated in several research papers. Karci and co-workers comparatively studied H₂O₂/UV-C oxidation and UV-C photolysis of NP-10 in terms of changes in acute inhibitory effect towards *V. fischeri* expressed as percent bioluminescence inhibition (Karci et al., 2013). The acute inhibitory effect gradually increased from 9% inhibition to 36% throughout the course of the 90 min UV-C treatment, which was speculated to be caused by the formation of photolysis products with shorter ethoxylate side chains including nonylphenol. The authors concluded that the H₂O₂/UV-C process could be more ecotoxicologically safely applied for the removal of aqueous NP-10 than UV-C photolysis, considering that the H₂O₂/UV-C oxidation of NP-10 did not result in any acute inhibitory effect worth mentioning in the reaction solution. Impact of ozonation of aqueous NP-10 on acute inhibitory effect towards *V. fischeri* was investigated by another research group (Ledakowicz et al., 2005). The initial acute inhibitory effect of NP-10 being 35% increased to approximately 90% abruptly already after 2 h ozonation and remained stagnant thereafter. Similar findings were obtained for the ozonation of Triton X-100 and X-705 (OP-70). The authors ascribed the abrupt increase in acute inhibitory effect during the

Table 2.5. Scientific studies documenting the toxicity changes during photolysis and chemical oxidation of alkylphenol polyethoxylates.

Compound	Treatment Process	Bioassay/Test Organism	Changes in Toxicity	Reference
NP-10 NP-70	UV-A, UV-B and UV-C photolysis	Genotoxic effect detected by generation of γ -H2AX	Depending on the energy of UV, the genotoxic effect of NP-10 was attenuated, while non-genotoxic NP-70 became genotoxic.	Kubota et al., 2013
NP-15 NP-70	UV-B photolysis	Genotoxic effect detected by generation of γ -H2AX	Genotoxic potential of NP-15 was significantly reduced, whereas non-genotoxic NP-70 became genotoxic.	Toyooka et al., 2013
NP-10	Direct UV-C photolysis H ₂ O ₂ /UV-C process	<i>Vibrio fischeri</i>	Slightly higher toxicity value compared to NP-10 after H ₂ O ₂ /UV-C Gradual increase in toxicity during UV-C	Karci et al., 2013
NP-1 NP-2	Ozonation	Estrogenic activity detected by means of breast cancer cells (MCF-7)	Estrogenic activity was reduced due to synergistic effects of other similar compounds being present in wastewater.	Bertanza et al., 2010
OP-10 OP-70 NP-10	Ozonation	<i>Vibrio fischeri</i>	Toxicity increased abruptly already at the beginning of the ozonation process and remained stagnant thereafter.	Ledakowicz et al., 2005
NP-10 NP-70	UV-B photolysis	Cytotoxic effect towards mammalian cell lines	The cytotoxicity of NP-10 decreased after UV-B irradiation, whereas the cytotoxicity of NP-70 first increased and then decreased.	Goto et al., 2004
NP-3	Ozonation	Estrogenic activity detected by the YES assay	A slight decrease in estrogenic activity was observed.	Lenz et al., 2004

initial stages of ozonation of Triton X-100 to the formation of dearomatization products being originated from the O₃ attack on aromatic ring, but still containing the original number of ethoxylate groups. Another important finding from the study was that there was no correlation between the acute inhibitory effect and biodegradability as assessed by the interpretation of the BOD₅ (5-day biochemical oxygen demand)/COD ratios.

Considering the endocrine disrupting potential of nonylphenol mono- and diethoxylates, several research groups aimed at clarifying the efficiency of ozonation mainly as a post-treatment in the abatement of estrogenic activity being contributed by these biotransformation products. For instance, Lenz and co-workers followed estrogenic activity of Marlophen NP3, a nonylphenol polyethoxylate with an average three ethoxy units during course of the ozonation with the help of the YES assay, an estrogen receptor binding assay (Lenz et al., 2004). Their findings indicated that ozonation resulted in only slight decrease in estrogenic activity due to the marginal elimination of nonylphenol mono- and diethoxylates (about 30%) being present in the original mixture. In a more recent investigation by Bertanza and co-workers, removal of nonylphenol mono- and diethoxylates from secondary effluents of municipal wastewater treatment plants by means of ozonation was studied with special emphasis on the effect on estrogenic activity being assessed by using breast cancer MCF-7 cells transfected with the luminescence luciferase gene (Bertanza et al., 2010). The authors reported that NP-1 and NP-2 concentrations being present at concentrations below 0.20 µg L⁻¹ in wastewater treatment plant effluent decreased to non-detectable levels after ozonation. Their findings delineated that the estrogenic activity being expressed as the fold induction decreased already after 15 min ozonation as a function of the ozone dosage.

Recently, change in the genotoxic effect of nonylphenol polyethoxylates when exposed to UV irradiation at different wavelengths was studied using the phosphorylation of histone H2AX (γ-H2AX) as a marker for DNA damage (Kubota et al., 2013; Toyooka et al., 2013). The overall findings of these parallel studies indicated that a remarkable number of γ-H2AX foci in the nucleus being produced by the untreated NP-10 and NP-15 decreased by applying UV-B irradiation, meaning that the genotoxic effect of NP-10 and NP-15 was significantly reduced after UV-B irradiation. On the other hand, NP-70 being originally non-genotoxic produced γ-H2AX (i.e. gained genotoxic potential) when exposed

to UV-B dose of 500 J cm^{-2} , but the genotoxic effect disappeared when exposed to an excess dose of UV-B irradiation (1000 J cm^{-2}). Combining bioassay results with the HPLC outputs, the authors concluded that the transformation of NP-70 into short side-chain intermediates like NP-10 and NP-15 was the cause of the appearance of genotoxic effect after medium dose of UV-B irradiation. Exactly the same findings were obtained when the cytotoxic effects of the untreated and UV-B – treated aqueous NP-10 and NP-70 on mammalian cultured cells were investigated and compared (Goto et al., 2004). The experimental findings being summarized in this last paragraph underlines the importance of taking the genotoxicity as well as the cytotoxicity of the transformation products of alkylphenol polyethoxylates into consideration before conducting a comprehensive risk assessment.

To sum up, a majority of the findings discussed in this section revealed that direct UV photolysis and ozonation have the inherent risk of transforming the relatively non-toxic alkylphenol polyethoxylates into toxic transformation products. At this point, AOP deserves focus as an efficient alternative for the ecotoxicologically safe treatment of alkylphenol polyethoxylates contaminated waters. Although most of the relevant references listed in Table 2.5 assume that increases in inhibitory effect being observed during advanced chemical treatment of alkylphenol polyethoxylates are the result of the shortening of the polyethoxylate side chain, more clear conclusions being drawn by using the capabilities of sophisticated analytical techniques seem to be necessary to relate the inhibitory effect to specific transformation products.

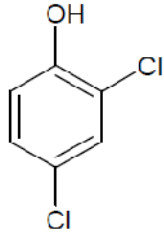
3. MATERIALS AND METHODS

3.1. Materials

3.1.1. 2,4-Dichlorophenol (2,4-DCP)

2,4-DCP was chosen as one of the two model pollutants representing chlorophenols. It is a common pollutant found in industrial wastewaters, being used as a chemical intermediate in the production of pesticides and herbicides including the widely used pesticide pentachlorophenol and the herbicide 2,4-dichlorophenoxy acetic acid. It is also used as a feedstock for the manufacture of certain methyl compounds included in mouth proofing, antiseptics and seed disinfectants (Al Momani et al., 2004). 2,4-DCP has also been found in pulp and paper effluents (Ali and Sreekrishnan, 2001). Other indirect routes for 2,4-DCP to enter into the environment are the photodegradation of the common antimicrobial agent triclosan (Latch et al., 2005), disinfection/treatment via chlorination and incineration flue gases of municipal waste (Chu et al., 2005). 2,4-DCP was purchased from Merck, Germany (purity > 98%) and used as received. The structural formula and some physicochemical properties of 2,4-DCP are shown in Table 3.1.

Table 3.1. Structural formula and selected physicochemical properties of 2,4-DCP.

2,4-DCP	
Molecular formula	C ₆ H ₄ Cl ₂ O
Molecular weight (g mol⁻¹)	163
TOC equivalent (g TOC g⁻¹ 2,4-DCP)	0.44
pK_a^a	7.85
Water solubility (g L⁻¹)	4.5 (20°C)
Structural formula	

^aShen et al. (1996).

3.1.2. Nonylphenol Decaethoxylate (NP-10)

The nonionic surfactant nonylphenol decaethoxylate was selected as the second model pollutant. This nonylphenol polyethoxylate is commercially abbreviated as “NP-10” and is widely employed as a wetting agent in different textile preparation processes at a concentration range of 0.5-1.5 g L⁻¹ and pH 10-11 (Arslan-Alaton et al., 2012b) as well as for cleaning purposes in household applications (Chen et al., 2007b). NP-10 was obtained from a local chemicals manufacturing plant being located in Tuzla, Istanbul and used as received. The structural formula and some physicochemical properties of NP-10 are shown in Table 3.2.

Table 3.2. Structural formula and selected physicochemical properties of NP-10.

NP-10	
Molecular formula	C ₉ H ₁₉ C ₆ H ₄ (OCH ₂ CH ₂) ₁₀ OH
Molecular weight (g mol⁻¹)	660
TOC equivalent (g TOC g⁻¹ NP-10)	0.64
log K_{ow}^a	4.09
Critical micelle concentration^b	75 μM (≅ 50 mg L ⁻¹)
Water solubility	Soluble ^c
Structural formula	

^aFan et al. (2011).

^bWang et al. (2011).

^cQuantitative data not available.

3.1.3. Synthetic Freshwater (SFW) Sample

Individual sets of experiments were performed in SFW to predict the treatment efficiencies, transformation products and toxicity for the cases where the selected treatment processes are applied to 2,4-DCP- and NP-10-polluted real natural waters. SFW was prepared in accordance with Standard Methods (APHA/AWWA/WEF, 1998) by adding reagent-grade chemicals to distilled water (DW) that was supplied by an Arium RO 61316 (Sartorius AG, Germany) reverse osmosis system (typical conductivity < 20 $\mu\text{S cm}^{-1}$). Two different stock solutions (called Solutions A and B) were used to prepare SFW of moderate hardness. “Solution A” was prepared by dissolving 2.4 g of $\text{MgSO}_4 \cdot 7\text{H}_2\text{O}$ (Merck, Germany), 1.9 g of NaHCO_3 (Merck, Germany) and 0.080 g of KCl (Merck, Germany) in 2 L DW. “Solution B” was prepared by dissolving 1.2 g of $\text{CaSO}_4 \cdot 2\text{H}_2\text{O}$ in 1 L DW under constant magnetic stirring and open atmosphere. DW was then fortified with the Stock Solutions A and B under constant agitation such that the concentrations of inorganic ingredients in the final aqueous solution were as in Table 3.3.

Table 3.3. Final composition and quality of SFW.

SFW	
NaHCO_3 (mg L^{-1})	96
$\text{CaSO}_4 \cdot 2\text{H}_2\text{O}$ (mg L^{-1})	60
$\text{MgSO}_4 \cdot 7\text{H}_2\text{O}$ (mg L^{-1})	123
KCl (mg L^{-1})	4.0
pH	7.4-7.8
Hardness (as mg $\text{CaCO}_3 \text{ L}^{-1}$)	80-100
Classification	Moderately hard
Alkalinity (as mg $\text{CaCO}_3 \text{ L}^{-1}$)	60-70
Conductivity ($\mu\text{S cm}^{-1}$)	324

3.1.4. Other Chemicals and Reagents

H_2O_2 (35%, w/w), $\text{FeSO}_4 \cdot 7\text{H}_2\text{O}$ (99.5-102.0% purity), hydroquinone (for synthesis), benzoquinone (for synthesis), phenol (99-100.5% purity), oxalic acid dihydrate ($\geq 99\%$ purity), formic acid (98-100% purity) and acetic acid (100% purity) were all purchased from Merck, Germany. Chlorohydroquinone ($\sim 85\%$ purity), maleic acid ($\geq 98.0\%$ purity) and catalase made from *Micrococcus lysodeikticus* (200181 AU mL^{-1}) were purchased

from Fluka, Switzerland. Catechol (> 99% purity) and fumaric acid (99% purity) were obtained from Acros Organics, Belgium and Sigma-Aldrich, USA, respectively. Methanol ($\geq 99.9\%$ purity, Merck, Germany), orthophosphoric acid (H_3PO_4 , 85.0-88.0% purity, Merck, Germany), acetic acid, sodium sulphate anhydrous (Na_2SO_4 , $\geq 99.0\%$ purity, Merck, Germany) and methane sulfonic acid ($\geq 99.5\%$ purity, Sigma-Aldrich, USA) were used to prepare mobile phases for the HPLC measurements. HPLC-gradient grade acetonitrile (Sigma-Aldrich, USA), LC-MS grade formic acid (Sigma-Aldrich, USA) and 25% NH_4OH (Merck, Germany) were used to prepare mobile phases for the LC-MS analyses. High purity dry air and high purity helium gas being used in the TOC and GC-MS analyses, respectively, were purchased from Linde AG, Germany. All other chemicals required for analytical and experimental procedures were at least of analytical grade, most of which being purchased from Merck, Germany. DW was used throughout the experiments, except that doubly distilled water with a conductivity of $0.055 \mu\text{S cm}^{-1}$ produced by an Arium 611UV system (Sartorius AG, Germany) was employed for the preparation of mobile phases for the HPLC measurements. For genotoxicity testing, the S9 fraction being supplied from Xenometrix, Switzerland was used as the metabolic activator system. 30% S9 mixture being employed in the *umu*-test method was prepared from the following reagents: 0.070 mL of 1.0 M KCl (Merck, Germany), 0.067 mL of 0.25 M $\text{MgCl}_2 \cdot 6\text{H}_2\text{O}$, 0.053 mL of 0.20 M glucose-6-phosphate (Sigma, USA), 0.21 mL of 0.04 M nicotinamide adenine dinucleotide phosphate, NADP (Sigma, USA) and 0.098 mL of the S9 mixture. 4-Nitroquinoline *N*-oxide and 2-aminoanthracene were purchased from Aldrich, USA, whereas dimethylsulfoxide was supplied by Sigma-Aldrich, USA.

3.2. Photoreactor and UV-C Light Source

All experiments were conducted in a 3250 mL capacity, cylindrical quartz photoreactor being covered by stainless steel (length: 84.5 cm; diameter: 8.0 cm) which is given in Figure 3.1. The UV-C light source was a 40 W low pressure mercury vapour lamp being located in the center of the photoreactor. The batch-operated photoreactor was mixed by means of a peristaltic pump at a flow rate of approximately 170 mL min^{-1} . The photon flux at 253.7 nm was determined by means of H_2O_2 actinometry (Nicole et al., 1990) as $7.9 (\pm 1.8) \times 10^{-2} \mu\text{E cm}^{-2} \text{ s}^{-1}$.

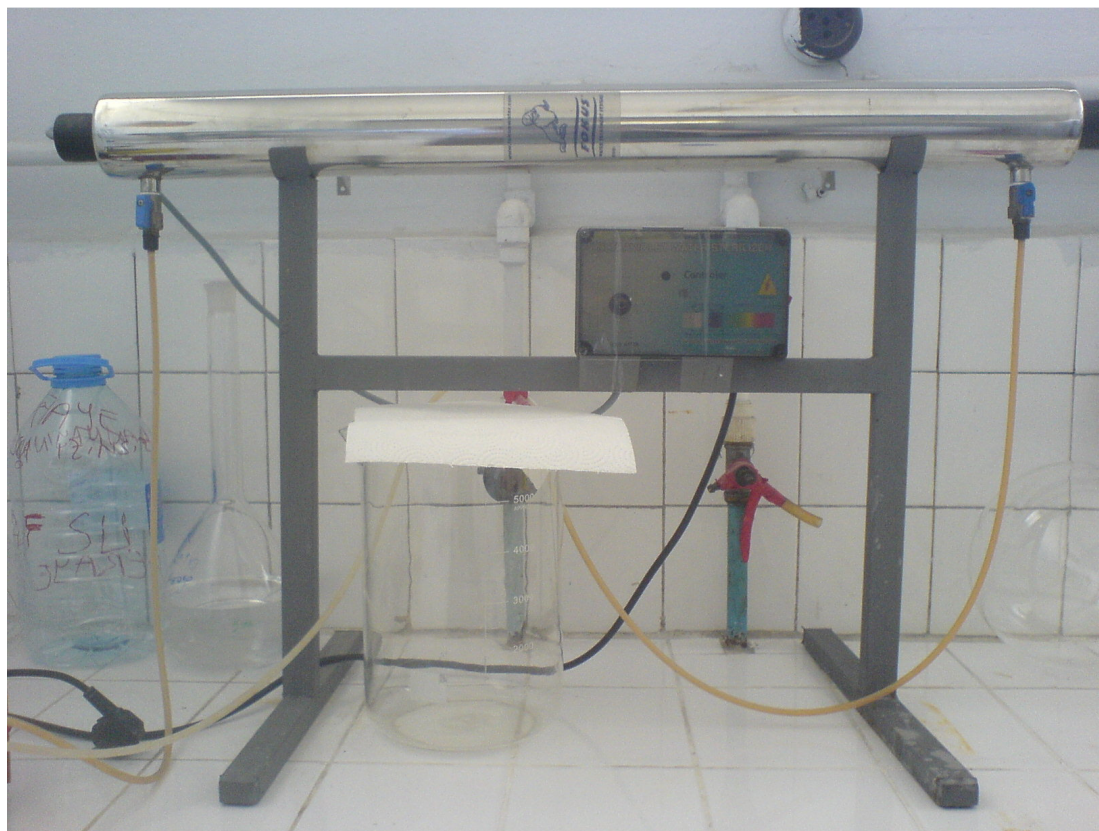


Figure 3.1. Experimental set-up being used throughout the treatment runs.

3.3. Experimental Procedures

Aqueous 2,4-DCP and NP-10 solutions were typically prepared at the concentrations of 25 mg L^{-1} ($150 \text{ }\mu\text{M}$) and 50 mg L^{-1} ($76 \text{ }\mu\text{M}$), respectively. Aqueous 2,4-DCP solutions were prepared by dissolving the crystalline solid form of 2,4-DCP directly in DW under magnetic stirring, whereas aqueous NP-10 solutions were made by diluting appropriate volumes of 2 g L^{-1} (3 mM) or 4 g L^{-1} (6 mM) NP-10 stock solution in DW under constant agitation. At the beginning of all experiments, the initial pH values of the 2,4-DCP and NP-10 solutions were adjusted to pre-determined values by using H_2SO_4 and NaOH solutions at varying concentrations. It should be emphasized here that the aqueous pollutant solutions were not pH-buffered, and therefore pH was not controlled throughout experiments. Before adding H_2O_2 to the aqueous pollutant solutions, an original sample was taken to confirm the prepared initial pollutant concentration by HPLC and TOC analyses. Following the addition of H_2O_2 to the aqueous pollutant solutions at pre-determined concentrations, the photoreactor was filled with the aqueous pollutant solutions

by means of a peristaltic pump. Before turning on the UV-C light source in the H₂O₂/UV-C process and adding the ferrous ion source in the Fenton and photo-Fenton processes, a $t = 0$ sample was taken. The H₂O₂/UV-C process was started by turning on the UV-C light source, whereas the addition of FeSO₄·7H₂O from a 5%, w/v (180 mM) or 10%, w/v (360 mM) stock solution was recognized as the starting point of the Fenton and photo-Fenton processes. Figure 3.2 shows outline of the study as a flow scheme which features experimental conditions and all analytical procedures applied in this research.

3.4. Analytical Procedures

Approximately 40 mL of treated sample aliquots were withdrawn from the photoreactor at pre-determined time intervals from the sampling valve. The Fenton and photo-Fenton reactions were quenched with the addition of a few drops of 1 N or 10 N NaOH solution to increase the pH to alkaline values and in this way to remove iron catalyst in the form of its hydroxides from the solution by filtering the sample through 0.45 µm PVDF syringe filters (Millipore, USA) in the case of 2,4-DCP and through 0.45 µm regenerated cellulose syringe filters (Sartorius AG, Germany) in the case of NP-10. The analytical procedures being performed on withdrawn samples are described in the following subsections.

3.4.1. HPLC Analyses

After 0.45 µm filtration, the treated samples were directly injected into the HPLC system except that the alkalified samples after the Fenton and photo-Fenton processes were re-acidified with concentrated H₂SO₄ to improve separation of the chromatographic peaks of carboxylic acids on the organic acid column. 2,4-DCP and NP-10 as well as their potential aromatic (phenol, catechol, hydroquinone, benzoquinone and chlorohydroquinone) and aliphatic transformation products (formic, acetic, oxalic, maleic and fumaric acids) were monitored by a 1100 Series HPLC (Agilent Technologies, USA) system equipped with a diode array (DAD) and fluorescence detector (FLD). Operating conditions of the HPLC for the selected target compounds are presented in Table 3.4. Analyte concentrations in the samples were determined according to the calculation of peak areas by external calibration. The detection limits were determined as the signal-to-

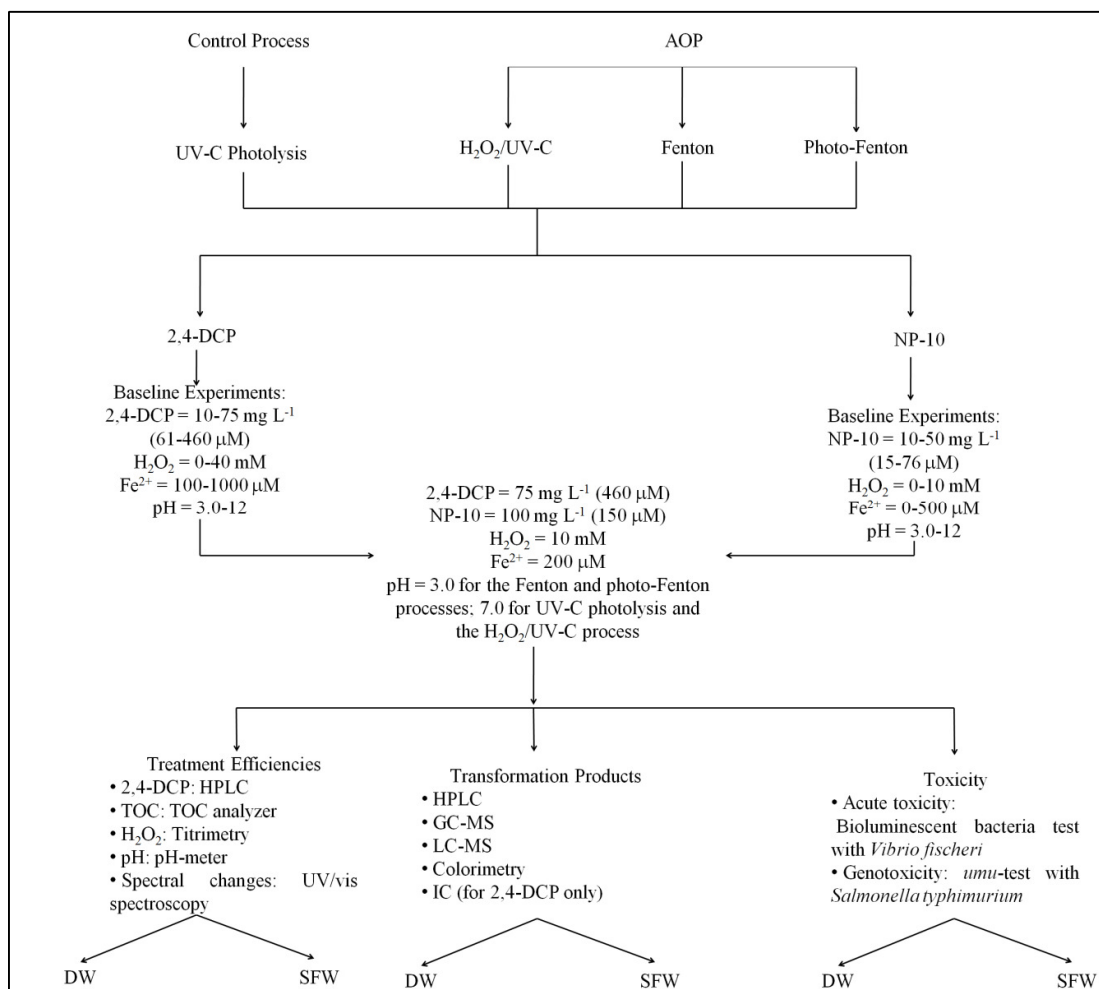


Figure 3.2. The flow scheme representing experimental conditions and all analytical procedures involved in the study.

noise ratio (S/N) of 3 and individually found as 0.069, 0.047, 0.063, 0.14, 0.053, 0.19, 0.074, 2.5, 1.4, 0.054 and 0.24 mg L^{-1} for 2,4-DCP, NP-10, phenol, catechol, hydroquinone, benzoquinone, chlorohydroquinone, formic acid, acetic acid, maleic acid and fumaric acid, respectively. Individual HPLC calibration curves being established for all target compounds are presented in Appendix A.

3.4.2. GC-MS Analyses

GC-MS analysis was also performed to identify transformation products of 2,4-DCP and NP-10 as well as to monitor their evolution during the $\text{H}_2\text{O}_2/\text{UV-C}$, Fenton and photo-Fenton treatment as well as UV-C photolysis. Prior to GC-MS analysis, solid phase

Table 3.4. HPLC operating conditions.

Compound	Column	Mobile phase	Flow rate (mL min ⁻¹)	Column temperature (°C)	Injection volume (μL)	Detection mode/ wavelength (nm)
2,4-DCP		Methanol:0.1% H ₃ PO ₄ in water (65:35, v/v)	1	20	100	DAD/280
NP-10		Methanol:water (80:20, v/v)	1	20	100	FLD/Ex: 230, Em: 290
Phenol Catechol Hydroquinone Benzoquinone	Novapack C18 (150 mm × 3.9 mm, Waters, USA)	Water:methanol:acetic acid (79.2:19.8:1, v/v/v)	0.8	40	40	DAD/270 DAD/276 DAD/290 DAD/245
Chlorohydroquinone		Methanol:acetic acid:water (60:2.5:37.5, v/v/v)	1	20	50	DAD/283
Formic acid Acetic acid Oxalic acid Maleic acid Fumaric acid	Acclaim OA (250 mm × 4 mm, Dionex, USA)	100 mM Na ₂ SO ₄ adjusted to pH 2.65 with methanesulfonic acid	0.6	30	50	DAD/210

extraction (SPE) was used to extract transformation products from aqueous samples. For this purpose, aqueous samples were first acidified to pH 2 with 20% H₂SO₄ solution in order to maintain polar transformation products in their cationic or neutral form as much as possible. The Oasis® hydrophilic-lipophilic balance, HLB (6 mL/200 mg, Waters, USA) cartridges were conditioned with 5 mL of methanol and 5 mL of DW. Then, 50 mL of the acidified sample was passed through the cartridges under a vacuum of 5 in Hg. After the entire sample was loaded, the HLB cartridges were dried under vacuum for several minutes. Finally, elution was performed with 2 mL of methanol under the lowest vacuum as possible, and the obtained eluates were injected into the 5975C Series (Agilent Technologies, USA) GC-MS system being equipped with an HP-5MS (5% phenyl methyl silox, Agilent Technologies, USA) 30 m × 250 μm × 0.25 μm film capillary column. Helium was used as the carrier gas at a constant flow rate of 1.0 and 0.53 mL min⁻¹ for analysis of the transformation products of 2,4-DCP and NP-10, respectively. For analysis of the transformation products of 2,4-DCP, the oven temperature was programmed to start under isothermal conditions at 80 °C for 6 min, then rise to 180 °C at a rate of 4 °C min⁻¹ and remain constant at 180 °C for 10 min. For analysis of the transformation products of NP-10, the oven temperature kept constant at 40 °C for 1 min, and then increased to 320 °C at a rate of 5 °C min⁻¹. The injection port and ion source temperatures were held at 280 and 230 °C, respectively, for 2,4-DCP and at 280 and 180 °C, respectively, for NP-10. A full scan from 30 to 700 *m/z* was performed. The injection volume was set at 2 μL and 4 μL for analysis of the transformation products of 2,4-DCP and NP-10, respectively. Transformation products were identified comparing the obtained fragmentation patterns as interpreted from the mass spectra with the identities being provided by the ChemStation™ (Agilent Technologies, USA) mass spectral library. Temporal evolution of the transformation products was evaluated by monitoring the changes in corrected peak areas of the individual transformation products with respect to treatment time.

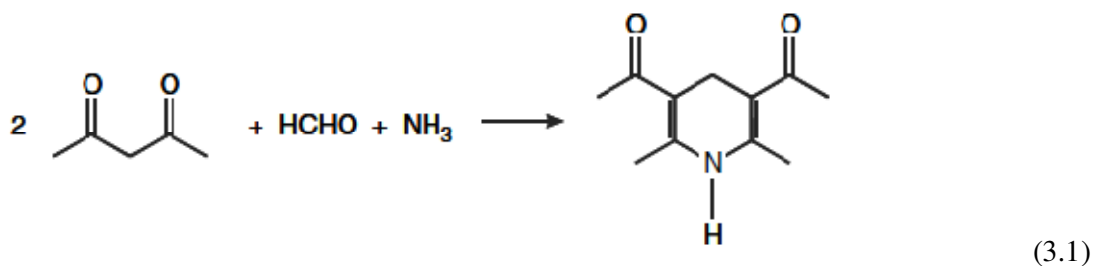
3.4.3. LC-MS Analyses

Transformation products of 2,4-DCP and NP-10 were additionally identified via direct infusion of the untreated and treated aqueous samples using the syringe pump of MS into a TSQ Quantum Access triple quadrupole mass spectrometer (Thermo Scientific, USA) under negative ion (NI) and positive ion (PI) electrospray modes. For NI mode,

mobile phase was acetonitrile:50 mM NH₄OH:water (30:20:50, v/v/v), whereas for PI mode, 1% formic acid:acetonitrile:water (10:30:60, v/v/v) was employed as the mobile phase. The spray voltage, capillary temperature and sheath gas pressure were set at 4000 V, 270 °C and 40 arb, respectively. Scan data were collected from 30 to 1000 *m/z*. Xcalibur™ software (Thermo Scientific, USA) was used for system control and data acquisition. Changes in intensity of the selected molecular ions were monitored to follow the temporal evolution of the identified transformation products.

3.4.4. Aldehyde Analysis

The so-called acetylacetone method, as described by Nash (1953), is widely applied as a standard procedure for the specific analysis of formaldehyde. The reaction, which is based on the Hantzsch synthesis, involves the cyclization of acetylacetone, ammonium acetate and formaldehyde, forming the diacetyldihydrolutidine according to Equation (3.1);



However, it should be underlined here that despite high specificity of the Nash's reagent towards formaldehyde, small quantities of other aldehydes, particularly acetaldehyde, can be also detected via the acetylacetone method. After addition of acetylacetone and ammonium acetate to the samples, the mixture was kept in an oven being previously equilibrated at 102 °C for 7 min to complete the reaction. Quantification was performed by a Novaspec II model UV-vis spectroscopy (Pharmacia Biotech, Sweden) at 412 nm. The calibration curve was established using formaldehyde as the standard in the concentration range of 0.5-10 mg L⁻¹ (Appendix A).

3.4.5. Chloride Analysis

Cl⁻ release during H₂O₂/UV-C, Fenton and photo-Fenton treatment as well as UV-C photolysis of 2,4-DCP was monitored on an ICS-1500 Ion Chromatography (IC) unit (Dionex, USA) equipped with a conductivity detector, an IonPac AS14A (4 × 250 mm) carbonate eluent anion-exchange column (Dionex, USA) and an IonPac AG14A (4 × 50 mm) guard column (Dionex, USA). The IC was operated in auto-suppression mode with 1 mM NaHCO₃/8 mM Na₂CO₃ eluent at a flow rate of 1 mL min⁻¹. The external calibration curve being established for Cl⁻ in the concentration range of 10-90 mg L⁻¹ is presented in Appendix A.

3.4.6. UV Absorbance Measurements

In order to measure the UV absorbance of aqueous 2,4-DCP and NP-10 solutions as well as the treated samples, spectrophotometric measurements were conducted. The obtained UV absorbance measurements were used to explain the patterns of aromatic ring cleavage as assessed by the UV absorbance at $\lambda = 280$ nm and of double bond cleavage as assessed by the UV absorbance at $\lambda = 254$ nm. The UV absorbances were monitored on a Lambda 25 model UV-vis double beam spectrophotometer (Perkin-Elmer, USA) in 1 cm-pathlength quartz cuvettes. As changes or shifts in absorption bands are possible with changing reaction pH due to slight structural changes including protonation/deprotonation, isomerization, alkaline elimination or hydrolysis, all samples were pH-adjusted to 2-3 before taking the absorption spectra.

3.4.7. Other Procedures

The TOC of the samples was monitored on a V_{PCN} model carbon analyzer (Shimadzu, Japan) equipped with an autosampler according to the combustion method. Residual H₂O₂ in the treated samples was traced by employing the molybdate-catalyzed iodometric method (Horwitz, 1980). Changes in pH values were recorded by an Orion 720⁺ model pH-meter (Thermo Scientific, USA) throughout the photochemical experiments.

3.5. Bioanalytical Procedures

In this study, two bacterial toxicity bioassays were selected, one utilizing *Vibrio fischeri* and the another employing *Salmonella typhimurium*. *V. fischeri* remains the most widely used organism for measurement of cytotoxicity in water samples. It suitably reflects the underlying baseline toxicity of all chemicals in the mixture. The bioluminescence inhibition test using *V. fischeri* was chosen not only due to its low cost and simplicity, but also considering that its application for evaluating AOP performances in various water matrices is well established in the scientific literature (Guzzella et al., 2002; Trovó et al., 2009; Sirtori et al., 2010) providing a large volume of comparative information. Although it does not reflect the specific mode of inhibitory effect of chemicals, *V. fischeri* is very useful for obtaining a first idea of overall acute toxicity resulting from transformation products.

The bioluminescence inhibition test using *V. fischeri* was complemented by the *umu*-test, a genotoxicity bioassay, to capture cases where transformation products have lost their non-specific mode of inhibitory effect, but developed a high specific toxicity. Genotoxicity is of special concern, because it may cause adverse reproductive damage to organisms directly or even lead to their extinction (Zhang et al., 2013). For genotoxicity testing, the *umu*-test was selected in this study due to its theoretical advantages that it is based on one of the standard Ames strains and uses the same S9 mix and its practical advantages of high throughput capacity (Escobar et al., 2013). Additionally, the *umu*-test has been already applied for several research groups to evaluate various water treatment options (Shishida et al., 2000; Reungoat et al., 2010; Tuerk et al., 2010) that would make the comparison of findings to be gathered in this study with those in the scientific literature possible.

The following subsections deal with the details of experimental procedures involved in acute toxicity and genotoxicity testing.

3.5.1. Acute Toxicity Testing

Changes in the acute inhibitory effect during application of UV-C photolysis, H₂O₂/UV-C, Fenton and photo-Fenton treatment processes were measured by using a

commercial assay kit marketed as BioTox™ (Aboatox, Finland). The reagent was a lyophilised preparation of the marine photobacterium *Vibrio fischeri* (NRRL B-11177). The assay is based on the decrease in light emission of *V. fischeri* resulting from its exposure to the toxicant. Prior to the assay, the pH was adjusted to 7.0 (± 0.2) with NaOH or H₂SO₄ for the cases where the pH of the sample was not between 6 and 8.5. NaCl was added to the samples to obtain a final salinity being equivalent to 2% NaCl, w/v solution. Prior to analysis, the sample solutions were oxygenated by stirring. In order to eliminate its positive effect on the toxicity test results, any unreacted H₂O₂ remaining in the samples was catalytically decomposed with catalase. After mixing 0.5 mL of raw and treated 2,4-DCP and NP-10 solutions with 0.5 mL luminescent bacterial suspension (dilution ratio = 50%, v/v), the luminescence intensities from the cuvettes containing bacterial suspension were measured after 0 and 15 min contact time at 15 °C, and the percent relative inhibition (INH%) was calculated relative to a non-toxic control (2%, w/v NaCl solution) by the help of Equation (3.2);

$$\text{INH\%} = 100 - 100 \times (\text{IT}_{15} / \text{KF} \times \text{IT}_0) \quad (3.2)$$

where IT_0 and IT_{15} are the luminescence intensities (in relative luminescence units abbreviated as RLU) of the sample at the beginning and after 15 min contact time, respectively, and KF is the correction factor (dimensionless) for the control;

$$\text{KF} = \text{IC}_{15}/\text{IC}_0 \quad (3.3)$$

where IC_0 and IC_{15} are the luminescence intensities (in RLU) of the control after 0 min and 15 min contact time, respectively. The effective concentrations of aqueous (untreated) 2,4-DCP and NP-10 causing 50% inhibition (EC_{50} ; in mg L⁻¹) were also determined.

3.5.2. Genotoxicity Testing

The genotoxic potential of raw and treated samples being previously 25-fold concentrated in methanol phase by means of SPE was assessed by using a commercial assay kit marketed as umuC Easy AQ (Xenometrix, Switzerland). The test is based on that upon exposure of *Salmonella typhimurium* TA 1535 [pSK 1002] bacteria to genotoxic

water samples, the *umuC* gene being contained in the plasmid pSK 1002 and fused to the *lacZ* reporter gene is induced as part of the bacterial SOS response. The SOS response is a global response to DNA damage in which the cell cycle is arrested and DNA repair and mutagenesis are induced. The induction of *lacZ* is measured by the conversion of colorless *o*-nitrophenyl- β -D-galactopyranoside (ONPG) substrate to the yellow product *o*-nitrophenol by the *lacZ*-encoded β -galactosidase. Individual stages of the *umu*-test are briefly described in the following paragraphs.

3.5.2.1. Preparation of the Bacterial Culture. 200 μ L of 1 \times (single strength) TG medium (1% bactotryptone, 0.5% NaCl, 0.2% glucose) was added to the vial containing *S. typhimurium* TA 1535 [pSK 1002] bacteria. 10 mL 1 \times TG medium was added to a 50 mL tube being labelled as “culture tube” and 3 mL 1 \times TG medium to a tube being labelled as “sterility control tube”. 10 μ L and 3 μ L of ampicillin (50 mg mL⁻¹) were added to the culture tube and the sterility control tube, respectively. Finally, 50 μ L of the bacterial dispersion was added into the culture tube. The tubes were then incubated in an environmental shaker set at 37 °C, 250 rpm for 14-16 h. After the overnight incubation, 900 μ L of 1 \times TG medium was added to two spectrophotometer cuvettes. 100 μ L aliquots from the culture and sterility control tubes were transferred to the cuvettes containing 900 μ L of 1 \times TG medium. The Epoch spectrophotometer (BioTek, USA) was blanked at 600 nm with 1000 μ L TG medium only. It was verified that the optical density values at 600 nm (OD₆₀₀) for the cultures were > 2, and that the OD₆₀₀ value of the negative control was \leq 0.5. The test was continued only if these criteria were met.

3.5.2.2. Reincubation of the Bacteria. The overnight culture was diluted 1:4 (1 mL culture + 3 mL 1 \times TG medium + 4 μ L ampicillin) and incubated as before for 1.5-2 h to obtain an OD₆₀₀ corresponding to 75% of the original OD of the overnight cultures.

3.5.2.3. Exposure of Bacteria to Test Samples. The 96-well microplate configuration in the *umu*-test system is presented in Appendix B. For one plate, 10 μ L ampicillin (50 mg mL⁻¹) was added to 10 mL TG medium, and 20 μ L of the resulting mixture was added to all wells. For the wells without S9 (rows A-D), 70 μ L of the reincubated bacteria was added to all wells except D10-D12 (blank) to which 70 μ L of TG medium was added. For

the S9 wells (rows E-H), a bacteria/S9 mix was prepared consisting of 35 μL of KCl, 33.5 μL of MgCl_2 , 26.5 μL of glucose-6-phosphate, 105.5 μL of NADP, 50 μL of S9 and 1.23 mL of re-incubated bacteria, and 70 μL of the resulting mixture was added to all wells except that for H10-H12 (blank) 235 μL of TG medium was added to 40 μL of the mixture consisting of 35 μL of KCl, 33.5 μL of MgCl_2 , 26.5 μL of glucose-6-phosphate, 105.5 μL of NADP and 50 μL of S9, and 70 μL of the resulting mixture was added to the blank wells H10-H12. 180 μL of test sample was then added to columns 1-12, rows A-C and E-G. 10 μL of 4-nitroquinoline *N*-oxide (12.5 $\mu\text{g mL}^{-1}$ in dimethyl sulfoxide) and 2-aminoanthracene (50 $\mu\text{g mL}^{-1}$ in dimethyl sulfoxide) as the positive controls were added to columns 1-3 of row D (- S9) and row H (+ S9), respectively, and 170 μL of sterile water was pipetted onto the positive controls. 10 μL of solvent control (dimethyl sulfoxide) was added to columns 4-6 of rows D and H, and 170 μL of sterile water was pipetted onto the solvent controls. 180 μL of water was added to the negative control and blank wells (columns 7-12 of rows D and H). Finally, the microplate was incubated for 2 h at 37 °C, 120-150 rpm.

3.5.2.4. Dilution Step and Second Incubation. For a second plate, 14 μL ampicillin was added to 14 mL TG medium, and 270 μL of the resulting mixture was pipetted to all wells. The microplate was placed in an incubator (Nüve, Turkey) at 37 °C. After 2 h incubation, 30 μL of the contents of the first plate was transferred to the second plate. The OD_{600} of the second plate was read. The second plate was then incubated for 2 h at 37 °C, with shaking (120-150 rpm). At the end of the 2 h incubation, the OD_{600} of the second plate was re-read.

3.5.2.5. Measurement of *umuC* Induction. A third plate was prepared with 7.5 mL of B buffer, 20.25 μL of β -mercaptoethanol and 0.5 mL of ONPG solution. 150 μL of the resulting mixture was transferred to all wells, and the microplate was then put at 37 °C for 15 min. 30 μL from each well of the second plate was transferred to the third plate. The third plate was incubated for 30 min at 37 °C, with shaking (120-150 rpm). After 30 min, 120 μL of Stop Reagent was added to each well, and the optical density at 420 nm (OD_{420}) was read.

3.5.2.6. Calculation. For each sample, the growth factor (G), the β -galactosidase activity (U_S) and the induction factor (I_F) were calculated using Equations (3.4), (3.5) and (3.6), respectively;

$$G = \frac{A_{600, S} - A_{600, B}}{A_{600, N} - A_{600, B}} \quad (3.4)$$

where $A_{600, S}$ is the absorbance of the sample S at 600 nm, $A_{600, B}$ the absorbance of the blank at 600 nm and $A_{600, N}$ the absorbance of the negative control at 600 nm.

$$U_S = \frac{A_{420, S} - A_{420; B}}{A_{600, S} - A_{600, B}} \quad (3.5)$$

where $A_{420, S}$ is the absorbance of the sample S at 420 nm and $A_{420, B}$ the absorbance of the blank at 420 nm.

$$I_F = \frac{1}{G} \times \frac{A_{420, S} - A_{420; B}}{A_{420, N} - A_{420, B}} \quad (3.6)$$

A sample was considered weakly genotoxic if $2 \leq I_F \leq 3$, moderately genotoxic if $3 \leq I_F \leq 6$ and strongly genotoxic if $I_F > 6$ (Oda et al., 1985; Nakamura et al., 1987; Shimada and Nakamura, 1987). The G value was above 0.5 for all tested samples which was indicative of a non-cytotoxic effect in the *umu*-test. The whole test was considered valid if the positive controls reached an $I_F \geq 2$. For all tested samples, the average OD₆₀₀ of the negative controls of the second plate increased by a factor of ≥ 2 during the 2 h incubation (growth control).

4. RESULTS AND DISCUSSION

4.1. Studies with 2,4-DCP

4.1.1. 2,4-DCP Baseline Experiments and Kinetics

The $\text{H}_2\text{O}_2/\text{UV-C}$, Fenton and photo-Fenton processes are affected by numerous parameters such as initial H_2O_2 , Fe^{2+} and pollutant concentrations as well as treatment time and pH (Olmez-Hanci et al., 2011; Tureli et al., 2010; Arslan-Alaton et al., 2010). Since it is too complicated to consider all process variables, the selection of those variables having a significant effect on treatment performance becomes important. Hence, baseline experiments are generally very useful to identify the major process variables and to decide for their most appropriate levels and ranges. In this section, results of the baseline experiments aiming at assessing the effect of initial pollutant, H_2O_2 and Fe^{2+} concentrations and pH on 2,4-DCP and TOC removal kinetics and efficiencies were presented and discussed. In addition, the studied treatment processes were comparatively evaluated on the basis of 2,4-DCP and TOC removal kinetics and efficiencies.

4.1.1.1. Single H_2O_2 and UV-C Photolysis Control Experiments. First of all, a control experiment was conducted in order to realize whether H_2O_2 alone with an initial concentration of 40 mM which was the highest initial H_2O_2 concentration being used in this experimental part, and an initial pH of 7 resulted in any reduction in 2,4-DCP concentration and TOC. 2,4-DCP, TOC and H_2O_2 decay kinetics being obtained during single H_2O_2 oxidation of 2,4-DCP are presented in Figure 4.1. The findings demonstrated that H_2O_2 without UV-C irradiation resulted in only 15% conversion of 2,4-DCP with an initial concentration of 25 mg L^{-1} after 90 min treatment, whereas practically no mineralization occurred under these experimental conditions. In systems in which H_2O_2 is used as the sole oxidant, the dominant reaction which is thermodynamically favorable is the dissociation of H_2O_2 as shown in Equation (4.1) and in this case, O_2 is the active oxidant responsible for the degradation and mineralization of the parent pollutant (Lee and Carberry, 1992):

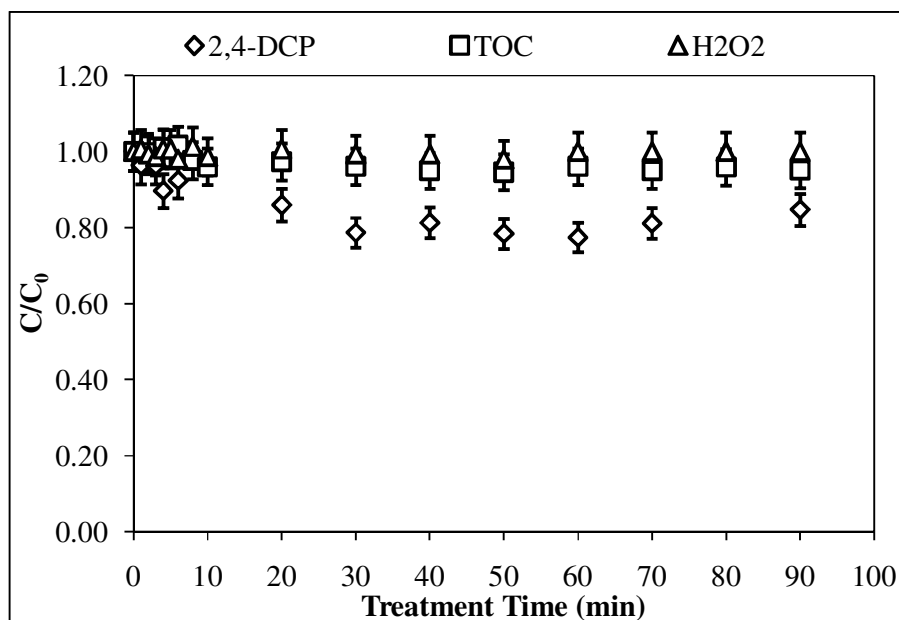


Figure 4.1. Normalized 2,4-DCP, TOC and H₂O₂ decays during single H₂O₂ oxidation of 2,4-DCP. Initial experimental conditions: 2,4-DCP = 25 mg L⁻¹ (150 μM), H₂O₂ = 40 mM, pH = 7.

However, O₂ has a much lower standard reduction potential (1.23 V vs. NHE, Normal Hydrogen Electrode; Muff, 2010) than HO[•] (2.80 V vs. NHE; Pera-Titus et al., 2004) which accounts for the low 2,4-DCP removal efficiency and negligible mineralization being obtained in the present study. H₂O₂ (Figure 4.1) and pH (data not shown) measurements during the treatment of 2,4-DCP with H₂O₂ alone also showed that the initial values of these two process parameters almost did not change during the course of the treatment, referring to the very low conversion of 2,4-DCP with H₂O₂ alone. The inefficiency of H₂O₂ alone in degrading chlorophenols has also been demonstrated by other authors (Trapido et al., 1998; Benitez et al., 2000b; Ghaly et al., 2001).

An additional experiment concerning the direct UV-C photolysis of 2,4-DCP was also conducted as a control for the H₂O₂/UV-C process. The obtained 2,4-DCP and TOC removal kinetics as well as pH evolution during direct UV-C photolysis of 2,4-DCP are demonstrated in Figure 4.2. Results showed that UV-C irradiation was able to achieve 91% removal of 2,4-DCP after 90 min treatment. During photochemical treatments using UV

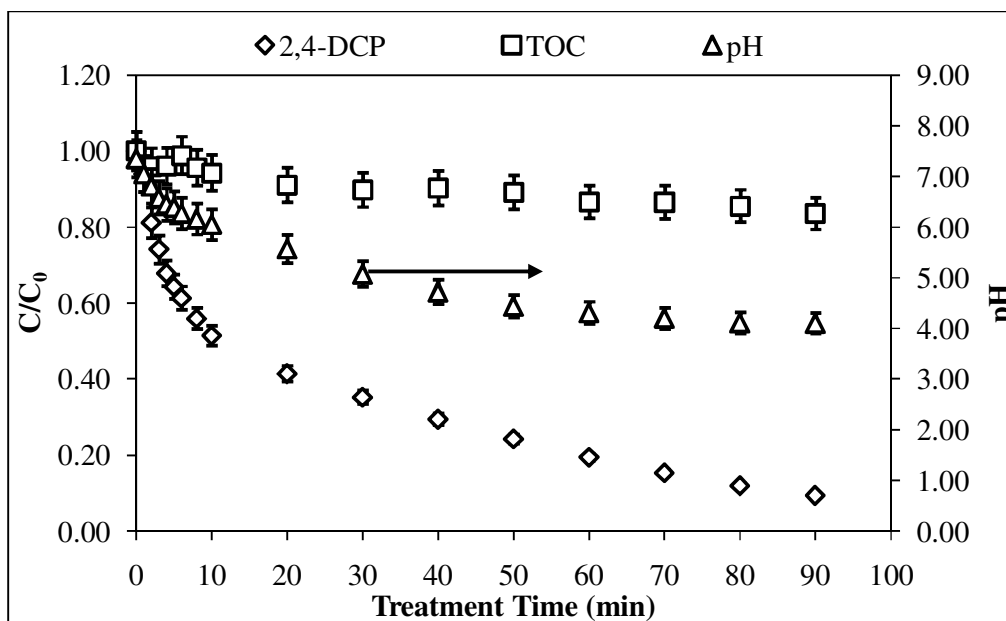


Figure 4.2. Normalized 2,4-DCP and TOC removals as well as pH evolutions during direct UV-C photolysis of 2,4-DCP. Initial experimental conditions: 2,4-DCP = 25 mg L⁻¹ (150 μM), pH = 7.

irradiation, electronically excited states of chlorophenols have been suggested to be generated as a result of their absorption of UV irradiation. In these excited states, chlorophenols can undergo intramolecular transformations and stabilize states with different electron distributions, in turn decomposing to radical or molecular products (Durand et al., 1992; Boule et al., 1982). However, this treatment was found to result in incomplete transformation of 2,4-DCP in this study even after a relatively long treatment time of 90 min. Furthermore, mineralization efficiency at the end of treatment was only 16%, indicating that UV-C photolysis alone was inefficient for the degradation of the organic photolysis products being generated during the treatment. This conclusion can also be withdrawn from the pH evolutions during direct UV-C photolysis of 2,4-DCP (Figure 4.2) which revealed that the formation of acidic photolysis products continued until the end of the photochemical process and was dominant over their mineralization to CO₂. Poor removal efficiencies for chlorophenols with direct UV photolysis have also been reported by many other authors (De et al., 1999; Trapido et al., 1998; Bayarri et al., 2007).

4.1.1.2. The H₂O₂/UV-C Experiments.

Effect of Initial 2,4-DCP Concentration. The experiments aiming to assess the effect of initial 2,4-DCP concentration on 2,4-DCP and TOC removals, H₂O₂ consumption and pH evolution were conducted at a constant initial H₂O₂ concentration of 10 mM, initial pH of 7, and four different initial 2,4-DCP concentrations, namely 10, 25, 50, and 75 mg L⁻¹ (61, 150, 310 and 460 μM). The concentration range of 10-75 mg L⁻¹ was selected in the present study, since this range is relevant in environmental conditions existing in heavily contaminated sites. Even higher concentrations of total chlorophenols up to 190 mg L⁻¹ have been shown to be present near a sawmill (Lampi et al., 1990).

Figure 4.3a shows the graph involving the effect of initial 2,4-DCP concentration on parent pollutant removal kinetics. Photochemical transformation of 2,4-DCP via the H₂O₂/UV-C process was well described by a first order model kinetic with regression coefficients (R^2) ≥ 0.978 for all studied initial 2,4-DCP concentrations. The calculated pseudo-first-order rate coefficients for the decays of 2,4-DCP, TOC and H₂O₂ as well as their conversion percentages via the H₂O₂/UV-C process are presented in Table 4.1 as a function of initial 2,4-DCP concentration. Data from the scientific literature have also indicated that photochemical treatment of chlorophenols via the H₂O₂/UV process was generally described by the pseudo-first-order kinetics (Pera-Titus et al., 2004). The obtained experimental findings in this work revealed that the pseudo-first-order 2,4-DCP removal rate coefficients decreased with increasing initial 2,4-DCP concentration under the studied experimental conditions (Table 4.1). At a concentration of 10 mg L⁻¹, 2,4-DCP disappeared to non-detectable levels after 4 min H₂O₂/UV-C treatment, whereas the disappearance time reached more than 20 min when the initial 2,4-DCP concentration was increased 7.5-fold. These results were in line with data from the scientific literature demonstrating the negative effect of increasing initial chlorophenol concentration on parent pollutant abatement rates and conversion percentages in the H₂O₂/UV process (Çatalkaya et al., 2003; Pouloupoulos et al., 2008; Shen et al., 1996). The decrease in 2,4-DCP removal rate with increasing initial 2,4-DCP concentration could be attributed to the competition of 2,4-DCP with H₂O₂ for the absorption of UV irradiation when its concentration was increased, thus impeding the HO[•] formation rate (Shen et al., 1996). The inhibitory effect of increasing 2,4-DCP concentration on 2,4-DCP removal kinetics may also be due to

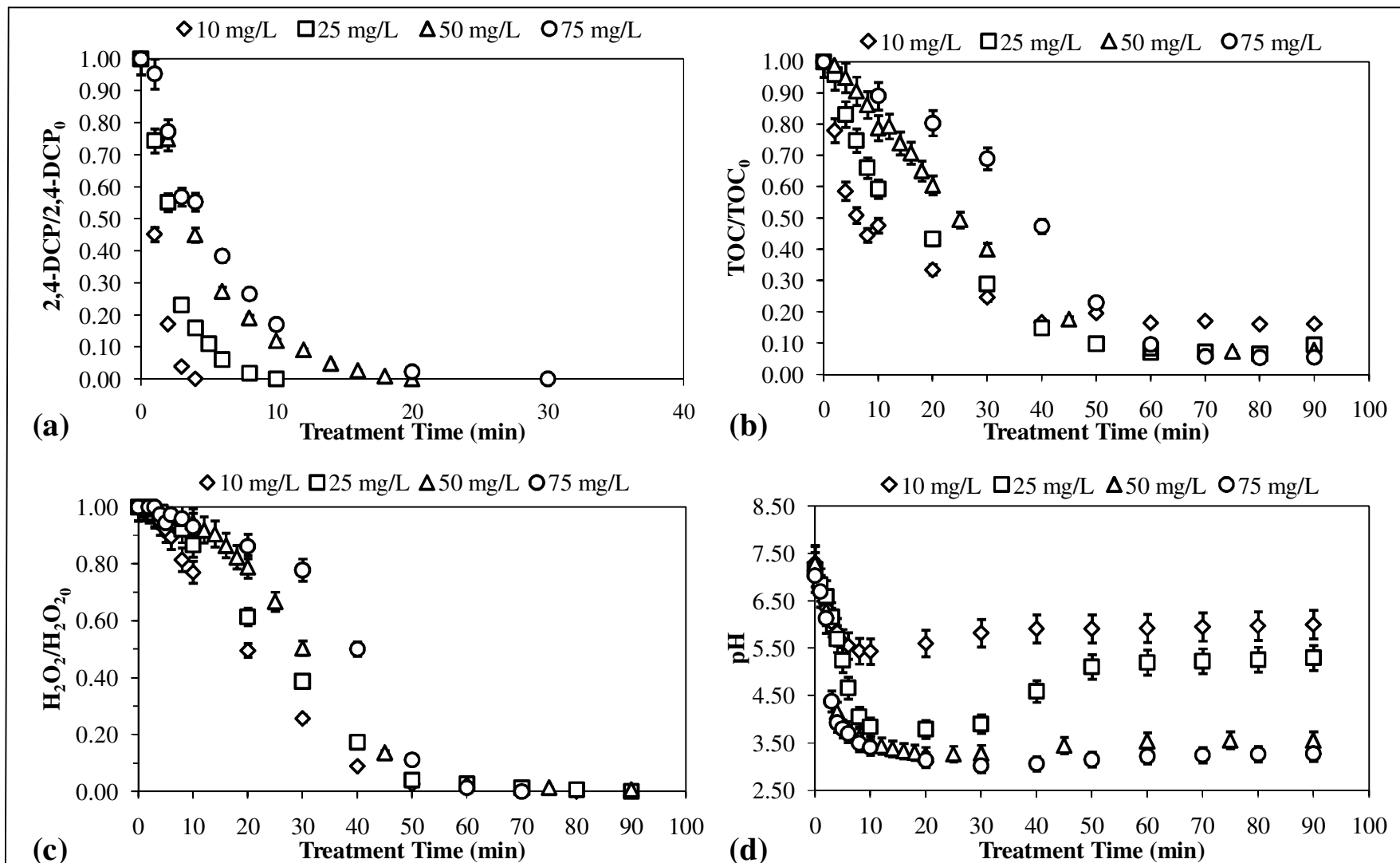


Figure 4.3. Effect of initial 2,4-DCP concentration on the decay of 2,4-DCP (a), TOC (b) and H₂O₂ (c) as well as the pH evolution (d) during H₂O₂/UV-C treatment of 2,4-DCP. Initial experimental conditions: H₂O₂ = 10 mM, pH = 7.

Table 4.1. The pseudo-first-order rate coefficients and removal percentages for 2,4-DCP, TOC and H₂O₂ decays by the H₂O₂/UV-C process as a function of initial 2,4-DCP concentration.

	2,4-DCP (mg L ⁻¹)			
	10	25	50	75
$k_{2,4-DCP}$ (min ⁻¹)	1.1	0.51	0.22	0.17
2,4-DCP removal (%)*	100	100	100	100
k_{TOC} (min ⁻¹)	0.046	0.040	0.030	0.012
TOC removal (%)*	84	91	92	95
$k_{H_2O_2}$ (min ⁻¹)	0.046	0.032	0.020	0.0086
H ₂ O ₂ consumption (%)*	100	100	99	100

*After 90 min treatment.

higher concentrations of Cl⁻ being released from 2,4-DCP with higher initial concentration, since Cl⁻ has been reported to have the ability to scavenge radicals which are largely responsible for chlorophenol degradation and mineralization (Krutzler and Bauer, 1999).

Figure 4.3b shows the graph involving the effect of initial 2,4-DCP concentration on TOC removal kinetics. As can be seen from Figure 4.3b, TOC removals were significantly slower than the 2,4-DCP removals. The pseudo-first-order TOC removal rate coefficients (0.046, 0.040, 0.030 and 0.012 min⁻¹ for the initial 2,4-DCP concentrations of 10, 25, 50 and 75 mg L⁻¹, respectively) were found to be one order of magnitude smaller than the pseudo-first-order rate coefficients for 2,4-DCP removal (1.1, 0.51, 0.22 and 0.17 min⁻¹ for 10, 25, 50 and 75 mg L⁻¹, respectively) as given in Table 4.1. Being similar to the pseudo-first-order 2,4-DCP removal rate coefficients, the pseudo-first-order TOC removal rate coefficients were also found to decrease with increasing initial 2,4-DCP concentration in accordance with findings from the scientific literature dealing with the H₂O₂/UV treatment of chlorophenols (Çatalakaya et al., 2003).

Figure 4.3c presents the H₂O₂ consumptions over time for each one of the studied initial 2,4-DCP concentrations. From Figure 4.3c, it could be readily seen that the H₂O₂ consumptions were slower with increasing initial 2,4-DCP concentration. When the initial 2,4-DCP concentration was increased from 10 to 75 mg L⁻¹, it became more difficult to photodecompose the H₂O₂, particularly at the initial stages of reaction. This trend was most

probably due to the higher competition of 2,4-DCP and its transformation products with H_2O_2 for UV-C irradiation at greater initial concentrations of 2,4-DCP. Since the molar absorptivity of chlorophenols is known to be relatively high in the UV-region (Trapido et al., 1997), increasing concentration of 2,4-DCP might have resulted in high UV absorbencies which compete seriously with H_2O_2 . In addition to the parent chlorophenol, higher concentrations of transformation products being generated from 2,4-DCP with greater initial concentrations could also contribute to the greater absorption of UV-C irradiation. Support for this suggestion could be deduced from Figure 4.3c which shows that, especially for the initial 2,4-DCP concentrations of 50 and 75 mg L^{-1} , H_2O_2 concentration only slightly changed during the first 10-20 min of the $\text{H}_2\text{O}_2/\text{UV-C}$ treatment, most probably due to the generation of transformation products in the system during this time course. Following this treatment time, H_2O_2 photodecomposition accelerated which most likely paralleled the rapid disappearance of transformation products. In fact, as could be realized from the comparison of Figure 4.3b and c, the rapid H_2O_2 consumptions being observed within 10-20 to 50-60 min of the $\text{H}_2\text{O}_2/\text{UV-C}$ treatment were well accompanied by the fast diminishments in the TOC values within the same time interval. Following this time interval where H_2O_2 was nearly completely consumed for all studied initial 2,4-DCP concentrations, however, TOC values did not significantly change, suggesting that H_2O_2 is essential for the progress of mineralization and UV-C irradiation alone could not lead to any significant decrease in TOC.

Figure 4.3d presents the pH changes over time for each one of the studied initial 2,4-DCP concentrations. From Figure 4.3d, it is apparent that the $\text{H}_2\text{O}_2/\text{UV-C}$ treatment of 2,4-DCP was accompanied by a rapid pH drop in the early part of treatment for all studied initial 2,4-DCP concentrations due to the formation of oxygenated acidic reaction intermediates during 2,4-DCP degradation (De et al., 1999). On the other hand, the extent of pH drop differed between the four initial 2,4-DCP concentrations. For example, a decrease of 4.0 pH units was measured for the initial 2,4-DCP concentration of 75 mg L^{-1} , while for 10 mg L^{-1} of 2,4-DCP, the amount of pH decrease was only 1.9 pH units. In addition to the amount of pH decrease, the time required for the pH to reach its minimum value was also found to increase with increasing initial concentration of 2,4-DCP. These findings suggested that higher concentrations of acidic transformation products were formed from 2,4-DCP with a higher initial concentration, but the treatment time necessary

for the concentrations of acidic products to reach their maximum values increased with increasing 2,4-DCP concentration. On the other hand, from pH profiles, it could be readily seen that pH tended to rise again after the minimum pH was reached. This was most probably due to the release of final mineralization product, CO₂, from the reaction solution (Olmez-Hanci et al., 2011). The amount of pH rise after the minimum value was reached decreased with increasing 2,4-DCP concentration, with the exception of 25 mg L⁻¹ of 2,4-DCP for which pH rise was most pronounced (from 3.8 to 5.3).

Effect of Initial pH. The second process variable which could potentially affect the efficiency of the H₂O₂/UV-C process is the pH of the reaction solution, and its effect on the pseudo-first-order rate coefficients and removal percentages for 2,4-DCP, TOC and H₂O₂ decays are summarized in Table 4.2. The initial pH values of 4, 7 and 11 were selected as the representatives of acidic, neutral and alkaline media, respectively, and the initial 2,4-DCP and H₂O₂ concentrations were kept constant at 25 mg L⁻¹ (150 μM) and 10 mM, respectively, in these experiments. In addition, experiments were also conducted at the initial pH of 12 to test the H₂O₂/UV-C treatment efficiency and kinetics above the pK_a value of H₂O₂ of 11.7 (Kawaguchi, 1993). The pH of the aqueous 2,4-DCP solutions was not buffered to avoid the scavenging of HO[•] by inorganic constituents being generally present in buffer solutions (Kang et al., 2009).

Table 4.2. The pseudo-first-order rate coefficients and removal percentages for 2,4-DCP, TOC and H₂O₂ decays by the H₂O₂/UV-C process as a function of initial pH.

	pH			
	4	7	11	12
$k_{2,4-DCP}$ (min ⁻¹)	0.51	0.51	0.36	0.19
2,4-DCP removal (%)*	100	100	100	100
k_{TOC} (min ⁻¹)	0.050	0.045	0.028	0.011
TOC removal (%)*	92	91	87	39
$k_{H_2O_2}$ (min ⁻¹)	0.044	0.032	0.025	0.13
H ₂ O ₂ consumption (%)*	100	100	99	100

*After 90 min treatment.

The effect of initial pH of the aqueous 2,4-DCP solution on the kinetics of 2,4-DCP and TOC abatements is represented in Figure 4.4a and b, respectively. The solution pH

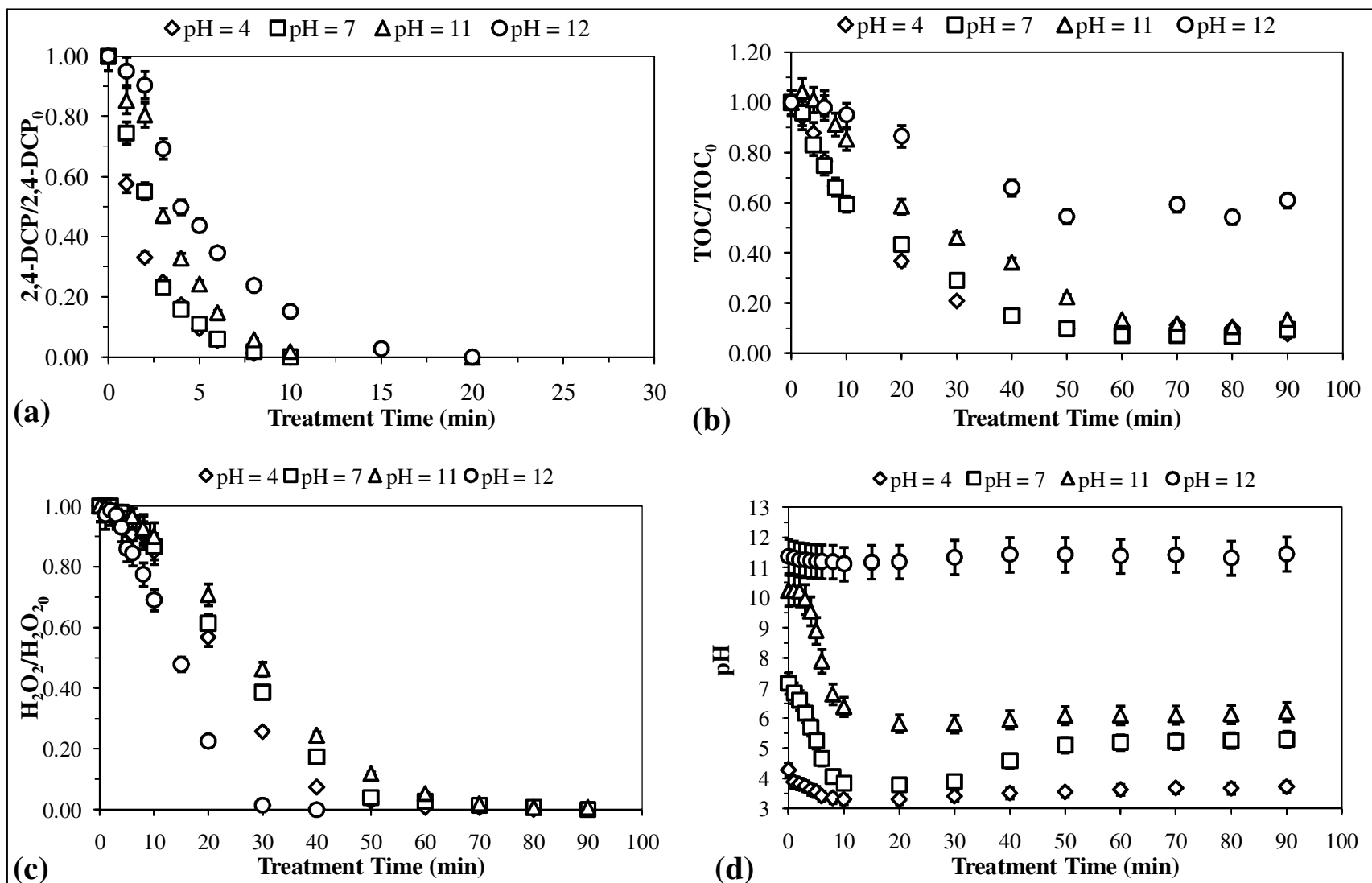


Figure 4.4. Effect of initial pH on the decay of 2,4-DCP (a), TOC (b) and H₂O₂ (c) as well as the pH evolution (d) during H₂O₂/UV-C treatment of 2,4-DCP. Initial experimental conditions: 2,4-DCP = 25 mg L⁻¹ (150 μM), H₂O₂ = 10 mM.

strongly affects the distribution of dissociated and undissociated species. Accordingly, the scientific literature has proved that the light absorbance and photolytic properties of chlorophenols and H_2O_2 are highly dependent on the pH of aqueous chlorophenolic solution (Shen et al., 1995, 1996). The obtained findings in the present work demonstrated that there was practically no difference between the pseudo-first-order 2,4-DCP removal rate coefficients being obtained at the initial pH values of 4 and 7 ($k_{2,4\text{-DCP}} = 0.51 \text{ min}^{-1}$) as given in Table 4.2. However, the pseudo-first-order rate coefficient for TOC removal at $\text{pH}_0 = 4$ (0.050 min^{-1}) was slightly higher than that at $\text{pH}_0 = 7$ (0.045 min^{-1}) during the first 40 min of the $\text{H}_2\text{O}_2/\text{UV-C}$ treatment. When the initial pH was adjusted to alkaline, the pseudo-first-order rate coefficients for 2,4-DCP and TOC removals both decreased, the most pronounced decrease being observed at the initial pH of 12 (0.19 and 0.011 min^{-1} , respectively). The scientific literature has previously reported that the effect of H_2O_2 on the $\text{H}_2\text{O}_2/\text{UV-C}$ treatment of chlorophenols is remarkable at acidic pH, while the photodecomposition of chlorophenols at alkaline pH, particularly above the pK_a value of H_2O_2 , is almost due to the direct photolysis (Kawaguchi, 1993; Hirvonen et al., 2000; Trapido et al., 1997, 1998). The decreased removal rates for both 2,4-DCP and TOC at alkaline initial pH values could be attributed to higher concentration of the anionic form of H_2O_2 (hydro-peroxide anion, HO_2^-) at these pH values which reacts two order faster with HO^\bullet ($k = 7.5 \times 10^9 \text{ M}^{-1} \text{ s}^{-1}$) than that at $\text{pH} < 10$ (Kralik et al., 2010):



The decrease in the parent pollutant and TOC elimination rates at alkaline conditions during the $\text{H}_2\text{O}_2/\text{UV}$ process has also been reported in other studies (Alaton et al., 2002; Schrank et al., 2005; Saritha et al., 2009).

Figure 4.4c demonstrates the effect of initial pH on the decomposition kinetics of H_2O_2 during application of the $\text{H}_2\text{O}_2/\text{UV-C}$ process. The pseudo-first-order rate coefficients for H_2O_2 consumption decreased from 0.044 min^{-1} to 0.025 min^{-1} , when the initial pH was increased from 4 to 11 (Table 4.2). On the other hand, when the initial pH was increased from 11 to 12, the pseudo-first-order rate coefficient for H_2O_2 consumption increased 5-fold. It is known that HO_2^- anions being predominant under alkaline conditions

display a higher molar absorptivity ($240 \text{ M}^{-1} \text{ cm}^{-1}$) than H_2O_2 ($20 \text{ M}^{-1} \text{ cm}^{-1}$) at 253.7 nm (Glaze et al., 1987) according to the following reaction:



This reaction most probably accounts for the much more rapid disappearance of H_2O_2 at $\text{pH} = 12$. On the other hand, rate of the removal of 2,4-DCP which has a $\text{p}K_a$ of 7.85 (Shen et al., 1996) and thus exists almost in phenolate ion at $\text{pH} 12$ (phenolate/phenol = 14125 according to the Henderson-Hasselbalch equation) seems to be only marginally affected by its speciation when considering large absorbance of 2,4-DCP in the alkaline solutions (Shen et al., 1995). Despite the higher molar absorptivity of HO_2^- anion, lower pseudo-first-order rate coefficients being obtained for both 2,4-DCP and TOC removals at $\text{pH} = 12$ (Table 4.2) could be explained by the knowledge that 2 moles of HO^\bullet are formed from H_2O_2 per incident photon absorbed, while from HO_2^- , it is only one (see Equation 4.3). In addition to Equation 4.3, Equation 4.2 and the homogeneous base-catalyzed decomposition of H_2O_2 (Duke and Haas, 1961; Equation 4.4a and b) may also be responsible for the much more rapid disappearance of H_2O_2 at $\text{pH} = 12$:



Figure 4.4d presents temporal evolution of the pH values during $\text{H}_2\text{O}_2/\text{UV-C}$ treatment of 2,4-DCP when started at different initial pH values. pH profiles during the $\text{H}_2\text{O}_2/\text{UV-C}$ process demonstrated that the amount of pH decrease was highest (4.4 pH units) at the initial pH of 11, while pH did not practically change in the solutions being adjusted to 12. On the other hand, the amount of pH rise after the minimum value was highest for the neutral 2,4-DCP solution. The time necessary for the initial pH to reach the minimum value was observed to increase with increasing initial pH (except for $\text{pH} = 12$).

Effect of Initial H_2O_2 Concentration. The third process variable which would have an anticipated effect on the $\text{H}_2\text{O}_2/\text{UV-C}$ process kinetics and efficiency is the initial H_2O_2 concentration, and its effect on the pseudo-first-order rate coefficients and removal

percentages for 2,4-DCP, TOC and H₂O₂ decays are summarized in Table 4.3. In this set of experiments, an initial 2,4-DCP concentration of 25 mg L⁻¹ (150 μM) and an initial pH of 7 were selected. Figure 4.5a and b present the effect of initial H₂O₂ concentration varying between 0 and 40 mM on the kinetics of 2,4-DCP and TOC abatements, respectively. From Figure 4.5a and b, it could be seen that the combination of H₂O₂ with UV-C irradiation at all studied initial H₂O₂ concentrations greatly enhanced the 2,4-DCP and TOC removals. This increase in the 2,4-DCP and TOC removals was mainly caused by HO[•] being generated in the system due to the photolysis of H₂O₂ with the quantum yield of 0.5 at 254 nm (Crittenden et al., 1999):



Table 4.3. The pseudo-first-order rate coefficients and removal percentages for 2,4-DCP, TOC and H₂O₂ decays by the H₂O₂/UV-C process as a function of initial H₂O₂ concentration.

H ₂ O ₂ (mM)	2,4-DCP		TOC		H ₂ O ₂	
	<i>k</i> _{2,4-DCP} (min ⁻¹)	Removal (%)*	<i>k</i> _{TOC} (min ⁻¹)	Removal (%)*	<i>k</i> _{H₂O₂} (min ⁻¹)	Consumption (%)*
0	0.076	91	0.004	16	—	—
2	0.36	100	0.028	92	0.037	100
5	0.49	100	0.062	93	0.045	100
10	0.51	100	0.055	91	0.032	100
15	0.52	100	0.051	91	0.027	100
20	0.41	100	0.050	94	0.021	100
30	0.29	100	0.041	94	0.015	99
40	0.24	100	0.040	94	0.011	99

*After 90 min treatment.

From the experimental results being presented in Table 4.3, it became evident that the pseudo-first-order rate coefficients for 2,4-DCP and TOC removals both increased with increasing H₂O₂ concentration and peaked at 15 mM (*k*_{2,4-DCP} = 0.52 min⁻¹) and 5 mM of H₂O₂ (*k*_{TOC} = 0.062 min⁻¹), respectively, after which H₂O₂ started to inhibit the 2,4-DCP and TOC removals. This is a well known phenomenon from the scientific literature (Ghaly et al., 2001; De et al., 1999) and known as HO[•] scavenging by H₂O₂ beyond a certain case-

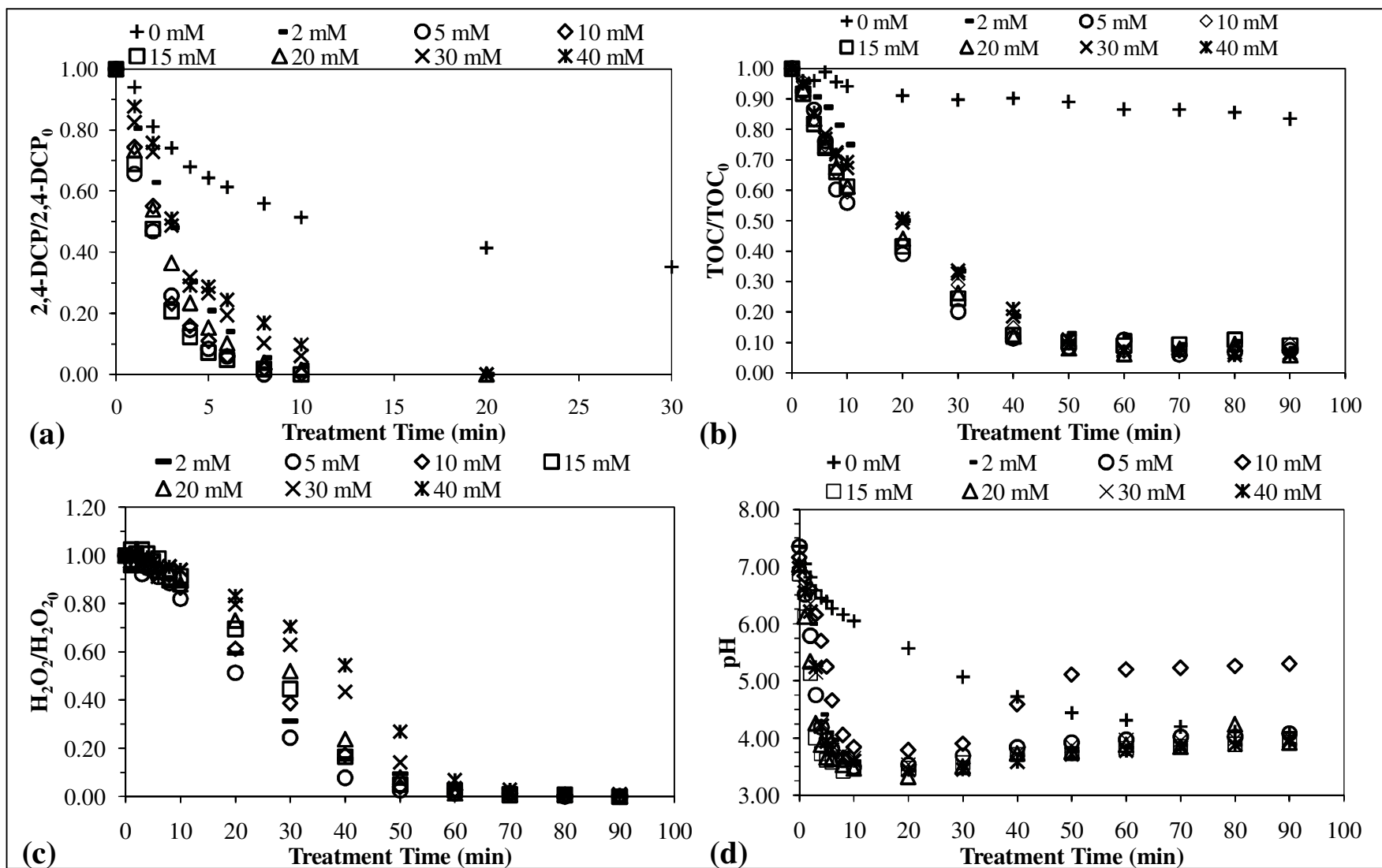


Figure 4.5. Effect of initial H_2O_2 concentration on the decay of 2,4-DCP (a), TOC (b) and H_2O_2 (c) as well as the pH evolution (d) during $\text{H}_2\text{O}_2/\text{UV-C}$ treatment of 2,4-DCP. Initial experimental conditions: 2,4-DCP = 25 mg L⁻¹ (150 μM), pH = 7.

specific concentration with second-order reaction rate coefficients between $1.2\text{-}4.5 \times 10^7 \text{ M}^{-1} \text{ s}^{-1}$ according to the reaction shown below in Equation (4.6);



The reduction potential of HO_2^\bullet is much lower (1.0 V; Mohan and Mittal, 1995) than that of HO^\bullet (2.8 V), and this is most probably the reason for the observed decrease in degradation and mineralization rates. Although the optimum H_2O_2 concentrations necessary for the achievement of maximum pseudo-first-order rate coefficients for 2,4-DCP and TOC removals were found to be different from each other (15 and 5 mM, respectively), the difference between the initial H_2O_2 concentrations of 5 and 15 mM in terms of the pseudo-first-order rate coefficients for 2,4-DCP removal (0.49 and 0.52 min^{-1} , respectively; see Table 4.3) was not significant. Hence, it could be concluded that the optimum H_2O_2 concentration for the treatment of 2,4-DCP-containing water based on the parent pollutant concentration and TOC parameters was 5 mM which corresponds to a H_2O_2 :2,4-DCP molar ratio of about 33:1. This result encourages the cost-effective use of the H_2O_2 /UV-C process for the treatment of waters being contaminated with chlorophenols, since 5 mM of H_2O_2 is a low concentration when considering the low molar absorptivity of H_2O_2 at 253.7 nm ($20 \text{ M}^{-1} \text{ cm}^{-1}$) which generally requires a relatively high dose of H_2O_2 for the efficient degradation and mineralization of refractory pollutants (Pera-Titus et al., 2004). On the other hand, other organic and inorganic constituents being potentially present in real waters which could also compete for HO^\bullet should not be ruled out when applying the H_2O_2 /UV-C process to real environmental matrices, since the presence of such constituents may increase the required H_2O_2 concentration. The results herein demonstrated the importance of optimization of the applied H_2O_2 dose to maximize treatment performance of the H_2O_2 /UV-C process as has also been underlined in many other experimental investigations (Hugül et al., 2000; Kralik et al., 2010; Saritha et al., 2009).

Figure 4.5c presents temporal evolution of the H_2O_2 concentrations varying between 2 and 40 mM during H_2O_2 /UV-C treatment of 2,4-DCP. From Table 4.3, it could be realized that being similar to the case in TOC removals, the pseudo-first-order rate coefficients for H_2O_2 consumption were found to increase up to the initial H_2O_2 concentration of 5 mM

and then decrease again with increasing initial H_2O_2 concentration. Several studies have also reported the decreased consumption rate and percentage of H_2O_2 with increasing H_2O_2 concentration (Hugül et al., 2000; Poulopoulos et al., 2008). Since the addition of higher concentrations of H_2O_2 could result in higher residual concentrations of the oxidant remaining in the reactor at the end of the reaction, and in turn, higher costs of the process, the use of a minimum concentration of H_2O_2 is essential in the $\text{H}_2\text{O}_2/\text{UV-C}$ process.

The pH evolutions at different initial H_2O_2 concentrations are given in Figure 4.5d. The results revealed that at all studied initial H_2O_2 concentrations pH decreased rapidly down to a certain value after which it started to increase again. The situation was different during direct UV-C photolysis of 2,4-DCP where pH decrease continued until the end of the treatment. From the findings, it could be suggested that with all studied H_2O_2 concentrations mineralization of the acidic transformation products to CO_2 took place during $\text{H}_2\text{O}_2/\text{UV-C}$ treatment of 2,4-DCP. The initial H_2O_2 concentration of 15 mM resulted in the most rapid decrease in pH from 6.9 to 3.4 after 8 min $\text{H}_2\text{O}_2/\text{UV-C}$ treatment in correlation with the highest pseudo-first-order rate coefficient for 2,4-DCP removal being achieved with 15 mM H_2O_2 .

4.1.1.3. The Fenton Experiments. Applicability of the Fenton process for the removal of 2,4-DCP was also investigated. The Fenton treatment of 25 mg L^{-1} ($150 \text{ } \mu\text{M}$) 2,4-DCP was carried out using two $\text{H}_2\text{O}_2:\text{Fe}^{2+}$ molar ratios, namely 10:1 ($10 \text{ mM}:1.0 \text{ mM}$) and 50:1 ($10 \text{ mM}:200 \text{ } \mu\text{M}$), and at an initial pH of 3. The calculated pseudo-first-order rate coefficients for 2,4-DCP and TOC removals as well as H_2O_2 consumptions during Fenton treatment of 2,4-DCP are summarized in Table 4.4.

At the $\text{H}_2\text{O}_2:\text{Fe}^{2+}$ molar ratio of 50:1, the complete removal of 2,4-DCP was achieved after approximately 40 min treatment, whereas at the $\text{H}_2\text{O}_2:\text{Fe}^{2+}$ molar ratio of 10:1, 80% of the initially spiked 2,4-DCP could be degraded during the first 3 min of the Fenton treatment. The latter finding proved that the Fenton process was able to remove 2,4-DCP very rapidly during initial stages of the treatment when applied at the $\text{H}_2\text{O}_2:\text{Fe}^{2+}$ molar ratio of 10:1. On the other hand, the removal of 2,4-DCP suddenly slowed down after 3 min Fenton treatment, resulting in the complete degradation of 2,4-DCP after approximately 50 min treatment at the $\text{H}_2\text{O}_2:\text{Fe}^{2+}$ molar ratio of 10:1. From the TOC data,

Table 4.4. The pseudo-first-order rate coefficients and removal percentages for 2,4-DCP, TOC and H₂O₂ decays by the Fenton process as a function of H₂O₂:Fe²⁺ molar ratio.

	H ₂ O ₂ :Fe ²⁺ molar ratio	
	10:1	50:1
$k_{2,4-DCP}$ (min ⁻¹)	n.d. **	0.072
2,4-DCP removal (%)*	100	100
k_{TOC} (min ⁻¹)	0.013	0.010
TOC removal (%)*	32	38
$k_{H_2O_2}$ (min ⁻¹)	n.d. **	0.11
H ₂ O ₂ consumption (%)*	99	100

*After 70 min treatment.

** not determined due to insufficient data.

it could be drawn that the Fenton treatment at both H₂O₂:Fe²⁺ molar ratios resulted in a relatively low TOC removal being ≤ 38%. In addition, no significant difference was found between the H₂O₂:Fe²⁺ molar ratios of 10:1 and 50:1 based on the ultimate TOC removals (Table 4.4). Overall, it could be argued that decreasing the H₂O₂:Fe²⁺ molar ratio from 50:1 to 10:1 by increasing the initial Fe²⁺ concentration from 200 μM to 1.0 mM did not have a net benefit on the 2,4-DCP and TOC removals.

The H₂O₂ decomposition kinetics shared close resemblance with the kinetics of 2,4-DCP removal. At the H₂O₂:Fe²⁺ molar ratio of 50:1, 2,4-DCP and H₂O₂ disappeared in parallel to each other, 95% of the initially added H₂O₂ being decomposed after 40 min Fenton treatment where the complete removal of 2,4-DCP was achieved. On the other hand, at the H₂O₂:Fe²⁺ molar ratio of 10:1, the very sharp decline in the 2,4-DCP concentration being observed after 3 min Fenton treatment was paralleled with an abrupt H₂O₂ decomposition pattern within the same time interval after which the residual H₂O₂ concentration only slightly changed. This was an anticipated outcome considering the catalyzing role of Fe²⁺ on H₂O₂ decomposition with second-order reaction rate coefficient of 63 M⁻¹ s⁻¹ according to the following equation (Arslan-Alaton and Gurses, 2004);



4.1.1.4. The Photo-Fenton Experiments.

Effect of Initial pH. The experimental sets investigating the effect of initial pH on 2,4-DCP and TOC removals as well as H₂O₂ consumption patterns during the photo-Fenton process were conducted under the following initial experimental conditions: 2,4-DCP = 25 mg L⁻¹ (150 μM), Fe²⁺ = 200 μM, H₂O₂ = 10 mM and three initial pH values, namely pH 3, 4 and 5. The pH range of 3-5 was chosen in this study, since this pH range is more relevant in studies concerning the removal of chlorophenols using the dark- and photo-Fenton processes (Ruppert et al., 1993; Basu and Wei, 1998; Ghaly et al., 2001). 2,4-DCP and TOC removals as well as H₂O₂ consumptions were all fitted to the first-order kinetics with $R^2 \geq 0.944$. The pseudo-first-order rate coefficients and conversion percentages for 2,4-DCP and TOC removals as well as H₂O₂ consumptions are summarized in Table 4.5.

Table 4.5. The pseudo-first-order rate coefficients and removal percentages for 2,4-DCP, TOC and H₂O₂ decays by the photo-Fenton process as a function of initial reaction pH.

	pH		
	3	4	5
$k_{2,4-DCP}$ (min ⁻¹)	0.65	0.61	0.63
2,4-DCP removal (%)*	100	100	100
k_{TOC} (min ⁻¹)	0.10	0.058	0.076
TOC removal (%)*	81	79	79
$k_{H_2O_2}$ (min ⁻¹)	0.18	0.12	0.11
H ₂ O ₂ consumption (%)*	100	100	100

*After 90 min treatment.

Reaction pH is one of the most important process parameters in the Fenton and photo-Fenton processes, since iron speciation which in turn determines the UV absorption, complexation and dissolution properties of the catalyst, is strongly affected by pH (Malato et al., 2009). The most suitable pH range for the removal of organic pollutants with the Fenton and photo-Fenton processes has already been established as 2-5 (Arslan-Alaton et al., 2010; Alaton and Teksoy, 2007). Between the pH range of 2-4, higher concentrations of Fe(OH)⁺ have been reported to be generated, and these species have been suggested to have a higher activity than Fe²⁺ in the photo-Fenton reactions (Kuo, 1992). Similarly, a pH of 2.8 has been stated to maximize the concentration of mono- and dihydroxylated Fe³⁺-

aquo complexes, which absorb UV irradiation more efficiently than the non-hydroxylated Fe^{3+} complexes (Malato et al., 2009). In addition, stability and the oxidation potential of HO^\bullet have been explained to be high between this pH range (Hsueh et al., 2005), which could be one of the reasons of the increase in the degradation efficiency within this range. Above this range, precipitation of Fe^{3+} as its hydroxides occurs, reducing its ability to catalyze the decomposition of H_2O_2 (Saritha et al., 2007) and the transmission of the radiation (Faust and Hoigne, 1990) and in turn, decreasing the degradation strongly. The formation of Fe^{2+} complexes with some matrix constituents at operating $\text{pH} > 4$ has also been reported to inhibit the formation of free radicals (Gogate and Pandit, 2004). Similarly, pH values below 2 have also been shown to exert detrimental effects due to the scavenging effect of increasing concentration of H^+ ions on HO^\bullet with second-order reaction rate coefficient of $7 \times 10^9 \text{ M}^{-1} \text{ s}^{-1}$ according to the following equation (Spinks and Woods, 1990):



The decrease in performance of the Fenton process under very acidic conditions has also been suggested to be caused by the low stability of H_2O_2 in very acidic conditions, less susceptibility of the neutral forms of phenols being predominant at very low pH to the electrophilic attack of HO^\bullet compared to their phenolate forms (Lipczynska-Kochany et al., 1995) and the regeneration of parent chlorophenol in strongly acidic solutions as a result of an acid-catalyzed dehydration (Barbeni et al., 1987).

Despite the potential effect of reaction pH on the Fenton and photo-Fenton process kinetics and efficiencies as being discussed in the above paragraph, experimental findings in the present study being presented in Table 4.5 indicated that 2,4-DCP removal rates were not significantly affected by changing the initial reaction pH from 3 to 4 and 5 ($k_{2,4\text{-DCP}} = 0.65, 0.61$ and 0.63 min^{-1} at $\text{pH} = 3, 4$ and 5 , respectively). Temporal change of the normalized 2,4-DCP concentration during application of the photo-Fenton process as affected by the initial reaction pH is presented in Figure 4.6a. From Figure 4.6a, it could be seen that at the investigated pH range of 3-5, 2,4-DCP completely disappeared to non-detectable levels after 8-10 min photo-Fenton treatment. It is thought that the rapid drop in

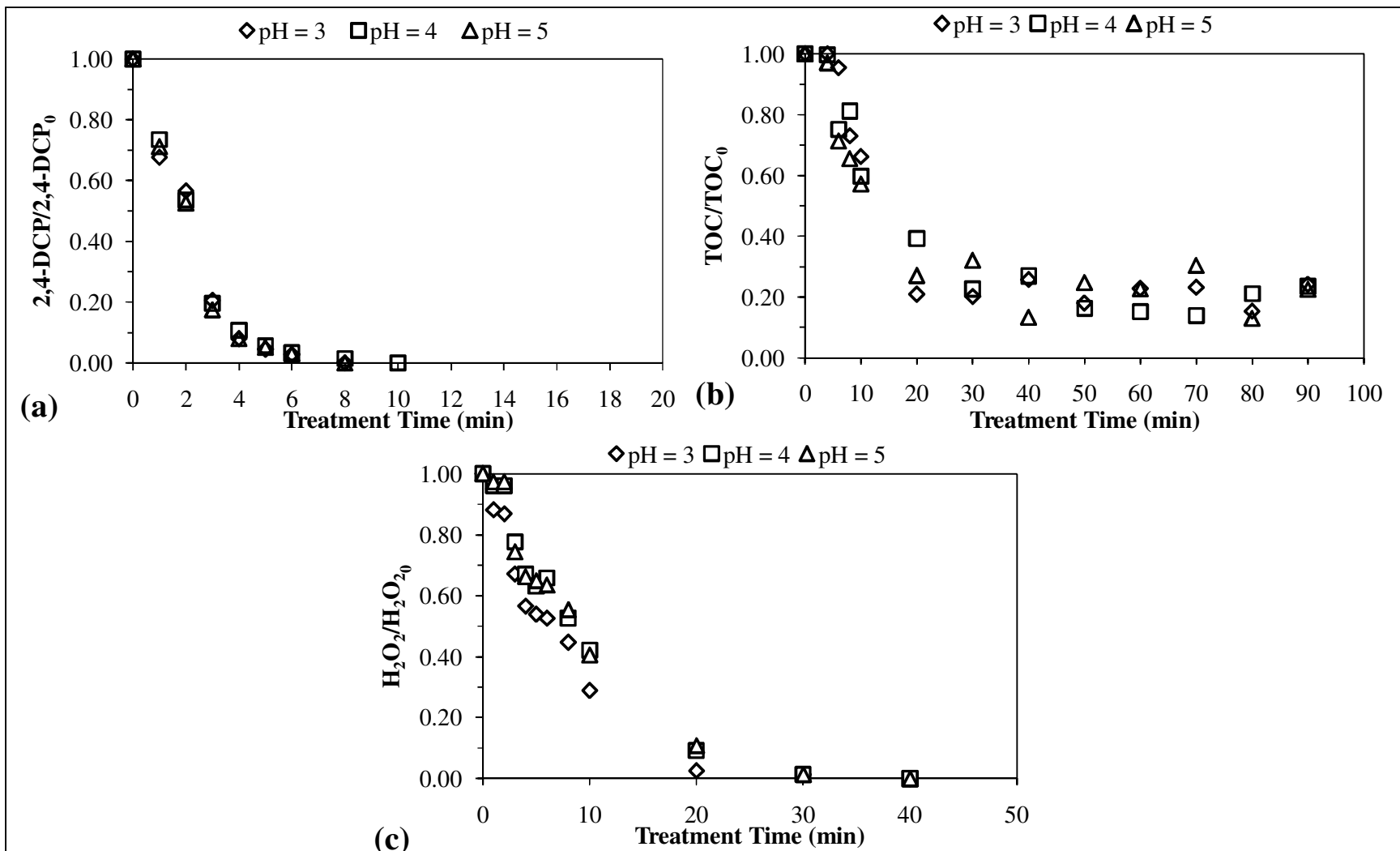


Figure 4.6. Effect of initial pH on the decay of 2,4-DCP (a), TOC (b) and H₂O₂ (c) during photo-Fenton treatment of 2,4-DCP. Initial experimental conditions: 2,4-DCP = 25 mg L⁻¹ (150 μM), H₂O₂ = 10 mM, Fe²⁺ = 200 μM.

pH down to values at which Fe^{2+} efficiently catalyzes the photo-Fenton reaction likely compensated the difference in the initially adjusted pH values.

The photo-Fenton treatment of 2,4-DCP initiated at pH 3 resulted in an appreciably higher mineralization rate ($k_{\text{TOC}} = 0.10 \text{ min}^{-1}$) as compared to experiments that were started at pH 4 and 5 ($k_{\text{TOC}} = 0.058$ and 0.076 min^{-1} , respectively) as given in Table 4.5. The pseudo-first-order rate coefficients for TOC removal were much smaller than those for 2,4-DCP removal. Temporal change of the normalized TOC during application of the photo-Fenton process as affected by the initial reaction pH is presented in Figure 4.6b. From Figure 4.6b, it could be seen that at all studied initial pH values, a minimum of 75% of the initial TOC was degraded after 20-30 min photo-Fenton treatment after which the residual TOC did not significantly change. As a result, complete mineralization of 2,4-DCP by the photo-Fenton process did not occur under the studied experimental conditions, about 2.5 mg L^{-1} TOC remaining in the treated solution after 90 min treatment at all investigated initial pH values. As a whole, it could be postulated that overall treatment results obtained for 2,4-DCP degradation and mineralization were still encouragingly high for the photo-Fenton treatment initiated at pH 5. The experimental results delineated that relatively high pH values could be effectively used for the oxidation of 2,4-DCP by the photo-Fenton process. This issue has some practical importance since decreasing the pH causes inevitable consumption of high amounts of acids and creates a major obstacle for the real-scale application of the photo-Fenton treatment process.

Figure 4.6c presents temporal evolution of the normalized H_2O_2 concentration during photo-Fenton treatment of 2,4-DCP as affected by the initial reaction pH. Most of the H_2O_2 (58-71%) was consumed during first 10 min of the photo-Fenton process at all studied initial reaction pH values. The obtained experimental findings indicated that the pseudo-first-order rate coefficient for H_2O_2 consumption was higher at pH = 3 (0.18 min^{-1}), while it was nearly the same at the pH = 4 and 5 ($k_{\text{H}_2\text{O}_2} = 0.12$ and 0.11 min^{-1} , respectively) as given in Table 4.5. This was most probably caused by the more efficient catalysis of the decomposition of H_2O_2 by Fe^{2+} at pH = 3 due to increase of the amount of soluble irons reacting with H_2O_2 (Zhang et al., 2005) and was in line with faster TOC removal kinetics being obtained at pH = 3. The dependence of continuation of the mineralization on the residual H_2O_2 concentration could be clearly realized from Figures 4.6b and 4.6c,

demonstrating that the residual TOC remained nearly stagnant after 20-30 min photo-Fenton treatment where almost complete consumption of H₂O₂ was obtained at all studied initial pH values.

Effect of Initial Fe²⁺ Concentration. Table 4.6 summarizes the overall pseudo-first-order rate coefficients and conversion percentages for 2,4-DCP and TOC removals as well as H₂O₂ consumptions during application of the photo-Fenton process as affected by the initial Fe²⁺ concentration. Figures 4.7a and b present temporal change of the normalized 2,4-DCP concentration and TOC throughout the course of the photo-Fenton process at different initial Fe²⁺ concentrations. The results indicated that the pseudo-first-order rate coefficients for 2,4-DCP removal were slightly affected by the initial Fe²⁺ concentration. 2,4-DCP degradation kinetics increased until an initial Fe²⁺ concentration of 200 μM was applied ($k_{2,4-DCP} = 0.65 \text{ min}^{-1}$). After this concentration, no significant change was observed in the reaction rate coefficients. However, the effect of initial Fe²⁺ concentration on TOC removal was more pronounced than its effect on 2,4-DCP removal. The pseudo-first-order rate coefficients for TOC removal peaked at 0.10 min⁻¹ at an initial Fe²⁺ concentration of 200 μM. A further increase in Fe²⁺ concentration decreased TOC removal rates due to the fact that the reaction of HO• with Fe²⁺ ($k_{Fe^{2+}; HO\bullet} = 3.0 \times 10^8 \text{ M}^{-1} \text{ s}^{-1}$) became more and more dominant at excessive Fe²⁺ concentrations according to Equation 4.9 (Hsueh et al., 2005);



Considering the above findings, 200 μM Fe²⁺ was found to be convenient for the photo-Fenton experiments which will be described in the forthcoming sections.

Temporal evolution of the normalized H₂O₂ concentrations was also investigated during photo-Fenton treatment of 2,4-DCP as affected by the initial Fe²⁺ concentration, and the results are presented in Figure 4.7c. From Figure 4.7c, it became evident that the initial decomposition rates of H₂O₂ as predicted from the H₂O₂ consumption data after 1 min photo-Fenton treatment were not significantly different within the initial Fe²⁺ concentration range of 100-400 μM. On the other hand, beyond the initial Fe²⁺ concentration of 400 μM (H₂O₂:Fe²⁺ molar ratio = 25:1), the initial decomposition rates of H₂O₂ considerably

increased according to Equation 4.7. However, an interesting pattern was that the stagnant phase being observed after the rapid initial decomposition of H_2O_2 also significantly prolonged above the initial Fe^{2+} concentration of 400 μM . A plausible explanation for this observation could be the formation of a higher concentration of $\text{Fe}^{3+}\text{-H}_2\text{O}_2$ complexes being originated from the oxidation of a higher initial concentration of Fe^{2+} which hinders the subsequent photodissociation of H_2O_2 . This suggests that the rate-limiting step in the photo-Fenton process is the photodecomposition of the formed Fe^{3+} -peroxide intermediate being similar to the reported cases in the thermal Fenton reaction (Pignatello et al., 2006). Overall, based on the H_2O_2 decomposition kinetics during the first 10 min of the photo-Fenton treatment, not a net difference was detected between the studied initial Fe^{2+} concentrations (Table 4.6).

Table 4.6. The pseudo-first-order rate coefficients and removal percentages for 2,4-DCP, TOC and H_2O_2 decays by the photo-Fenton process as a function of initial Fe^{2+} concentration.

Fe^{2+} (μM)	2,4-DCP		TOC		H_2O_2	
	$k_{2,4\text{-DCP}}$ (min^{-1})	Removal (%)*	k_{TOC} (min^{-1})	Removal (%)*	$k_{\text{H}_2\text{O}_2}$ (min^{-1})	Consumption (%)*
100	0.50	100	0.057	76	0.15	100
150	0.50	100	0.058	49	0.11	100
200	0.65	100	0.10	81	0.13	100
400	0.62	100	0.062	57	0.11	100
500	0.63	100	0.051	56	0.13	100
800	0.68	100	0.038	49	0.17	100

*After 90 min treatment.

4.1.1.5. Comparative Evaluation of Kinetics and Efficiencies of the Studied Treatment Processes. After determining the most appropriate reaction conditions ($\text{H}_2\text{O}_2 = 10 \text{ mM}$, $\text{Fe}^{2+} = 200 \mu\text{M}$, $\text{pH} = 7$ for the $\text{H}_2\text{O}_2/\text{UV-C}$ process and $\text{pH} = 3$ for the Fenton and photo-Fenton processes) for effective treatment of aqueous 2,4-DCP by means of the baseline experiments, the $\text{H}_2\text{O}_2/\text{UV-C}$, Fenton and photo-Fenton processes were compared in terms of 2,4-DCP and TOC removals, H_2O_2 consumptions as well as pH and $\text{UV}_{254/280}$ absorbance evolutions. On the other hand, since an initial 2,4-DCP concentration of 75 mg L^{-1} (460 μM) was selected for experiments where transformation product identification and toxicity assessment were targeted, comparative evaluations of the studied treatment processes were made choosing 75 mg L^{-1} initial 2,4-DCP concentration instead of 25 mg L^{-1}

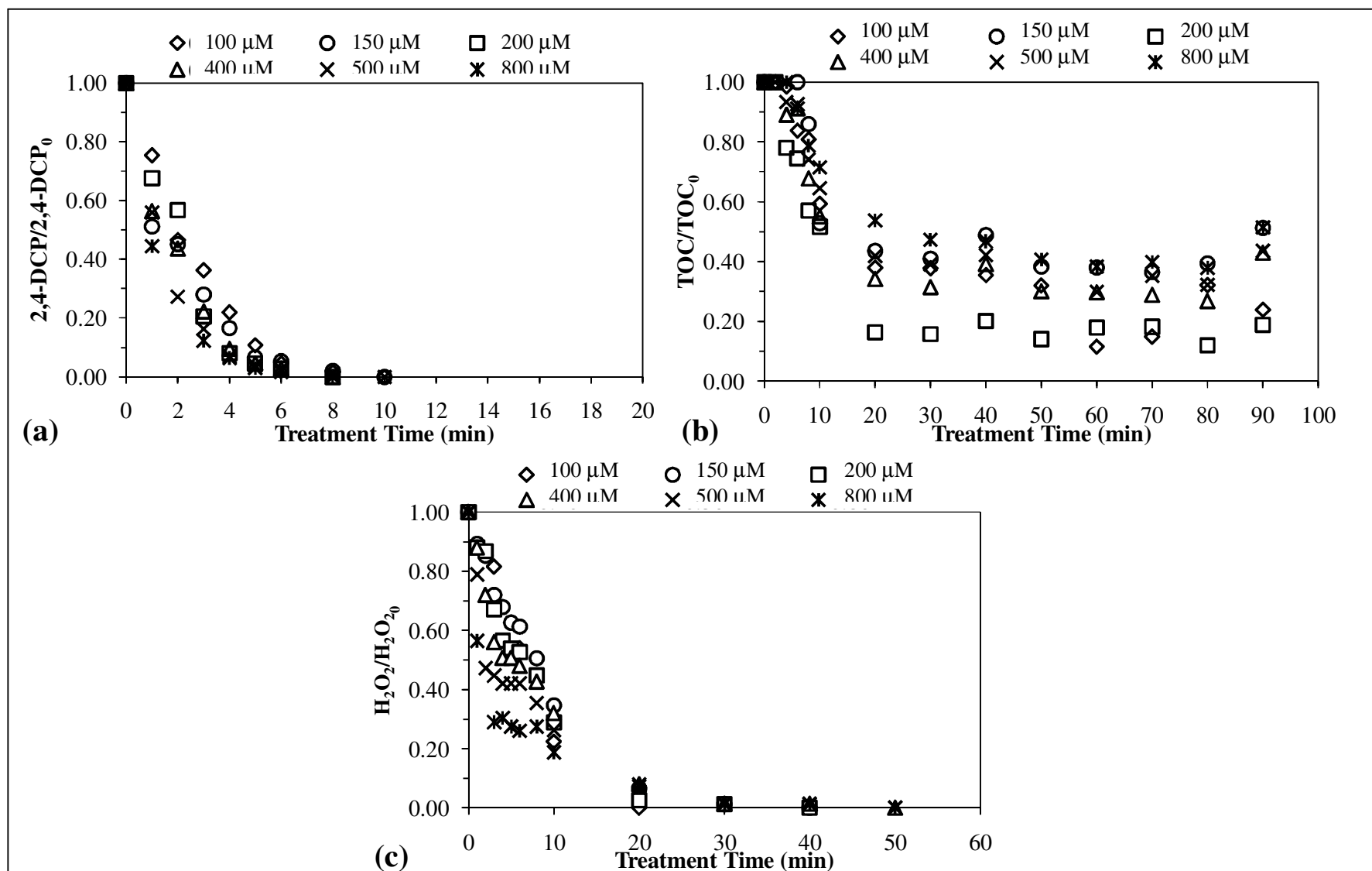


Figure 4.7. Effect of initial Fe^{2+} concentration on the decay of 2,4-DCP (a), TOC (b) and H_2O_2 (c) during photo-Fenton treatment of 2,4-DCP. Initial experimental conditions: 2,4-DCP = 25 mg L⁻¹ (150 μM), H_2O_2 = 10 mM, pH = 3.

¹ (150 μM) 2,4-DCP that was previously used in the baseline runs. UV-C photolysis as a control treatment process was also included in the comparisons.

The degradation of 2,4-DCP with the $\text{H}_2\text{O}_2/\text{UV-C}$, Fenton and photo-Fenton processes as well as UV-C photolysis followed pseudo-first-order kinetics ($R^2 \geq 0.964$) with respect to 2,4-DCP concentration and TOC. In addition, H_2O_2 decomposition kinetics being observed during application of the $\text{H}_2\text{O}_2/\text{UV-C}$, Fenton and photo-Fenton processes were also fitted to the pseudo-first-order reaction kinetics ($R^2 \geq 0.958$). The pseudo-first-order rate coefficients and conversion percentages for 2,4-DCP and TOC removals as well as H_2O_2 consumptions during $\text{H}_2\text{O}_2/\text{UV-C}$, Fenton and photo-Fenton treatment as well as UV-C photolysis of 2,4-DCP are summarized in Table 4.7. It could be demonstrated that 72% 2,4-DCP removal could be achieved via UV-C photolysis after 90 min treatment (Figure 4.8a), whereas no significant mineralization ($\leq 10\%$) was obtained throughout the course of UV-C photolysis (Figure 4.8b). From Figure 4.8d depicting the temporal change of pH during UV-C photolysis of 2,4-DCP, it could be realized that the pH kept decreasing to 3.7 after 90 min UV-C photolysis. The experimental results revealed that the parent pollutant was most rapidly degraded by the photo-Fenton process ($k_{2,4\text{-DCP}} = 0.26 \text{ min}^{-1}$) followed by the $\text{H}_2\text{O}_2/\text{UV-C}$ process ($k_{2,4\text{-DCP}} = 0.17 \text{ min}^{-1}$), the Fenton process ($k_{2,4\text{-DCP}} = 0.098 \text{ min}^{-1}$) and UV-C photolysis ($k_{2,4\text{-DCP}} = 0.040 \text{ min}^{-1}$) as given in Table 4.7. During application of the photo-Fenton treatment, 2,4-DCP disappeared to non-detectable levels after 20 min treatment, while it took up to 70 min with the Fenton's reagent. The enhancement of 2,4-DCP removal rate in the photo-Fenton process was most probably caused by the generation of additional HO^\bullet via photoreduction of Fe^{3+} to Fe^{2+} with a quantum yield of approximately 0.07 at 254 nm according to the following equation (Arslan-Alaton and Gurses, 2004);



Despite complete degradation of 2,4-DCP during application of the dark Fenton's process, 66% of the initial TOC remained in the treated solution after 90 min treatment (Table 4.7), indicating that Fenton's reagent was not effective in 2,4-DCP mineralization; a major limitation of this process as also observed in relevant studies (Arslan-Alaton, 2007;

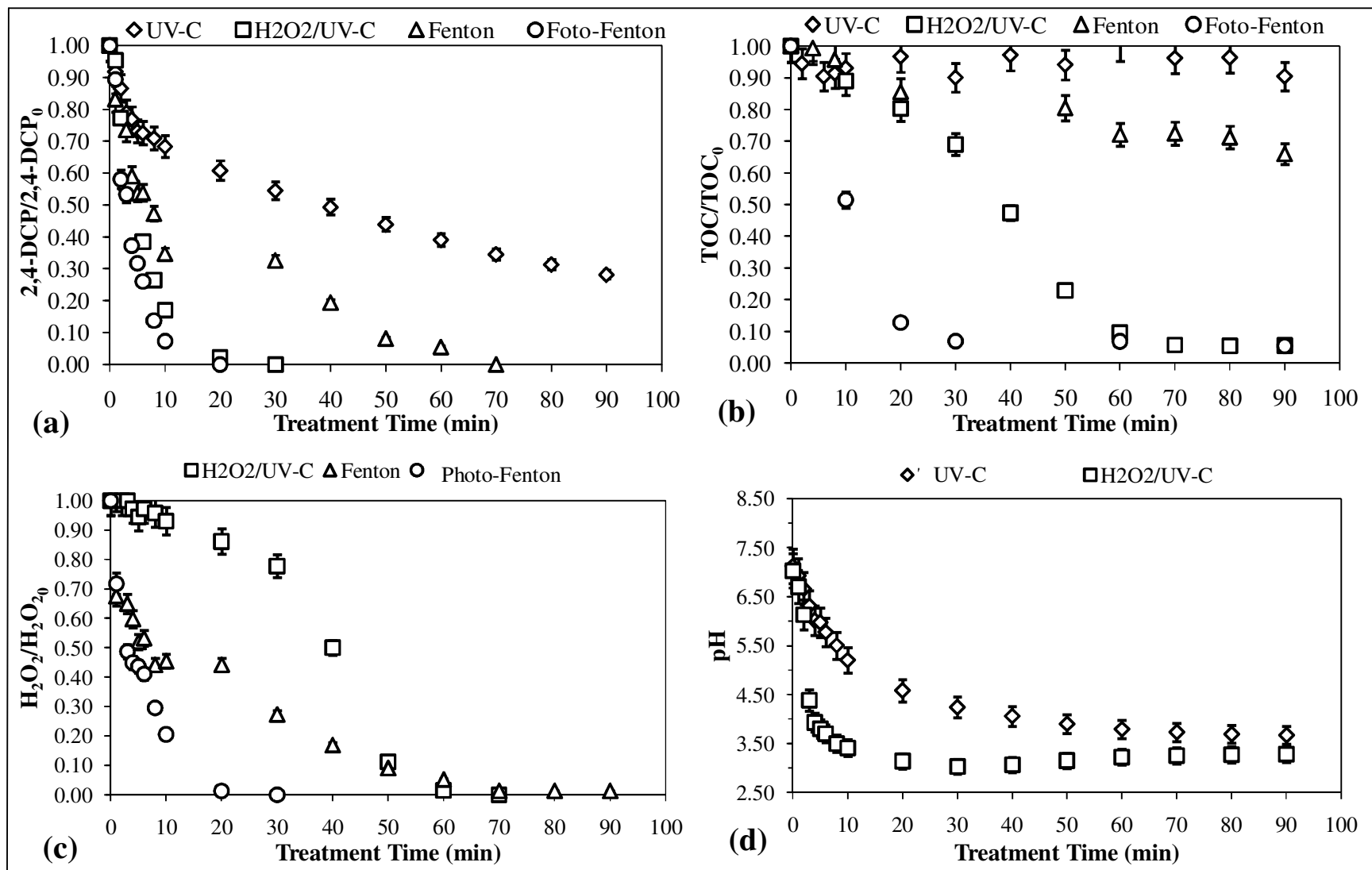


Figure 4.8. Comparison of the decay of 2,4-DCP (a), TOC (b) and H₂O₂ (c) as well as pH change (d) during H₂O₂/UV-C, Fenton and photo-Fenton treatment as well as UV-C photolysis of 2,4-DCP. Initial experimental conditions: 2,4-DCP = 75 mg L⁻¹ (460 μM), H₂O₂ = 10 mM, Fe²⁺ = 200 μM, pH = 7 for UV-C photolysis and the H₂O₂/UV-C process and pH = 3 for the Fenton and photo-Fenton processes.

Zimbron and Reardon, 2009). Although the TOC removal obtained during the first 30 min of the photo-Fenton process was higher as compared with the TOC removal achieved by applying the H₂O₂/UV-C oxidation, it completely stopped after this treatment time, an outcome most probably caused by the complete consumption of H₂O₂ during the first 30 min of the photo-Fenton's reaction. The obtained findings also revealed that UV-C photoreduction of Fe³⁺ was not sufficient to continue significant HO[•] generation after complete exhaustion of H₂O₂ in the photo-Fenton process. The inefficiency of the Fe³⁺/UV-C combination for the mineralization of 2,4-DCP was confirmed by a control experiment conducted with 200 μM of Fe³⁺ and UV-C irradiation. In this experiment, TOC removal obtained after 90 min treatment was low (only 12%; data not shown). Considering the above experimental findings as a whole, the application of the H₂O₂/UV-C and photo-Fenton treatment processes resulted in higher removals both in terms of 2,4-DCP and TOC.

Table 4.7. The pseudo-first-order rate coefficients and removal percentages for 2,4-DCP, TOC and H₂O₂ decays by the studied treatment processes.

	Treatment Process			
	UV-C	H ₂ O ₂ /UV-C	Fenton	Photo-Fenton
$k_{2,4-DCP}$ (min ⁻¹)	0.040	0.17	0.098	0.26
2,4-DCP removal (%)*	72	100	100	100
k_{TOC} (min ⁻¹)	n.d.**	0.012	0.009	0.094
TOC removal (%)*	10	95	34	95
$k_{H_2O_2}$ (min ⁻¹)	—	0.009	0.022	0.21
H ₂ O ₂ consumption (%)*	—	100	99	100

*After 90 min treatment.

**not determined due to insignificant removal.

The absorption spectra of untreated and treated samples during application of the H₂O₂/UV-C, Fenton and photo-Fenton processes as well as UV-C photolysis were depicted in Appendix C. 2,4-DCP had a maximum absorption band at around $\lambda = 280$ nm. The same wavelength was considered to follow dearomatization of the original compound during treatment with AOP and UV-C photolysis. In addition, being characteristic for unsaturated carbon bonds, absorbance at $\lambda = 254$ nm was also followed during the course of the studied treatment processes. Temporal evolution of the UV₂₈₀ and UV₂₅₄ absorbances during

advanced oxidation and UV-C photolysis of 2,4-DCP is presented in Figure 4.9a and b, respectively. UV₂₈₀ absorbing moieties showed an initial increase after 30 min and 3 min of UV-C photolysis and the H₂O₂/UV-C process, respectively. The initial increases being observed in the UV₂₅₄ absorbances were more pronounced than those in the UV₂₈₀ absorbances and were evident for all studied AOP. For UV-C photolysis, however, UV₂₅₄ absorbances were found to gradually increase throughout the course of 90 min treatment being different from the findings obtained for the studied AOP. The increases in UV_{280/254} absorbing moieties (Figure 4.9a and b) can be attributable to the formation of condensation products being typical during HO[•]-mediated as well as photolytic degradation of phenolic compounds (Arslan-Alaton, 2007). The abatement rates of UV_{280/254} absorbances were in the following order: the photo-Fenton process > the H₂O₂/UV-C process > the Fenton process, being the same order established for the pseudo-first-order rate coefficients for 2,4-DCP and TOC removals. Overall, based on the data for the abatements of UV_{280/254} absorbances, it could be concluded that the photo-Fenton followed by the the H₂O₂/UV-C process were most effective in the attack and rupture of high electron density sites, i.e. dearomatization and cleavage of unsaturated carbon bonds.

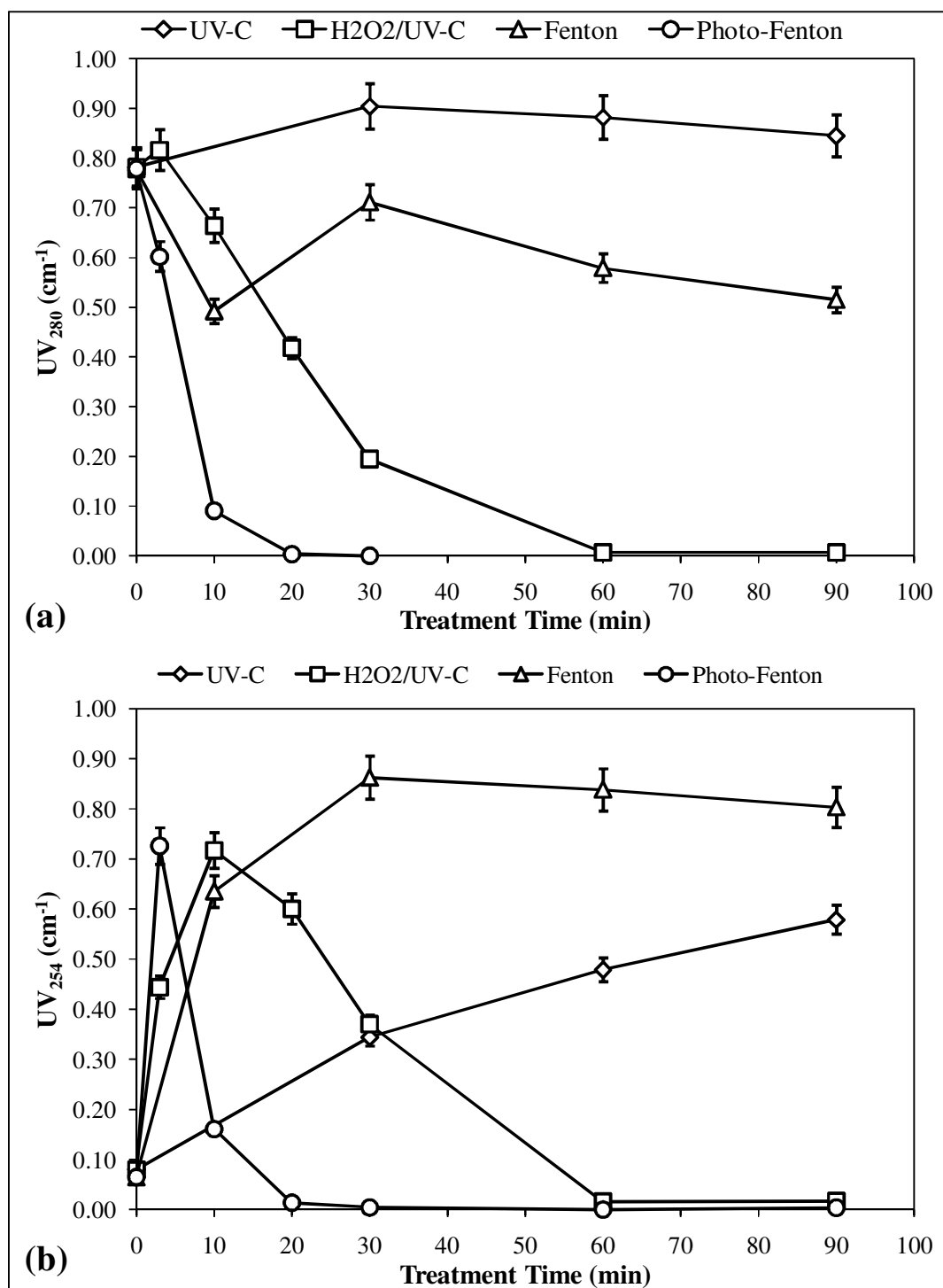


Figure 4.9. Temporal evolution of the UV absorbances at $\lambda = 280$ nm (a) and $\lambda = 254$ nm (b) during UV-C, H₂O₂/UV-C, Fenton and photo-Fenton treatment of 2,4-DCP. Initial experimental conditions: 2,4-DCP = 75 mg L⁻¹ (460 μ M), H₂O₂ = 10 mM, Fe²⁺ = 200 μ M, pH = 7 for UV-C photolysis and the H₂O₂/UV-C process and pH = 3 for the Fenton and photo-Fenton processes.

4.1.2. Evolution of Transformation Products

The main concern about application of AOP is formation of various transformation products as a consequence of the non-selectivity of HO^\bullet , that trigger complex, parallel, consecutive pathways of transformation products (Radjenović et al., 2009). Considering the potential hazards of transformation products of organic pollutants generated during AOP (Rizzo, 2011; Escher and Fenner, 2011), their identification and quantification, as well as elucidation of main reaction mechanisms, are therefore of crucial importance for safe application of such processes for water treatment. The major motivation of this section was to identify the transformation products of 2,4-DCP and highlight the evolution patterns of such products during application of UV-C, $\text{H}_2\text{O}_2/\text{UV-C}$, Fenton and photo-Fenton treatment. For experiments where transformation product identification was targeted, the highest initial 2,4-DCP concentration of 75 mg L^{-1} ($460 \text{ }\mu\text{M}$) studied in the baseline experiments was selected in order to improve the analytical conditions for the detection of transformation products.

4.1.2.1. Chloride Release. Figure 4.10 displays Cl^- release versus treatment time profiles during UV-C, $\text{H}_2\text{O}_2/\text{UV-C}$, Fenton and photo-Fenton treatment of aqueous 2,4-DCP. As is evident from Figure 4.10, the $\text{H}_2\text{O}_2/\text{UV-C}$ process ultimately resulted in a slightly lower Cl^- release than the photo-Fenton process. For both photochemical oxidation processes, dechlorination was practically complete within 20 min so that Cl^- concentrations reached asymptotic values beyond this treatment time. Obtained findings indicated that 2,4-DCP degradation and dechlorination proceeded simultaneously, since 75 mg L^{-1} aqueous 2,4-DCP was completely removed after 20 and 30 min for the photo-Fenton and $\text{H}_2\text{O}_2/\text{UV-C}$ treatment processes, respectively. These results also revealed that dechlorination was one of the initial stages of photochemical 2,4-DCP oxidation as has also been evidenced in former related work (Krebel et al., 2011). The dechlorination trend observed during the Fenton process was somewhat different; it proceeded at a relatively slow rate during the first 10 min of the reaction, but continued until the end of the treatment process,

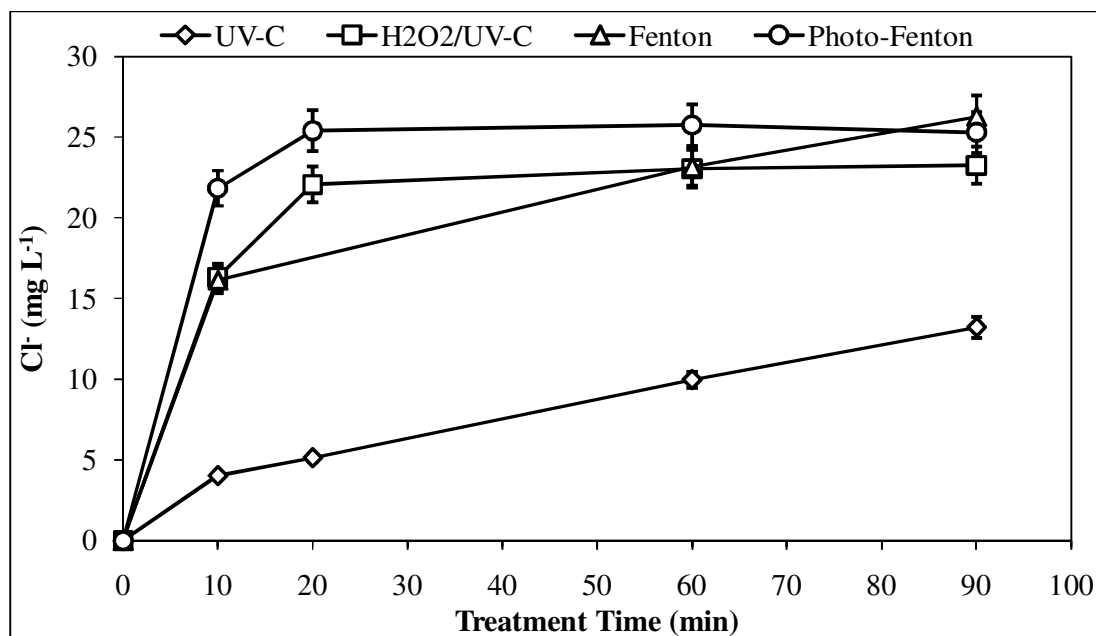


Figure 4.10. Cl⁻ release observed during UV-C, H₂O₂/UV-C, Fenton and photo-Fenton treatment of 2,4-DCP. Initial experimental conditions: 2,4-DCP = 75 mg L⁻¹ (460 μM), H₂O₂ = 10 mM, Fe²⁺ = 200 μM, pH = 7 for UV-C and H₂O₂/UV-C and pH = 3 for Fenton and photo-Fenton treatments.

reaching levels similar to those obtained for the photo-Fenton experiment after around 80 min. The parallel trend between 2,4-DCP removal and Cl⁻ release was also evident for the Fenton's reaction. During UV-C photolysis of 2,4-DCP, Cl⁻ release was also observed, but at a relatively slow rate as compared to the studied AOP. At the end of treatment, 26, 25, 23 and 13 mg L⁻¹ Cl⁻ were obtained for Fenton, photo-Fenton, H₂O₂/UV-C and UV-C treatment, respectively. When the Cl⁻ concentrations released after each treatment processes were compared with the theoretically maximum possible amount of Cl⁻ release of about 33 mg L⁻¹, it was realized that the measured Cl⁻ concentrations were always below the theoretically maximum possible amount of Cl⁻ releases. The amount of Cl⁻ hypothetically found in organic products was calculated as the difference between the amount of Cl⁻ initially found in 2,4-DCP and the amounts of Cl⁻ found in 2,4-DCP and measured in the treated solution at time *t*. According to the calculated Cl mass balances, the amount of Cl⁻ found in products levels after the studied treatment processes followed the order: UV-C (9.3 mg L⁻¹) > Fenton (5 mg L⁻¹) > Photo-Fenton (4 mg L⁻¹) > H₂O₂/UV-

C (3 mg L^{-1}). Mass balances analysis therefore suggested that recalcitrant chlorinated products were formed during all studied treatment processes.

4.1.2.2. Aromatic Transformation Products. Based on the literature review discussed in Section 2.3.1, the potential formation of five selected aromatic compounds, namely phenol (1), catechol (2), hydroquinone (3), benzoquinone (4) and chlorohydroquinone (5) was investigated and compared during 2,4-DCP transformation by UV-C, $\text{H}_2\text{O}_2/\text{UV-C}$, Fenton and photo-Fenton treatment. The 2,4-DCP solution exhibited colour changes during UV-C and $\text{H}_2\text{O}_2/\text{UV-C}$ treatment. It turned from colourless to a light brownish colour after 10 min, fading to yellow and ultimately to colourless after 20 min $\text{H}_2\text{O}_2/\text{UV-C}$ treatment, whereas the colour continuously became darker throughout the course of UV-C photolysis. The yellow colour generated during the oxidation of phenol is believed to be caused by *p*-benzoquinone (Li et al., 2005). The HPLC peak corresponding to *p*-benzoquinone could only be detected after 70 min UV-C photolysis at a low concentration (0.10 mg L^{-1}), therefore the monitoring of its evolution was not allowed by the analytical conditions used. On the other hand, chlorohydroquinone could be followed in the UV-C photolyzed samples, which gradually increased throughout the course of UV-C photolysis reaching 3.4 mg L^{-1} after 90 min treatment. As for the $\text{H}_2\text{O}_2/\text{UV-C}$ process, although catechol formation was peaked after approximately 8 min treatment, its concentration was too low (0.35 mg L^{-1}) for the monitoring of the catechol evolution by the used HPLC method. On the other hand, phenol could be followed in samples treated with the $\text{H}_2\text{O}_2/\text{UV-C}$ process, reaching the highest concentration of 0.71 mg L^{-1} after 6 min treatment and disappeared after approximately 10 min.

Hydroquinone was found to be the only common aromatic transformation product of the studied treatment processes. For comparative purposes, hydroquinone evolution was demonstrated in Figure 4.11 for UV-C, $\text{H}_2\text{O}_2/\text{UV-C}$, Fenton and photo-Fenton treatment. Hydroquinone concentration did not significantly increase during the course of the UV-C photolysis (from 0.21 mg L^{-1} after 40 min treatment to 0.27 mg L^{-1} after 90 min treatment), speculatively due to the parallel transformation of hydroquinone into other oxidation products. As is obvious from Figure 4.11, the highest hydroquinone formation of 1.5 mg L^{-1} was found during $\text{H}_2\text{O}_2/\text{UV-C}$ treatment of 2,4-DCP, while the lowest hydroquinone generation was observed during UV-C photolysis. During the $\text{H}_2\text{O}_2/\text{UV-C}$ process, hydro-

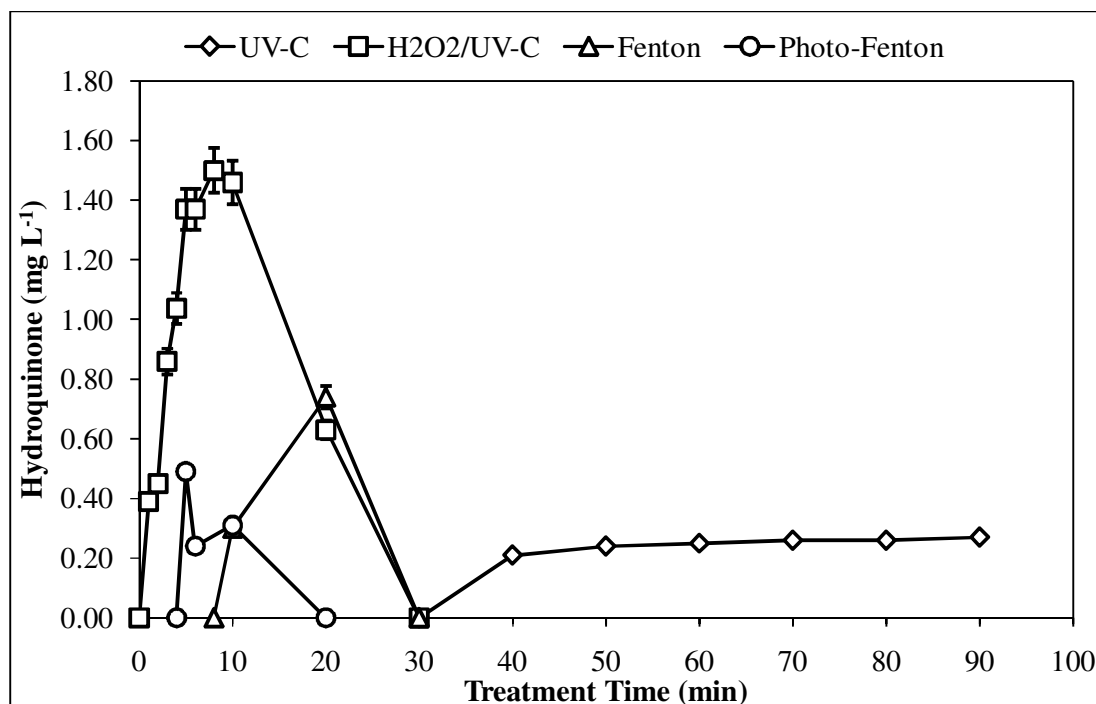


Figure 4.11. Temporal evolution of hydroquinone during UV-C, H₂O₂/UV-C, Fenton and photo-Fenton treatment of 2,4-DCP. Initial experimental conditions: 2,4-DCP = 75 mg L⁻¹ (460 μM), H₂O₂ = 10 mM, Fe²⁺ = 200 μM, pH = 7 for UV-C and H₂O₂/UV-C and pH = 3 for the Fenton and photo-Fenton treatments.

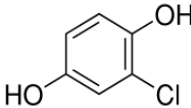
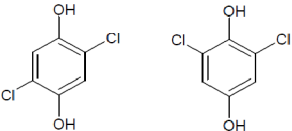
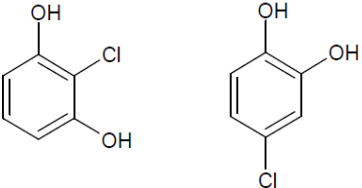

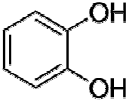

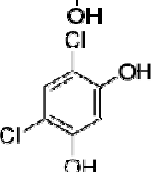
quinone concentration increased very rapidly during the first 5 min of the reaction, peaked after about 10 min and completely disappeared after 30 min treatment. On the other hand, dark Fenton's reaction of 2,4-DCP resulted in a maximum hydroquinone formation of 0.74 mg L⁻¹ after 20 min treatment. In conclusion, obtained experimental findings delineated that hydroquinone did not accumulate in the reaction solution and during all studied AOP, hydroquinone could be further degraded, whereas the H₂O₂/UV-C and Fenton processes required longer treatment times for disappearance of hydroquinone to non-detectable levels as compared to the photo-Fenton process. On the other hand, the formed hydroquinone persisted after applying UV-C photolysis, indicating that UV-C irradiation alone was relatively inefficient for the degradation of hydroquinone generated during treatment.

For the mass spectrometric analysis of the transformation products of chlorophenols, GC-MS has been largely used in previous studies (Pera-Titus et al., 2004). For this reason, besides the HPLC measurements of the selected transformation products, GC-MS analyses

were also performed on samples which were subjected to UV-C, H₂O₂/UV-C, Fenton and photo-Fenton treatment in order to characterize the identity of the formed products. The obtained findings are summarized in Table 4.8. Chlorinated transformation products (chlorohydroquinone, dichlorohydroquinone and chlorobenzenediol) were most detected in samples taken after UV-C and H₂O₂/UV-C treatment. The non-chlorinated transformation products catechol and hydroquinone were also detected in the UV-C photolyzed samples taken after 60-90 min treatment. In addition to catechol and hydroquinone, the non-chlorinated 1,3-cyclopentenedione was also apparent with its characteristic fragmentation pattern (*m/z* 31, 42 and 96) in the UV-C treated samples, but only after 40 min photolysis, most probably due to its relatively low concentration generated during UV-C photolysis. Photodecomposition of aqueous pentachlorophenol has been previously reported to give a dichloro-substituted form of 1,3-cyclopentenedione which was most likely originated from the oxidative ring cleavage of the corresponding hydroquinone and/or resorcinol structures (Wong and Crosby, 1981). The non-chlorinated products started to form only after 40 min UV-C photolysis in relation with the relatively slow 2,4-DCP degradation kinetics observed in that treatment process. 4,6-dichlororesorcinol was detected at the initial stages (3-10 min) of the H₂O₂/UV-C process, but not in UV-C photolysis, as a result of direct attack of HO[•] to the non-substituted *meta* position of 2,4-DCP with respect to the —OH group. The H₂O₂/UV-C process ensured disappearance of all identified transformation products to non-detectable levels after a maximum of approximately 20 min treatment which was not the case in UV-C photolysis where the formed transformation products excluding 1,3-cyclopentenedione were all present in the treated solution after 90 min treatment in parallel with the insignificant mineralization ($\leq 10\%$) obtained by this treatment process.

According to the obtained GC-MS data presented in Table 4.8, the only identified transformation product of the Fenton treatment was chlorohydroquinone, which was detected after 10 min reaction and disappeared after 30 min treatment. At the initial stages (3 min) of the photo-Fenton treatment, 4,6-dichlororesorcinol was also detected in addition to chlorohydroquinone. The generation of chlorohydroquinone and hydroquinone (the latter assessed by the HPLC measurements, as seen in Figure 4.11) as the common transformation products of the studied treatment processes suggested that the

Table 4.8. Transformation products identified by GC-MS during UV-C, H₂O₂/UV-C, Fenton and photo-Fenton treatment of 2,4-DCP.

Name	Structure	<i>m/z</i> (Relative Abundance)	Retention Time (min)	Treatment Process/Time (min)
Chlorohydroquinone		144 (100); 52 (68); 80 (34); 146 (33)	18	UV-C/30, 40, 60, 90 H ₂ O ₂ /UV-C/3, 10, 20 Fenton/10 Photo-Fenton/3
2,5-Dichlorohydroquinone or 2,6-Dichlorohydroquinone		178 (100); 32 (97); 180 (55); 182 (10)	19	UV-C/30, 40, 60, 90 H ₂ O ₂ /UV-C/3, 10, 20
2-Chlororesorcinol or 4-Chlorocatechol		144 (100); 63 (33); 146 (31)	21	UV-C/30, 40, 60, 90 H ₂ O ₂ /UV-C/3, 10, 20
1,3-Cyclopentenedione		31 (100); 42 (49); 96 (49)	3.9	UV-C/40
Catechol		110 (100); 32 (61); 64 (35)	13	UV-C/60, 90
Hydroquinone		110 (100); 32 (42); 81 (35); 53 (33)	16	UV-C/90
4,6-Dichlororesorcinol		178 (100); 180 (61); 32 (45); 51 (31); 86 (24); 115 (22); 182 (11)	18	H ₂ O ₂ /UV-C/3, 10 Photo-Fenton/3

disappearance of chlorohydroquinone during the studied treatment processes proceeds via a dechlorination pathway where it is transformed into hydroquinone. Based on the overall GC-MS findings, a general pathway for the degradation of 2,4-DCP during application of UV-C, $H_2O_2/UV-C$, Fenton and photo-Fenton treatments is represented in Figure 4.12. Accordingly, an initial HO^\bullet addition to the aromatic ring and dechlorination should be the governing mechanism for the studied AOP. The possible addition of Cl^\bullet to the aromatic ring, however, should not be ruled out as evident from the generation of dichlorohydroquinone. By contrast, formation of the hydroxylated transformation products during UV-C photolysis of 2,4-DCP could be mainly explained by the homolytic cleavage of the C—Cl bond yielding the hydroxyphenyl radical and its subsequent reaction with dissolved oxygen in the water, as has been suggested by Al-Ekabi et al. (1989).

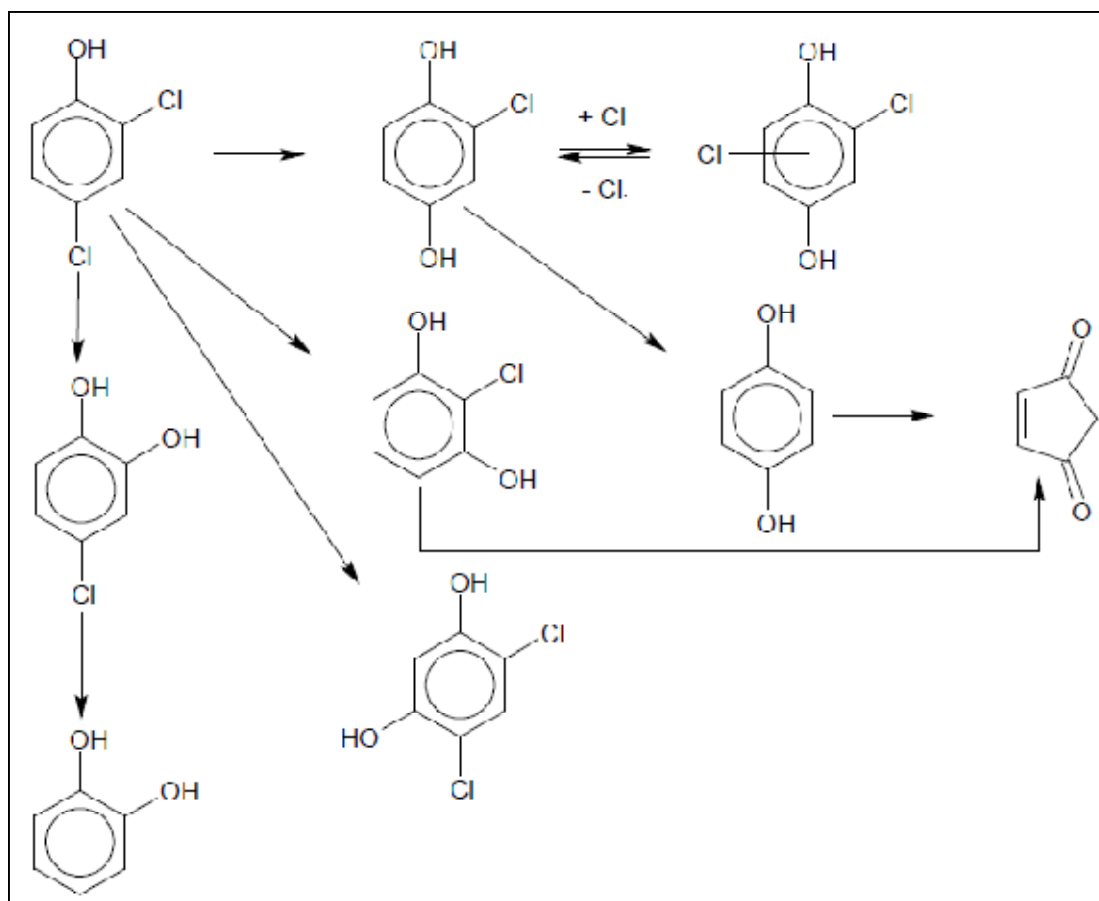


Figure 4.12. A general scheme describing the degradation routes of 2,4-DCP by UV-C, $H_2O_2/UV-C$, Fenton and photo-Fenton treatments based on the GC-MS results.

4.1.2.3. Aliphatic Transformation Products. The above-discussed GC-MS findings mainly clarified the formation patterns of the initial transformation products being aromatic in nature. However, the identities and evolution trends of the late transformation products, most likely polar and non-volatile in nature, remained still unknown. To address this question, aliphatic transformation products, namely C1-C4 carboxylic acids and aldehydes, were analyzed in the treated samples. In general, maleic and fumaric acids have been reported to be generated at the first stages following the cleavage of the aromatic ring, which was followed by the formation of simpler structured carboxylic acids including formic, acetic and oxalic acids (Gu et al., 2008; Zazo et al., 2005). Accordingly, temporal evolution of maleic and fumaric acids was first investigated during application of the studied AOP and represented in Figure 4.13.

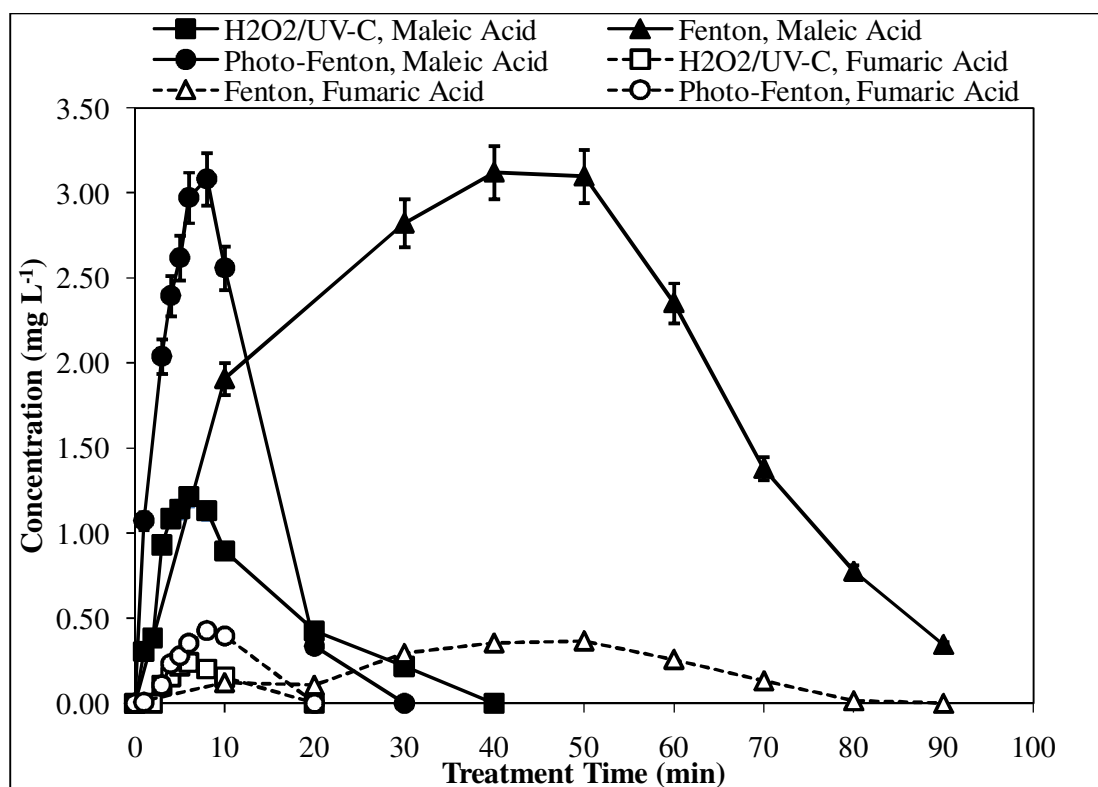


Figure 4.13. Temporal evolution of maleic and fumaric acids during H₂O₂/UV-C, Fenton and photo-Fenton treatment of 2,4-DCP. Initial experimental conditions: 2,4-DCP = 75 mg L⁻¹ (460 μM), H₂O₂ = 10 mM, Fe²⁺ = 200 μM, pH = 7 for the H₂O₂/UV-C and pH = 3 for the Fenton and photo-Fenton processes.

For the sake of simplicity, the UV-C findings were not included in Figure 4.13. During application of UV-C photolysis, the formation pattern of maleic acid presented similarities with that of hydroquinone (Figure 4.11), which appeared after approximately 30 min UV-C photolysis and slowly increased to 0.84 mg L^{-1} after 90 min treatment. On the other hand, its *trans* isomer fumaric acid could not be detected at measurable concentrations in the UV-C photolyzed samples. According to the obtained experimental results given in Figure 4.13, maleic and fumaric acids were found to be the common aliphatic oxidation products for all studied AOP. Although the formation of maleic and fumaric acids was evident as soon as the treatment was started in all studied AOP, it took a longer time (40-50 min) for maleic and fumaric acids to reach their peak concentrations via the Fenton process as compared to the $\text{H}_2\text{O}_2/\text{UV-C}$ and photo-Fenton processes in parallel to the slower 2,4-DCP removal kinetics observed in the Fenton process. Due to the relatively high recalcitrance of maleic and fumaric acids upon the Fenton oxidation, their concentration decreased more slowly in the later stages of the Fenton treatment as compared to the $\text{H}_2\text{O}_2/\text{UV-C}$ and photo-Fenton processes, which resulted in a residual maleic acid concentration of 0.34 mg L^{-1} after 90 min Fenton treatment. The peak maleic and fumaric acids concentrations obtained after approximately 8 min photo-Fenton treatment (3.1 and 0.43 mg L^{-1} , respectively) were found to be near to the levels generated during application of the Fenton process (3.1 and 0.37 mg L^{-1} , respectively), whereas the $\text{H}_2\text{O}_2/\text{UV-C}$ process resulted in the formation of significantly lower concentrations of maleic and fumaric acids (1.2 and 0.24 mg L^{-1} , respectively) after about 6 min treatment. An important observation was that the maximum formed maleic and fumaric acid concentrations were negatively correlated with the peak hydroquinone concentrations via the studied AOP (Figure 4.11), suggesting that maleic and fumaric acids were in part originated from the oxidative cleavage of hydroquinone ring. Overall, the experimental findings indicated that maleic and fumaric acids could be degraded to non-detectable levels after 20-40 min treatment by applying the $\text{H}_2\text{O}_2/\text{UV-C}$ and photo-Fenton processes.

The simpler structured saturated carboxylic acids, i.e. formic, acetic and oxalic acids, were also analyzed in the treated samples. According to the analytical results, oxalic acid could only be reliably detected after approximately 70 min UV-C photolysis, increasing to 1.2 mg L^{-1} after 80 min treatment and remaining nearly stagnant thereafter. Although from the scientific literature, it is known that oxalic acid gives complexes with Fe^{3+} ,

speculatively leading to false negative results in solutions treated by iron-based AOP (Brillas et al., 1998), the exact reason of why oxalic acid was not detected during application of the Fenton and photo-Fenton processes in this study remains unknown. However, the absence of oxalic acid in treated samples throughout the course of Fe^{3+} -mediated UV-C photolysis (data not shown) favored the argument of the formation of Fe^{3+} -oxalate complexes.

Evolution of acetic and formic acids during treatment of 2,4-DCP via the $\text{H}_2\text{O}_2/\text{UV-C}$, Fenton and photo-Fenton processes is displayed in Figure 4.14a and b, respectively. Again, for simplicity, UV-C photolysis data were not included in Figure 4.14a and b. During UV-C photolysis, acetic acid formation was first evident after 20 min treatment, increasing to 11 mg L^{-1} after 50 min treatment and very slightly decreasing to 10 mg L^{-1} after 90 min UV-C photolysis. In parallel to the slight degradation of acetic acid observed between 50-90 min of the UV-C photolysis, a slight, but gradual accumulation of formic acid to 6.5 mg L^{-1} was evident, suggesting that the generated formic acid was originated by the parallel transformation of acetic acid in the reaction medium. According to Figure 4.14b, formic acid was found to be the common aliphatic transformation product of the studied AOP, whereas acetic acid was not detected in 2,4-DCP solutions treated with the $\text{H}_2\text{O}_2/\text{UV-C}$ process. The acetic acid evolution pattern was different for the Fenton and photo-Fenton treatment of 2,4-DCP; more acetic acid was generated during the Fenton process (41 mg L^{-1}) than in the photo-Fenton process (25 mg L^{-1}). The higher acetic acid production in the Fenton process as compared to the photo-Fenton process could be due to the behaviour of acetic acid as a photo-active complex in the presence of Fe^{3+} at acidic pH resulting in its faster oxidation in photo-Fenton treatment (Kavitha and Palanivelu, 2004). During application of the Fenton treatment, acetic acid formation started immediately, and its concentration continued to increase up to 40 min treatment at a slower rate than in the photo-Fenton process. Acetic acid disappeared to non-detectable levels at the end of the treatment. Unlike acetic acid, formic acid remained almost unchanged throughout the Fenton's reaction. These findings imply that formic acid could not be further oxidized via the dark Fenton process, and the introduction of UV-C light was necessary to enable its further oxidation. Among the studied treatment processes, the highest formic acid formation (20 mg L^{-1}) was observed during the $\text{H}_2\text{O}_2/\text{UV-C}$ treatment of 2,4-DCP, and its

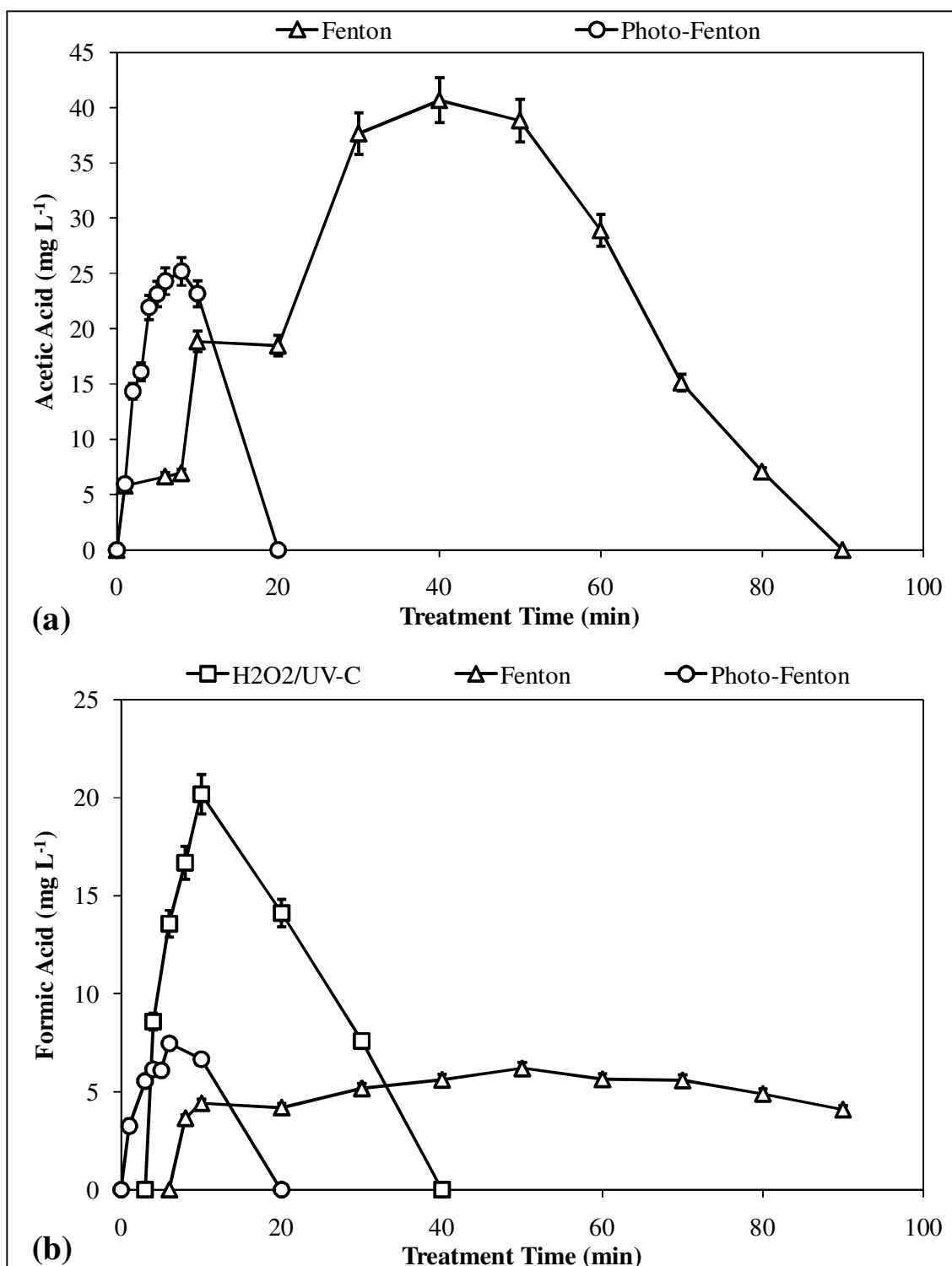


Figure 4.14. Temporal evolution of acetic acid (a) and formic acid (b) during H₂O₂/UV-C, Fenton and photo-Fenton treatment of 2,4-DCP. Initial experimental conditions: 2,4-DCP = 75 mg L⁻¹ (460 μM), H₂O₂ = 10 mM, Fe²⁺ = 200 μM, pH = 7 for the H₂O₂/UV-C and pH = 3 for the Fenton and photo-Fenton processes.

degradation was complete after 40 min treatment which was twice the time required for formic acid removal with the photo-Fenton process.

Although less frequently reported as compared to the aliphatic carboxylic acids, aldehydes with an aliphatic structure could also form as a result of oxidative cleavage of the aromatic ring during AOP treatment of chlorophenols (Abe and Tanaka, 1997; Cravotto et al., 2010). Therefore, aldehyde evolution was also investigated in this study, however rather as a sum parameter. Temporal evolution of aldehydes during the studied treatment processes is presented in Figure 4.15.

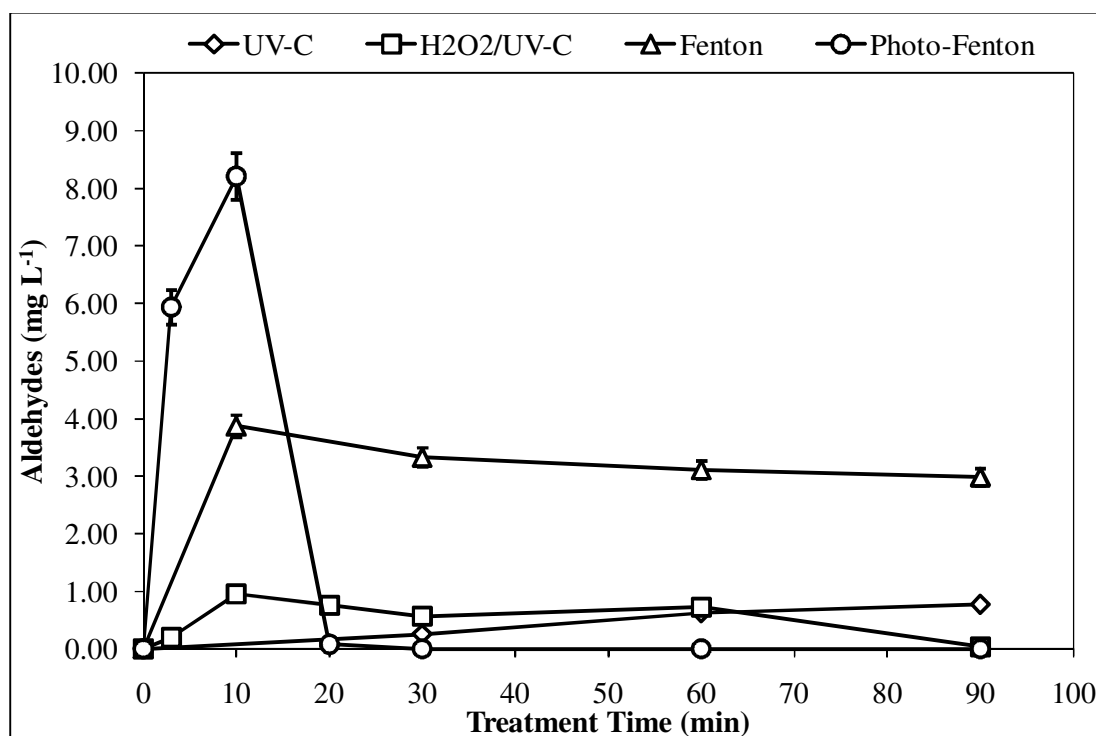


Figure 4.15. Temporal evolution of aldehydes during UV-C, H₂O₂/UV-C, Fenton and photo-Fenton treatment of 2,4-DCP. Initial experimental conditions: 2,4-DCP = 75 mg L⁻¹ (460 μM), H₂O₂ = 10 mM, Fe²⁺ = 200 μM, pH = 7 for UV-C and H₂O₂/UV-C and pH = 3 for Fenton and photo-Fenton treatments.

Aldehydes were formed during application of each studied treatment processes. A slow, but gradual accumulation of aldehydes to 0.77 mg L⁻¹ was evidenced throughout the course of UV-C photolysis in parallel to the slow 2,4-DCP and TOC removal kinetics achieved by this treatment process. On the other hand, it became evident from Figure 4.15

that during application of the H₂O₂/UV-C, Fenton and photo-Fenton processes, the aldehyde concentrations first increased to the peak concentrations of 0.96, 3.9 and 8.2 mg L⁻¹, respectively, after 10 min treatment and decreased thereafter. However, a slight re-increase in the aldehyde concentration from 0.56 mg L⁻¹ to 0.73 mg L⁻¹ was observed after 60 min H₂O₂/UV-C treatment. Considering that the highest formic acid formation was obtained during H₂O₂/UV-C treatment which was followed by the photo-Fenton and Fenton processes (Figure 4.14b), it was speculated that formaldehyde was quickly oxidized once it was produced during the H₂O₂/UV-C process to generate formic acid. Overall, the experimental findings indicated that the H₂O₂/UV-C and photo-Fenton processes were capable of nearly completely degrading the formed aldehydes, whereas a major fraction of the generated aldehydes (3.0 mg L⁻¹) was still present in the treated solution after 90 min Fenton treatment.

4.1.2.4. LC-MS Analyses. LC-MS analyses primarily aimed at characterizing the chemical structures of transformation products which were highly polar (e.g., chlorinated aliphatic transformation products) and thus could not be identified by means of GC-MS. Proposed identities of overall transformation products generated during UV-C, H₂O₂/UV-C, Fenton and photo-Fenton treatment of 2,4-DCP are listed in Table 4.9.

Table 4.9. Proposed identities of transformation products formed during UV-C, H₂O₂/UV-C, Fenton and photo-Fenton treatment of 2,4-DCP.

Indication ^a	Compound	Ionization mode	Mass (<i>m/z</i>)
(1)	Chlorobenzenediol	[M-H] ⁻	143
(2)	Dichlorobenzenediol	[M-H] ⁻	177/179
(3)	Trichlorodihydroxybiphenyl	[M-H] ⁻	287/289
(4)	2,4-Dichlorohexanedioic acid	[M-H] ⁻	213/215
(5)	Chlorocyclohexene-1,4-dione	[M+H] ⁺	145/147
(6)	Formic acid	[M-H] ⁻	45
(7)	Chloromethanediol	[M-H] ⁻	81/83
(8)	Oxalic acid	[M-H] ⁻	89
(9)	Malonic acid	[M-H] ⁻	103
(10)	Malic acid	[M-H] ⁻	133
(11)	Chloromaleic acid	[M-H] ⁻	149/151

Table 4.9. *Continued*

Indication ^a	Compound	Ionization mode	Mass (<i>m/z</i>)
(12)	2,3,4,5-Tetrahydroxycyclohexa-2,4-diene-1-carboxylic acid	[M-H] ⁻	187
(13)	2-Hydroxy-3,5-dichloro-1,4-benzoquinone	[M-H] ⁻	191/193
(14)	2-Chloro-3,4-dihydroxypent-2-enedioic acid	[M-H] ⁻	195
(15)	Maleic acid	[M-H] ⁻	115
(16)	Chloromalonic acid	[M-H] ⁻	137
(17)	2-Chloro-4-hydroxybenzaldehyde	[M-H] ⁻	155/157
(18)	3,5-Dichlorohexa-3,5-dien-2-one	[M+H] ⁺	165
(19)	Dibenzodioxin	[M+H-1] ⁺	184
(20)	4-Chlorodibenzo[<i>b,d</i>]furan-2,8-diol	[M-H] ⁻	233
(21)	8-Chlorooxanthrene-2-carboxylic acid	[M-H] ⁻ [M+H] ⁺	260/261 263
(22)	5-Chlorobiphenyl-2,2'-dicarboxylic acid	[M-H] ⁻	274/275
(23)	1-Chloro-2,3-dihydroxyprop-2-ene-1,1,3-tricarboxylic acid	[M-H] ⁻	239

^a The compound indication numbers of identified products correspond to those in Figures 4.16-4.18.

Proposed pathways for the generation of photolysis products during UV-C treatment of 2,4-DCP are schematized in Figure 4.16. From the LC-MS data, it was evidenced that four types of transformation products were formed during UV-C photolysis of 2,4-DCP. The first group consisted of chlorobenzenediols, namely chloro- (1) and dichlorobenzenediol (2). As was discussed previously to explain the GC-MS findings, hydroxylated derivatives of 2,4-DCP have been proposed to be generated via the homolytic cleavage of the C—Cl bond yielding the hydroxyphenyl radical and the subsequent reaction of this radical with molecular oxygen. As has been reviewed by Czaplicka (2006), the Cl atom is photo-reactive more in *ortho*- and *para*-position than in *meta*-position, so the photolytic transformation of 2,4-DCP into chlorohydroquinone and *p*-chlorocatechol

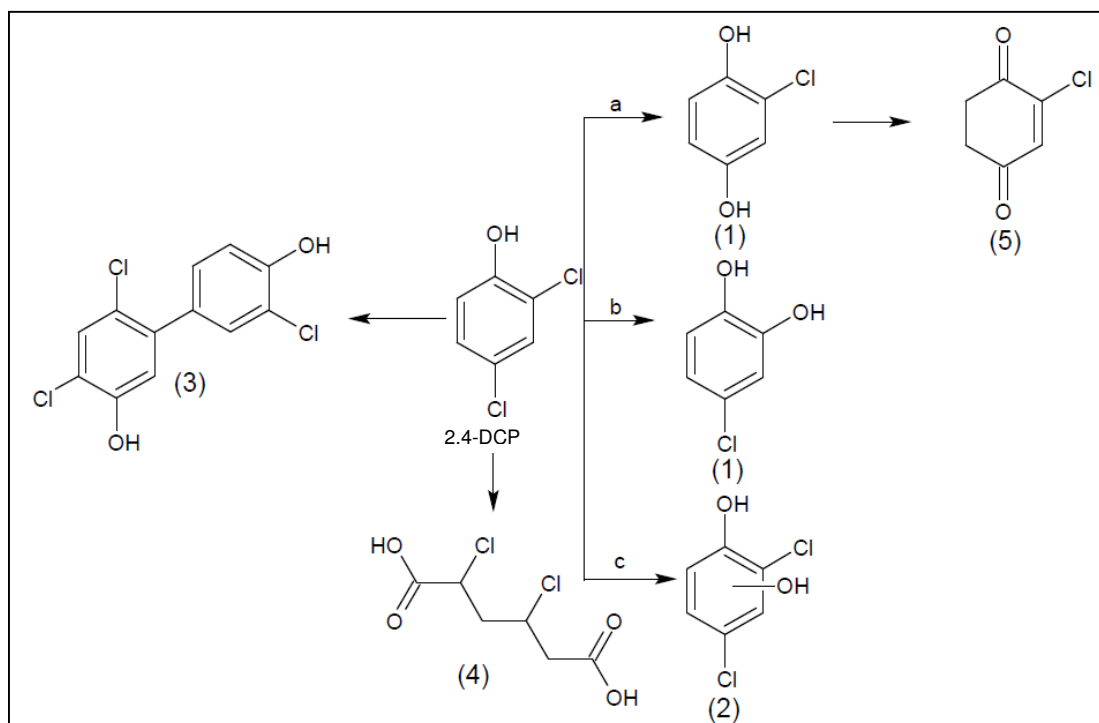


Figure 4.16. Proposed pathway for UV-C photolysis of 2,4-DCP based on LC-MS data.

(route a and b in Figure 4.16, respectively) is more possible. On the other hand, the formation of dichlorobenzenediol indicated that a —OH group was added to the aromatic ring of 2,4-DCP without any dechlorination. The hydroxyphenyl radical being responsible for the generation of chlorobenzenediol could also be a precursor of the second type transformation product in this study, i.e. biphenyl derivatives, as has also been suggested by Al-Ekabi et al. (1989). Accordingly, trichlorodihydroxybiphenyl (3) was detected in the UV-C photolyzed samples as a result of the coupling of the generated chloro hydroxyphenyl radicals. 2,4-dichlorohexanedioic acid (4), the third type of photolysis product of a chlorinated and saturated dicarboxylic acid structure was speculatively formed as a result of the hydrogenation of 2,4-DCP to 2,4-dichlorocyclohexanol followed by the oxidation of 2,4-dichlorocyclohexanol to 2,4-dichlorohexanedioic acid. In fact, the generation of cyclohexanyl type compounds during UV-induced photodegradation of NP-10, a nonylphenol ethoxylated surfactant, has been previously reported (Chen et al., 2007a, 2007b). Another molecular ion with m/z 194.36-194.54 was also found to gradually increase throughout the course of UV-C photolysis of 2,4-DCP, presumably originating from the deprotonation of another carboxylic acid molecule, but it could not be reliably proposed as a photolysis product due to the interferent molecular ions having similar

masses. The fourth type of transformation product was characterized with a cyclic diketone structure bearing an unsaturated C=C bond and a —Cl group which was proposed as chlorocyclohexene-1,4-dione (5). Although m/z 145 also corresponded to the protonated form of chlorobenzenediol, it was distinguished from chlorobenzenediol with the different temporal evolution patterns observed for m/z 143 and 145. The formation of chlorocyclohexene-1,4-dione could be explained by the partial hydrogenation of chloro-*p*-benzoquinone, a transformation product whose generation has been previously reported during photodegradation of chlorophenols (Tamer et al., 2006).

Masses and proposed identities and degradation pathways of transformation products formed during H₂O₂/UV-C treatment of 2,4-DCP are presented in Table 4.9 and Figure 4.17. The experimental results regarding the H₂O₂/UV-C treatment of 2,4-DCP delineated that direct addition of HO• to the aromatic ring without dechlorination first resulted in the formation of the major molecular ion of m/z 177 (2). Formation of hydroxylated 2,4-DCP as a result of the H₂O₂/UV treatment of 2,4-DCP has been already demonstrated in the scientific literature (Hirvonen et al., 2000), which is in line with the suggestions in the present study. Further hydroxylation of the aromatic ring without dechlorination and subsequent oxidation of —OH groups to carbonyl brought about the formation of a chlorohydroxybenzoquinone product (13) which was evident from the molecular ions of m/z 191 and 193. The molecular ion of m/z 187 (12) was supposed to be formed by means of a Kolbe-like reaction via the reaction of phenoxide ion with carbon dioxide which was accompanied by the nucleophilic substitution of HO• with Cl. From Figure 4.17, it could be concluded that the H₂O₂/UV-C-treated solution was predominantly constituted by ring cleavage products. A number of saturated and unsaturated aliphatic mono- and dicarboxylic acids, from the simplest formic acid of m/z 45 (6) to the largest molecule 2,4-dichlorohexanedioic acid of m/z 213 and 215 (4), were detected. Formation of these carboxylic acids was paralleled by a sharp decrease in pH and aromaticity represented by the collective parameter UV₂₈₀. The results were in line with the findings obtained via the HPLC analyses.

Table 4.9 and Figure 4.18 present masses and proposed identities of transformation products and their degradation pathways for the Fenton treatment of 2,4-DCP based on LC-MS data. The Fenton and H₂O₂/UV-C treatment of 2,4-DCP showed distinct

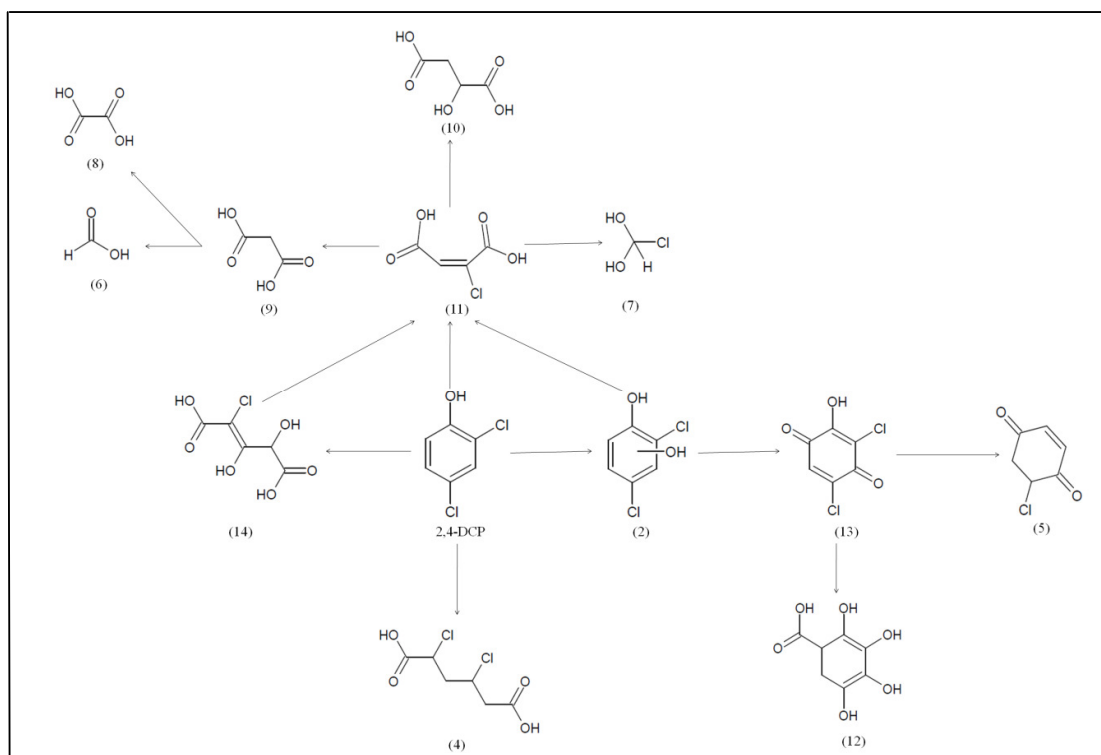


Figure 4.17. Transformation products identified by means of LC-MS during degradation of 2,4-DCP via the $\text{H}_2\text{O}_2/\text{UV-C}$ process and proposed degradation pathway.

differences in the transformation product distribution and mechanistic aspects. Transformation products generated during application of the Fenton process could be classified under two categories: a) hydroxylation, dechlorination and ring cleavage products, and b) condensation products. Several transformation products in the first category, namely oxalic acid of m/z 89 (8), chloromethanediol of m/z 81 and 83 (7), chlorocyclohexenedione of m/z 145 and 147 (5) and tetrahydroxycyclohexadienecarboxylic acid of m/z 187 (12) were found to be the common oxidation intermediates of the Fenton and $\text{H}_2\text{O}_2/\text{UV-C}$ processes. Additional aldehydic and ketonic transformation products were detected during application of the Fenton process and identified as 2-chloro-4-hydroxybenzaldehyde of m/z 155 and 157 (17) and 3,5-dichlorohexa-3,5-dien-2-one of m/z 165 (18). On the other hand, the major difference between the Fenton and $\text{H}_2\text{O}_2/\text{UV-C}$ processes was the condensation products generated in the former process. The suggested condensation products included dibenzodioxin of m/z 184 (19), 4-chlorodibenzo[*b,d*]furan-2,8-diol of m/z 233 (20), 8-chlorooxanthrene-2-carboxylic acid of m/z 260/261 (21) and 5-chlorobiphenyl-2,2'-dicarboxylic acid of m/z 274/275 (22). Formation of condensation products upon Fenton and photo-Fenton oxidation of chlorophenols has been reported in

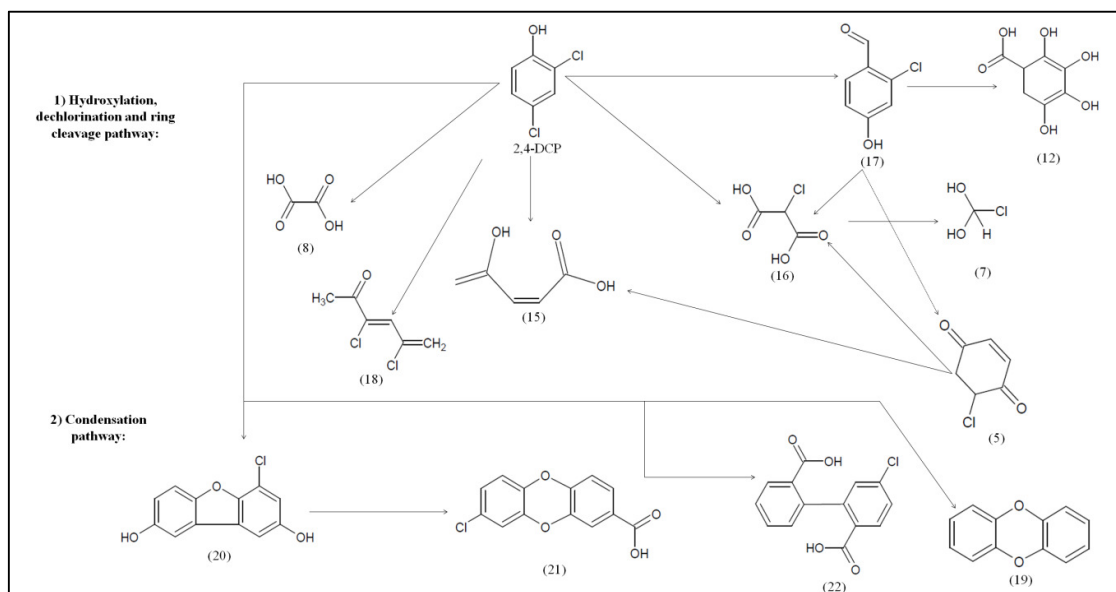


Figure 4.18. Transformation products of 2,4-DCP identified by means of LC-MS during application of the Fenton process and proposed degradation pathway.

the scientific literature and suggested to be caused by a variety of combinations of resonance-stabilized radicals originating from the substituted or nonsubstituted dihydroxycyclohexadienyl radicals (Munoz et al., 2011; Poerschmann et al., 2009; Fukushima and Tatsumi, 2001). In a more recent study, Fenton oxidation of the landfill leachates has been demonstrated to cause the formation of polychlorinated dibenzodioxins and dibenzofurans which increased sample toxicity (Vallejo et al., 2013). Overall, it could be argued that condensation products generated via the Fenton process contributed to the overall TOC remaining after treatment.

LC-MS analyses of the photo-Fenton-treated samples revealed that product distribution in the photo-Fenton process was very similar to that in the Fenton process. Masses and proposed identities and degradation pathways of transformation products formed during photo-Fenton treatment of 2,4-DCP are presented in Table 4.9 and Figure 4.19. Similar to the case in the Fenton process, detected transformation products were predominated by condensation products being relatively refractory to further oxidation which suggested that a close resemblance existed between degradation pathways of 2,4-DCP via the Fenton (Figure 4.18) and photo-Fenton processes (Figure 4.19). As a result, the relatively low residual TOC remaining after 90 min photo-Fenton treatment (1.8 mg L^{-1}) was speculated to be mainly contributed by the condensation products. In fact, the lower

number of transformation products in the Fenton- and photo-Fenton-treated samples than in the UV-C- and H₂O₂/UV-C-treated samples as assessed by the GC-MS analyses could be accounted for by the generation of this type of higher molecular weight products during application of the Fenton and photo-Fenton processes.

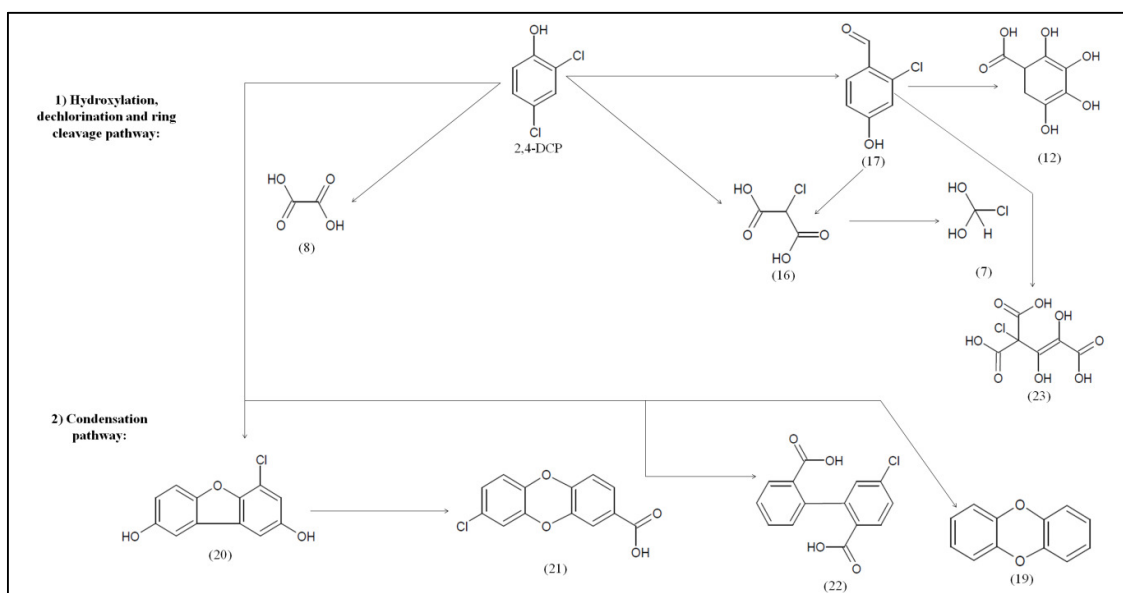


Figure 4.19. Transformation products of 2,4-DCP identified by means of LC-MS during application of the photo-Fenton process and proposed degradation pathway.

4.1.3. Toxicity Evolution During Transformation of 2,4-DCP

It has been previously reported that photolysis and AOP may cause the formation of undesired transformation products which exert a higher toxic impact than the parent compounds (Fernández-Alba et al., 2002; Fatta-Kassinos et al., 2011). For this reason, two toxicity types, i.e. acute toxicity and genotoxicity, were assessed during application of UV-C, H₂O₂/UV-C, Fenton and photo-Fenton treatment processes for the removal of aqueous 2,4-DCP. Relationships between the formed transformation products and observed toxic effects were evaluated and discussed in the following paragraphs.

4.1.3.1. Acute Toxicity Evolution. Figure 4.20 presents changes in percent relative inhibition after exposing *V. fischeri* to raw (untreated) 2,4-DCP in the concentration range of 0.39 to 50 mg L⁻¹ (2.4-307 μM). According to Figure 4.20, the *EC*₅₀ and *EC*₂₀ of 2,4-DCP were found as 8.4 and 4.2 mg L⁻¹, respectively, indicating that 2,4-DCP is toxic towards *V. fischeri*. The measured *EC*₅₀ of 8.4 mg L⁻¹ that was outside the range of 1.2-6.1 mg L⁻¹ reported in the scientific literature for the Microtox® toxicity of 2,4-DCP (Bojanowska-Czajka et al., 2010) could be ascribed to potential differences in testing conditions including the purity of used test chemicals and equipments in the two commercial test systems (BioTox™ and Microtox®).

Table 4.10 shows changes in the acute toxic effect of 2,4-DCP towards *V. fischeri* in terms of percent relative inhibition of the luminescence intensities during UV-C (pH 7), H₂O₂/UV-C (pH 7), Fenton (pH 3) and photo-Fenton (pH 3) treatment of 75 mg L⁻¹ (460 μM) 2,4-DCP versus treatment time for 10 mM H₂O₂ and 200 μM Fe²⁺. As can be seen from Table 4.10, during UV-C photolysis the acute toxicity of 2,4-DCP first diminished from 86 (± 11)% to 78 (± 1.0)% after 30 min treatment. Thereafter, the inhibitory effect slightly increased reaching 84 (± 0.23)% after 40 min UV-C photolysis. The trends observed in the acute inhibitory effect during UV-C photolysis of 2,4-DCP were investigated in parallel to the evolution of transformation products as assessed by LC-MS analyses. The observed changes in the acute toxic effect in the early stages of UV-C treatment were paralleled by the formation of four chlorinated transformation products, namely chlorobenzenediol, dichlorobenzenediol, trichlorodihydroxybiphenyl and chlorocyclohexenedione which were indicated by the numbers (1), (2), (3) and (5), respec-

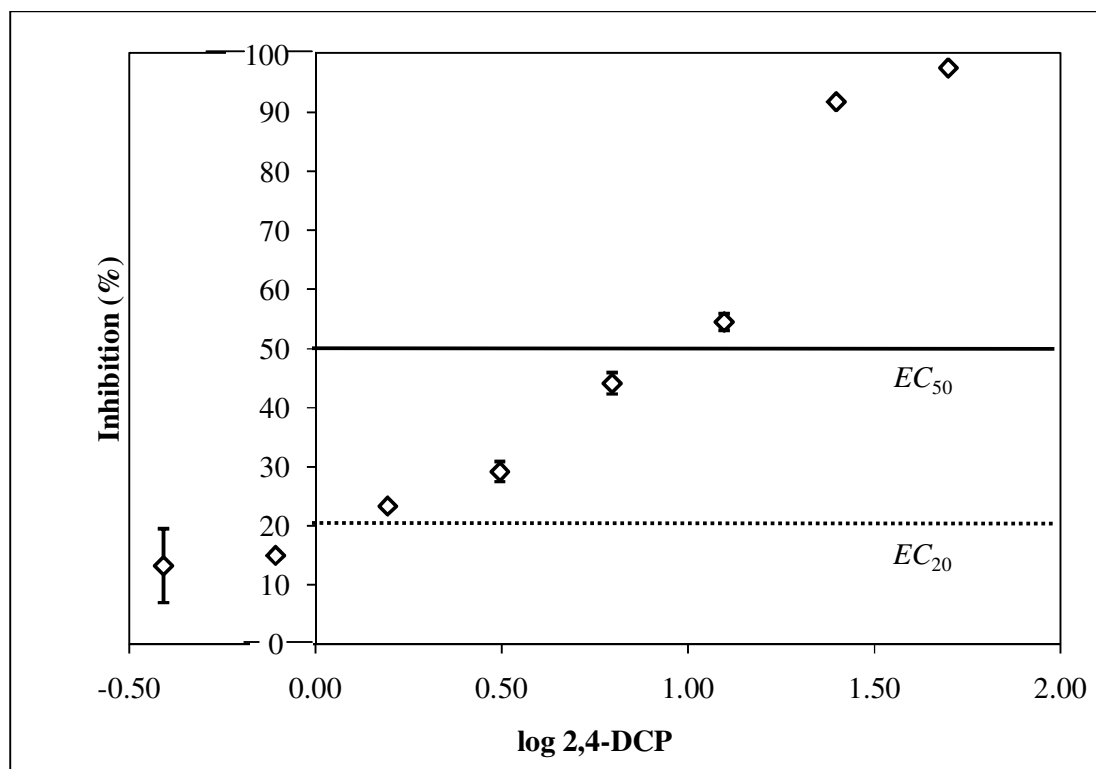


Figure 4.20. Changes in percent relative inhibition within the 2,4-DCP concentration range of 1.6-50 mg L⁻¹ (9.8-307 μM).

tively in Figure 4.16. In a previous study, 4-chlorocatechol, a chlorobenzenediol, has been reported to be generated as a result of UV irradiation of *p*-chlorophenol exerting an EC_{50} of 5.9 mg L⁻¹ on *V. fischeri* which was at the same order of magnitude as that of the parent pollutant (Krebel et al., 2011). These authors have also concluded that unidentified chlorinated photolysis products as evident from the discrepancy between theoretical and experimentally found adsorbable organic halogen content should be taken into account in explaining the observed toxicity as well. For the other possible chlorobenzenediol, i.e. chlorohydroquinone, an EC_{50} value of 5.8 mg L⁻¹ on *V. fischeri* has been reported in the scientific literature (Kaiser and Palabrica, 1991). On the other hand, particularly after 60 min UV-C photolysis, acute inhibitory effect caused by the treated solution relatively efficiently decreased due to the 2,4-DCP removal above 61% (Table 4.10) which was accompanied by a decrease in the signal intensities of chlorobenzenediol, dichlorobenzenediol and chlorocyclohexenedione and the generation of 2,4-dichlorohexanedioic acid indicated by the number (4) in Figure 4.16. It should also be emphasized here that the incomplete degradation of 2,4-DCP, chlorobenzenediol, dichloro-

Table 4.10. Acute toxic effects observed during UV-C, H₂O₂/UV-C, Fenton and photo-Fenton treatment of 2,4-DCP.

Treatment Process and Time	Inhibition (%)	2,4-DCP Removal (%)	TOC Removal (%)
Original 2,4-DCP solution (75 mg L ⁻¹ , 460 μM)	86 (± 11)	—	—
<i>UV-C photolysis</i>			
30 min	78 (± 1.0)	46	≤ 10
40 min	84 (± 0.23)	51	≤ 10
60 min	74 (± 1.1)	61	≤ 10
90 min	34 (± 0.83)	72	≤ 10
<i>H₂O₂/UV-C</i>			
10 min	81 (± 0.61)	83	11
20 min	20 (± 0.26)	98	20
30 min	17 (± 1.2)	100	31
60 min	59 (± 6.9)	100	90
90 min	76 (± 0.14)	100	95
<i>Fenton</i>			
10 min	79 (± 0.81)	65	≤ 10
30 min	69 (± 1.0)	80	14
60 min	54 (± 1.5)	95	28
90 min	54 (± 3.2)	100	34
<i>Photo-Fenton</i>			
10 min	35 (± 1.4)	93	48
20 min	21 (± 2.8)	100	87
30 min	3.6 (± 2.2)	100	93
60 min	2.3 (± 3.3)	100	93
90 min	10 (± 5.3)	100	95

benzenediol and chlorocyclohexenedione together with the persistence of trichlorodihydroxybiphenyl accounted for the insignificant TOC removal obtained throughout 90 min UV-C photolysis.

For the H₂O₂/UV-C process, the acute inhibitory effect only slightly decreased from 86 (± 11)% to 81 (± 0.61)% during first 10 min of the H₂O₂/UV-C treatment, although 83% 2,4-DCP removal was achieved within this time interval (Table 4.10), indicating that relatively toxic transformation products were formed during initial stages of the H₂O₂/UV-C treatment. For the purpose of supporting this suggestion, acute inhibitory effects were evaluated in relation with transformation products identified by LC-MS throughout the

course of the H₂O₂/UV-C process. Figure 4.21a, b, c and d present relationships between the measured acute inhibitory effect and identified 2,4-DCP transformation products whose signal intensities peaked after 10, 20, 30 and 90 min H₂O₂/UV-C treatment, respectively. From the patterns given in Figure 4.21a, it was evidenced that the slight decrease in the acute inhibitory effect observed during first 10 min of the H₂O₂/UV-C process was accompanied by the formation of chloromaleic acid, dichlorobenzenediol, hydroxydichlorobenzoquinone and 2,4-dichlorohexanedioic acid which were indicated by the numbers (11), (2), (13) and (4), respectively in Figure 4.21a. Between 10 and 20 min treatment, however, a very fast detoxification was observed in parallel to the degradation of the above-mentioned transformation products which was accompanied by the generation of the non-chlorinated carboxylic acids malic acid and tetrahydroxycyclohexadiene carboxylic acid indicated by the numbers (10) and (12), respectively in Figure 4.21b. In fact, a higher *EC*₅₀ value for malic acid (59 mg L⁻¹) on *V. fischeri* than found for 2,4-DCP has been reported in the scientific literature (Kaiser and Palabrica, 1991), accounting for the decreased acute inhibitory effect via the formation of malic acid. No reported data were available on the acute inhibitory effect of tetrahydroxycyclohexadiene carboxylic acid towards *V. fischeri*. After 30 min H₂O₂/UV-C treatment, the acute inhibitory effect decreased to the minimum level of 17 (± 1.2)% where complete 2,4-DCP removal and the asymptotic level of Cl⁻ release were achieved. This observation was in line with the literature data postulating that the dechlorination of phenolic compounds is at least partially responsible for biodegradability enhancement and toxicity reduction (Adams et al., 1997; Trovó et al., 2006). From Figure 4.21c, it became clear that chlorodihydroxypentenedioic acid, malonic acid, formic acid and oxalic acid which were indicated by the numbers (14), (9), (6) and (8), respectively, peaked after 30 min H₂O₂/UV-C treatment where the toxicity minimum was observed. Accordingly, it could be suggested that transformation of 2,4-DCP into aliphatic carboxylic acids together with the rapid dechlorination mainly governed the detoxification mechanism evidenced during first 30 min of the H₂O₂/UV-C process. This was supported by the general conclusions from the relevant studies which indicated that the formation of aliphatic carboxylic acids resulting from the degradation of phenolic pollutants renders the treated waters more biodegradable for a subsequent biological process (Wu and Zhou, 2001).

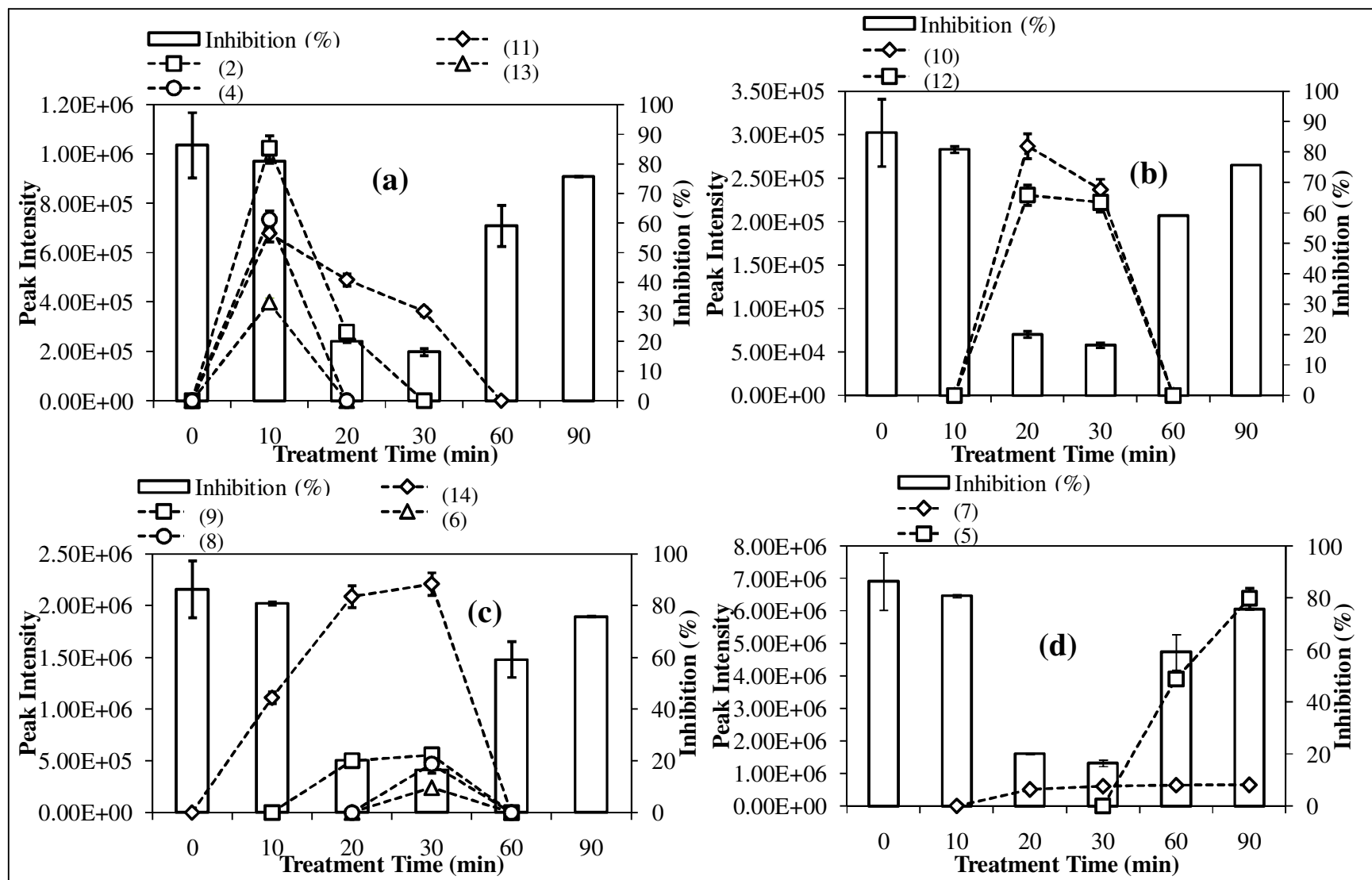


Figure 4.21. Temporal evolution of the acute inhibitory effect in relation with the identified 2,4-DCP transformation products whose signal intensities peaked after 10 (a), 20 (b), 30 (c) and 90 min (d) H₂O₂/UV-C treatment.

Although the abrupt detoxification pattern observed during first 30 min of the $\text{H}_2\text{O}_2/\text{UV-C}$ process, the acute inhibitory effect started to re-increase, suggesting that during the later stages of treatment relatively inhibitory transformation products were formed and/or the inhibitory effects of some transformation products became pronounced after 30 min treatment. The elucidation of Figure 4.21d, in fact, indicated that the increasing trend in the acute inhibitory effect was correlated to the gradual increase in the signal intensities of chloromethanediol and particularly to the formation of chlorocyclohexenedione which were labelled by the numbers (7) and (5), respectively. This evidence has an interesting aspect, as the re-appearance patterns in the acute inhibitory effect reported in the scientific literature could not in general attributed directly to a specific transformation product. Rather, they have been often ascribed to the formation of ring-opening products (Santiago et al., 2011; Jiménez et al., 2011).

As can be followed from Table 4.10, during Fenton treatment of 2,4-DCP the original acute inhibitory effect decreased to $54 (\pm 1.5)\%$ after 60 min and remained stagnant until the end of the 90 min-Fenton process where 2,4-DCP and TOC removals were found as 100% and 34%, respectively. In other words, the acute inhibitory effect remaining after 90 min Fenton treatment was relatively high, although 2,4-DCP was completely degraded. LC-MS analyses revealed that a number of transformation products from different chemical classes were present in the treated solution which rendered the ascription of the acute inhibitory effect measured after 90 min Fenton treatment to a specific transformation product difficult. Taking into account the poor TOC removal and accumulation of different transformation products during application of the Fenton treatment as assessed by the LC-MS analyses, the Fenton's reagent was less efficient than the $\text{H}_2\text{O}_2/\text{UV-C}$ and photo-Fenton treatment processes. The acute inhibitory effect after homogeneous Fenton-like ($\text{Fe}^{3+}/\text{H}_2\text{O}_2$) treatment of several monochlorophenols, dichlorophenols (including 2,4-DCP) and trichlorophenols has been attributed to chlorinated condensation byproducts including diphenyl ethers, biphenyls and dibenzodioxins in two recent studies (Munoz et al., 2011, 2012b). In those cases, higher acute inhibitory effects than exerted by the parent compounds except for 4-chlorophenol, 2,4-DCP and 3,5-dichlorophenol have been reported after applying 20% of the stoichiometric H_2O_2 concentration. The present study, on the other hand, suggested that condensation products of 2,4-DCP persisting after 90 min

Fenton treatment presented a lower acute toxic potential as compared to the untreated 2,4-DCP, at least at their concentrations in the treated solution.

Figure 4.22 displays percent relative inhibition values for the original and 10, 20, 30, 60 and 90 min photo-Fenton-treated 2,4-DCP solutions in relation with unreacted 2,4-DCP concentration and the TOC originating from intermediates. The acute toxicity evolution during photo-Fenton treatment of 2,4-DCP showed a similar trend as the treatment of 2,4-DCP with the H₂O₂/UV-C process within the first 30 min of the treatment processes (Figure 4.21 and 4.22). As in the case of the H₂O₂/UV-C process, the rapid degradation of 2,4-DCP and sharp release of Cl⁻ at the beginning of the photo-Fenton process was accompanied with an abrupt detoxification pattern. From the results presented in Figure 4.22, it could be inferred that relatively less toxic transformation products were formed during photo-Fenton treatment of 2,4-DCP under the pre-established experimental conditions. The inhibition rates (81 (± 0.61)% for the H₂O₂/UV-C process; 35 (± 1.4)% for the photo-Fenton process) obtained after 10 min 2,4-DCP treatment as well as the corresponding treatment efficiencies indicated that at the early stages of photochemical oxidation, the concentration and speciation of transformation products were different for the H₂O₂/UV-C and photo-Fenton processes. In fact, a comparison of the LC-MS identifications indicated that chloromaleic acid, dichlorobenzenediol, dichloromonohydroxybenzoquinone and 2,4-dichlorohexanedioic acid being the potential sources of the relatively high acute inhibitory effect measured after 10 min H₂O₂/UV-C treatment were not formed throughout the course of the photo-Fenton process. In the same manner, TOC removals and the TOC values originating from intermediates were found to be completely different for these processes at the same treatment time (11% and 27 mg L⁻¹ for the H₂O₂/UV-C process; 48% and 15 mg L⁻¹ for the photo-Fenton process after 10 min treatment) as could be interpreted from Table 4.10 and Figure 4.22. More importantly, the re-increase in the acute inhibitory effect starting from 30 min of H₂O₂/UV-C treatment was not evident in the case of the photo-Fenton process. The latter evidence could also be attributed to the difference between the type of generated transformation products, since the accumulation of chloromethandiol and chlorocyclohexenedione which were suspected of being the origin of the acute toxicity re-increase in the H₂O₂/UV-C process was not observed during application of the photo-Fenton treatment. For the photo-Fenton process, detoxification was more rapid and exhibited a parallel trend to 2,4-DCP degradation,

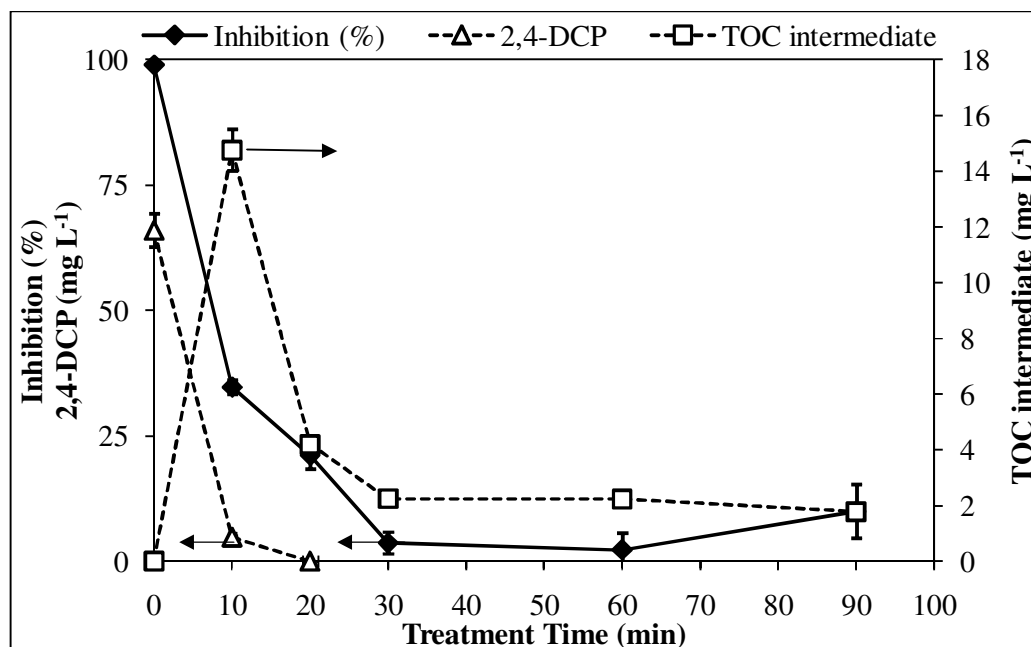


Figure 4.22. Temporal evolution of acute inhibitory effect in relation with unreacted 2,4-DCP concentration and the TOC originating from intermediates during photo-Fenton treatment of 2,4-DCP. Initial experimental conditions: 2,4-DCP = 75 mg L⁻¹ (460 μM), H₂O₂ = 10 mM, Fe²⁺ = 200 μM, pH = 3.

dechlorination and mineralization rates. This observation was supported by the general statement made in most related work for the superiority of the photo-Fenton treatment (Poulopoulos et al., 2008).

Figure 4.23 presents the acute inhibitory effects as a function of 2,4-DCP removal for UV-C, H₂O₂/UV-C, Fenton and photo-Fenton treatment processes. As observed in Figure 4.23, there is a negative correlation between 2,4-DCP conversion and acute toxic effect regardless of the studied treatment processes. According to this relationship, it could be anticipated that treatment processes being more effective in removing aqueous 2,4-DCP would have a greater detoxification capacity. The latter suggestion could account for the most rapid alleviation in the acute inhibitory effect evidenced within the first 30 min of the H₂O₂/UV-C and photo-Fenton processes. However, it should be kept in mind that complete removal of 2,4-DCP does not necessarily mean that the acute toxic effect decreased to ecotoxicologically safe levels. For instance, the Fenton's reagent, although ensured complete 2,4-DCP degradation after 90 min treatment, could not decrease the acute

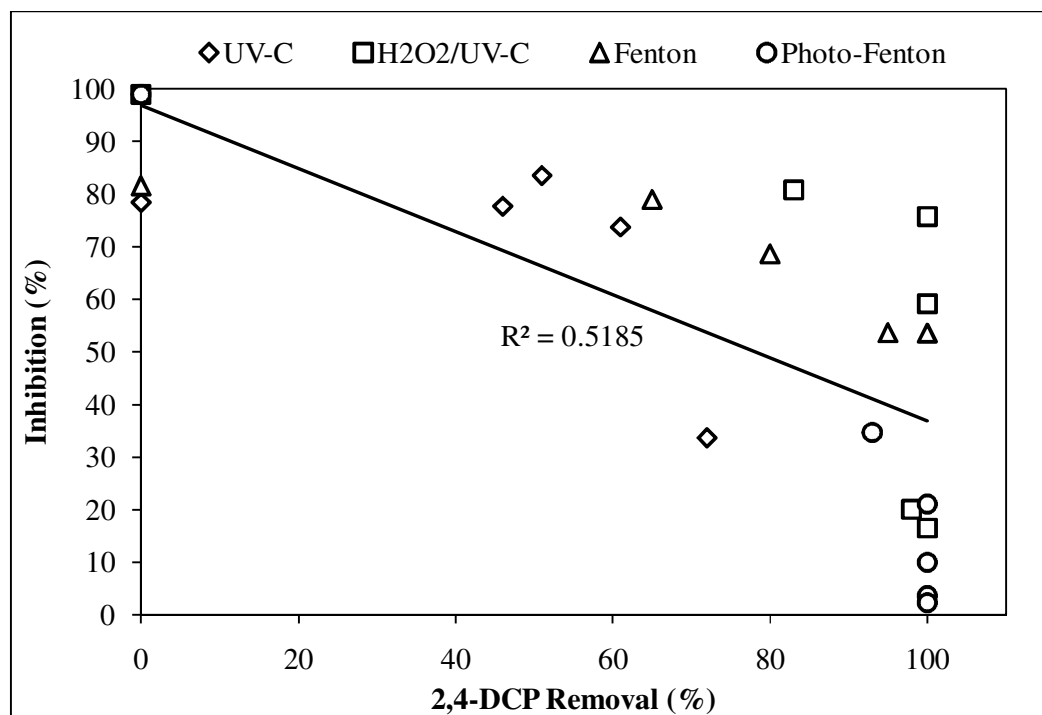


Figure 4.23. Evolution of acute inhibitory effect with 2,4-DCP removal for UV-C, H₂O₂/UV-C, Fenton and photo-Fenton treatment processes. Initial experimental conditions: 2,4-DCP = 75 mg L⁻¹ (460 μM), H₂O₂ = 10 mM, Fe²⁺ = 200 μM, pH = 7 for UV-C and H₂O₂/UV-C and pH = 3 for Fenton and photo-Fenton treatment processes.

inhibitory effect below 50%. In addition, the H₂O₂/UV-C and photo-Fenton processes should not be prolonged much beyond the treatment time where complete 2,4-DCP removal was obtained in order to avoid potential re-increases in acute inhibitory effect and unnecessary operation costs. Accordingly, 30 min H₂O₂/UV-C and photo-Fenton treatment could be regarded efficient to provide effluents with insignificant acute toxic effect under pre-established experimental conditions.

4.1.3.2. Genotoxicity Evolution. Genotoxicity testing is important for ecotoxicological characterization of oxidative water treatment processes for degradation of chlorophenols which exhibit potential genotoxicity, mutagenicity and carcinogenicity (Michałowicz et al., 2007). For this reason, this section aimed at investigating genotoxicity patterns during UV-C, H₂O₂/UV-C, Fenton and photo-Fenton treatment of 2,4-DCP by means of the *umu*-test in relation with the identified transformation products. The pre-established initial H₂O₂ and

Fe^{2+} concentrations of 10 mM and 200 μM were used for the degradation of 75 mg L^{-1} (460 μM) 2,4-DCP by the studied AOP.

Firstly, changes in genotoxic response expressed by the induction factor with the pollutant concentration were assessed for the 2,4-DCP concentration range of 17-67 mg L^{-1} (104-411 μM) in the absence and presence of metabolic activation which were abbreviated as - S9 and + S9, respectively. The results are demonstrated in Figure 4.24.

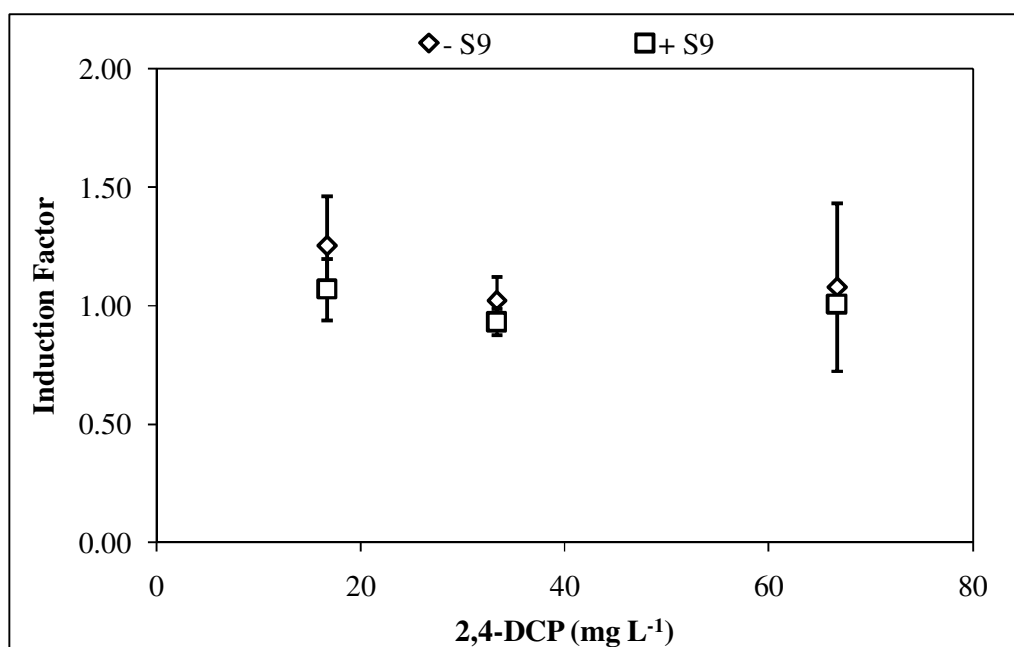


Figure 4.24. The genotoxic effect versus 2,4-DCP concentration graph.

Figure 4.24 indicates that all studied 2,4-DCP concentrations exerted a similar level of genotoxic effect. Accordingly, increasing 2,4-DCP concentration over the range 17-67 mg L^{-1} did not have a net effect on the measured genotoxic effect. It could be inferred from the induction factors, all of which being below 1.5, that 2,4-DCP did not exert any significant genotoxic effect over the studied concentration range of 17-67 mg L^{-1} . This observation was in line with the *umu*-test results by Yasunaga et al. (2004) who reported that the induction factors in the 2,4-DCP concentration range of 5-200 mg L^{-1} were all below 1.6. Although genotoxic effects measured in the absence of S9 mix were slightly higher than those recorded in the presence of S9 mix in the present study, differences between them were not significant within the experimental errors. Therefore, it could be concluded that

metabolic activation by S9 mixture had no significant effect on the genotoxic potential of 2,4-DCP.

Temporal evolution of genotoxic effect during UV-C, H₂O₂/UV-C, Fenton and photo-Fenton treatment of 2,4-DCP in the absence and presence of S9 mix is given in Table 4.11. A general remark could be made in that during application of the studied treatment processes no significant genotoxic effect was observed, as was evident from the induction factors found below 2.0 with and without S9 mix (Table 4.11). During application of UV-C photolysis an initial increase in the genotoxic effect from an induction factor of 0.971 to 1.49 was apparent in the absence of S9 mix during first 40 min of the treatment. From this result, it was evidenced that photolysis products being more genotoxic than 2,4-DCP were generated in parallel to disappearance of 2,4-DCP. An increase in the mutagenic effect measured by means of the Ames test during photodegradation of 2,4-DCP has been already reported by Czaplicka and Mielżyńska (2007) which was in line with the results from the present study. The parallel slight increase in the acute inhibitory effect towards *V. fischeri* after 40 min UV-C photolysis as described in Section 4.1.3.1 suggested that photolysis products causing increase in the genotoxic effect were acutely toxic as well. The genotoxic effect, however, significantly decreased to the induction factor of 1.13 after 60 min UV-C photolysis and remained nearly stagnant thereafter, indicating that photolysis products causing genotoxic effect increase were degraded to some extent. The observed genotoxicity patterns were elucidated in relation with transformation products identified by LC-MS in order to shed light into possible relationships between transformation products and genotoxicity. Genotoxic effect measured during UV-C photolysis of 2,4-DCP followed exactly the same pattern as the evolution of trichlorodihydroxybiphenyl, a hydroxylated polychlorinated biphenyl (PCB) product, which was indicated by the number (3) in Figure 4.16. Being a potential metabolite of PCB, 4,4'-dihydroxy-3,3',5,5'-tetrachlorobiphenyl has been previously demonstrated to give a weak, but statistically significant inhibition of growth in the DRAG assay (Johansson et al., 2004) which refers to the genotoxic potential of this hydroxylated PCB. Accordingly, although the induction factors observed during UV-C photolysis of 2,4-DCP did not indicate a significant genotoxic effect in the present study, the genotoxicity fluctuations evidenced in this treatment process were suspected to be mainly governed by the evolution of trichlorodihydroxybiphenyl product.

Table 4.11. Genotoxic effects observed at different stages of 2,4-DCP degradation by UV-C, H₂O₂/UV-C, Fenton and photo-Fenton treatment processes.

Treatment Time (min)	Induction Factor (- S9)				Induction Factor (+ S9)			
	UV-C	H ₂ O ₂ /UV-C	Fenton	Photo-Fenton	UV-C	H ₂ O ₂ /UV-C	Fenton	Photo-Fenton
0		0.971				1.47		
3	n.d.*	1.33	n.d.	1.30	n.d.	1.47	n.d.	1.68
10	n.d.	1.39	0.918	0.917	n.d.	1.20	1.38	1.50
20	n.d.	1.27	n.d.	0.920	n.d.	1.32	n.d.	1.93
30	1.45	1.34	1.35	0.960	1.55	1.15	0.968	1.45
40	1.49	n.d.	n.d.	n.d.	1.26	n.d.	n.d.	n.d.
60	1.13	1.02	0.893	1.24	1.05	1.22	1.30	1.03
90	1.16	1.45	0.839	0.934	1.10	1.00	1.39	1.26

*Not determined.

The initial increase in genotoxic effect described for UV-C photolysis above was also evident during H₂O₂/UV-C treatment of 2,4-DCP, resulting in two peak points after 10 and 30 min H₂O₂/UV-C treatment (Table 4.11). These initial increases were attributed to several transformation products characterized by LC-MS whose temporal evolution is illustrated in Figure 4.25.

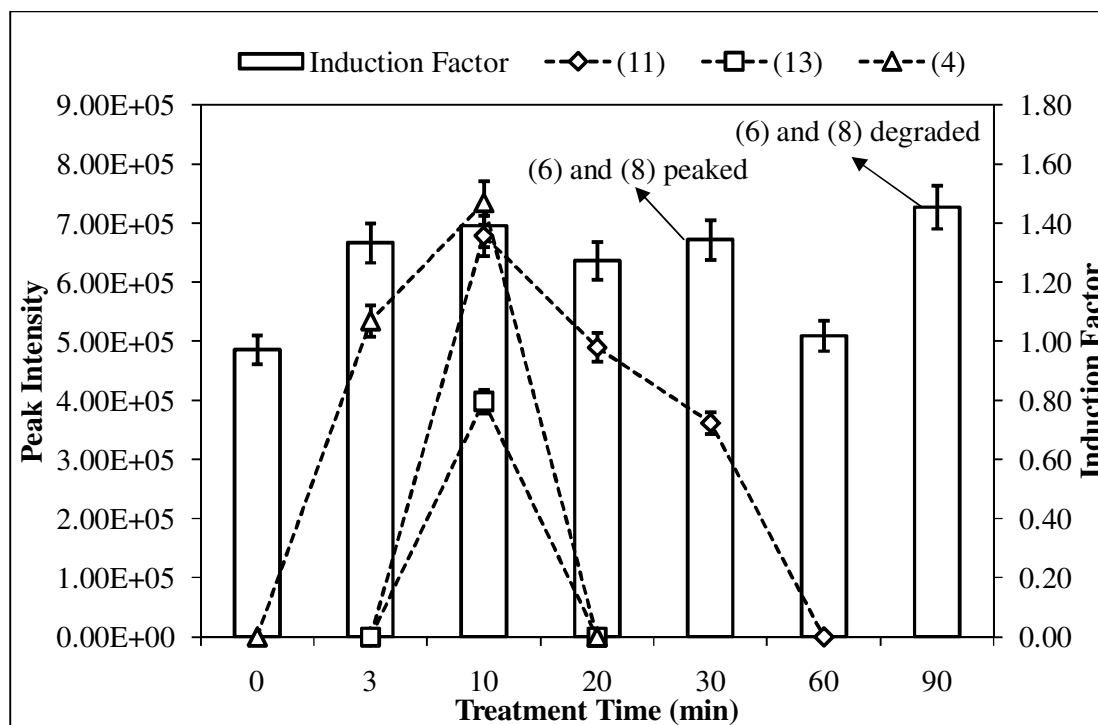


Figure 4.25. Temporal evolution of genotoxic effect without S9 mix during H₂O₂/UV-C treatment of 2,4-DCP in relation with transformation products identified by LC-MS.

LC-MS analyses indicated that the rapid degradation of 2,4-DCP by the H₂O₂/UV-C process was accompanied by the formation of several chlorinated aliphatic and aromatic transformation products during initial stages of the H₂O₂/UV-C treatment. Among them, chloromaleic acid, hydroxydichlorobenzoquinone and dichlorohexanedioic acid which were indicated by the numbers (11), (13) and (4), respectively in Figure 4.25 followed a similar trend as the genotoxic effect during first 10 min of the H₂O₂/UV-C treatment, suggesting that these transformation products caused the initial increase in the induction factor from 0.971 to 1.39. It is already known from the scientific literature that dichloro- and trichloroacetic acid are not genotoxic towards mammalian cells (Plewa et al., 2010). However, the suggestion drawn from the present study differed from the above-referenced

report presumably due to differences in the chemical structures of dichloroacetic acid, trichloroacetic acid, chloromaleic acid and dichlorohexanedioic acid and the employed test systems. Haloquinones formed as disinfection byproducts have been reported to be a potential carcinogen (Bull et al., 2011), although no clear data are available regarding the genotoxic potential of their hydroxylated metabolites. After 30 min H₂O₂/UV-C treatment, a slight re-increase in the genotoxic effect to an induction factor of 1.34 was evident most probably due to accumulation of formic and oxalic acids which were indicated by the numbers (6) and (8), respectively in Figure 4.25. Although the genotoxic effect efficiently decreased to an induction factor of 1.02, thus reaching to that of the original 2,4-DCP solution, after 60 min H₂O₂/UV-C treatment, a second re-increase to the induction factor of 1.45 was apparent after 90 min treatment which was similar to the re-increase in the acute inhibitory effect after the same treatment time (Figure 4.21). Therefore, chloromethanediol and chlorocyclohexenedione suspected of being the sources of the acute inhibitory effect at the end of the H₂O₂/UV-C treatment were also speculated to be the potential origins of the second re-increase in the genotoxic effect. Another important point to mention is that transformation products causing genotoxicity fluctuations could be metabolized into less genotoxic products, as evident from the lower induction factors obtained in the presence of S9 mix (Table 4.11).

For the Fenton process, the genotoxic effect followed a similar trend as that noticed during course of the UV-C photolysis of 2,4-DCP without S9 mix (Table 4.11). However, Fenton treatment of 2,4-DCP resulted in a lower genotoxic effect after all selected treatment times as compared to UV-C photolysis. After 30 min Fenton treatment, the genotoxic effect significantly increased from 0.918 to 1.35, indicating that transformation products more genotoxic than 2,4-DCP were formed. According to the complementary LC-MS analyses, when the mass intensity of 8-chlorooxanthrene-2-carboxylic acid, a dibenzodioxin derivative indicated by the number (21) in Figure 4.18, peaked, the genotoxic effect also reached its maximum value. The genotoxic effect significantly decreased after 90 min Fenton treatment even below the level recorded for the untreated 2,4-DCP. The *umu*-test results also delineated that transformation products being the origin of the increase in genotoxic effect evidenced after 30 min Fenton treatment could be metabolized into less genotoxic products in the presence of the rat liver enzyme S9 (Table 4.11).

During application of the photo-Fenton process, two maximum induction factors of 1.30 and 1.24 were noticed after 3 and 60 min treatment, respectively. The first suggestion could be that the above-mentioned maximum genotoxicity levels evidenced in the photo-Fenton process were caused by the formation of different types of early and late transformation products, as in case of the $\text{H}_2\text{O}_2/\text{UV-C}$ treatment of 2,4-DCP. Elucidation of LC-MS results revealed that temporal evolution of the mass intensity of 2-chloro-4-hydroxybenzaldehyde indicated by the number (17) in Figure 4.19 perfectly correlated with genotoxicity patterns throughout the course of the photo-Fenton treatment of 2,4-DCP. From Figure 4.26 where this relationship is presented, it could be followed that both the genotoxic effect and the mass intensity of 2-chloro-4-hydroxybenzaldehyde reached the maximum levels after the same treatment times. The re-increase in mass intensity of 2-chloro-4-hydroxybenzaldehyde observed between 30 and 60 min of the photo-Fenton process was most likely caused by the degradation of generated condensation products to give the corresponding aldehyde structure. Overall, the investigation of genotoxic patterns in relation with identified transformation products could serve as a practical guide in ecological risk assessment.

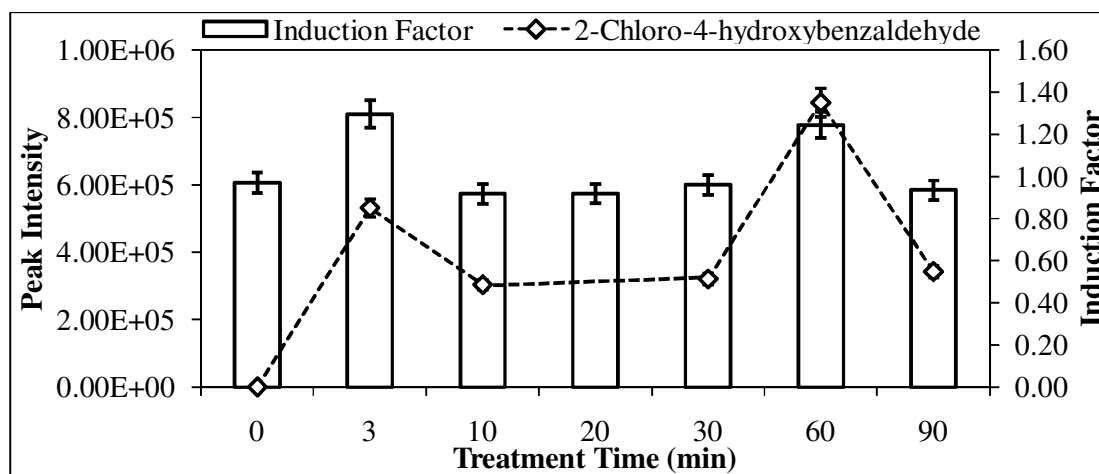


Figure 4.26. Temporal evolution of genotoxic effect in the absence of S9 mix during photo-Fenton treatment of 2,4-DCP in relation with the identified 2-chloro-4-hydroxybenzaldehyde product. Initial experimental conditions: 2,4-DCP = 75 mg L^{-1} ($460 \text{ } \mu\text{M}$), $\text{H}_2\text{O}_2 = 10 \text{ mM}$, $\text{Fe}^{2+} = 200 \text{ } \mu\text{M}$, $\text{pH} = 3$.

4.1.4. 2,4-DCP Removal in Synthetic Freshwater

4.1.4.1. Treatment Performances and Kinetics. Previous studies from the scientific literature have demonstrated that varying degrees of treatment efficiencies based on parent pollutant concentration and/or TOC were attained during application of AOP in different types of aqueous environmental matrices (Michael et al., 2012; Postigo et al., 2011b; Achilleos et al., 2010). For this reason, this subsection aimed at evaluating the effect of water matrix on treatment performances and kinetics. The pre-established initial H_2O_2 and Fe^{2+} concentrations of 10 mM and 200 μM , respectively, were used to degrade 75 mg L^{-1} (460 μM) 2,4-DCP in synthetic freshwater (SFW) samples under the initial pH conditions of 7.0 for UV-C and $\text{H}_2\text{O}_2/\text{UV-C}$ and 3.0 for Fenton and photo-Fenton treatment processes. 2,4-DCP and TOC abatements in SFW are shown in Figure 4.27a and b, respectively. The pseudo-first-order abatement rate coefficients with respect to 2,4-DCP, TOC and H_2O_2 concentrations ($R^2 \geq 0.987$) were also calculated for suitable time intervals in all studied treatment processes, and the results for degradation of 2,4-DCP are given in Table 4.12 in comparison with those obtained in distilled water (DW).

Table 4.12. Pseudo-first-order abatement rate coefficients and percent removal efficiencies obtained for degradation of 2,4-DCP by UV-C, $\text{H}_2\text{O}_2/\text{UV-C}$, Fenton and photo-Fenton treatment processes in DW and SFW.

	$k_{2,4\text{-DCP}} (\text{min}^{-1})$		2,4-DCP Removal (%)*	
	DW	SFW	DW	SFW
UV-C	0.011	0.020	72	88
$\text{H}_2\text{O}_2/\text{UV-C}$	0.178	0.154	100	100
Fenton	0.104	0.087	100	99
Photo-Fenton	0.260	0.229	100	100

*After 90 min treatment.

As seen in Figure 4.27a, the $\text{H}_2\text{O}_2/\text{UV-C}$ and photo-Fenton processes ensured complete disappearance of 2,4-DCP in SFW after approximately 40 and 30 min treatment, respectively. Although 99% 2,4-DCP removal was achieved after 40 min Fenton treatment in SFW, traces of 2,4-DCP were still detectable at a concentration of 0.74 mg L^{-1} after 90

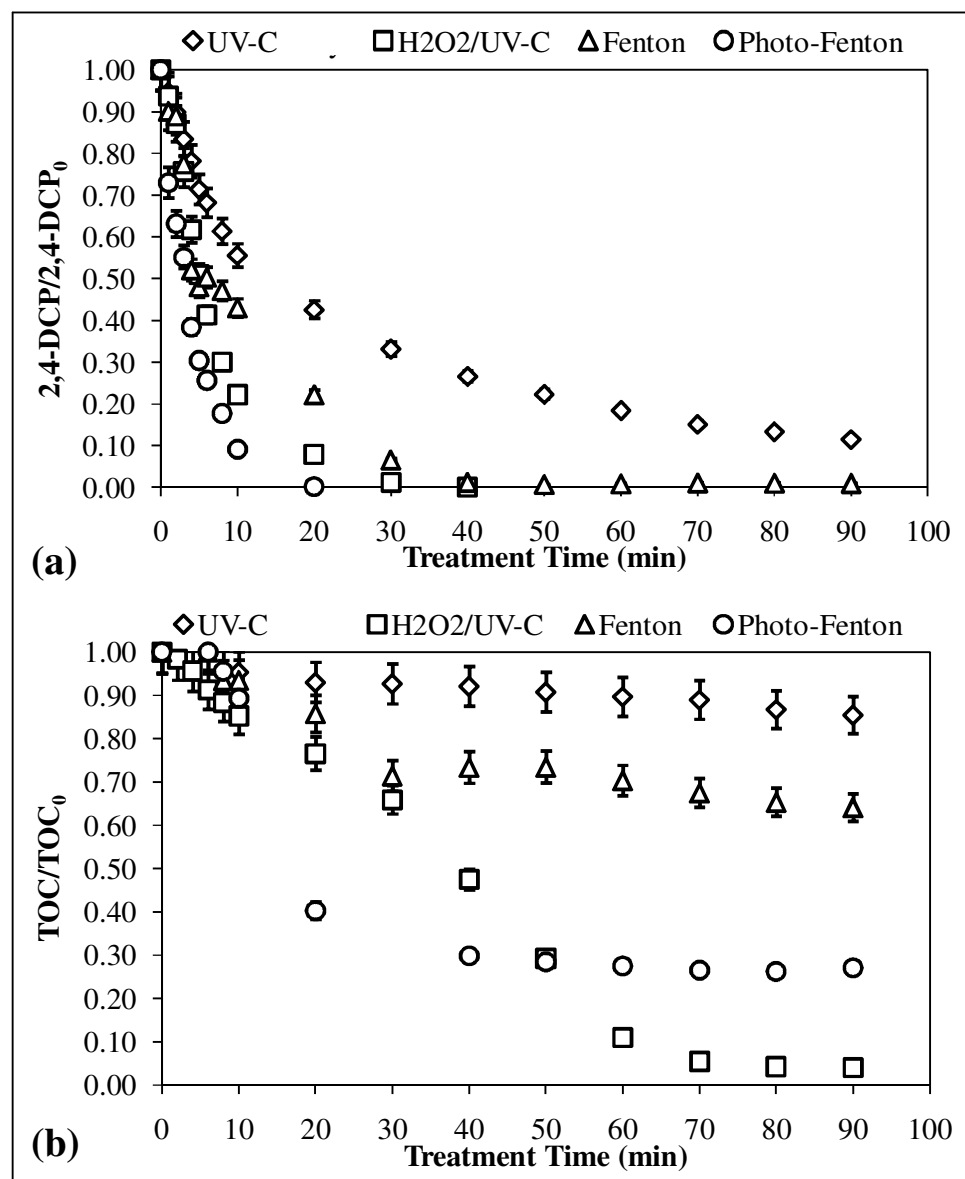


Figure 4.27. 2,4-DCP (a) and TOC removals (b) during UV-C, H₂O₂/UV-C, Fenton and photo-Fenton treatment of 2,4-DCP in SFW. Initial experimental conditions: 2,4-DCP = 75 mg L⁻¹ (460 μM), H₂O₂ = 10 mM, Fe²⁺ = 200 μM, pH = 7 for UV-C and H₂O₂/UV-C and pH = 3 for Fenton and photo-Fenton treatment.

min treatment. On the other hand, 12% of the initially present 2,4-DCP was still existent in the SFW samples being subjected to UV-C photolysis. Comparative evaluation of the studied treatment processes between DW and SFW revealed that slightly higher residual 2,4-DCP concentrations were detected during UV-C photolysis when performed in DW as compared to SFW, whereas the opposite was the case during application of the H₂O₂/UV-C

and photo-Fenton processes. On the other hand, the major difference was that the complete 2,4-DCP removal was achieved via Fenton treatment of DW unlike the case in SFW. Slightly better performances of the H₂O₂/UV-C, Fenton and photo-Fenton processes for degradation of 2,4-DCP in DW than those observed in SFW correlated with the higher pseudo-first-order rate coefficients for H₂O₂ consumption in DW than in SFW as evident from Table 4.13. The lower pseudo-first-order abatement rate coefficients for 2,4-DCP in SFW could not be attributed to radical scavenging effect of anionic constituents of SFW, i.e. SO₄²⁻, Cl⁻ and HCO₃⁻, as suggested in the relevant scientific literature (Lipczynska-Kochany et al., 1995), since if it would be the case, H₂O₂ consumption rates achieved in the studied systems would be higher in SFW than in DW. Although the UV₂₅₄ absorbance of water matrix could also affect the consumption kinetics of H₂O₂, contribution from the SFW constituents to the overall UV₂₅₄ absorbance was of minor importance considering the insignificant difference between the UV₂₅₄ absorbances of DW and SFW contaminated with 2,4-DCP (0.072 (± 0.011) cm⁻¹ and 0.078 (± 0.011) cm⁻¹, respectively). Former work has demonstrated that the presence of SO₄²⁻ or Cl⁻ could markedly retard the catalytic decomposition of H₂O₂ by Fe³⁺ and the oxidation of organic compounds due to the generation of complexes of Fe³⁺ by Cl⁻ or SO₄²⁻ which hinder photoreduction of Fe³⁺ and cause the generation of less reactive SO₄^{•-} and Cl₂^{•-} (De Laat et al., 2004). This latter supports the lower pseudo-first-order abatement rate coefficients for 2,4-DCP in SFW evidenced in the present study.

Table 4.13. Pseudo-first-order abatement rate coefficients and percent consumptions obtained for H₂O₂ during H₂O₂/UV-C, Fenton and photo-Fenton treatment of 2,4-DCP in DW and SFW.

	$k_{H_2O_2}$ (min ⁻¹)		Consumption (%)*	
	DW	SFW	DW	SFW
H ₂ O ₂ /UV-C	0.009	0.008	100	99
Fenton	0.043	0.020	99	94
Photo-Fenton	0.216	0.109	100	100

*After 90 min treatment.

From the experimental findings regarding the TOC removal during application of the studied treatment processes in SFW, it became apparent that significantly lower mineralization efficiencies were obtained via UV-C and Fenton treatment processes as

compared to the H₂O₂/UV-C and photo-Fenton processes (Figure 4.27b and Table 4.14). The H₂O₂/UV-C process provided the highest TOC removal of 96% after 90 min treatment, whereas TOC decreased at a faster rate during the first 40 min of photo-Fenton treatment ($k_{TOC} = 0.036 \text{ min}^{-1}$) than in H₂O₂/UV-C treatment ($k_{TOC} = 0.019 \text{ min}^{-1}$). The pseudo-first-order abatement rate coefficients for TOC followed exactly the same order as for the pseudo-first-order abatement rate coefficients for 2,4-DCP, i.e. photo-Fenton > H₂O₂/UV-C > Fenton > UV-C. Comparison of the obtained TOC removals between DW and SFW revealed that although UV-C, H₂O₂/UV-C and Fenton treatments provided comparable results in DW and SFW, removal efficiencies and pseudo-first-order abatement rate coefficients for TOC by the photo-Fenton process were significantly higher in DW (95% and 0.094 min^{-1} , respectively) than in SFW (73% and 0.068 min^{-1} , respectively) presumably due to the same reason as discussed above to account for the slower 2,4-DCP degradation kinetics in SFW. Unlike the case in the photo-Fenton process, the indifference between the pseudo-first-order abatement rate coefficients and percent removal efficiencies for TOC achieved during Fenton treatment in DW and SFW (Table 4.14) could be explained by that the reaction of Fe³⁺ with H₂O₂ is much slower ($k = 0.001\text{--}0.01 \text{ M}^{-1} \text{ s}^{-1}$; Walling and Goosen, 1973) than the reaction of Fe²⁺ with H₂O₂ ($k = 51 \text{ M}^{-1} \text{ s}^{-1}$; Walling, 1975), thus rendering the role of the potential formation of Fe³⁺---SO₄²⁻ and/or Fe³⁺---Cl complexes less critical for the Fenton process. Overall speaking, TOC removal efficiencies of the H₂O₂/UV-C and photo-Fenton processes were still high in the case of SFW. Therefore, if the only criteria for the selection of a treatment process to be applied to natural freshwaters would be 2,4-DCP and TOC removals, then H₂O₂/UV-C and photo-Fenton processes would be superior to Fenton and UV-C treatments. However, it should be underlined here that another prevalent constituent of natural waters is the dissolved natural organic matter which could be an important free radical scavenger in the case of AOP (Lindsey and Tarr, 2000) and act as a photosensitizer in the case of photolysis (Chin et al., 2004). Since in reality, the processes are applied in real water matrices, dissolved natural organic matter should be taken into account to reach a more rigid conclusion on the effectiveness of the studied treatment processes for degradation of 2,4-DCP in natural waters.

Table 4.14. Pseudo-first-order abatement rate coefficients and percent removal efficiencies obtained for TOC removal by UV-C, H₂O₂/UV-C, Fenton and photo-Fenton treatment of 2,4-DCP in DW and SFW.

	$k_{TOC} \text{ (min}^{-1}\text{)}$		Removal Efficiency (%)	
	DW	SFW	DW	SFW
UV-C	—*	—*	10	15
H ₂ O ₂ /UV-C	0.012	0.019	95	96
Fenton	0.004	0.004	34	36
Photo-Fenton	0.094	0.068	95	73

*Not determined because of insignificant removal rate.

Figure 4.28 presents the evolution of UV₂₈₀ (a), (b) and UV₂₅₄ (c), (d) absorbances during UV-C, H₂O₂/UV-C (a), (c), Fenton and photo-Fenton (b), (d) treatment of 2,4-DCP in DW and SFW. The absorption spectra of 2,4-DCP-containing SFW samples subjected to the studied treatment processes are also depicted in Appendix C. Overall, the Fenton and photo-Fenton processes ensured the highest UV₂₈₀ abatement rates in SFW among the studied treatment processes, whereas the UV₂₈₀ absorbance after 90 min UV-C photolysis of SFW contaminated with 2,4-DCP was even higher than that of the parent pollutant. The residual UV₂₅₄ absorbances in SFW after 90 min treatment followed the order: UV-C > Fenton > H₂O₂/UV-C > photo-Fenton. Although UV₂₈₀ absorbances throughout the course of photo-Fenton treatment of 2,4-DCP were practically the same in DW and SFW, UV-C and H₂O₂/UV-C treatment processes resulted in slightly higher UV₂₈₀ absorbances when applied in SFW. However, the major difference was that Fenton treatment of 2,4-DCP in SFW resulted in significantly faster abatement of UV₂₈₀ absorbance than achieved in DW. Considering that nearly the same TOC removal efficiencies were reached via the Fenton process in both aqueous matrices (Table 4.14), one could speculate that different types of transformation products were formed through Fenton treatment of 2,4-DCP in DW and SFW. As for the UV₂₅₄ absorbances, some differences were observed between DW and SFW. Throughout the course of UV-C photolysis of 2,4-DCP in SFW, the UV₂₅₄ absorbances were higher than those observed in DW which was parallel to the higher pseudo-first-order abatement rate coefficients and percent removal efficiencies for 2,4-DCP achieved in SFW (Table 4.12). From the scientific literature it is known that HO• and Cl• could be formed as a result of UV-C photolysis of acidic free chlorine (HOCl) with the quantum yield of 1.4 mol E⁻¹ at 254 nm according to the following reaction (Watts and

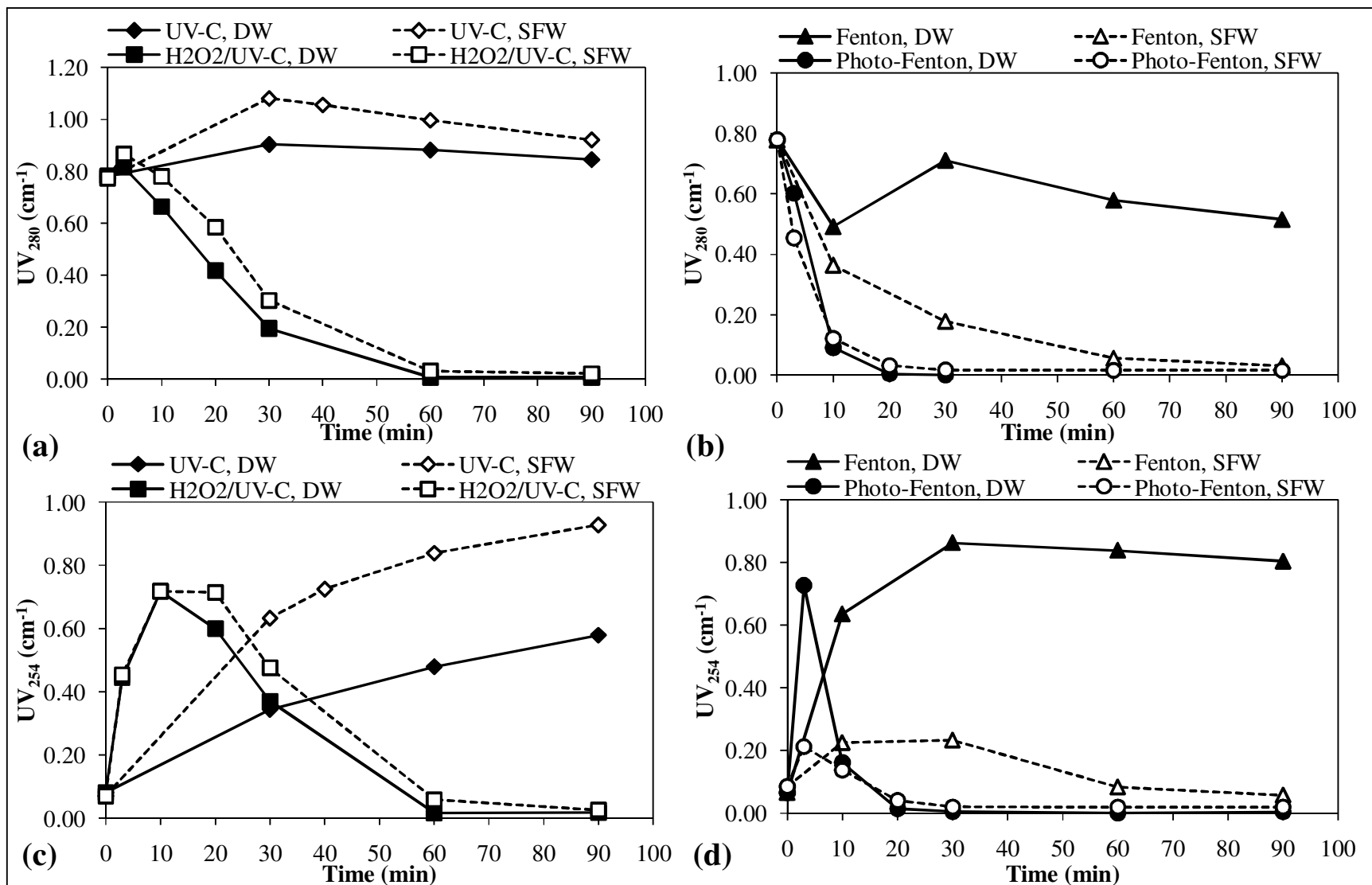


Figure 4.28. Evolution of UV₂₈₀ (a), (b) and UV₂₅₄ (c), (d) absorbances during UV-C, H₂O₂/UV-C (a), (c), Fenton and photo-Fenton (b), (d) treatment of 2,4-DCP in DW and SFW. Initial experimental conditions: 2,4-DCP = 75 mg L⁻¹ (460 μM), H₂O₂ = 10 mM, Fe²⁺ = 200 μM, pH = 7 for UV-C and H₂O₂/UV-C and pH = 3 for Fenton and photo-Fenton treatment processes.

Linden, 2007);



However, scientific evidence on potential formation of HOCl from the photolytic oxidation of Cl⁻ is not available. Being the potential photolysis products of aqueous phenolic pollutants, specific types of condensed structures including aromatic ketones and quinones have been postulated to be able to photosensitize the transformation of aqueous phenols (Canonica et al., 1995). Accordingly, greater formation of such structures during UV-C photolysis of 2,4-DCP in SFW as speculated from the higher UV_{280/254} absorbances might account for the higher 2,4-DCP removal achieved in SFW, but requires further evidence. For the H₂O₂/UV-C process, although the UV₂₅₄ absorbances observed during the first 10 min of treatment were not different between DW and SFW, abatement of the UV₂₅₄ absorbance after its maximum level proceeded at a slower rate in SFW than in DW which was similar to the difference in the observed H₂O₂ decomposition patterns in both aqueous matrices. However, the major differences between the observed UV₂₅₄ absorbances in DW and SFW were evident during application of the Fenton and photo-Fenton processes. Throughout the course of Fenton treatment and during the first 3 min of photo-Fenton treatment of 2,4-DCP, considerably lower UV₂₅₄ absorbances were recorded in SFW than in DW which contrasted with the findings obtained via UV-C and H₂O₂/UV-C treatment processes. This might indicate the formation of lower number of transformation products exhibiting a significant absorption at 254 nm during application of the Fenton and photo-Fenton processes in SFW.

4.1.4.2. Chloride Release. As an indicator of the efficiency of the studied treatment processes in SFW, Cl⁻ releases were also followed in SFW, and the results are depicted in Figure 4.29a and b in comparison with those obtained in DW. It should also be underlined here that since the SFW samples already contained Cl⁻ in its composition, this initial Cl⁻ content was subtracted from the concentrations determined in the treated samples. The most rapid dechlorination in SFW was achieved via the photo-Fenton process in correlation with the largest pseudo-first-order abatement rate coefficient for 2,4-DCP in this AOP (Table 4.12), whereas the rate and extent of Cl⁻ releases during application of the

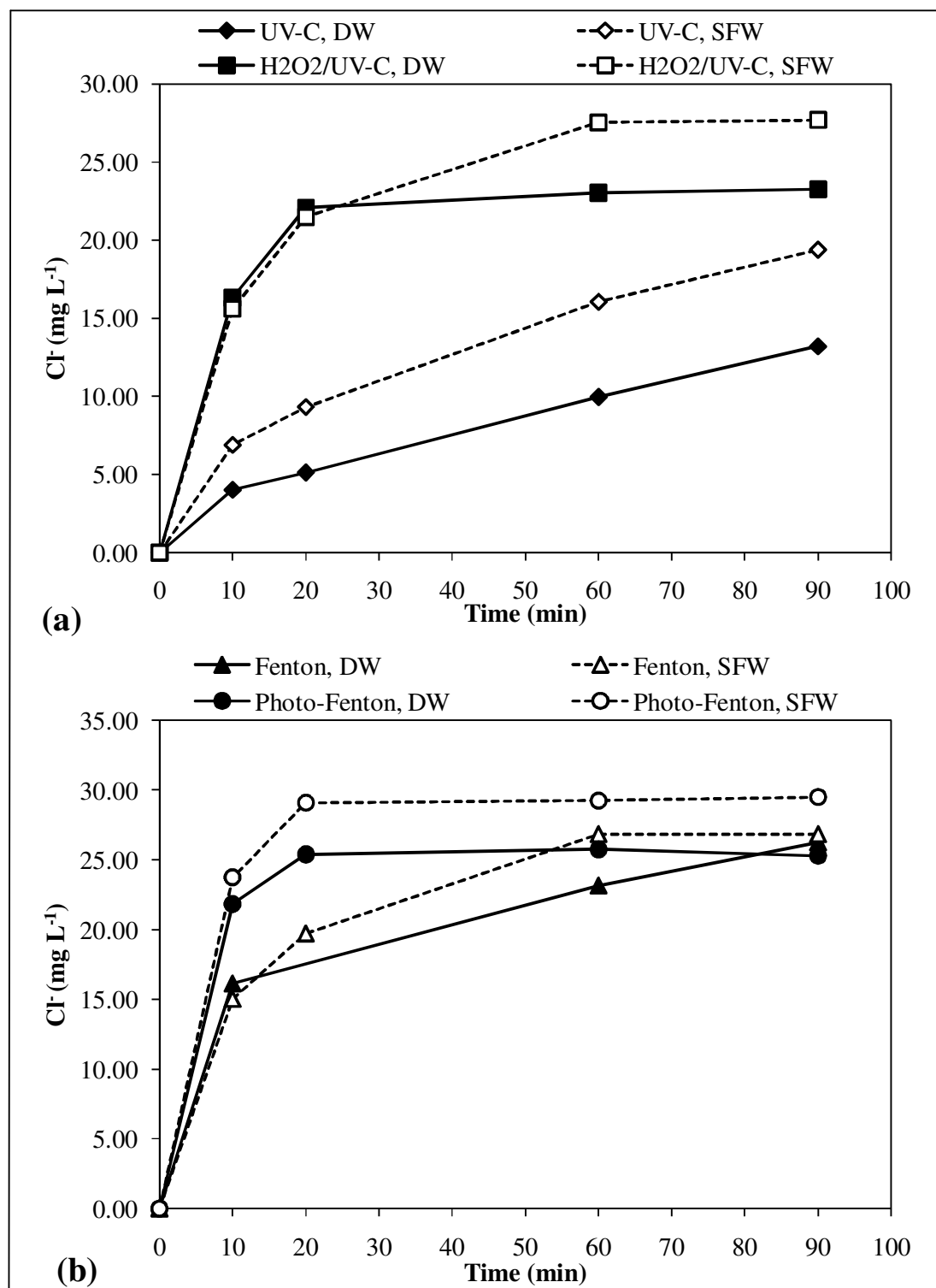


Figure 4.29. Cl⁻ releases during UV-C, H₂O₂/UV-C (a), Fenton and photo-Fenton (b) treatment of 2,4-DCP in DW and SFW. Initial experimental conditions: 2,4-DCP = 75 mg L⁻¹ (460 μM), H₂O₂ = 10 mM, Fe²⁺ = 200 μM, pH = 7 for UV-C and H₂O₂/UV-C and pH = 3 for Fenton and photo-Fenton treatment.

H₂O₂/UV-C and Fenton processes in SFW were not significantly different from each other. Although the released concentration of Cl⁻ gradually increased during UV-C photolysis in parallel to the gradual decomposition of 2,4-DCP, the ultimate dechlorination was considerably lower than achieved via the studied AOP. The important point here is that the released Cl⁻ concentrations in SFW were close to the theoretically maximum possible amount of Cl⁻ release of 33 mg L⁻¹ in all studied AOP, particularly after a short treatment time in the photo-Fenton process. The comparison of Cl⁻ releases in DW and SFW revealed that similar to the patterns obtained for the UV₂₅₄ absorbances, throughout the course of UV-C photolysis and starting from approximately 20 min of H₂O₂/UV-C treatment, the released Cl⁻ concentrations were higher in SFW than in DW. Similarly, application of the photo-Fenton process in SFW resulted in the release of a slightly higher ultimate Cl⁻ concentration of 29 mg L⁻¹ than found in DW after 90 min photo-Fenton treatment (25 mg L⁻¹). The higher Cl⁻ concentrations in SFW samples subjected to UV-C photolysis could be directly correlated with the higher 2,4-DCP removals achieved in SFW. On the other hand, the greater extent of dechlorination obtained by applying the H₂O₂/UV-C and photo-Fenton processes in SFW as compared to DW was speculated to be caused by the generation of reactive Cl species including Cl[•] and Cl₂^{•-}, thereby inducing release of the organically bound chlorine in the form of inorganic Cl⁻ according to the following reactions;



for which the second-order reaction rate coefficients of 4.3×10^9 , 1.0×10^5 and 2.1×10^{10} M⁻¹ s⁻¹ were reported, respectively (Grebel et al., 2010).

4.1.4.3. Aromatic Transformation Products. HPLC and GC-MS analyses were performed in SFW to explore the effect of water matrix on the identity and concentration of aromatic transformation products obtained during the studied treatment processes. The analytical assessment revealed that the common non-chlorinated aromatic transformation product of the studied treatment processes in SFW was hydroquinone whose temporal evolution in

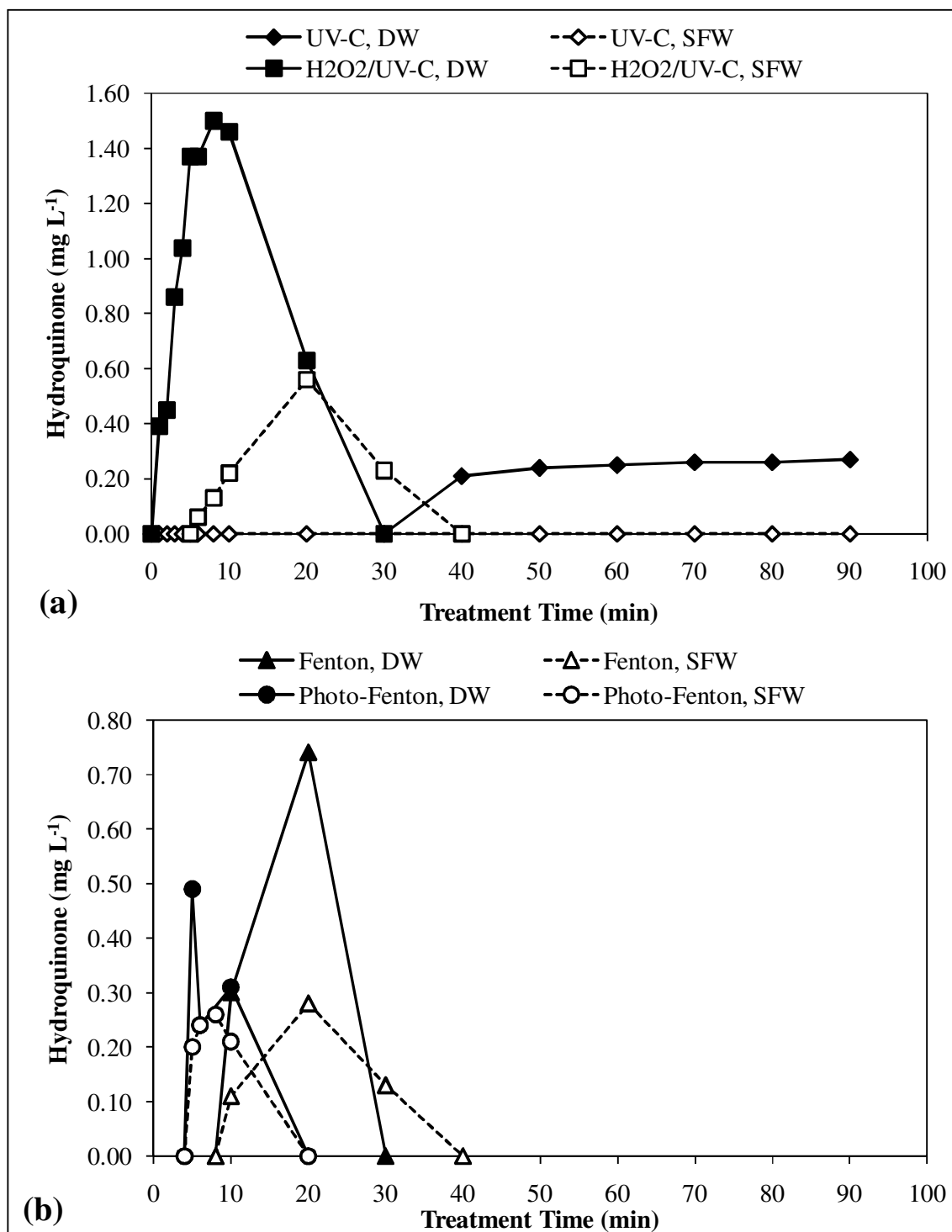


Figure 4.30. Hydroquinone formation during UV-C, H₂O₂/UV-C (a), Fenton and photo-Fenton (b) treatment of 2,4-DCP in DW and SFW. Initial experimental conditions: 2,4-DCP = 75 mg L⁻¹ (460 μM), H₂O₂ = 10 mM, Fe²⁺ = 200 μM, pH = 7 for UV-C and H₂O₂/UV-C and pH = 3 for Fenton and photo-Fenton treatment.

DW and SFW is comparatively shown in Figure 4.30a and b. From Figure 4.30 it could be followed that the relatively low concentrations of hydroquinone of 0.21-0.27 mg L⁻¹ being detected during the later stages (≥ 40 min) of UV-C photolysis of 2,4-DCP in DW were not apparent when UV-C photolysis was performed in SFW. It could also be realized that after 6 min H₂O₂/UV-C treatment in SFW hydroquinone was quantified at a concentration of 0.06 mg L⁻¹, whereas after the same treatment time in DW hydroquinone concentration rapidly reached nearly the peak concentration of 1.5 mg L⁻¹. In the similar manner, the higher initial formation rate of hydroquinone in DW as compared to SFW was also evident during Fenton and photo-Fenton treatments. As a result, higher peak hydroquinone concentrations were reached in DW than in SFW for all studied treatment processes. These findings speculated that the slightly higher residual 2,4-DCP concentrations in SFW might be a reason of the lower concentrations of hydroquinone formation during application of the H₂O₂/UV-C, Fenton and photo-Fenton processes. However, the Cl⁻ release and hydroquinone formation patterns were completely different between DW and SFW, i.e. lower hydroquinone generation and higher Cl⁻ releases occurred together during UV-C, H₂O₂/UV-C, Fenton and photo-Fenton treatment of 2,4-DCP. Finally, it could be demonstrated that for the complete disappearance of the formed hydroquinone during the application of H₂O₂/UV-C and Fenton processes in SFW a slightly longer time (40 min) was required than in DW (30 min).

According to the GC-MS results, 4-chlorophenol was identified as the only transformation product that was formed in SFW samples being subjected to the photo-Fenton process, but not in DW. During the first 3 min of photo-Fenton treatment of 2,4-DCP the peak area of 4-chlorophenol increased from 2.9×10^6 to 7.0×10^6 and decreased to non-detectable levels after 20 min photo-Fenton treatment, demonstrating that 2,4-DCP was rapidly dechlorinated to form 4-chlorophenol during initial stages of the treatment. The formation of 4-chlorophenol from the electrochemical degradation (Wang et al., 2010a, 2010b), ultrasonic degradation and microwave-assisted treatment with sodium percarbonate, an adduct of sodium carbonate and hydrogen peroxide with the formula $2\text{Na}_2\text{CO}_3 \cdot 3\text{H}_2\text{O}_2$ (Cravotto et al., 2010) and electro-Fenton degradation (Song-hu and Xiao-hua, 2005) of 2,4-DCP has also been reported in the scientific literature. Although not identified in DW samples subjected to the H₂O₂/UV-C process, catechol was detected in the H₂O₂/UV-C-treated SFW samples, reaching the peak level after 10 min treatment

and disappearing to non-detectable levels after 30 min treatment. Another difference between DW and SFW results was that chlorohydroquinone identified during application of the Fenton and photo-Fenton processes in DW could not be detected when the processes were applied in SFW. Also, 4,6-dichlororesorcinol could not be detected in the photo-Fenton-treated SFW samples, although available in the photo-Fenton-treated DW samples. Similarly, dichlorohydroquinone and chlorobenzenediol formed during UV-C and H₂O₂/UV-C treatment of 2,4-DCP in DW were non-detectable in the treated SFW samples.

4.1.4.4. Aliphatic Transformation Products. After the identification of aromatic transformation products of 2,4-DCP in SFW, aliphatic transformation products, namely C1-C4 carboxylic acids and aldehydes, were analyzed with HPLC and colorimetry in treated SFW samples and compared with the findings obtained in DW. According to the obtained HPLC results, maleic acid was found as the common carboxylic acid product of the studied treatment processes in SFW samples. Figure 4.31a and b present temporal evolution of maleic acid during UV-C, H₂O₂/UV-C, Fenton and photo-Fenton treatment of 2,4-DCP in DW and SFW. The results indicated that the maximum concentrations of maleic acid measured in SFW samples were in general slightly lower than those recorded in DW except for the Fenton process where the measured maximum concentrations of maleic acid were not significant between DW and SFW. However, it should be noted that maleic acid was degraded below undetectable levels after the same treatment time in H₂O₂/UV-C and photo-Fenton processes regardless of the water matrix. Additionally, the residual maleic acid concentrations obtained after 90 min Fenton treatment were not significantly different between DW (0.34 mg L⁻¹) and SFW (0.47 mg L⁻¹).

Temporal change of the concentration of formic acid, one of the possible simplest structured transformation products before final mineralization, was also investigated during application of the studied treatment processes in SFW, and the results are shown in Figure 4.31c and d in comparison with the findings obtained in DW. A remarkable observation was that formic acid was not detected throughout the course of H₂O₂/UV-C treatment in SFW, although a high concentration of formic acid of 20 mg L⁻¹ was obtained in DW subjected to the H₂O₂/UV-C process only for 10 min (Figure 4.31c). Instead, 11 mg L⁻¹ acetic acid was found in SFW after 10 min H₂O₂/UV-C treatment (data not shown). As for the Fenton and photo-Fenton processes, no significant difference was evidenced between

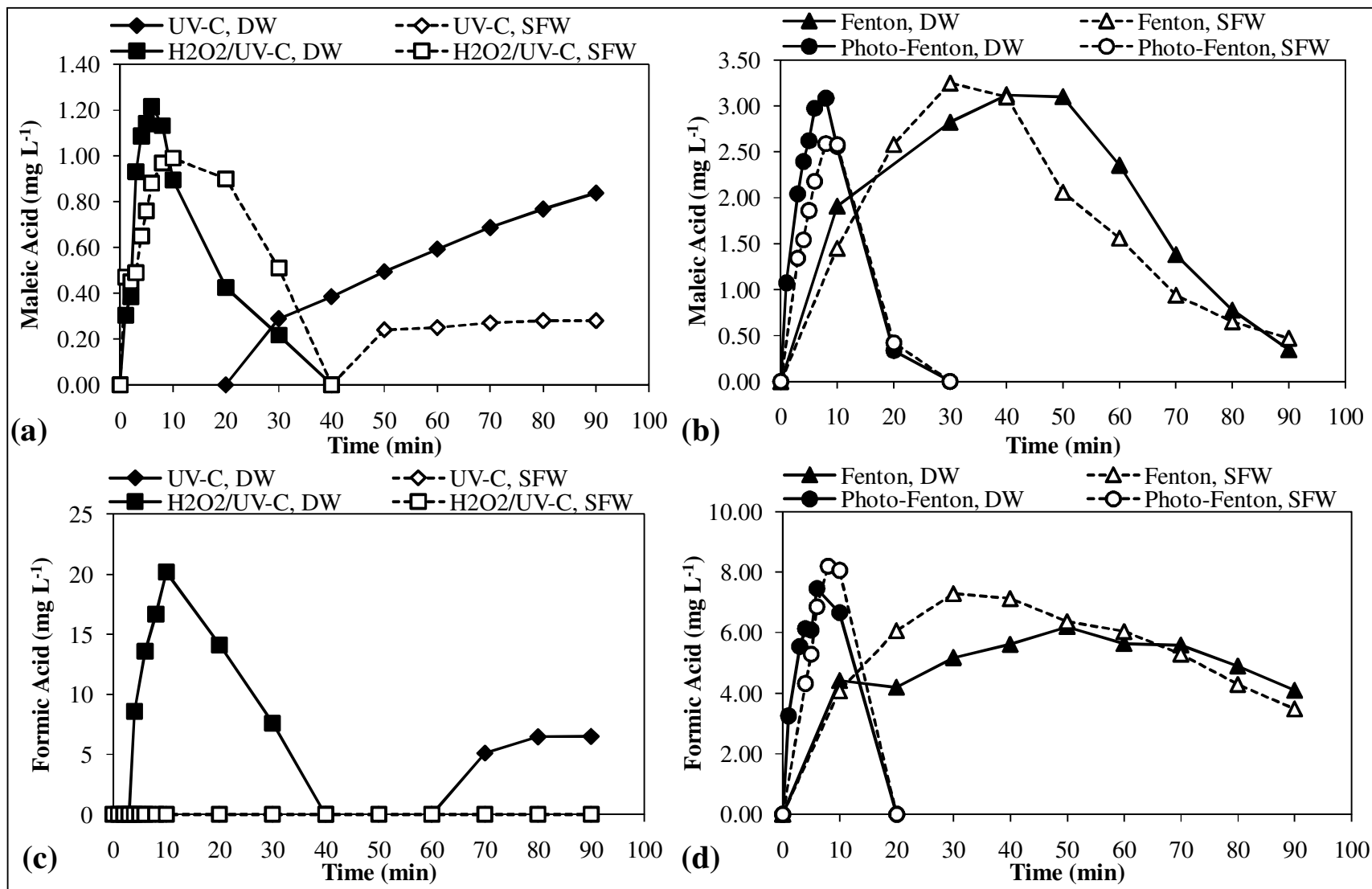


Figure 4.31. Evolution of maleic (a), (b) and formic (c), (d) acid products during UV-C, H₂O₂/UV-C (a), (c), Fenton and photo-Fenton (b), (d) treatment of 2,4-DCP in DW and SFW. Initial experimental conditions: 2,4-DCP = 75 mg L⁻¹ (460 μM), H₂O₂ = 10 mM, Fe²⁺ = 200 μM, pH = 7 for UV-C and H₂O₂/UV-C and pH = 3 for Fenton and photo-Fenton treatment processes.

the formic acid concentrations recorded in DW and SFW during treatment (Figure 4.31d). Overall speaking, when applied in SFW, the H₂O₂/UV-C and photo-Fenton processes were still capable of completely degrading the identified carboxylic acids after the same treatment time, and Fenton treatment provided a comparable efficiency in removing them as that achieved in DW.

Figure 4.32a and b present temporal evolution of aldehydes during UV-C, H₂O₂/UV-C, Fenton and photo-Fenton treatment of 2,4-DCP in DW and SFW samples. As could be followed from Figure 4.32a, higher aldehyde concentrations were detected in SFW samples subjected to UV-C photolysis than in DW samples that was correlated with the higher parent pollutant removal obtained in SFW by UV-C treatment. Similar to the case of maleic acid, aldehyde concentrations observed during the H₂O₂/UV-C process in the SFW system were slightly lower than that in the DW system. However, the major difference was obtained for the Fenton and photo-Fenton processes where aldehyde formation was completely hindered in SFW samples (Figure 4.32b). The absence of aldehydes in the Fenton and photo-Fenton systems performed in SFW might be due to potential interaction of aldehydes with Ca²⁺ and Mg²⁺ in the composition of SFW samples and Fe³⁺ during its precipitation after quenching the reaction.

4.1.4.5. Acute Toxicity. The *V. fischeri* bioluminescence inhibition assay was performed for the studied treatment processes, namely UV-C, H₂O₂/UV-C, Fenton and photo-Fenton treatments, in order to evaluate potential differences between the acute inhibitory effects arising from the degradation of 2,4-DCP in DW and SFW. The results obtained for UV-C, H₂O₂/UV-C (a), Fenton and photo-Fenton (b) treatments are depicted in Figure 4.33. There was not a significant difference between the inhibition values of the original 2,4-DCP solution in DW and SFW, indicating that the ionic constituents of SFW did not exhibit any synergistic or antagonistic effect on acute toxicity of 2,4-DCP. On the other hand, distinct differences were found between the acute toxicity patterns of DW and SFW contaminated with 2,4-DCP that were subjected to UV-C, H₂O₂/UV-C and Fenton treatment. The acute inhibitory effect of 2,4-DCP decreased from 96 (± 0.011) to 71 (± 0.80)% upon 40 min UV-C photolysis of SFW, whereas 40 min-UV-C photolysis resulted in a slight increase in the acute toxic effect of DW samples contaminated with 2,4-DCP. The observed trend in the acute inhibitory effect within the first 40 min of UV-C photolysis delineated that unlike

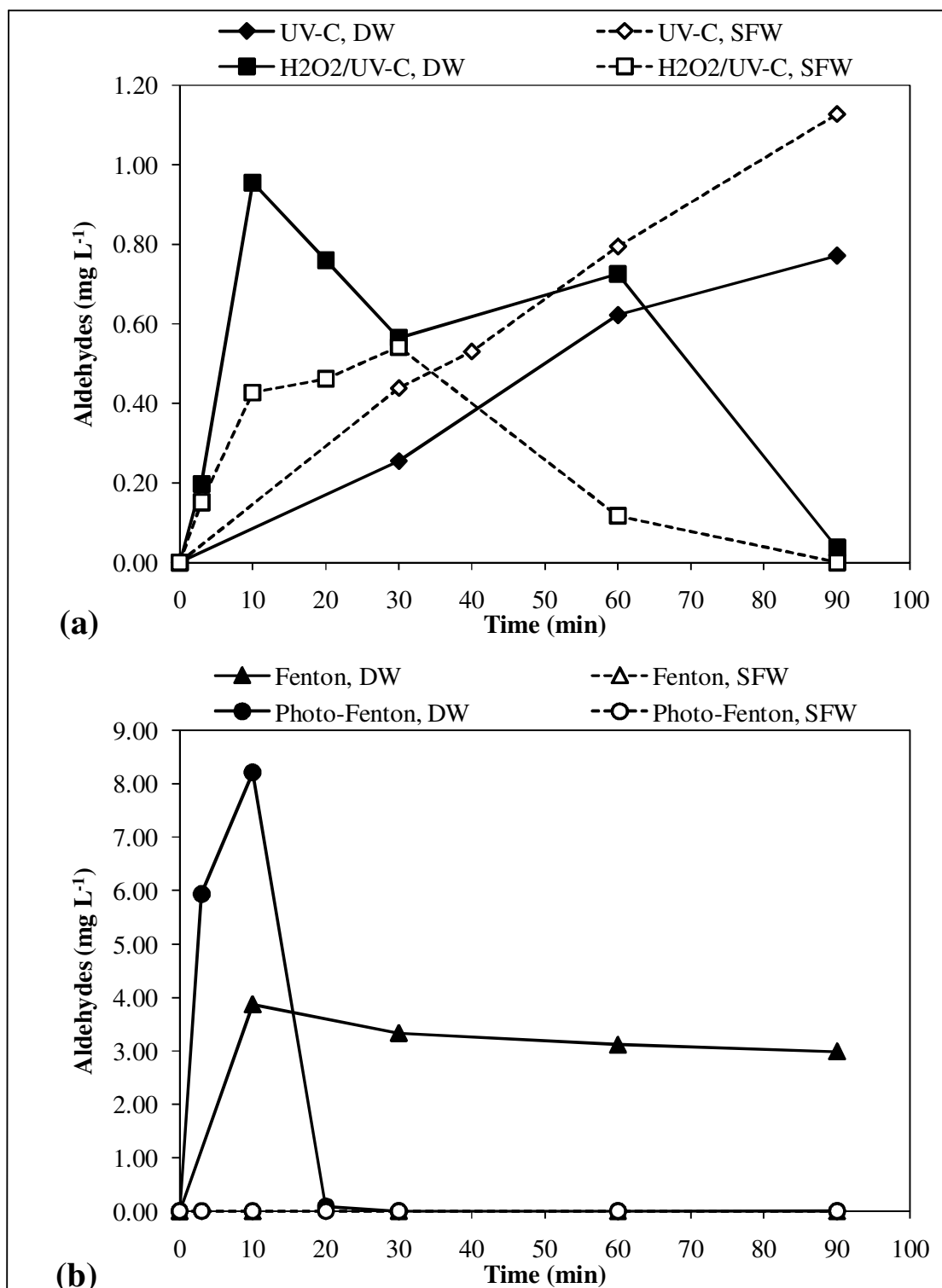


Figure 4.32. Aldehyde formation during UV-C, H₂O₂/UV-C (a), Fenton and photo-Fenton (b) treatment of 2,4-DCP in DW and SFW. Initial experimental conditions: 2,4-DCP = 75 mg L⁻¹ (460 μM), H₂O₂ = 10 mM, Fe²⁺ = 200 μM, pH = 7 for UV-C and H₂O₂/UV-C and pH = 3 for Fenton and photo-Fenton treatment.

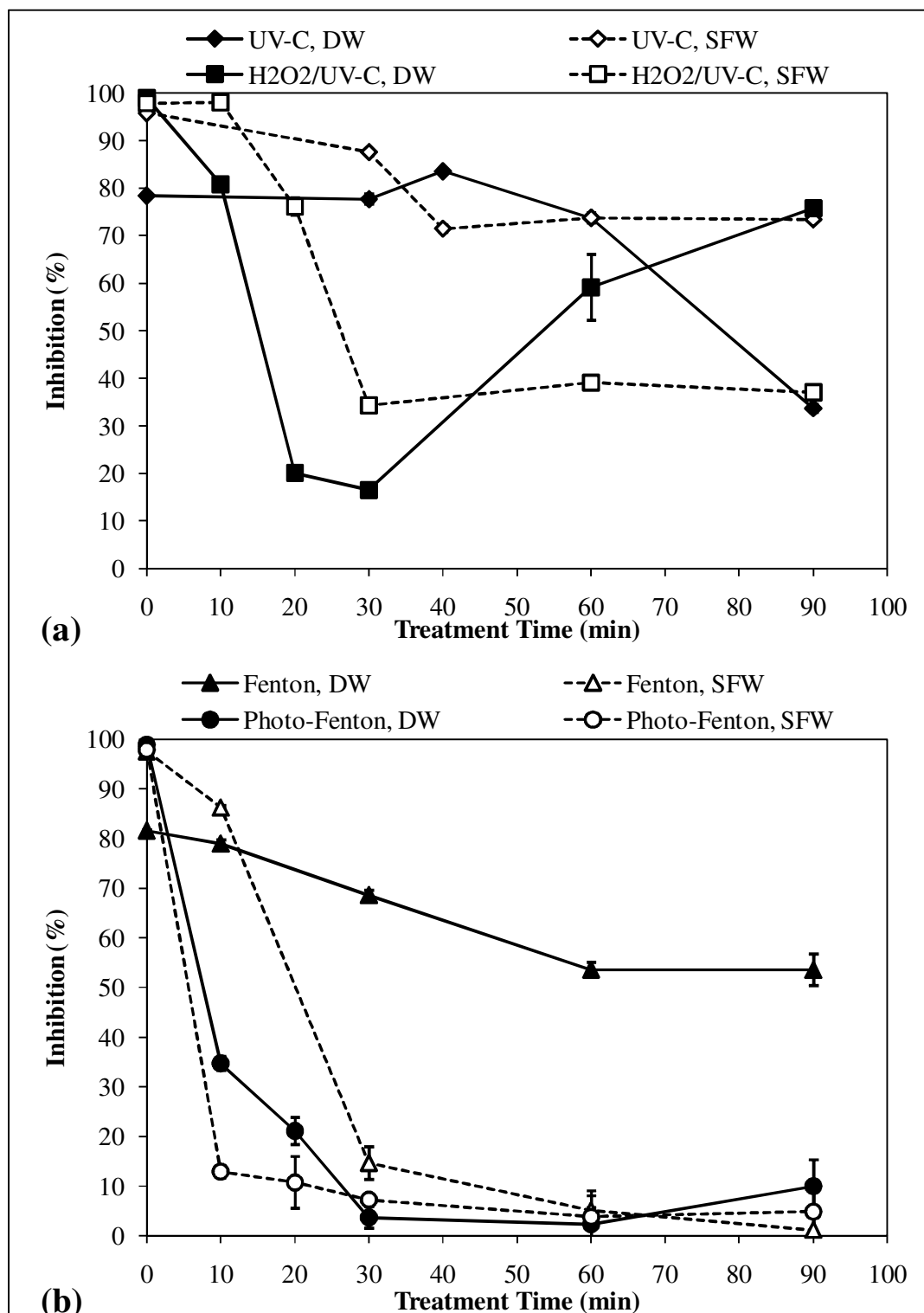


Figure 4.33. Temporal evolution of acute inhibitory effect during UV-C, H₂O₂/UV-C (a), Fenton and photo-Fenton (b) treatment of 2,4-DCP in DW and SFW. Initial experimental conditions: 2,4-DCP = 75 mg L⁻¹ (460 μM), H₂O₂ = 10 mM, Fe²⁺ = 200 μM, pH = 7 for UV-C and H₂O₂/UV-C and pH = 3 for Fenton and photo-Fenton treatment.

the case in DW, the formation and accumulation of photolysis products more toxic than 2,4-DCP were not noticed in SFW. However, the most pronounced difference between UV-C photolysis results in DW and SFW was that the acute inhibitory effect observed in SFW did not significantly change starting from 40 min UV-C photolysis, whereas a considerable reduction in acute toxic effect was evident in DW between 40-90 min of the UV-C treatment. Considering that the residual 2,4-DCP concentration in SFW after 90 min UV-C photolysis (8.6 mg L^{-1}) was nearly at the same level as its experimentally measured EC_{50} of 8.4 mg L^{-1} , the relatively high level of acute inhibitory effect of $73 (\pm 0.033)\%$ remaining in SFW after 90 min UV-C photolysis was partly contributed by 2,4-DCP photolysis products. Overall, 90 min-UV-C photolysis could not reduce the acute inhibitory effect of SFW contaminated with 2,4-DCP below 50% that proved the necessity of an additional oxidant and/or catalyst in order to provide reasonable extent of detoxification.

For the $\text{H}_2\text{O}_2/\text{UV-C}$ process, the acute inhibitory effect being observed in DW and SFW showed different trends during first 10 min of the treatment in that the acute toxic effect did not change in SFW after 10 min treatment, whereas a slight diminishment in the relative inhibition from $99 (\pm 0.0073)$ to $81 (\pm 0.61)\%$ was evidenced in DW within the same treatment time (Figure 4.33a). This strongly suggested that acutely toxic early transformation products were formed when 2,4-DCP was subjected to the $\text{H}_2\text{O}_2/\text{UV-C}$ process in SFW. Although the acute inhibitory effect noticeably decreased both in DW and SFW between 10-30 min of the $\text{H}_2\text{O}_2/\text{UV-C}$ process, the inhibition rates obtained in SFW within this time interval were greater than those achieved in DW, indicating that the concentration and identity of the formed oxidation intermediates were different for DW and SFW. According to the obtained experimental results, the re-increase in the acute inhibitory effect observed in DW was not evidenced in SFW, suggesting that the inhibitory late oxidation products identified in DW were not generated in SFW when the treatment time was prolonged beyond 30 min. Considering that the inhibition value of $34 (\pm 0.55)\%$ attained after 30 min $\text{H}_2\text{O}_2/\text{UV-C}$ treatment in SFW did not practically change further with treatment time, 30 min- $\text{H}_2\text{O}_2/\text{UV-C}$ process could be regarded as suitable for the treatment of 2,4-DCP-contaminated SFW based on acute toxicity test results.

The Fenton's reagent provided a significantly faster detoxification of 2,4-DCP in SFW as compared to that achieved in DW during first 30 min of treatment (Figure 4.33b). Ultimately, the inhibition rate measured in SFW after 90 min Fenton treatment was considerably lower ($1.2 (\pm 2.4)\%$) than that recorded in DW ($54 (\pm 3.2)\%$) after the same treatment time. It could be speculated that temporal evolution of the acute inhibitory effect during Fenton treatment of SFW contaminated with 2,4-DCP was mainly governed by the abatement of the parent pollutant. Accordingly, it may be inferred that relatively non-toxic 2,4-DCP transformation products were formed in SFW starting approximately 30 min Fenton treatment where 93% 2,4-DCP removal was achieved. Taking into account the slight decrease in relative inhibition between 30-90 min of treatment, 30 min exposure of SFW samples to the Fenton's reagent which provided an acute toxicity reduction to $15 (\pm 3.3)\%$ was sufficient to obtain a relatively safe water in terms of the acute inhibitory effect. It should also be noted that the Fenton's reagent was more effective for the detoxification of SFW contaminated with 2,4-DCP as compared to the $\text{H}_2\text{O}_2/\text{UV-C}$ process.

According to the experiments results obtained for the photo-Fenton process, the acute inhibitory effects measured in SFW during first 20 min of the treatment were slightly lower than those recorded in DW (Figure 4.33b). However, starting from 30 min photo-Fenton treatment differences between the acute toxic effects observed in DW and SFW were less pronounced. The acute inhibitory effect significantly decreased to $13 (\pm 1.2)\%$ only after 10 min photo-Fenton treatment of SFW where 91% 2,4-DCP and 11% TOC abatements were obtained. The acute inhibitory effect only slightly decreased to $4.9 (\pm 5.6)\%$ by extending the treatment time to 90 min. Therefore, it was safe to conclude that partial mineralization of 2,4-DCP in SFW by the photo-Fenton process resulted in the generation of transformation products being non-toxic towards *V. fischeri*. 10 min-photo-Fenton treatment would be recommended over other studied treatment processes for the detoxification of SFW contaminated with 2,4-DCP.

4.1.4.6. Genotoxicity. Figure 4.34 presents temporal evolution of the genotoxic effect expressed as the induction factor during UV-C, $\text{H}_2\text{O}_2/\text{UV-C}$ (a), (c), Fenton and photo-Fenton treatment (b), (d) of 2,4-DCP in DW and SFW with (c), (d) and without (a), (b) metabolic activation. According to the obtained experimental results, UV-C photolysis of 2,4-DCP in SFW resulted in an initial increase in the induction factor from 0.88 to 2.8

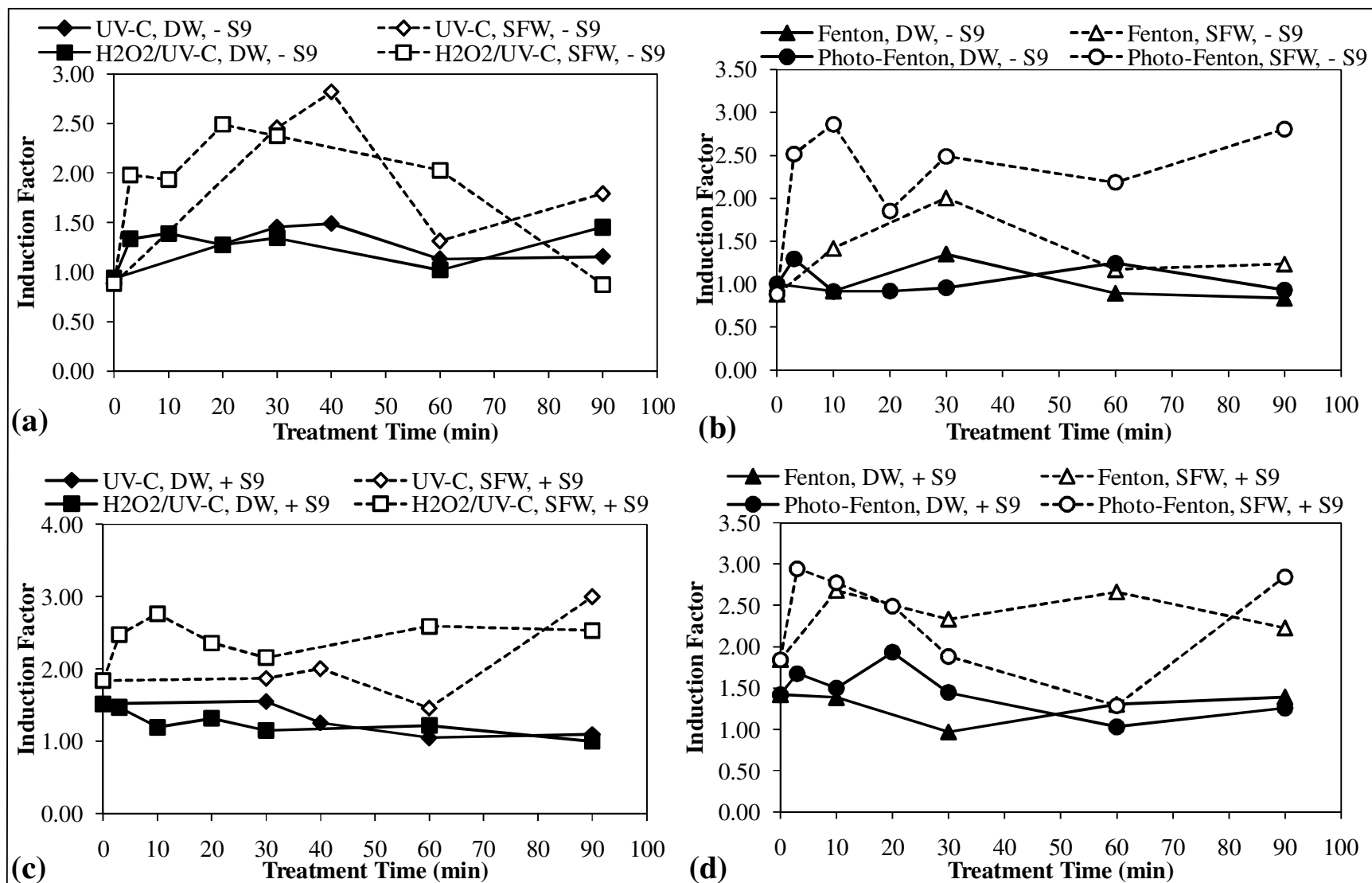


Figure 4.34. Temporal evolution of the genotoxic effect in the absence (a), (b) and presence of metabolic activation (c), (d) during UV-C, H₂O₂/UV-C (a), (c), Fenton and photo-Fenton (b), (d) treatment of 2,4-DCP in DW and SFW. Initial experimental conditions: 2,4-DCP = 75 mg L⁻¹ (460 μM), H₂O₂ = 10 mM, Fe²⁺ = 200 μM, pH = 7 for UV-C and H₂O₂/UV-C and pH = 3 for Fenton and photo-Fenton treatment.

without metabolic activation and from 1.8 to 2.0 with metabolic activation after 40 min treatment. Therefore, the first 40 min of UV-C photolysis presented risk of the formation of directly and indirectly acting, weakly genotoxic transformation products. Although the induction factor decreased to 1.8 in the absence of metabolic activation after 90 min UV-C photolysis, it increased further to 3.0 in the presence of metabolic activation. This delineated that although transformation products generated after 90 min UV-C photolysis were non-genotoxic, their metabolization brought about the formation of products exerting moderately genotoxic effect.

During H_2O_2 /UV-C treatment of 2,4-DCP in SFW, the induction factor initially increased to 2.5 and 2.8 without and with metabolic activation, respectively, indicating that 2,4-DCP was first converted into directly and indirectly acting, weakly genotoxic transformation products after 10-20 min treatment (Figure 4.34a and c). It should be noted that after 30 min H_2O_2 /UV-C treatment where a fair acute inhibitory effect of 34% was observed, the treated SFW was of weakly genotoxic character. Although the genotoxic effect obtained after 90 min H_2O_2 /UV-C treatment was far below the induction factor threshold level of 2.0 in the absence of metabolic activation, a weak genotoxic effect corresponding to an induction factor of 2.5 was noticed with metabolic activation by the liver enzyme fraction S9. Therefore, it could be concluded that H_2O_2 /UV-C treatment of 2,4-DCP in SFW was relatively unsafe based on the genotoxicity results, although it sufficiently decreased the acute inhibitory effect of the original 2,4-DCP solution.

The Fenton's reagent resulted in the generation of directly acting, weakly genotoxic transformation products during the first 30 min of treatment of SFW contaminated with 2,4-DCP, but the induction factor decreased to non-genotoxic levels following this treatment time (Figure 4.34b). The observed increase in the genotoxic effect during the first 30 min of Fenton treatment again negatively correlated with the significant decrease in the acute inhibitory effect. Unlike the case in the absence of metabolic activation, a weak genotoxic effect was apparent with metabolic activation throughout the course of Fenton treatment of SFW, which clearly indicated that the liver metabolization of transformation products brought about a higher genotoxic effect during Fenton treatment of SFW contaminated with 2,4-DCP (Figure 4.34d).

During photo-Fenton treatment of 2,4-DCP in SFW, the induction factor first increased to a near-moderate level of genotoxic effect after 3-10 min treatment without and with metabolic activation due to the generation of early transformation products (Figure 4.34b and d). These transformation products caused only slight acute inhibition as could be drawn from Figure 4.33b. The induction factor was below 2.0 only in one sample taken after 20 min photo-Fenton process, but in the presence of metabolic activation weakly genotoxic transformation products were evidenced in the same sample. Accordingly, although favorable based on acute toxicity results, the photo-Fenton process resulted in the generation of weak to near-moderate level of genotoxic effect during degradation of 2,4-DCP in SFW.

As could be deduced from this part of study, the genotoxic effects obtained in SFW were in general higher than those recorded in DW for all studied treatment processes. This might be attributed to potential differences of the identities of transformation products generated in the two water matrices. In fact, the inorganic content in the water matrix may lead to the production of some reactive species like Cl^\bullet , and in turn, chlorinated organic products which are known to be very harmful, and in some cases, persistent (Sirtori et al., 2012). Therefore, care should be taken in the genotoxic effect of AOP when dealing with inorganic salt matrices.

4.2. Studies with NP-10

4.2.1. NP-10 Baseline Experiments and Kinetics

In this thesis section, results of the baseline experiments aiming at exploring the kinetics and efficiencies of H₂O₂/UV-C, Fenton and photo-Fenton treatments for the degradation of aqueous NP-10 are described. These baseline experiments also aimed at assessing the most suitable reaction conditions for the effective removal of NP-10 via H₂O₂/UV-C, Fenton and photo-Fenton processes.

4.2.1.1. Single H₂O₂ and UV-C Photolysis Control Experiments. Single H₂O₂ oxidation and UV-C photolysis were studied mainly as control treatment processes to evidence the separate effects of oxidant and UV-C irradiation. Figure 4.35 presents changes in NP-10, TOC and H₂O₂ concentrations during treatment of NP-10 by H₂O₂ alone. Treatment of 50 mg L⁻¹ (76 μM) NP-10 with 10 mM H₂O₂ at pH 7 in the absence of UV-C irradiation for 90 min resulted in only 10% NP-10 removal, while no mineralization occurred under these conditions. H₂O₂ concentration (Figure 4.35) and pH (data not shown) did not practically change throughout the course of treatment of NP-10 by H₂O₂ alone, indirectly referring to the negligible NP-10 degradation by this control treatment process. From the obtained findings it was obvious that the conventional oxidant H₂O₂ remained inefficient for the degradation of NP-10 when applied alone.

Figure 4.36 presents changes in NP-10 concentration and TOC as well as pH during UV-C photolysis of 50 mg L⁻¹ (76 μM) NP-10. Although UV-C photolysis of NP-10 at pH 7 for 90 min ensured 85% removal of NP-10, percent TOC removal achieved by this treatment process after 90 min photolysis was negligible. The latter finding spoke for the inefficiency of UV-C irradiation alone in the degradation of NP-10 photolysis products; a major shortcoming that has also been reported in a relevant study on advanced oxidation of alkylphenol polyethoxylates (de la Fuente et al., 2010). From pH evolutions demonstrated in Figure 4.36 it could be inferred that the formation of acidic photolysis products occurred to a limited extent after 90 min UV-C photolysis.

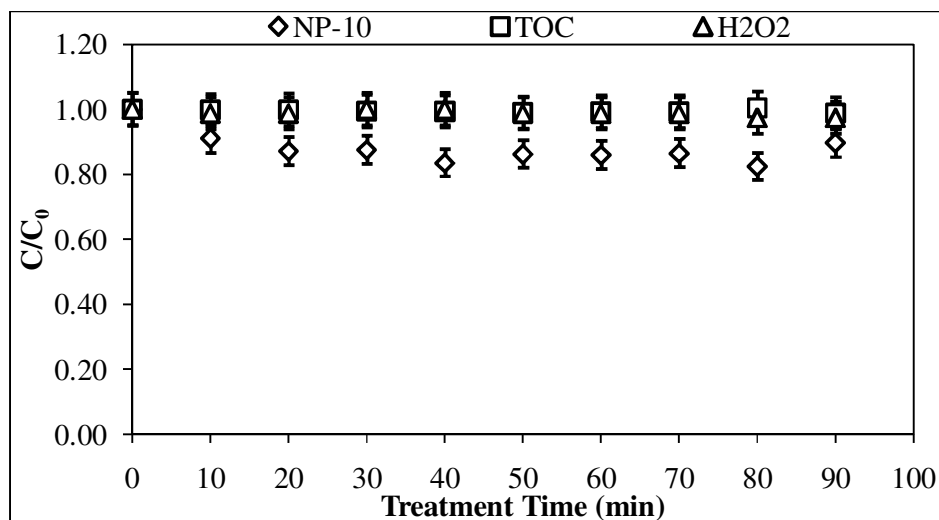


Figure 4.35. Changes in NP-10, TOC and H₂O₂ concentrations during treatment of NP-10 by H₂O₂ alone. Initial experimental conditions: NP-10 = 50 mg L⁻¹ (76 μM), H₂O₂ = 10 mM, pH = 7.

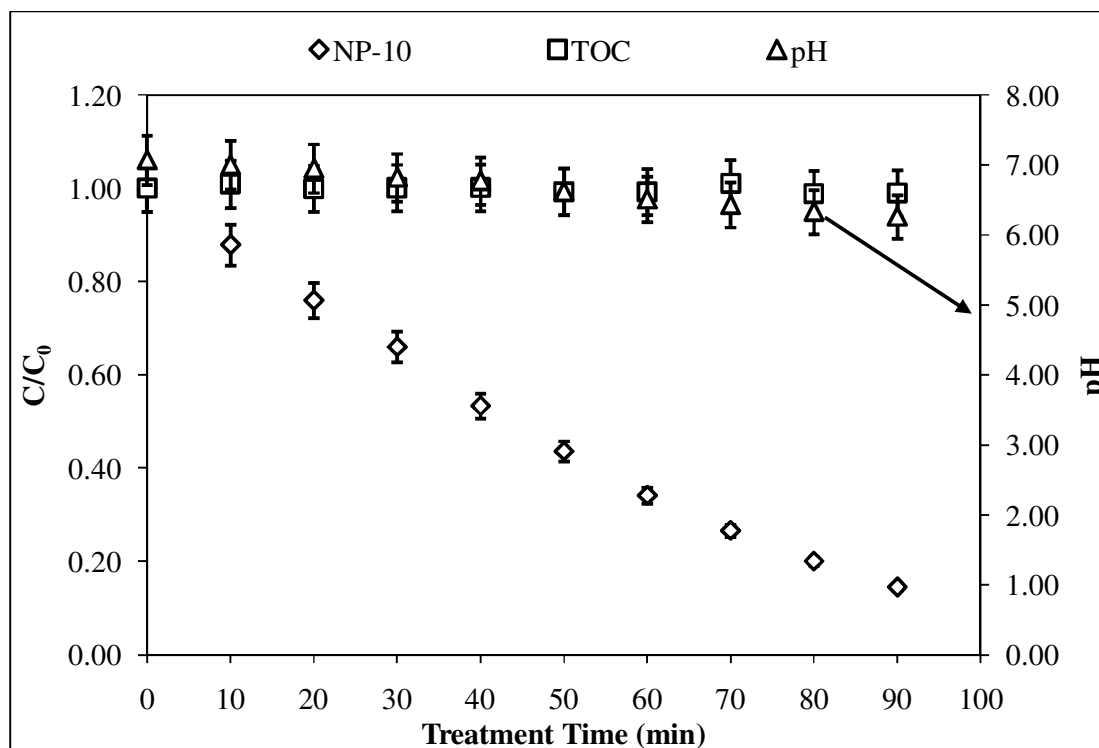


Figure 4.36. Changes in NP-10 concentration and TOC as well as pH during UV-C photolysis of NP-10. Initial experimental conditions: NP-10 = 50 mg L⁻¹ (76 μM), pH = 7.

4.2.1.2. The H₂O₂/UV-C Experiments.

Effect of Initial NP-10 Concentration. Experiments aiming at assessing the effect of initial NP-10 concentration on NP-10 and TOC removals, H₂O₂ consumption and pH evolution were performed at three different NP-10 concentrations, namely 10, 25 and 50 mg L⁻¹ (15, 38 and 76 μM), with 1 mM H₂O₂ and at an initial pH of 7. Figure 4.37a-d shows the graphs involving the effect of initial NP-10 concentration on NP-10 and TOC removal and H₂O₂ consumption kinetics as well as temporal evolution of pH. NP-10 and TOC abatements and H₂O₂ consumptions during the H₂O₂/UV-C process were fitted to the pseudo-first-order kinetics with $R^2 \geq 0.968$ for all studied initial NP-10 concentrations. The percent NP-10 and TOC removals and H₂O₂ consumptions as well as the respective pseudo-first-order abatement rate coefficients for the H₂O₂/UV-C process are summarized in Table 4.15 as a function of initial NP-10 concentration.

Table 4.15. Pseudo-first-order abatement rate coefficients and percent removal efficiencies obtained for NP-10, TOC and H₂O₂ by the H₂O₂/UV-C process as a function of initial NP-10 concentration.

	NP-10 (mg L ⁻¹)		
	10	25	50
k_{NP-10} (min ⁻¹)	2.2	0.93	0.41
NP-10 removal (%)*	100	100	100
k_{TOC} (min ⁻¹)	0.048	0.0069	—**
TOC removal (%)*	89	34	10
$k_{H_2O_2}$ (min ⁻¹)	0.057	0.041	0.038
H ₂ O ₂ consumption (%)*	100	100	97

*After 90 min treatment.

**Not determined because of insignificant removal

As is evident in Figure 4.37a, under all circumstances NP-10 removal was complete in < 20 min under the studied treatment conditions, although pseudo-first-order rate coefficients for NP-10 removal seriously decreased upon increasing the initial NP-10 concentration thereby keeping the oxidant concentration (1 mM H₂O₂) constant (Table 4.15). The inhibitory effect was also evident and even more dramatic on the basis of TOC abatements; pseudo-first-order rate coefficients for TOC removal were significantly

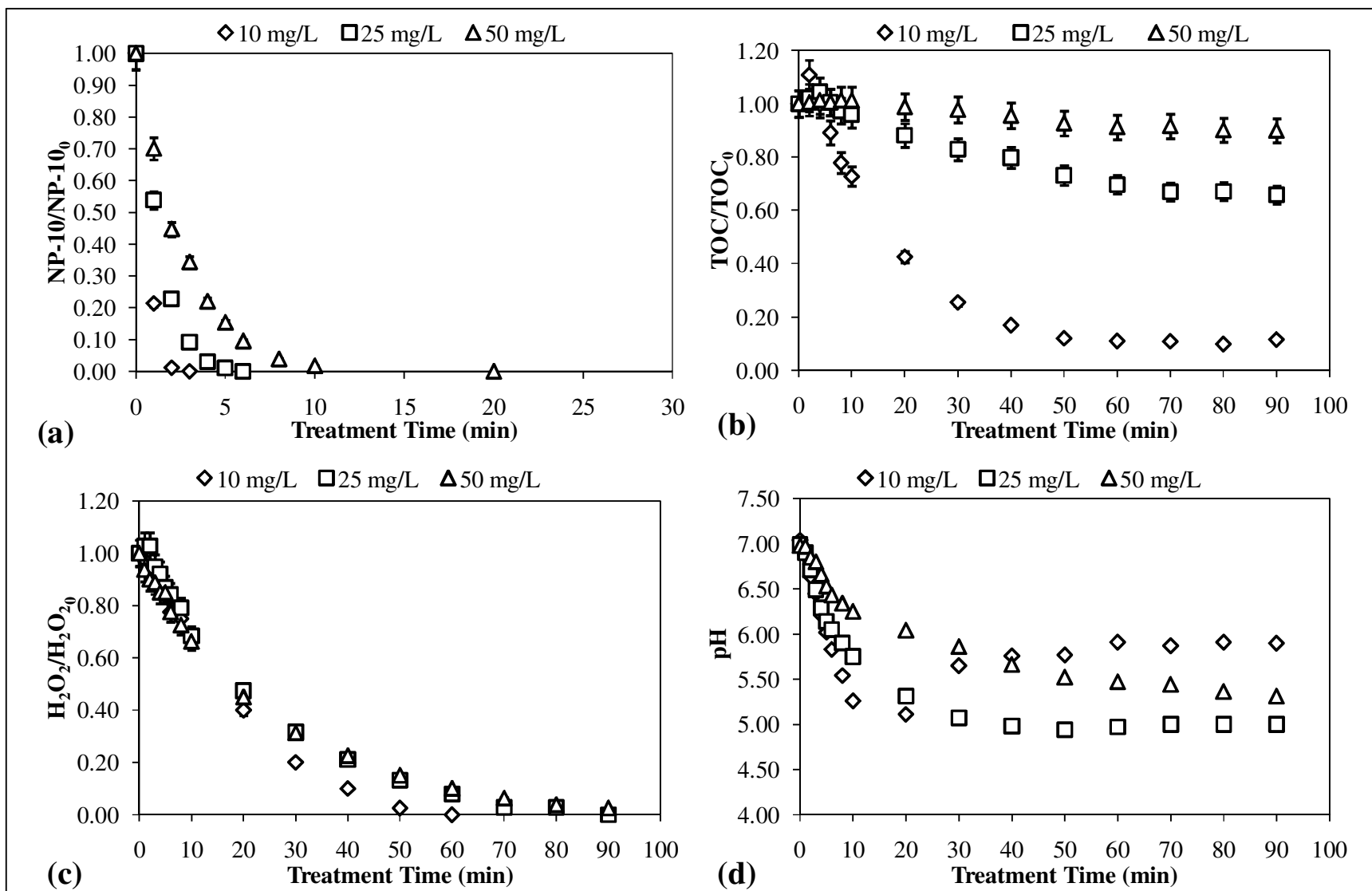


Figure 4.37. Effect of initial NP-10 concentration on the decay of NP-10 (a), TOC (b) and H₂O₂ (c) as well as the pH evolution (d) during H₂O₂/UV-C treatment of NP-10. Initial experimental conditions: H₂O₂ = 1 mM, pH = 7.

reduced, and percent TOC removals decreased from 89% for 10 mg L⁻¹ NP-10 down to 10% for 50 mg L⁻¹ NP-10 after 90 min treatment (Figure 4.37b and Table 4.15). From Figure 4.37c it could be deduced that H₂O₂ consumption was complete or near-complete (≥ 97%) after 90 min at all studied initial NP-10 concentrations. At higher NP-10 concentrations, complete or near-complete consumption of H₂O₂ may result in secondary reactions, such as accumulation and dimerization of intermediates which will affect the NP-10 degradation dramatically. The accumulation of acidic transformation products at the highest studied NP-10 concentration of 50 mg L⁻¹ was indirectly evidenced from the gradual decrease in pH as illustrated in Figure 4.37d, whereas at 10 and 25 mg L⁻¹ NP-10 the pH was stabilized or showed a re-increase starting from a certain treatment time due to faster TOC removals at these lower NP-10 concentrations. From the overall findings it is clear that for the removal of higher NP-10 concentrations the applied H₂O₂ concentration should be elevated in parallel particularly if mineralization of NP-10 is aimed.

Effect of Initial pH. The effect of initial pH varying between 3.0 and 12 during H₂O₂/UV-C treatment of 50 mg L⁻¹ (76 μM) NP-10 was investigated under the initial H₂O₂ concentration of 5 mM. The percent NP-10 and TOC removals and H₂O₂ consumptions as well as the respective pseudo-first-order abatement rate coefficients for the H₂O₂/UV-C process are summarized in Table 4.16 as a function of initial pH. In addition, NP-10 (a) and TOC removal (b) and H₂O₂ consumption kinetics (c) as well as temporal evolution of pH (d) at different initial pH values are graphically shown in Figure 4.38.

Table 4.16. Pseudo-first-order abatement rate coefficients and percent removal efficiencies obtained for NP-10, TOC and H₂O₂ by the H₂O₂/UV-C process as a function of initial pH.

	pH			
	3	7	11	12
k_{NP-10} (min ⁻¹)	0.46	0.59	0.57	0.37
NP-10 removal (%)*	100	100	100	100
k_{TOC} (min ⁻¹)	0.035	0.026	0.015	0.0093
TOC removal (%)*	76	82	73	18
$k_{H_2O_2}$ (min ⁻¹)	0.028	0.028	0.042	0.21
H ₂ O ₂ consumption (%)*	100	100	97	100

*After 90 min treatment.

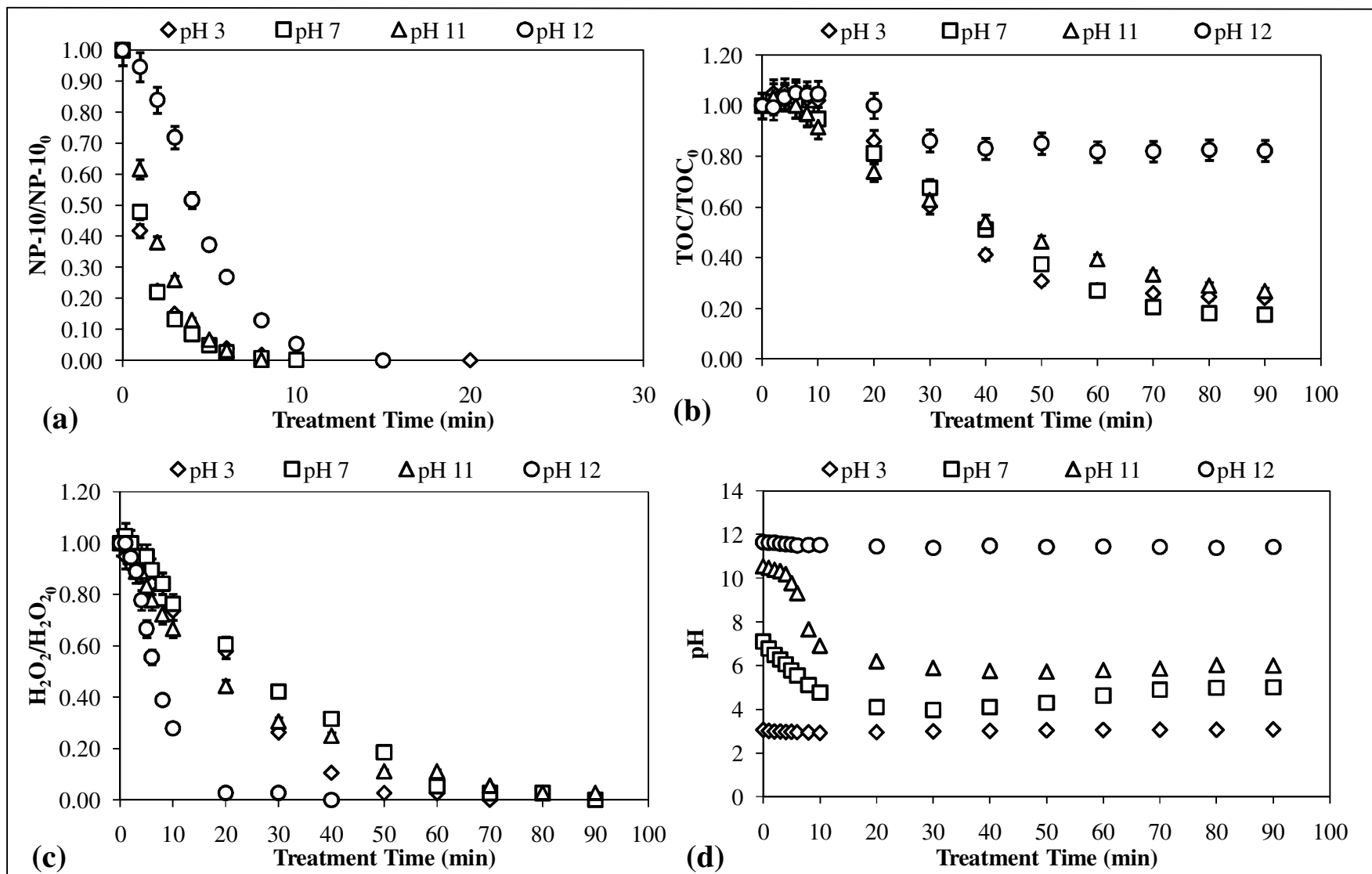


Figure 4.38. Effect of initial pH on the decay of NP-10 (a), TOC (b) and H_2O_2 (c) as well as the pH evolution (d) during $H_2O_2/UV-C$ treatment of NP-10. Initial experimental conditions: NP-10 = 50 mg L^{-1} ($76 \mu\text{M}$), $H_2O_2 = 5 \text{ mM}$.

As can be seen in Figure 4.38d, during the $\text{H}_2\text{O}_2/\text{UV-C}$ process the reaction pH which was initially adjusted to 7.0 and 11 decreased to 4.0 and 5.7, respectively, whereas it remained nearly unchanged when the reaction was initiated at pH 3.0 and 12. The pH decrease being observed within the first 30 and 50 min of reaction initiated at pH 7.0 and 11, respectively, is a consequence of the formation of acidic oxidation products (Olmez-Hanci et al., 2011). Experimental results presented in Figure 4.38a revealed that at the initial pH of 11 complete NP-10 removal was achieved after approximately 8 min treatment, whereas the time for complete NP-10 removal slightly increased to about 15 min at pH 3.0 and 12. The corresponding pseudo-first-order rate coefficients obtained for NP-10 abatement exhibited the following decreasing order; $\text{pH } 7 \approx \text{pH } 11 > \text{pH } 3 > \text{pH } 12$ (Table 4.16). Overall, it could be concluded that there was no distinct optimum pH value for NP-10 abatement by the $\text{H}_2\text{O}_2/\text{UV-C}$ process. The above results are in accord with previous studies which reported that the nonionic surfactant removal with the $\text{H}_2\text{O}_2/\text{UV-C}$ process is not pH-sensitive in the range of 3-11 (Arslan-Alaton and Erdinc, 2006; Arslan-Alaton et al., 2010). However, pseudo-first-order rate coefficients obtained for TOC abatement were found to decrease with increasing pH in the present study (Table 4.16). According to Figure 4.38b, TOC removals achieved at the initial pH values of 3.0, 7.0 and 11 were not significantly different from each other (76, 82 and 73%, respectively), whereas TOC abatement considerably slowed down at pH 12 that resulted in an ultimate TOC removal as low as 18%. This was in line with the relevant scientific literature which delineated that surfactant degradation with the $\text{H}_2\text{O}_2/\text{UV-C}$ process was seriously inhibited at $\text{pHs} > 11$ due to the enhanced dissociation rate of H_2O_2 to its conjugate base HO_2^- at extremely alkaline pH (Arslan-Alaton et al., 2007). In fact, H_2O_2 consumption patterns given in Figure 4.38c proved that the H_2O_2 was most rapidly (< 40 min) consumed when the $\text{H}_2\text{O}_2/\text{UV-C}$ process was initiated at initial pH of 12. The experimental findings support the fact that in the pH range where the self-decomposition of H_2O_2 dominantly occurs ($\text{pH} \geq 9$) less free radicals (HO^\bullet , HO_2^\bullet) can be formed via UV-C photolysis (Beltran-Heredia et al., 2001; Xu et al., 2005) which in turn retards the surfactant degradation.

Effect of Initial H_2O_2 Concentration. The effect of the initial H_2O_2 concentration on $\text{H}_2\text{O}_2/\text{UV-C}$ oxidation of 50 mg L^{-1} ($76 \mu\text{M}$) NP-10 was examined at four concentrations of H_2O_2 (1, 2, 5 and 10 mM) and at an initial pH of 7. Pseudo-first-order abatement rate coefficients and percent removal efficiencies obtained for NP-10, TOC and H_2O_2 with the

H₂O₂/UV-C process are summarized in Table 4.17 as a function of initial H₂O₂ concentration. In addition, Figure 4.39 presents the effects of increasing H₂O₂ concentration on NP-10 (a) and TOC (b) abatements, H₂O₂ consumptions (c) and pH changes (d) during H₂O₂/UV-C treatment. As evident from Table 4.17, combination of H₂O₂ with UV-C irradiation greatly enhanced the pseudo-first-order rate coefficients obtained for NP-10 abatement even at the lowest studied H₂O₂ concentration of 1 mM as compared to UV-C photolysis alone, although the pseudo-first-order rate coefficient obtained for TOC abatement was still negligibly low at this lowest H₂O₂ concentration. From Figure 4.39a it is apparent that NP-10 degradation was complete after 20 and 8 min H₂O₂/UV-C treatment when elevating the initial H₂O₂ concentration from 1 to 10 mM under the investigated reaction conditions. Accordingly, increasing H₂O₂ concentration resulted in an observable increase in pseudo-first-order rate coefficients obtained for NP-10 abatement (Table 4.17). However, the effect of initial H₂O₂ concentration was much more evident from the pseudo-first-order rate coefficients for TOC abatement for which the increment was nearly 10-fold when the initial H₂O₂ concentration was increased from 2 to 10 mM. H₂O₂ consumption patterns at varying initial H₂O₂ concentrations during H₂O₂/UV-C treatment shown in Figure 4.39c indicated that the initially added H₂O₂ was completely consumed ($\geq 97\%$ H₂O₂ consumption) at all studied initial H₂O₂ concentrations after 90 min treatment. From the obtained findings it is evident that the residual H₂O₂ con-

Table 4.17. Pseudo-first-order abatement rate coefficients and percent removal efficiencies obtained for NP-10, TOC and H₂O₂ by the H₂O₂/UV-C process as a function of initial H₂O₂ concentration.

	H ₂ O ₂ (mM)				
	0	1	2	5	10
k_{NP-10} (min ⁻¹)	0.014	0.41	0.46	0.59	0.69
NP-10 removal (%) [*]	85	100	100	100	100
k_{TOC} (min ⁻¹)	—**	—**	0.0050	0.016	0.042
TOC removal (%) [*]	1	10	28	82	97
$k_{H_2O_2}$ (min ⁻¹)	—	0.040	0.032	0.028	0.024
H ₂ O ₂ consumption (%) [*]	—	97	97	100	100

^{*}After 90 min treatment.

^{**}Not determined because of insignificant removal.

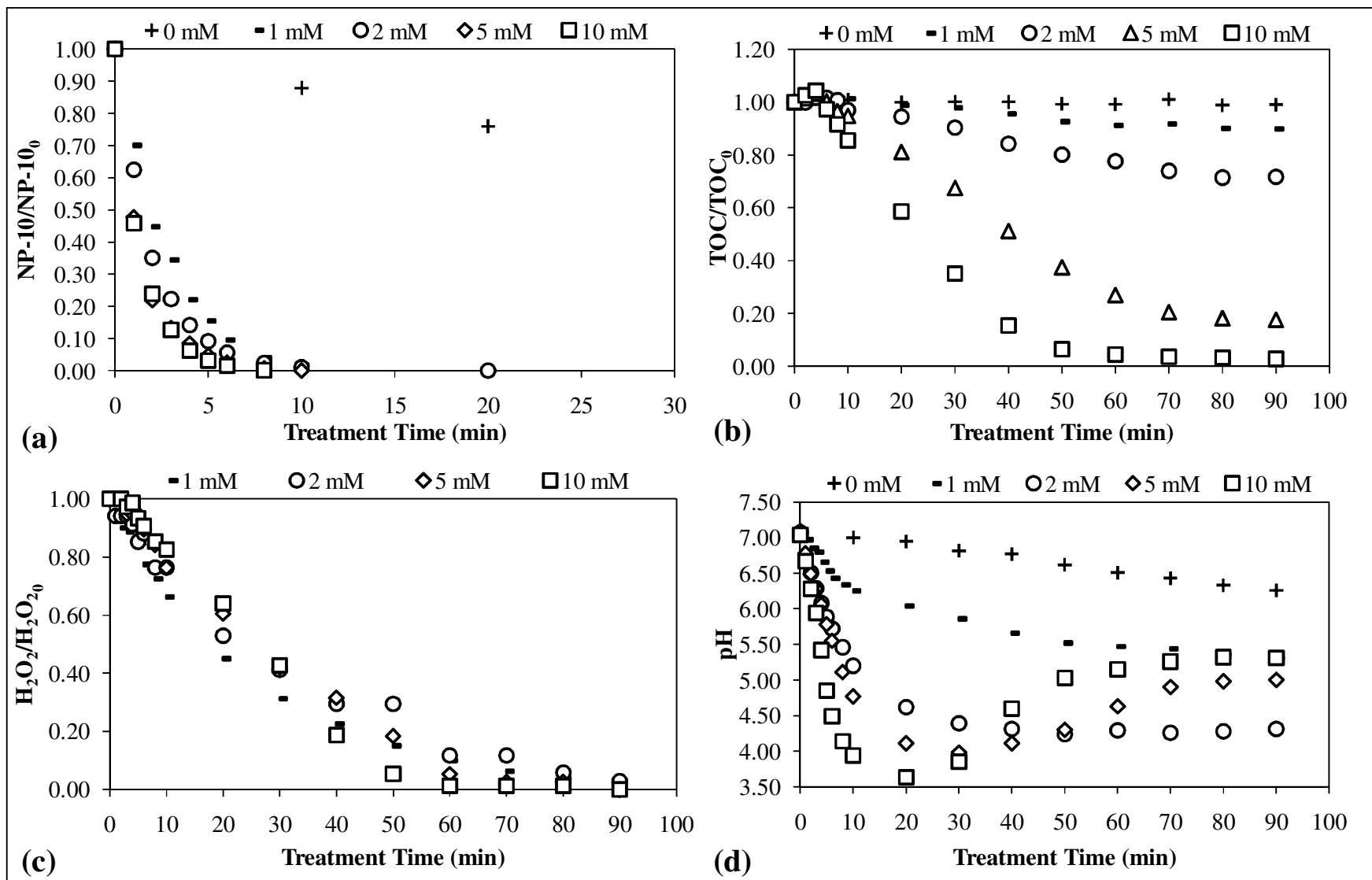


Figure 4.39. Effect of initial H₂O₂ concentration on the decay of NP-10 (a), TOC (b) and H₂O₂ (c) as well as the pH evolution (d) during H₂O₂/UV-C treatment of NP-10. Initial experimental conditions: NP-10 = 50 mg L⁻¹ (76 μM), pH = 7.

centration is the major limiting factor for mineralization of NP-10 with the H₂O₂/UV-C process. From the pH profiles given in Figure 4.39d it could be drawn that the minimum pH reached during H₂O₂/UV-C treatment of NP-10 increased and the treatment time required to reach the minimum pH level decreased with the initial H₂O₂ concentration, supporting that higher concentrations of acidic transformation products were rapidly formed by applying a higher concentration of H₂O₂. It was also found that the extent of pH re-increase after reaching the minimum level significantly increased with increasing initial H₂O₂ concentration in parallel with the higher TOC removal efficiencies obtained at greater initial H₂O₂ concentrations.

4.2.1.3. The Fenton Experiments. The 90 min-Fenton experiments were performed at an initial pH of 3 with 50 mg L⁻¹ (76 μM) NP-10, 5 mM H₂O₂ and two H₂O₂:Fe²⁺ molar ratios, namely 10:1 (5 mM:500 μM) and 50:1 (5 mM:100 μM). Pseudo-first-order abatement rate coefficients and percent removal efficiencies obtained for NP-10, TOC and H₂O₂ with the Fenton process are summarized in Table 4.18 as a function of H₂O₂:Fe²⁺ molar ratio. From Table 4.18 it is apparent that Fenton treatment performed by applying a H₂O₂:Fe²⁺ molar ratio of 10:1 resulted in a lower NP-10 removal of 38% after 90 min treatment as compared to that achieved by the H₂O₂:Fe²⁺ molar ratio of 50:1 (14% NP-10 removal). It should be underlined here that the NP-10 removal kinetics and efficiencies during Fenton treatment could be further improved by modifying the H₂O₂:Fe²⁺ molar ratios. For instance, Pagano et al. (2008) found an optimal H₂O₂:Fe²⁺ molar ratio in the range 1.4-2.1 for the Fenton oxidation of a number of alcohol and alkylphenol ethoxylates, each of which being at a concentration of 1.4 and 14 mg L⁻¹. In parallel, Kitis et al. (1999) reported that the percent COD removal of ethylene oxide/propylene oxide copolymer Pluronic L35 decreased at H₂O₂:Fe²⁺ molar ratios greater than unity.

From Table 4.18 it was also evidenced that insignificant TOC removals (≤ 10%) were obtained after 90 min Fenton treatment at both studied H₂O₂:Fe²⁺ molar ratios, indicating that the extent of surfactant mineralization was negligible under the studied experimental conditions. The residual H₂O₂ concentrations recorded during Fenton treatment of NP-10 by applying the H₂O₂:Fe²⁺ molar ratio of 10:1 was significantly lower than those obtained by applying the H₂O₂:Fe²⁺ molar ratio of 50:1 which might refer to that H₂O₂ was more efficiently transformed to generate reactive species in the presence of a higher concentrati-

Table 4.18. Pseudo-first-order abatement rate coefficients and percent removal efficiencies obtained for NP-10, TOC and H₂O₂ by the Fenton process as a function of H₂O₂:Fe²⁺ molar ratio.

	H ₂ O ₂ :Fe ²⁺ molar ratio	
	10:1	50:1
k_{NP-10} (min ⁻¹)	0.0058	—**
NP-10 removal (%)*	38	14
k_{TOC} (min ⁻¹)	—**	—**
TOC removal (%)*	≤ 10	≤ 10
$k_{H_2O_2}$ (min ⁻¹)	0.034	0.020
H ₂ O ₂ consumption (%)*	97	59

*After 90 min treatment.

**Not determined because of insignificant removal.

on of Fe²⁺. As a result, 41% of the initially added H₂O₂ was remained unreacted when a H₂O₂:Fe²⁺ molar ratio of 50:1 that also correlated with the lower NP-10 removal efficiency achieved under these experimental conditions.

4.2.1.4. Photo-Fenton Experiments.

Effect of Initial pH. Experiments with the specific aim of assessing the effect of initial pH on photo-Fenton oxidation of NP-10 were performed with initial NP-10, H₂O₂ and Fe²⁺ concentrations of 50 mg L⁻¹ (76 μM), 5 mM and 100 μM, respectively, and four initial pH values (pH 3, 4, 5 and 7). Pseudo-first-order abatement rate coefficients and percent removal efficiencies obtained for NP-10, TOC and H₂O₂ with the photo-Fenton process are summarized in Table 4.19 as a function of initial pH. Temporal decrease of normalized NP-10 (a), TOC (b) and H₂O₂ (c) concentrations was also followed during course of the photo-Fenton treatment and presented in Figure 4.40.

The results illustrated in Figure 4.40a indicated that complete NP-10 removal was achieved in < 20 min at all investigated initial pH values, and no significant difference was evidenced between the NP-10 abatement kinetics between the initial pH range of 3-7. According to Figure 4.40b, the most pronounced difference in percent TOC removal efficiencies was observed during the first 20 min of photo-Fenton treatment where a mar-

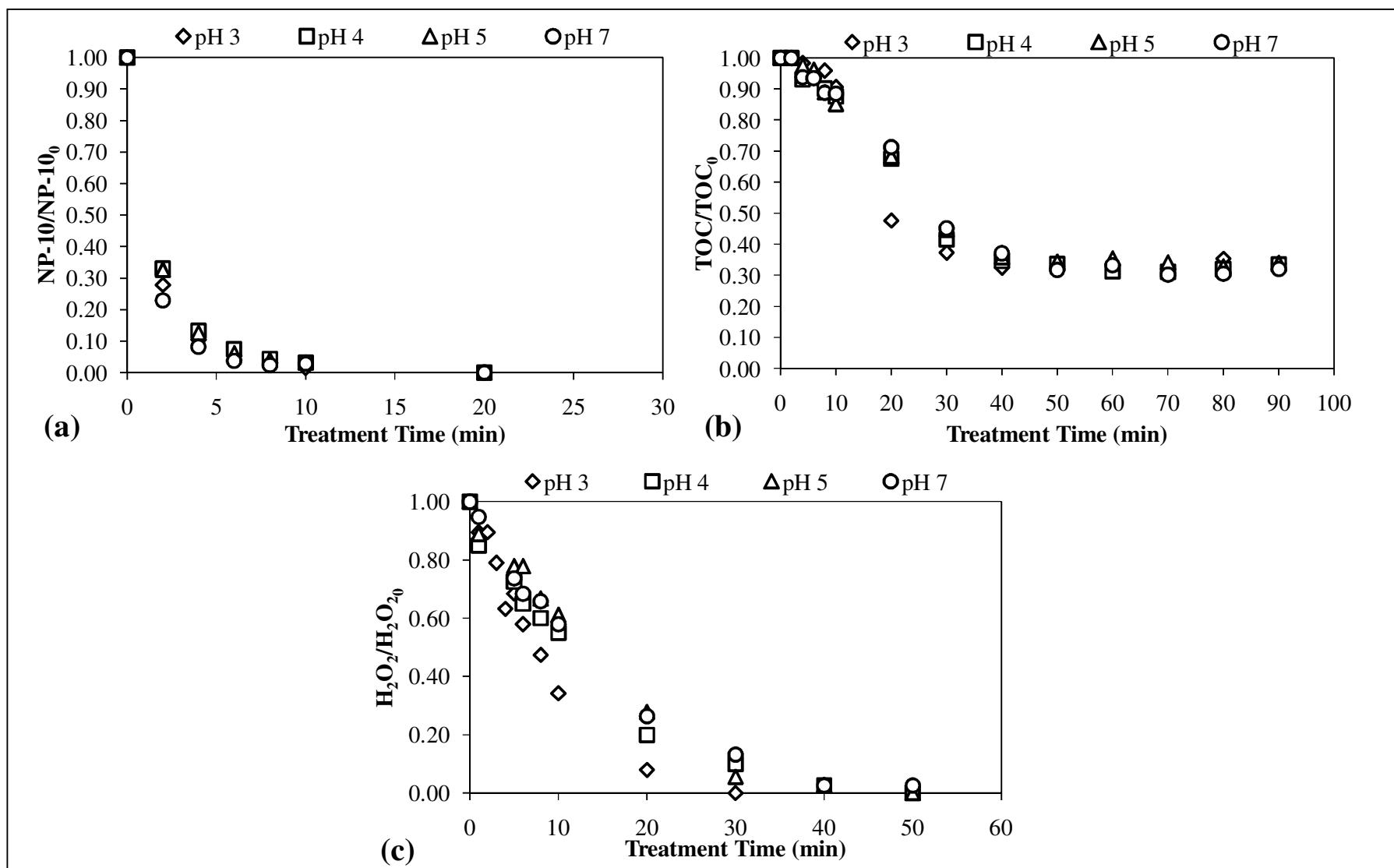


Figure 4.40. Effect of initial pH on the decay of NP-10 (a), TOC (b) and H₂O₂ (c) during photo-Fenton treatment of NP-10. Initial experimental conditions: NP-10 = 50 mg L⁻¹ (76 μM), H₂O₂ = 5 mM, Fe²⁺ = 100 μM.

Table 4.19. Pseudo-first-order abatement rate coefficients and percent removal efficiencies for NP-10, TOC and H₂O₂ during photo-Fenton process as a function of initial pH.

	pH			
	3	4	5	7
k_{NP-10} (min ⁻¹)	0.36	0.29	0.28	0.24
NP-10 removal (%) [*]	100	100	100	100
k_{TOC} (min ⁻¹)	0.043	0.036	0.032	0.031
TOC removal (%) [*]	66	66	66	68
$k_{H_2O_2}$ (min ⁻¹)	0.13	0.079	0.064	0.066
H ₂ O ₂ consumption (%) [*]	100	100	100	100

^{*}After 90 min treatment.

edly higher TOC abatement was apparent at an initial pH of 3 (52%) as compared to those obtained at pH 4-7 (29-33%). However, starting from 30 min photo-Fenton treatment on, the difference between the percent TOC removal efficiencies at varying initial pH levels was compensated due to consumption of a major fraction of H₂O₂ at all pH values after this treatment time (Figure 4.40c). Accordingly, practically same ultimate TOC removal efficiencies were obtained at all initial pH values after 90 min photo-Fenton treatment (Table 4.19). Overall speaking, photo-Fenton treatment was not significantly affected by varying the initial pH up to the neutral level (pH 7). These results encouraged to apply the photo-Fenton process for degradation of other nonylphenol polyethoxylates without significantly modifying the neutral pH conditions of water. However, it should be stressed that in the present study insensitivity of photo-Fenton treatment to varying initial pH values was most probably caused by the rapid decrease of the initially adjusted pH values already at the early stages of the photo-Fenton process to a range of 2.5-2.8 which avoided the precipitation of iron at all studied initial pH levels. Therefore, for natural waters where certain anionic constituents could buffer the pH and hinder the decrease in pH, pH might still have the critical role in photo-Fenton treatment.

Effect of Initial Fe²⁺ Concentration. Effect of initial Fe²⁺ concentration in the range 25-200 μM on photo-Fenton treatment performance for degradation of 50 mg L⁻¹ (76 μM) NP-10 was investigated under an initial H₂O₂ concentration of 5 mM and an initial pH of 3. Pseudo-first-order abatement rate coefficients and percent removal efficiencies obtained for NP-10, TOC and H₂O₂ with the photo-Fenton process are summarized in Table 4.20 as

a function of initial Fe^{2+} concentration. In parallel, Figure 4.41 presents temporal decrease in the normalized concentrations of NP-10 (a), TOC (b) and H_2O_2 (c) during photo-Fenton treatment at varying initial Fe^{2+} concentrations.

Table 4.20. Pseudo-first-order abatement rate coefficients and percent removal efficiencies for NP-10, TOC and H_2O_2 during photo-Fenton process as a function of initial Fe^{2+} concentration.

	Fe^{2+} (μM)				
	0	25	50	100	200
$k_{\text{NP-10}}$ (min^{-1})	0.45	0.41	0.38	0.36	0.25
NP-10 removal (%)*	100	100	100	100	100
k_{TOC} (min^{-1})	0.026	0.035	0.043	0.043	0.050
TOC removal (%)*	76	63	61	66	61
$k_{\text{H}_2\text{O}_2}$ (min^{-1})	0.028	0.12	0.12	0.13	0.091
H_2O_2 consumption (%)*	100	100	100	100	100

*After 90 min treatment.

As can be followed from Figure 4.41a, degradation of NP-10 was rather rapid and complete in < 20 min photo-Fenton treatment at all studied initial Fe^{2+} concentrations. Although the pseudo-first-order rate coefficients obtained for NP-10 abatement were found to follow a decreasing trend with increasing initial Fe^{2+} concentration (Table 4.20), the difference between them was considered to be insignificant. As for the percent TOC removal efficiencies (Figure 4.41b), only a slight improvement was found with increasing initial Fe^{2+} concentration during first 20-30 min of the photo-Fenton treatment. As is also apparent from Table 4.20, an increase in initial Fe^{2+} concentration from 25 to 200 μM resulted in a slight increase in the pseudo-first-order rate coefficients for TOC abatement from 0.035 to 0.050 min^{-1} . However, from comparison of Figure 4.41b and c it could be realized that TOC removal at all studied initial Fe^{2+} concentrations practically stopped after 30 min photo-Fenton treatment where $\geq 97\%$ of the initially added H_2O_2 was consumed from the reaction solution. As a result, comparable TOC removal efficiencies (61-66%) were obtained within the initial Fe^{2+} concentration range of 25-200 μM after 90 min photo-Fenton treatment. Keeping the above findings in mind, one could conclude that modification of the photo-Fenton reaction conditions in the initial Fe^{2+} concentration range of 25-200 μM only limitedly affected the treatment efficiency of photo-Fenton treatment

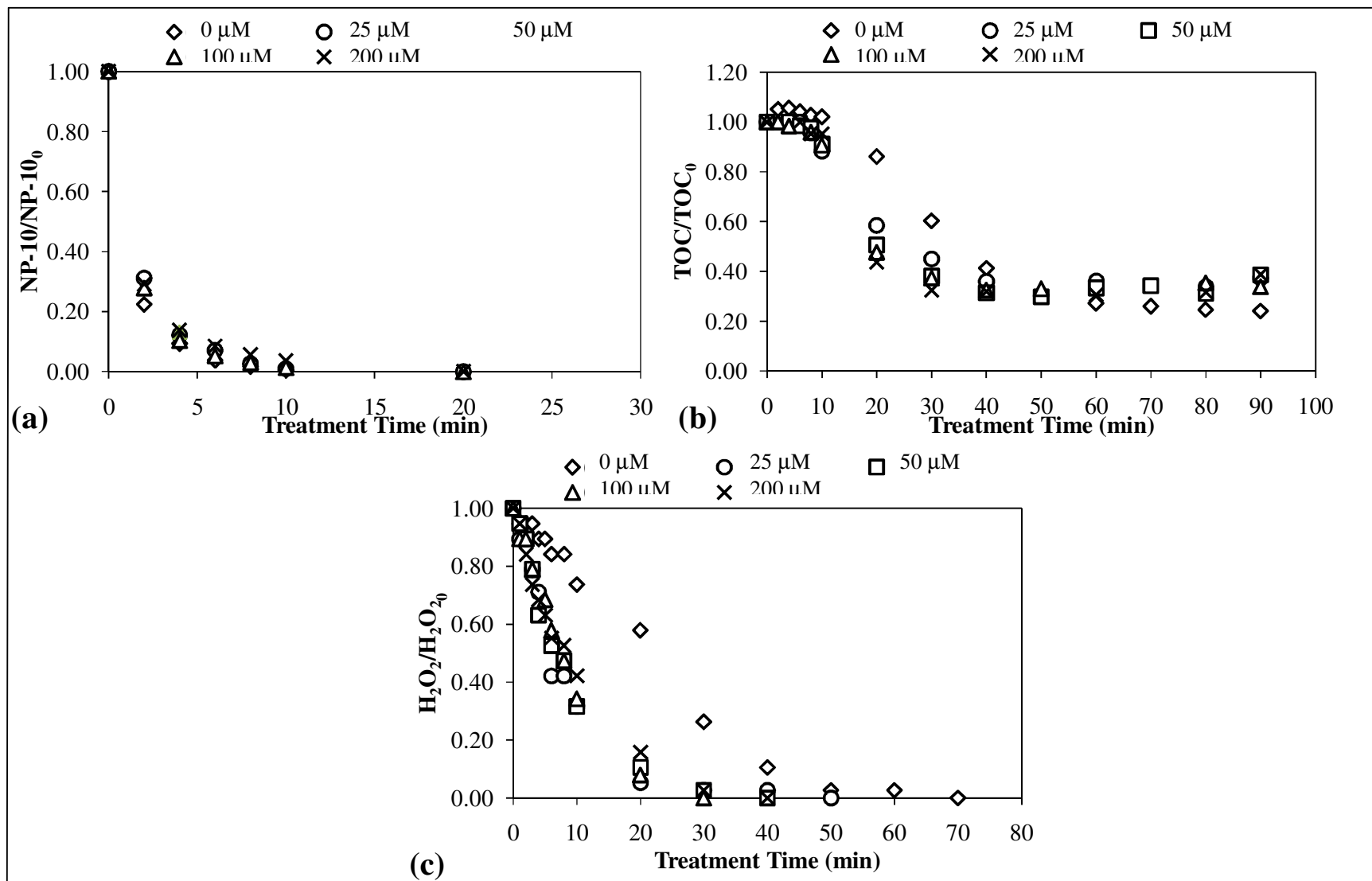


Figure 4.41. Effect of initial Fe^{2+} concentration on the decay of NP-10 (a), TOC (b) and H_2O_2 (c) during photo-Fenton treatment of NP-10.

Initial experimental conditions: NP-10 = 50 mg L⁻¹ (76 μM), H_2O_2 = 5 mM, pH = 3.

for degradation of NP-10.

4.2.1.5. Comparative Evaluation of Kinetics and Efficiencies of the Studied Treatment Processes. Prior to transformation product and toxicity assessment, H₂O₂/UV-C, Fenton and photo-Fenton treatments were also compared in terms of NP-10 and TOC abatements, H₂O₂ consumptions as well as pH and UV_{254/280} absorbance changes. Considering the findings from the above baseline experiments, 10 mM H₂O₂ and 200 μM Fe²⁺ and the initial pH values of 7.0 (for the H₂O₂/UV-C process) and 3.0 (for the Fenton and photo-Fenton processes) were chosen for the forthcoming experimental sets where an initial NP-10 concentration of 100 mg L⁻¹ (150 μM) was selected instead of 50 mg L⁻¹ (76 μM) that was used in the previous experimental runs. Accordingly, the treatment time was extended from 90 min to 120 min. UV-C photolysis as a control treatment process was also included in the comparisons. Degradation of NP-10 by UV-C, H₂O₂/UV-C, Fenton and photo-Fenton treatments was fitted to the pseudo-first-order kinetics with respect to the parent compound and TOC concentrations with $R^2 \geq 0.990$. H₂O₂ consumption during application of the studied AOP was also expressed by the pseudo-first-order kinetics with $R^2 \geq 0.990$. The pseudo-first-order abatement rate coefficients and percent removal efficiencies for NP-10, TOC and H₂O₂ during UV-C, H₂O₂/UV-C, Fenton and photo-Fenton treatment of NP-10 are summarized in Table 4.21. Additionally, temporal decrease of the normalized concentrations of NP-10 (a), TOC (b) and H₂O₂ (c) and the evolution of pH (d) during UV-C, H₂O₂/UV-C, Fenton and photo-Fenton treatment processes were depicted in Figure 4.42.

As is evident from Table 4.21 and Figure 4.42a and b, the least efficient treatment process was the Fenton treatment where low NP-10 degradation (20%) and insignificant TOC abatement (< 10%) could be achieved after 120 min treatment. The slow kinetics observed during application of the Fenton process was paralleled by a low H₂O₂ consumption rate that was incomplete (nearly 84%) at the end of treatment (Figure 4.42c). UV-C photolysis when applied alone achieved 92% NP-10 removal in 120 min, whereas the TOC removal efficiency obtained with this treatment process was < 10% at the end of treatment (Table 4.21 and Figure 4.42a and b). These findings clearly pointed out that Fenton and UV-C treatment should be replaced by more efficient treatment processes if the NP-10 and/or TOC removals would be the sole criteria.

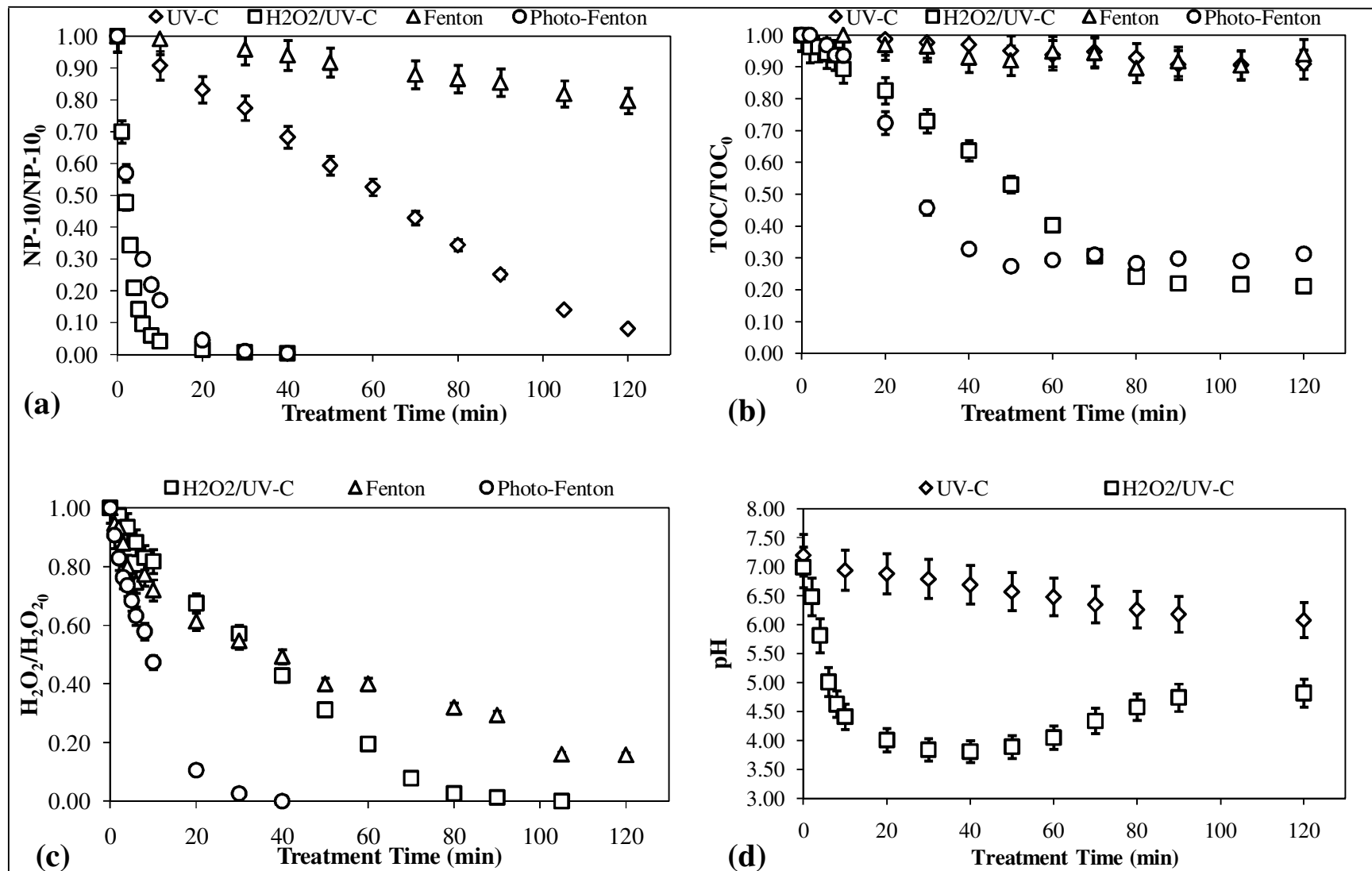


Figure 4.42. Comparison of NP-10 (a) and TOC (b) abatements, H₂O₂ consumptions (c) and pH changes (d) during UV-C, H₂O₂/UV-C, Fenton and photo-Fenton treatment of NP-10. Initial experimental conditions: NP-10 = 100 mg L⁻¹ (150 μM), H₂O₂ = 10 mM, Fe²⁺ = 200 μM, pH = 7 for UV-C and H₂O₂/UV-C and pH = 3 for Fenton and photo-Fenton treatment.

Table 4.21. Pseudo-first-order abatement rate coefficients and percent removal efficiencies obtained for NP-10, TOC and H₂O₂ by applying UV-C, H₂O₂/UV-C, Fenton and photo-Fenton treatments.

	Treatment Processes			
	UV-C	H ₂ O ₂ /UV-C	Fenton	Photo-Fenton
k_{NP-10} (min ⁻¹)	0.0085	0.40	–**	0.16
NP-10 removal (%)*	92	100	20	100
k_{TOC} (min ⁻¹)	–**	0.011	–**	0.032
TOC removal (%)*	< 10	79	< 10	69
$k_{H_2O_2}$ (min ⁻¹)	–	0.021	0.031	0.073
H ₂ O ₂ consumption (%)*	–	100	84	100

*After 120 min treatment.

**Not determined because of insignificant removal.

From Figure 4.42a and b and Table 4.21 it is evident that complete NP-10 and partial TOC abatements (79% and 69%) were obtained after 120 min treatment of NP-10 with the H₂O₂/UV-C and photo-Fenton processes, respectively. The lower ultimate TOC removal achieved by the photo-Fenton process as compared to the H₂O₂/UV-C oxidation was due to the complete consumption of H₂O₂ during first 40 min of the photo-Fenton process (Figure 4.42c). However, the slower NP-10 removal particularly observed during first 10 min of the photo-Fenton process as compared to the H₂O₂/UV-C process was attributed to the formation of Fe³⁺-NP-10 complexes at NP-10 concentration used in the present work that was above the critical micelle concentration of NP-10 of about 50 mg L⁻¹ (Wang et al., 2011). The resulting complexes might reduce the availability of NP-10 and Fe³⁺ for HO[•] attack and photoreduction, respectively (Kong and Lemley, 2007). In addition, the scientific literature reported that Fe complexes often show lower catalytic abilities for H₂O₂ decomposition as compared to free Fe ions (Ono et al., 2012) which could also account for the incomplete H₂O₂ consumption and low NP-10 removal achieved by applying the Fenton process in the present research. Considering the above experimental findings as a whole, application of the H₂O₂/UV-C and photo-Fenton processes resulted in much higher removals both in terms of NP-10 and TOC. On the other hand, incomplete mineralization achieved by these two photochemical AOP rendered the oxidation products and their toxic effects the critical point when establishing the benefits of these applied technologies.

Changes in pH were also compared during UV-C and H₂O₂/UV-C treatment of NP-10; the reaction pH gradually, but slowly decreased from its original value being 7.2 to 6.1 during UV-C photolysis of NP-10 (Figure 4.42d). On the other hand, the reaction pH rapidly decreased to 3.8 during first 40 min of the H₂O₂/UV-C treatment. The significantly lower decrease of pH being observed throughout the course of UV-C photolysis as compared to H₂O₂/UV-C treatment was most probably due to the generation of lower concentrations of acidic transformation products in the former treatment process. After 40 min H₂O₂/UV-C treatment, the pH started to increase because of the degradation of acidic transformation products and finally reached pH 4.8. This increase pattern was not observed during UV-C photolysis in parallel to the obtained insignificant TOC removal (Table 4.21).

UV absorbances were also monitored against treatment time to further evaluate efficiencies of the studied treatment processes in degrading NP-10, and the obtained results are depicted in Figure 4.43 for UV₂₈₀ (a) and UV₂₅₄ (b) absorbances. Absorbance spectra of treated and untreated aqueous NP-10 are also given in Appendix C. From Figure 4.43a it became evident that the UV₂₈₀ absorbances did not significantly change during application of UV-C and Fenton treatments in parallel to the insignificant TOC removals achieved with these treatment processes. On the other hand, initial increases in UV₂₈₀ absorbances were observed during first 20-30 min of the H₂O₂/UV-C and photo-Fenton processes which was more pronounced in the former AOP. These initial increases were also evident for UV₂₅₄ absorbances during first 20-30 min of the H₂O₂/UV-C and photo-Fenton processes, suggesting that highly aromatic early transformation products were formed during initial stages of the H₂O₂/UV-C and photo-Fenton processes (Figure 4.43b). Although no significant changes in UV₂₈₀ absorbances were apparent during application of UV-C and Fenton treatments as mentioned above, the UV₂₅₄ absorbances followed a gradually increasing trend particularly for UV-C photolysis. From the experimental results it could be established that the extent of UV₂₅₄ absorbance increase positively correlated with the pseudo-first-order rate coefficients obtained for NP-10 removal during studied treatment processes. The latter finding suggested that UV₂₅₄ parameter could be efficiently used to predict the transformation rate of NP-10 into its degradation products with different treatment processes.

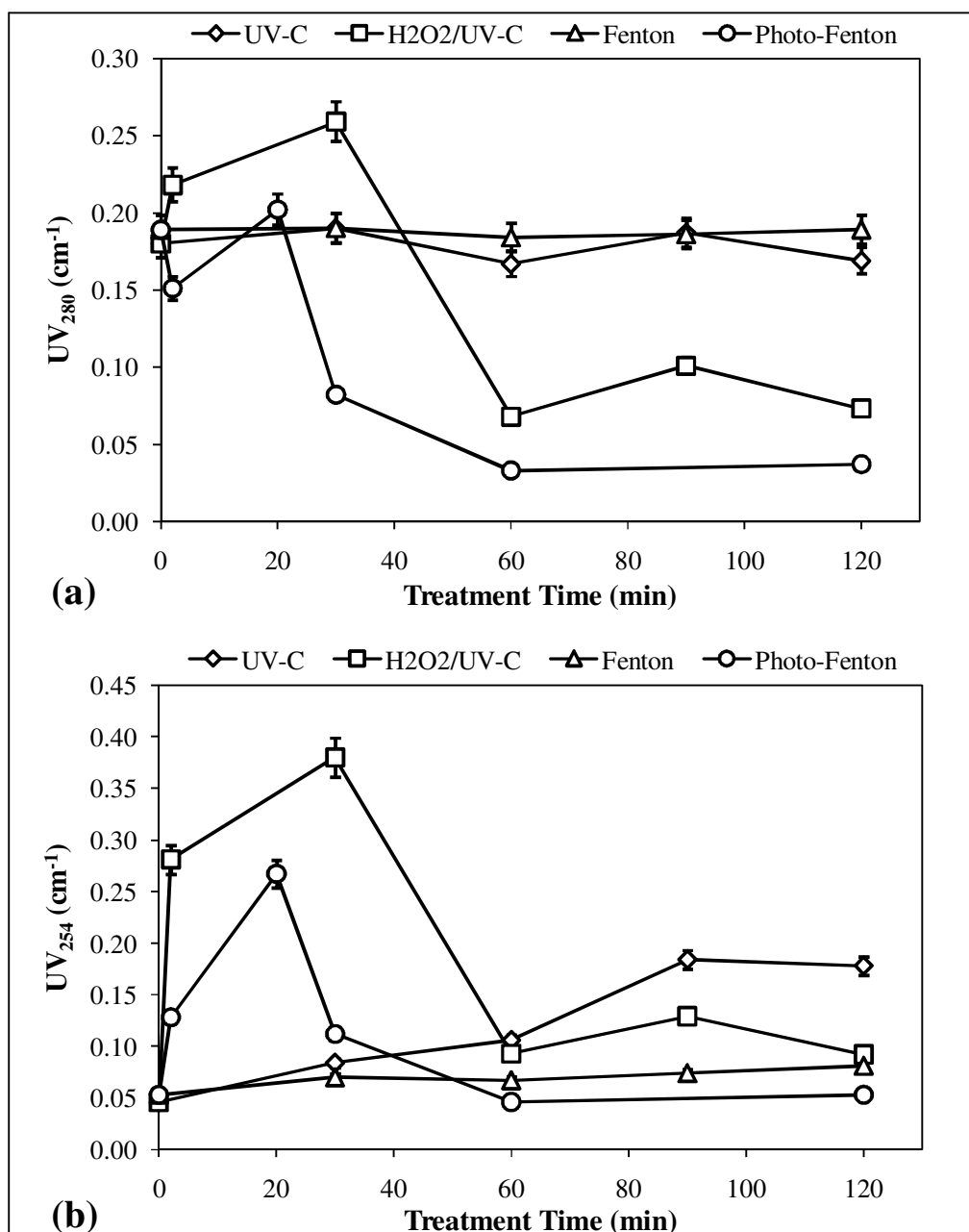


Figure 4.43. Temporal evolution of the UV absorbances at $\lambda = 280$ nm (a) and $\lambda = 254$ nm (b) during UV-C, H₂O₂/UV-C, Fenton and photo-Fenton treatment of NP-10. Initial experimental conditions: NP-10 = 100 mg L⁻¹ (150 μ M), H₂O₂ = 10 mM, Fe²⁺ = 200 μ M, pH = 7 for UV-C and H₂O₂/UV-C and pH = 3 for Fenton and photo-Fenton treatment.

4.2.2. Evolution of Transformation Products

Several previous studies have already demonstrated that UV-C, H₂O₂/UV-C, Fenton and photo-Fenton treatment could be a viable option for the efficient removal of aqueous nonylphenol polyethoxylates (Nagarnaik and Boulanger, 2011; de la Fuente et al., 2010). On the other hand, the reaction pathways and generation of transformation products arising from UV-C photolysis and AOP treatment of nonylphenol polyethoxylates have been poorly understood up to date. The identification of transformation products and the elucidation of photon- and radical-driven reaction pathways are two important tasks since they aid in optimizing the overall process efficiency by providing a more complete chemical characterization of the studied treatment processes (Fatta-Kassinos et al., 2011). Therefore, transformation products formed during UV-C, H₂O₂/UV-C, Fenton and photo-Fenton treatment of NP-10 were analyzed by HPLC, colorimetry and GC-MS throughout the course of 120 min treatment under optimized conditions (NP-10 = 100 mg L⁻¹, 150 μM; H₂O₂ = 10 mM; Fe²⁺ = 200 μM; pH 7 for UV-C and H₂O₂/UV-C and pH 3 for Fenton and photo-Fenton treatment). These experimental conditions also rendered the determination of transformation products possible.

4.2.2.1. Aromatic Transformation Products. Generally speaking, the following route has been reported in the scientific literature for the degradation of alkylphenol polyethoxylates by photolysis and AOP: fragmentation of the polyethoxylate chain length corresponding to the production of shorter-chained alkylphenol polyethoxylates and ultimately octyl- and nonylphenol (Chen et al., 2007b; Nagarnaik and Boulanger, 2011). The shortening of the aliphatic chain during the degradation of octyl- and nonylphenol may in turn lead to various transformation products including phenol, hydroquinone, benzoquinone and catechol (Neamțu and Frimmel, 2006; Brand et al., 2000) which are also the typical oxidation products of phenolic pollutants. Based on these literature data, the potential formation of six selected aromatic compounds, namely nonylphenol (1), octylphenol (2), phenol (3), catechol (4), hydroquinone (5) and benzoquinone (6) was investigated by HPLC during NP-10 degradation with UV-C, H₂O₂/UV-C, Fenton and photo-Fenton treatment.

Experimental findings indicated that octylphenol, a potential dealkylation product of nonylphenol, was not formed at detectable concentrations in any of the studied treatment processes. The HPLC analyses also revealed that phenol, catechol, hydroquinone and benzoquinone were not present in treated samples, suggesting that complete dealkylation and deethoxylation of NP-10 was never achieved by the studied treatment processes. Instead, nonylphenol was detected in NP-10 solutions that were subjected to UV-C photolysis for 50-90 min and to H₂O₂/UV-C treatment for 2 min, but could not be reliably quantified due to rather low peak areas. This was in agreement with the former study by Brand et al. (1998) who reported formation of octylphenol from the photoinduced degradation of Igepal CA 520 by Fe³⁺, an octylphenol polyethoxylate, in aqueous solution. Detection of nonylphenol in aqueous samples subjected to UV-C and H₂O₂/UV-C treatment discouraged practical application of these photochemical processes considering the toxic and endocrine disrupting potential of nonylphenol.

4.2.2.2. Aliphatic Transformation Products. Besides aromatic transformation products, generation of aliphatic compounds may also be anticipated during degradation of NP-10 by UV-C photolysis and AOP. As is known from the relevant scientific literature, HO[•] attack on the benzene ring and polyethoxylate chain could result in the formation of low molecular mass aliphatic carboxylic acids. Formic and acetic acids have been identified by Horikoshi et al. (2002) in the photodegradation of NP-9 catalyzed by TiO₂. Oxalic acid has been identified by Vinodgopal et al. (2001) as the only organic species remaining in Teric GN9 (a nonylphenol polyethoxylate with an average of nine ethylene oxide units) surfactant solution subjected to ultrasonic irradiation. Although not reported for alkylphenol polyethoxylates so far, maleic acid formation has been evidenced during wet oxidation of sodium salt of dodecylbenzene sulfonate, an anionic surfactant (Dhale and Mahajani, 2001). Considering the above-cited works, the HPLC analysis of formic, acetic, oxalic and maleic acids was performed for the studied treatment processes.

Maleic acid which is the indicator of the opening of benzene ring was not detected during the course of the studied treatment processes excluding two samples taken after 105 and 120 min Fenton treatment where maleic acid was measured only at concentrations close to the detection limit (0.10 mg L⁻¹). On the other hand, formic, acetic and oxalic acids were all identified as the degradation products of NP-10. Temporal evolution of oxalic (a),

acetic (b) and formic (c) acids during UV-C, H₂O₂/UV-C, Fenton and photo-Fenton treatment of NP-10 is displayed in Figure 4.44. As could be deduced from 4.44a, oxalic acid could be detected only in samples subjected to the H₂O₂/UV-C process after prolonged treatment (60-120 min) and at relatively low concentrations between 1.4 and 4.1 mg L⁻¹. Oxalic acid reached its maximum concentration 30 min after its first appearance in the treated samples, decreased thereafter and ultimately remained unchanged after 105 min H₂O₂/UV-C treatment where H₂O₂ was completely consumed. This finding suggested that degradation of oxalic acid with the H₂O₂/UV-C process was induced by the HO[•] attack rather than UV-C photolysis.

Acetic acid was formed during application of the H₂O₂/UV-C and photo-Fenton processes, whereas Fenton and UV-C treatment did not result in the generation of acetic acid at detectable concentrations. The absence of acetic acid in the samples subjected to UV-C and Fenton treatment was speculatively due to the incomplete and even low NP-10 transformation as well as insignificant mineralization obtained with these treatment processes. As could be interpreted from Figure 4.44b, temporal evolution of acetic acid during H₂O₂/UV-C and photo-Fenton treatment of NP-10 showed different patterns. Acetic acid formation observed at initial stages of the photo-Fenton process did not significantly change starting from 40 min treatment where H₂O₂ was completely consumed, suggesting that acetic acid could not be eliminated from the reaction solution by UV-C irradiation alone and/or in the presence of Fe³⁺. As for the H₂O₂/UV-C process, although complete consumption of H₂O₂ was apparent after 105 min H₂O₂/UV-C treatment, acetic acid concentration did not necessarily change starting from 80 min treatment. Comparative evaluation of the H₂O₂/UV-C and photo-Fenton processes in terms of acetic acid formation demonstrated that a higher acetic acid concentration of 23 mg L⁻¹ was reached in the H₂O₂/UV-C process than that measured in the photo-Fenton process (14 mg L⁻¹). Acetic acid reached its maximum concentration after 40 min H₂O₂/UV-C treatment where complete NP-10 removal was achieved, and thereafter decreased to 14 mg L⁻¹ after 120 min treatment. For the photo-Fenton process, acetic acid concentration increased throughout the course of 120 min treatment, although the increase notably slowed down starting from 40 min treatment. Exactly same level of acetic acid of 14 mg L⁻¹ was found in samples taken after 120 min H₂O₂/UV-C and photo-Fenton processes.

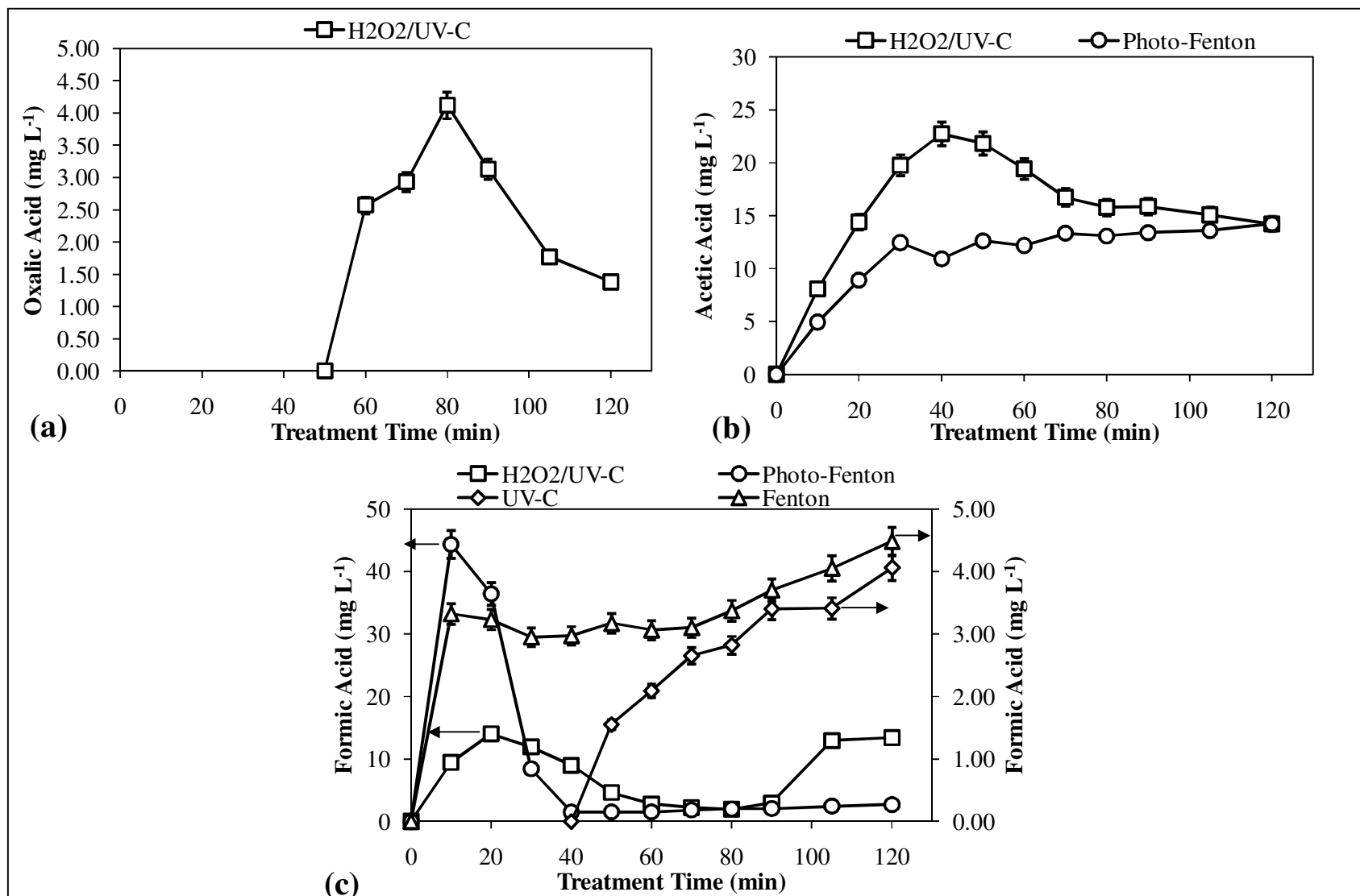


Figure 4.44. Temporal evolution of oxalic (a), acetic (b) and formic (c) acids during UV-C, H₂O₂/UV-C, Fenton and photo-Fenton treatment of NP-10. Initial experimental conditions: NP-10 = 100 mg L⁻¹ (150 μM), H₂O₂ = 10 mM, Fe²⁺ = 200 μM, pH = 7 for UV-C and H₂O₂/UV-C and pH = 3 for Fenton and photo-Fenton treatment.

As is evident from Figure 4.44c, only a small concentration of formic acid was detected at the end of 120 min Fenton and UV-C treatment, verifying the low NP-10 and TOC removals achieved by these treatment processes. On the other hand, rapid degradation of NP-10 observed during the first 10-20 min of H₂O₂/UV-C and photo-Fenton treatment was accompanied by immediate formation of formic acid. Among the studied treatment processes, the highest formic acid concentration of 44 mg L⁻¹ was measured during the photo-Fenton process which was followed by H₂O₂/UV-C (14 mg L⁻¹), Fenton (4.5 mg L⁻¹) and UV-C treatment (4.1 mg L⁻¹). During application of the H₂O₂/UV-C and photo-Fenton processes, formic acid reached its peak concentration after the respective NP-10 removals of 98 and 83% were obtained. An interesting finding drawn from this experimental part of the study was that formic acid concentration started to re-increase towards end of the H₂O₂/UV-C and photo-Fenton processes where mineralization practically stopped due to complete consumption of H₂O₂. This re-increase occurred to a greater extent during the H₂O₂/UV-C process than in the photo-Fenton system. A close inspection of Figure 4.44a and c revealed that the re-increase in formic acid concentration in the H₂O₂/UV-C process was paralleled by the degradation of oxalic acid after its peak concentration, suggesting that the re-appearance of formic acid towards the end of H₂O₂/UV-C treatment was mainly originated from degradation of oxalic acid according to the following reaction:



From the scientific literature, generation of aliphatic aldehydes including formaldehyde, acetaldehyde, glyoxal and methylglyoxal has been reported during transformation of nonylphenol polyethoxylates by the AOP (Kim et al., 2005), and therefore, the colorimetric determination of aliphatic aldehydes as a sum parameter was also performed for the studied treatment processes. According to the obtained results, aldehyde formation was evident for all studied treatment processes. Evolution of aldehydes during UV-C, H₂O₂/UV-C, Fenton and photo-Fenton treatment of NP-10 is displayed in Figure 4.45. Formation of only 0.14 mg L⁻¹ aldehydes at the end of 120 min Fenton process correlated well with the respective NP-10 and TOC removals of 20 and < 10% obtained by this AOP. As for UV-C photolysis, despite the lower pseudo-first-order rate coefficient obtained for NP-10 abatement as compared to those achieved by the H₂O₂/UV-

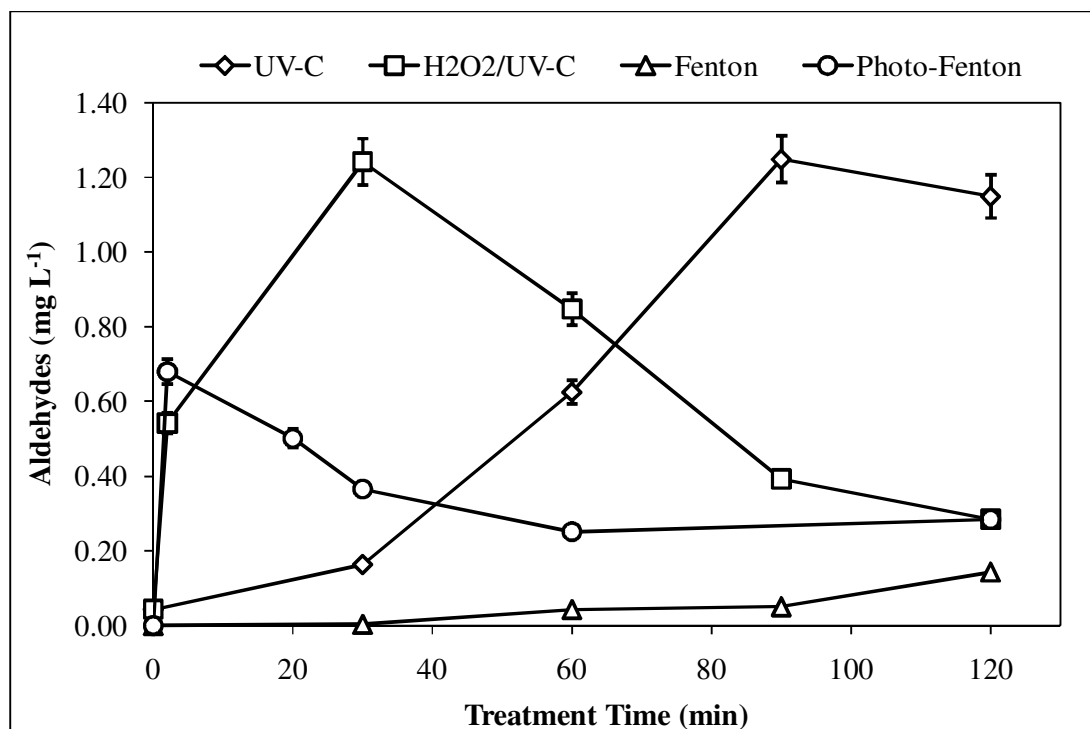


Figure 4.45. Temporal evolution of aldehydes during UV-C, H₂O₂/UV-C, Fenton and photo-Fenton treatment of NP-10. Initial experimental conditions: NP-10 = 100 mg L⁻¹ (150 μM), H₂O₂ = 10 mM, Fe²⁺ = 200 μM, pH = 7 for UV-C and H₂O₂/UV-C and pH = 3 for Fenton and photo-Fenton treatment.

C and photo-Fenton processes, the same maximum aldehyde concentration of 1.2 mg L⁻¹ was reached during UV-C and H₂O₂/UV-C treatment of NP-10. During UV-C photolysis, however it took 90 min for aldehydes to reach their maximum concentration in parallel to the insignificant mineralization obtained by applying this treatment process. In the H₂O₂/UV-C and photo-Fenton processes, aldehydes reached their respective peak concentrations of 1.2 and 0.68 mg L⁻¹ after 30 and 2 min treatment, respectively where the respective NP-10 removals of 99 and 43% were achieved via the H₂O₂/UV-C and photo-Fenton processes. The higher production of aldehydes in the H₂O₂/UV-C process as compared to the photo-Fenton process after 30 min treatment could be well explained by the finding that a higher extent of mineralization being 54% was achieved by applying photo-Fenton treatment within first 30 min of the reaction. Higher production of aldehydes during H₂O₂/UV-C and UV-C treatment of a nonylphenol polyethoxylate compound than in the photo-Fenton process has also been reported in a previous study by de la Fuente et al. (2010) in agreement with the present findings. However, it should be noted that

aldehydes were more efficiently eliminated by the H₂O₂/UV-C process in relation with the availability of H₂O₂ still after 30 min treatment, whereas the reaction practically stopped due to nearly complete consumption of H₂O₂ in the photo-Fenton process after the same treatment time.

The experimental results described in this subsection delineated that a degree of aliphatic carboxylic acids and aldehydes was still existent at the end of studied treatment processes which was most pronounced for H₂O₂/UV-C treatment. Overall speaking, the studied treatment processes did not ensure complete disappearance of aliphatic aldehydes and carboxylic acids even after 120 min treatment under the pre-established experimental conditions based on NP-10 and TOC removals.

4.2.2.3. GC-MS Analyses. GC-MS analyses were performed on samples being subjected to UV-C, H₂O₂/UV-C, Fenton and photo-Fenton treatment to characterize the oxidation products of volatile nature. Table 4.22 presents chemical structures, major mass fragments and their relative abundances for transformation products identified in different treatment processes. According to the obtained results, nonylphenol was identified as a transformation product of NP-10 only during UV-C photolysis. It produced a base peak of m/z 149 and the major fragment ions of m/z 107 and 121, but no other major fragments in the region of m/z 151-219 and molecular mass ion (m/z 220). This fragmentation pattern was assigned an alpha-methyl, beta-methyl configuration as suggested by Wheeler et al. (1997) and given in Table 4.22. The experimental findings revealed that nonylphenol was detectable starting from 30 min UV-C photolysis and persisted in the reaction solution after 120 min treatment.

As is evident from Table 4.22, PEG were identified as a common oxidation product of the studied treatment processes, suggesting that deethoxylation was the primary pathway for NP-10 degradation regardless of the type of treatment process. The total ion chromatogram obtained after full-scan GC-MS analysis of the sample, which was subjected to photo-Fenton treatment for 2 min, and the mass spectra of identified PEG were given in Appendix D. The base peak in the mass spectra was (C₂H₄O)H⁺ at m/z 45 in all cases, whereas the major fragment ions were HO=CH₂⁺, C₂H₃O⁺, (C₂H₄O)₂H⁺ and (C₂H₄O)₂C₂H₃O⁺ at m/z 31, 43, 89 and 87, respectively. The high mass ions in the m/z range

Table 4.22. Transformation products identified by GC-MS during UV-C, H₂O₂/UV-C, Fenton and photo-Fenton treatment of NP-10.

Structure	Name	Retention Time (min)	Major fragments, <i>m/z</i> (Relative Abundance, %)	Treatment Process
	Nonylphenol	31	149 (100); 107 (61); 121 (33)	UV-C
	Diethylene glycol	11	45 (100); 31 (36); 43 (24)	UV-C; H ₂ O ₂ /UV-C
	Triethylene glycol	26	45 (100); 31 (22); 89 (21)	UV-C; H ₂ O ₂ /UV-C; Fenton; Photo-Fenton
	Tetraethylene glycol	32	45 (100); 89 (24); 43 (14)	UV-C; H ₂ O ₂ /UV-C; Fenton; Photo-Fenton
	Pentaethylene glycol	38	45 (100); 89 (28); 43 (13)	UV-C; H ₂ O ₂ /UV-C; Fenton; Photo-Fenton
	Hexaethylene glycol	43	45 (100); 89 (31); 43 (13)	UV-C; H ₂ O ₂ /UV-C; Fenton; Photo-Fenton
	Heptaethylene glycol	47	45 (100); 89 (34); 87 (14)	UV-C; H ₂ O ₂ /UV-C; Fenton; Photo-Fenton
	Octaethylene glycol	51	45 (100); 89 (36); 87 (15)	UV-C; H ₂ O ₂ /UV-C; Fenton; Photo-Fenton

of 177 to 353 which were separated by 44 mass units of an ethoxy unit, together with retention times also allowed the differentiation of the PEG oligomers containing 3-8 ethoxy units after logarithmic scaling of the relative abundances to compensate the difference between major and minor mass fragments. Although commercial nonylphenol polyethoxylates may also contain PEG as an impurity in their formulations (Brand et al., 1998), GC-MS chromatograms of the original NP-10 solution did not indicate the presence of these substances at detectable levels, revealing that PEG were originated from the degradation of NP-10 by the studied treatment processes. Formation of PEG during advanced oxidation of nonylphenol polyethoxylates has already been reported in previous studies (Castillo et al., 2001; Petrovic et al., 2004; Schrank et al., 2004; Petrovic et al., 2007), speaking for a degradation pathway involving cleavage of the oxyethylene monomeric units and/or central fission as a consequence of HO^\bullet attack. Although identified for all studied treatment processes, the formation and degradation patterns of PEG differed between different processes as could be drawn from Figure 4.46. For instance, PEG being immediately generated at initial stages of the $\text{H}_2\text{O}_2/\text{UV-C}$ and photo-Fenton processes were found to disappear to non-detectable levels after 30 min treatment, whereas for UV-C and Fenton treatment formation of these transformation products was evident only after 30 and 60 min treatment, respectively, due to the slow degradation of NP-10 during these latter treatment processes. Additionally, a lower PEG yield was obtained in the first 2 min of $\text{H}_2\text{O}_2/\text{UV-C}$ process (total peak area = 3.9×10^8) as compared to the photo-Fenton process (total peak area = 1.1×10^9), which could be attributed to the degradation of PEG concurrent with their generation proceeding at a faster rate in the former AOP. This faster PEG transformation observed in the $\text{H}_2\text{O}_2/\text{UV-C}$ process was correlated with the higher pseudo-first-order rate coefficient of 0.40 min^{-1} for NP-10 removal obtained in this treatment process, suggesting the hindering role of Fe^{3+} -PEG complexes in the photo-Fenton process that delays the initial degradation of PEG by HO^\bullet , similar to the case of Fe^{3+} -NP-10 complexes.

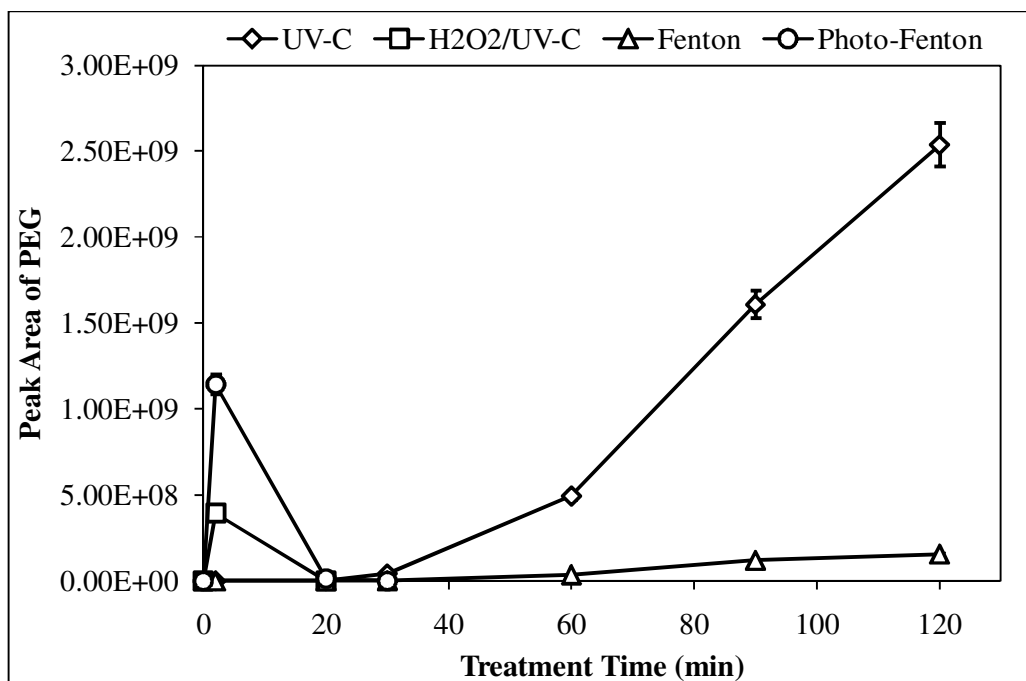


Figure 4.46. Temporal evolution of PEG during UV-C, H₂O₂/UV-C, Fenton and photo-Fenton treatment of NP-10. Initial experimental conditions: NP-10 = 100 mg L⁻¹ (150 μM), H₂O₂ = 10 mM, Fe²⁺ = 200 μM, pH = 7 for UV-C and H₂O₂/UV-C and pH = 3 for Fenton and photo-Fenton treatment.

4.2.3. Toxicity Evolution During Transformation of NP-10

4.2.3.1. Acute Toxicity Evolution. According to Figure 4.47, there was no clear concentration-inhibition relationship evident for NP-10 within the concentration range of 3.9-31 mg L⁻¹ (log NP-10 = 0.59-1.5) (for 15 min exposure time), which is below the critical micelle concentration of NP-10 (about 50 mg L⁻¹; Wang et al., 2011). However, surprisingly, above the critical micelle concentration (log NP-10 > 1.5), acute inhibitory effect inversely correlated with the surfactant concentration for which the reason is unknown. In the study conducted by Goel et al. (2003), the *EC*₂₀ value of NP-10 for 30 min exposure time was found as 32 mg L⁻¹ by means of the *V. fischeri* luminescence inhibition test. In the present study, after 30 min exposure, 31 mg L⁻¹ NP-10 caused a 24 (± 0.35)% inhibition (data not shown), showing a close proximity to the finding provided by Goel et al. (2003). Overall, from these tests, it became possible to verify that NP-10 is non-toxic to the *V. fischeri* photobacteria.

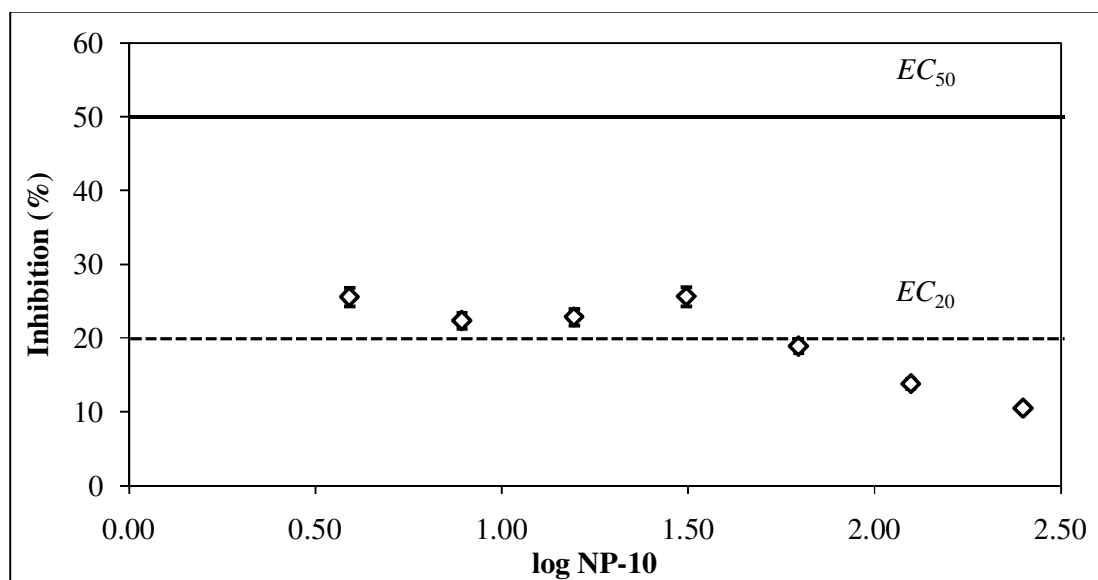


Figure 4.47. Changes in percent relative inhibition within the NP-10 concentration range of 3.9-250 mg L⁻¹ (5.8-375 μM).

Temporal evolution of acute toxicity towards *V. fischeri* during UV-C photolysis as well as H₂O₂/UV-C, Fenton and photo-Fenton treatment of 100 mg L⁻¹ NP-10 is depicted in Figures 4.48-4.50 in terms of percent relative inhibition of the luminescence intensities.

Possible relationships between the acute toxicity changes and common transformation products of the studied treatment processes, namely aliphatic carboxylic acids, aldehydes and PEG, were also evaluated. During UV-C photolysis, relative inhibition of NP-10 originally being $8.9 (\pm 5.4)$ reached $36 (\pm 0.27)\%$ after 90 min treatment and thereafter (> 90 min) did not significantly change (Figure 4.48). The increase in acute inhibitory effect being observed during UV-C photolysis was caused by the degradation of NP-10 to more toxic transformation products and the accumulation of these degradation products throughout UV-C photolysis. From Figure 4.48, it can be realized that the formed photolysis products increased gradually during UV-C photolysis, verifying the above suggestion. On the other hand, a more careful elucidation of Figure 4.48 revealed that the evolution of acute inhibitory effect followed almost exactly the same pattern with aldehydes and nonylphenol. Formaldehyde is already well known for its bacteriostatic and bactericidal properties even at low concentrations (Vighi et al., 2009), and hence, toxicity changes in parallel to the evolution of aldehydes as suggested for the UV-C photolysis in the present study could be anticipated. In addition, Goto et al. (2004) concluded that the cytotoxicity of NP-70 which had no cytotoxicity by itself, increased by UV-B photolysis as a result of the shortening of the ethoxylate side chain. Therefore, nonylphenol may have also been contributed to the overall acute inhibitory effect observed during UV-C photolysis of NP-10.

As can be followed from Figure 4.49, for the Fenton process, there was at first glance no relationship apparent between the very low aldehyde, carboxylic acid and PEG formation and the toxicity increase (to $26 (\pm 0.29)\%$ inhibition) being observed after 60 min treatment. However, it should be noted that the inhibition values were in general below 25%, indicating that only a slight inhibition was observed throughout the course of the Fenton process due to the low concentrations of detected oxidation products. The relative inhibition observed after 120 min Fenton treatment ($12 (\pm 1.1)\%$) was not practically different from that of the untreated NP-10 ($11 (\pm 5.8)\%$) due to limited transformation of NP-10 (20%) into its oxidation products including PEG, aldehydes and carboxylic acids.

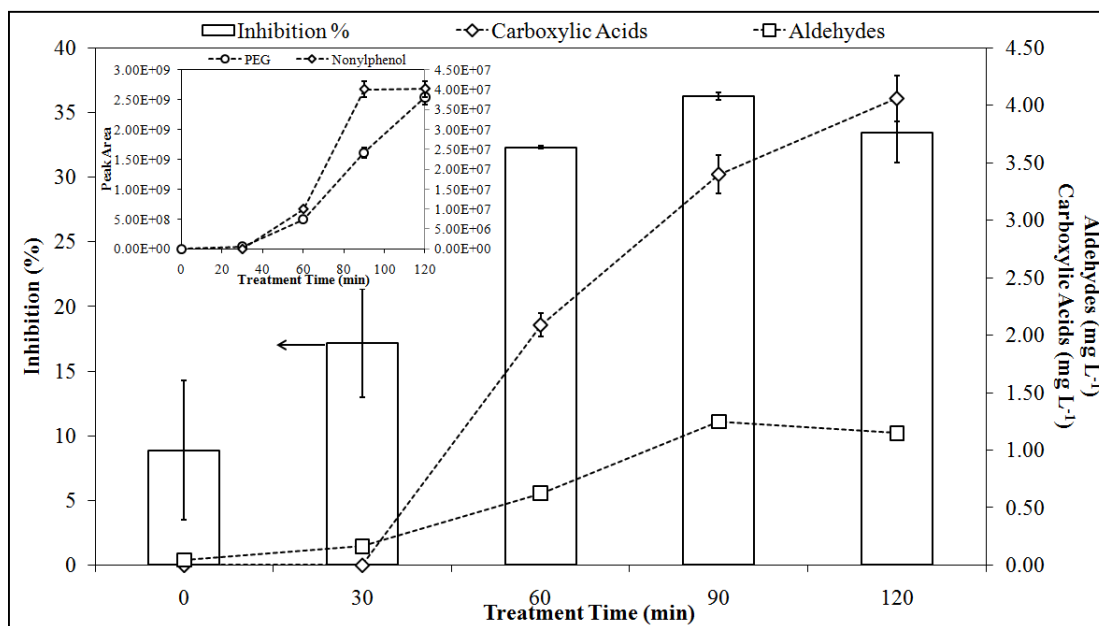


Figure 4.48. Temporal evolution of the acute inhibitory effect in relation with the identified transformation products during UV-C photolysis of NP-10. Initial experimental conditions: NP-10 = 100 mg L⁻¹ (150 μ M), pH = 7.

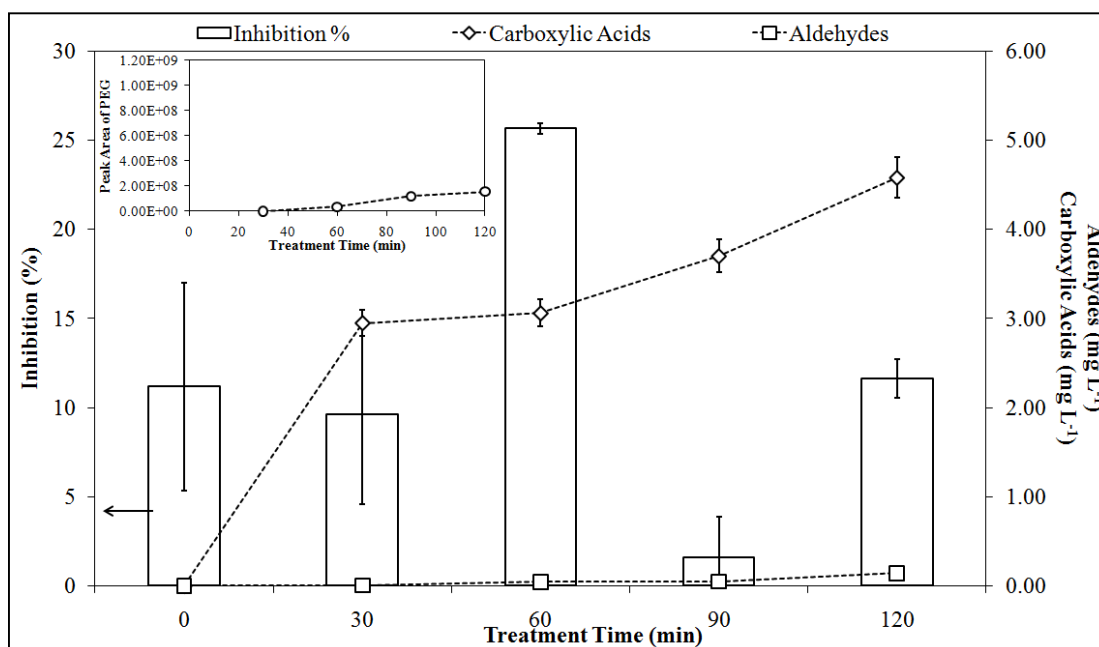


Figure 4.49. Temporal evolution of the acute inhibitory effect in relation with the identified transformation products during Fenton treatment of NP-10. Initial experimental conditions: NP-10 = 100 mg L⁻¹ (150 μ M), H₂O₂ = 10 mM, Fe²⁺ = 200 μ M, pH = 3.

Acute toxicity profiles observed during application of the H₂O₂/UV-C and photo-Fenton processes followed similar trends for both AOP. From Figure 4.50, it is evident that inhibition values showed an initial increase to 21 (\pm 4.0)% and 16 (\pm 2.8)% during first 30 min of the H₂O₂/UV-C and photo-Fenton processes, respectively, where nearly complete elimination of the parent substance was achieved, due to the generation of early transformation products exerting higher inhibitory effect than the original pollutant, as is also evident from previous related studies (Calza et al., 2006; Wu and Zhou, 2001). This initial toxicity increase could not be attributed to PEG due to their disappearance to non-detectable levels after 30 min of the H₂O₂/UV-C and photo-Fenton processes where the inhibitory effect peaked. This finding is supported by a previous study by Farré et al. (2001) who calculated an *EC*₅₀ of as high as 379 mg L⁻¹ for PEG using Microtox[®] bioluminescence inhibition assay. A closer inspection of Figure 4.50 revealed that the increase in inhibitory effect being observed during first 30 min of the H₂O₂/UV-C and photo-Fenton treatments was paralleled by an increase in the concentration of aldehydes and carboxylic acids, suggesting the contribution of these oxidation products to the overall toxicity. The subsequent reductions in inhibition values by 11% and 14% between 30-60 min of the H₂O₂/UV-C and photo-Fenton processes, respectively, well coincide with the time interval where parallel reductions of TOC, aldehyde and carboxylic acid concentrations occurred. However, a re-increase in the inhibitory effect to 24 (\pm 4.5)% and 8.0 (\pm 5.5)% was evident after 120 min treatment for the H₂O₂/UV-C and photo-Fenton processes, respectively. Considering that aldehyde concentration decreased further between 60-120 min of the H₂O₂/UV-C treatment (Figure 4.50a), the re-increase in acute toxicity towards the end of the H₂O₂/UV-C process could be related to the increase of carboxylic acid concentration within this time interval. Similarly, since the aldehyde concentration was almost unchanged between 60-120 min of the photo-Fenton treatment (Figure 4.50b), the re-appearance of the inhibitory effect in this AOP was most likely originated from the increase of carboxylic acid concentration. The toxicity of carboxylic acids to *V. fischeri* has been already demonstrated by Pintar et al. (2004), supporting the conclusions drawn from the present H₂O₂/UV-C and photo-Fenton experiments.

To verify the finding that carboxylic acids were one of the major oxidation products causing acute toxicity fluctuations during the H₂O₂/UV-C and photo-Fenton processes, synthetic samples containing the same concentrations of carboxylic acids as the reaction

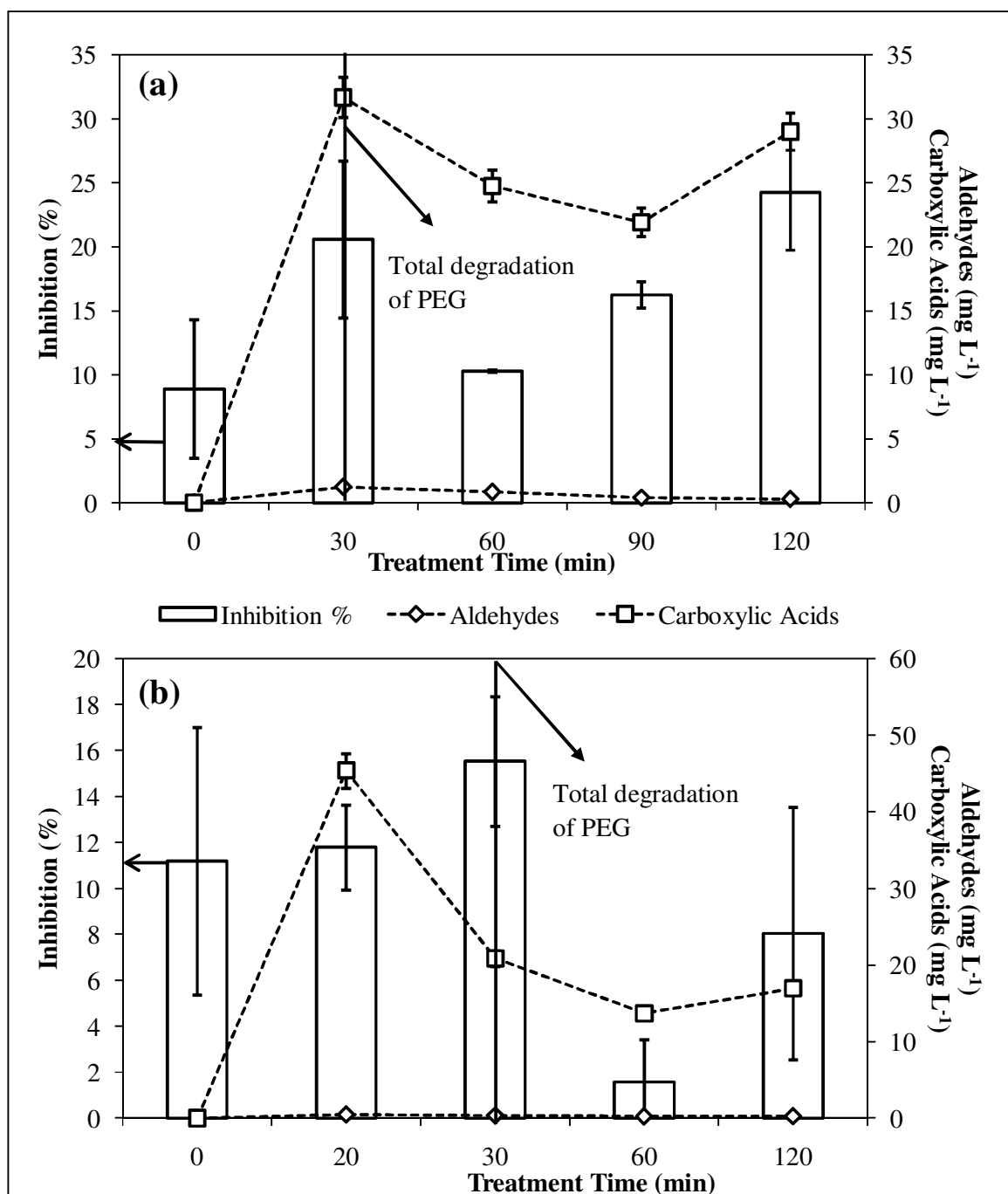


Figure 4.50. Temporal evolution of the acute inhibitory effect in relation with the identified transformation products during H₂O₂/UV-C (a) and photo-Fenton (b) treatment of NP-10. Initial experimental conditions: NP-10 = 100 mg L⁻¹ (150 μM), H₂O₂ = 10 mM, Fe²⁺ = 200 μM, pH = 7 and 3 for the H₂O₂/UV-C and photo-Fenton processes, respectively.

samples were prepared and assayed for their toxicity towards *V. fischeri*. The lower inhibition values observed in the synthetic samples as compared to the reaction samples taken after 120 min H₂O₂/UV-C (Figure 4.51a) and photo-Fenton processes (Figure 4.51b) suggested a level of synergism between formed carboxylic acids and one or more oxidation products, speculatively aldehydes. On the other hand, the results revealed that the ecotoxicity patterns of synthetic samples were consistent with those of reaction samples within the experimental errors (Figure 4.51), demonstrating that carboxylic acid evolution had a major impact on acute toxicity profiles during the H₂O₂/UV-C and photo-Fenton oxidation of NP-10. This latter finding suggested that the higher level of inhibitory effect observed at the end of the H₂O₂/UV-C process as compared to the photo-Fenton process was most probably caused by the lower concentrations of carboxylic acids detected in the photo-Fenton process.

A comparison of the H₂O₂/UV-C and photo-Fenton processes, being the most efficient AOPs for the removal of aqueous NP-10, in terms of acute toxicity changes in distilled water (Table 4.23) demonstrated that the H₂O₂/UV-C-treated NP-10 resulted in an inhibition (24 (± 4.5)%) being higher than the original NP-10, whereas no significant change in inhibition values was detected after the photo-Fenton treatment (from 11 (± 5.8)% to 8.0 (± 5.5)%). This finding proved that the photo-Fenton process was the ecotoxicologically safest treatment method among the studied others. Accordingly, the photo-Fenton process should be the method of choice for the efficient and safe treatment of aqueous nonylphenol ethoxylates including NP-10.

Table 4.23. Comparison of the initial and final acute inhibitory effects for H₂O₂/UV-C, Fenton and photo-Fenton treatment as well as UV-C photolysis of NP-10.

Treatment Process	Inhibition (± Standard Deviation)%	
	Before Treatment	After 120 min Treatment
UV-C	8.9 (± 5.4)	33 (± 2.3)
H ₂ O ₂ /UV-C	8.9 (± 5.4)	24 (± 4.5)
Fenton	11 (± 5.8)	12 (± 1.1)
Photo-Fenton	11 (± 5.8)	8.0 (± 5.5)

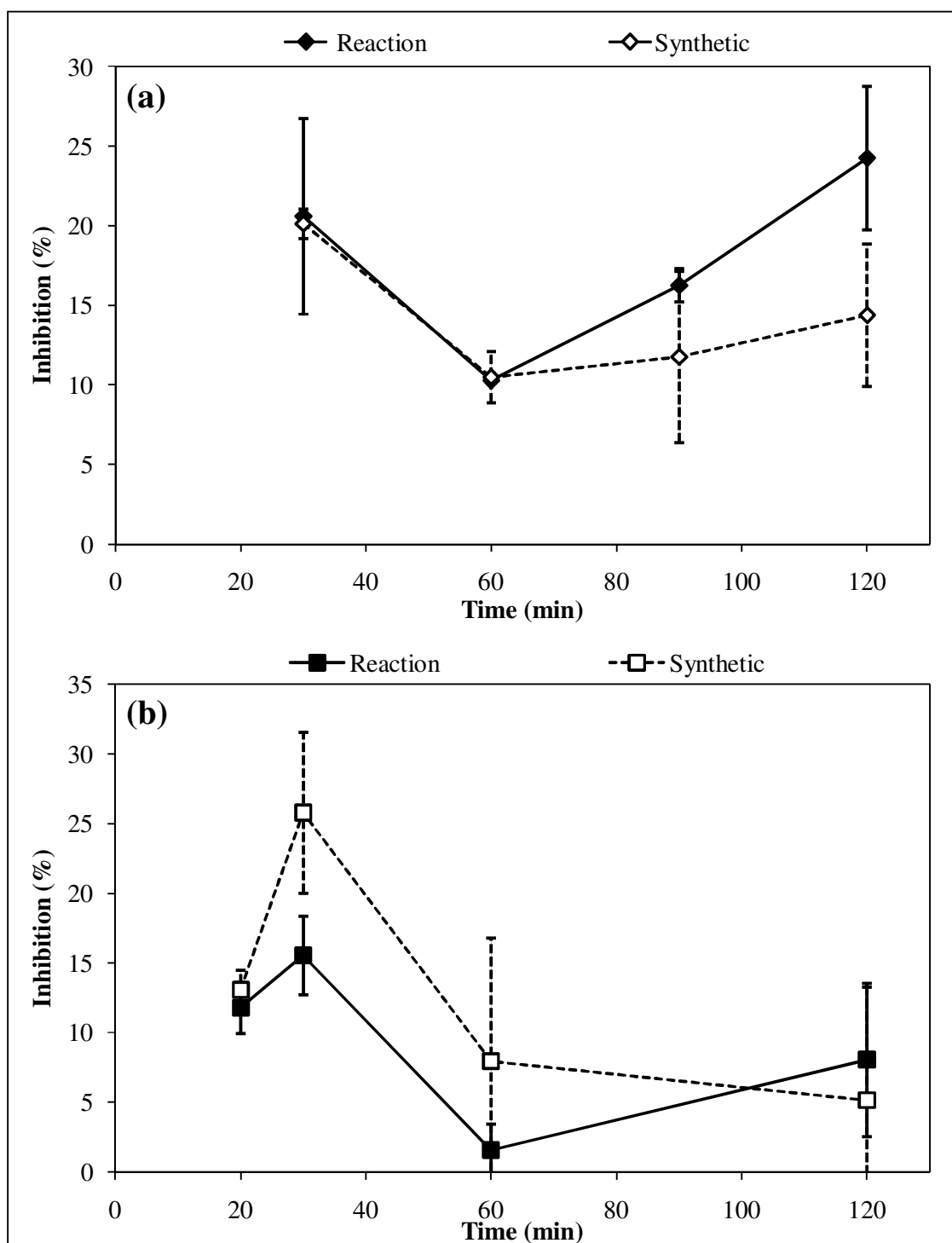


Figure 4.51. Evolution of acute toxicity in synthetic samples and reaction samples treated by the H₂O₂/UV-C (a) and photo-Fenton (b) processes. Initial experimental conditions for the reaction samples: NP-10 = 100 mg L⁻¹ (150 μM), H₂O₂ = 10 mM, Fe²⁺ = 200 μM, pH = 7 for the H₂O₂/UV-C and pH = 3 for the photo-Fenton processes.

4.2.3.2. Genotoxicity Evolution. Figure 4.52 depicts the changes of induction factors against NP-10 concentrations in the absence and presence of metabolic activation evaluated using unconcentrated aqueous samples. In the absence of metabolic activation, induction factors gradually increased with increasing NP-10 concentration. Similarly the highest induction factor was obtained for the highest NP-10 concentration tested (2667 mg L⁻¹) in the presence of metabolic activation. However, it should be noted that the differences being observed between the induction factors for the selected NP-10 concentrations were not statistically significant, implying that the genotoxic effect did not considerably change over the relatively broad concentration range of 333-2667 mg L⁻¹. In addition, induction factors were below the threshold level of 2 in all cases, indicating that NP-10 did not exert a significant genotoxic effect even at rather high concentrations. Accordingly, the recent findings obtained by Frassinetti et al. (2011) demonstrated that an industrial mixture of nonylphenol ethoxylates with an average ethoxylation degree of 5 did not induce genotoxic effects on the D7 strain of *Saccharomyces cerevisiae*. From the present findings, it was also found that the induction factors were not significantly different in the absence and presence of metabolic activation, indicating that the metabolism of non-genotoxic NP-10 by the rat liver extract did not cause the formation of genotoxic compounds.

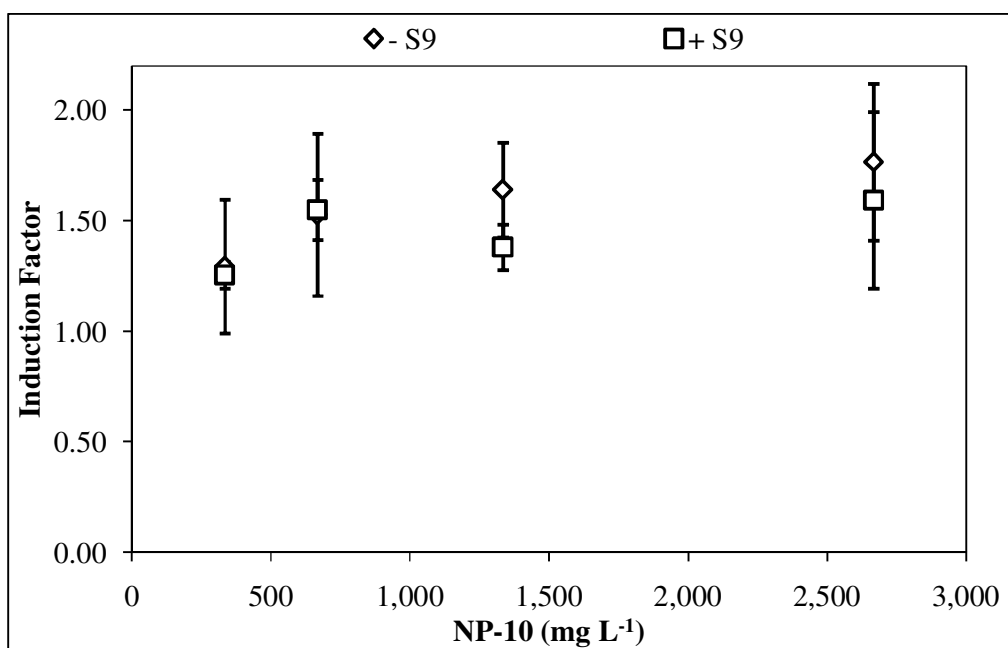


Figure 4.52. The genotoxic effect versus NP-10 concentration graph.

The overall genotoxicity results obtained during H₂O₂/UV-C, Fenton and photo-Fenton treatment as well as UV-C photolysis of NP-10 are given in Table 4.24. The comparative evaluation of the studied treatment processes revealed that magnitudes of the incubation factors both in the absence and presence of metabolic activation followed the order: Fenton > H₂O₂/UV-C > photo-Fenton > UV-C, although the difference was not statistically significant. The UV-C photolysis of NP-10 originally being non-genotoxic (induction factor = 0.92) did not result in any significant change in genotoxic effect in the absence of metabolic activation after 90 min photolysis where 75% NP-10 removal accompanied by an insignificant mineralization (< 10%) was obtained. However, after 90 min treatment, a significant increase in genotoxic effect to an induction factor of 2.4 was observed, indicating that weakly genotoxic transformation products were formed at the end of 120 min UV-C photolysis. Although formic acid accumulated gradually throughout the course of UV-C photolysis, increase of the genotoxic effect could not be directly attributed to the formed formic acid considering that this compound is non-genotoxic as assessed on cultured mammalian cells (Morita et al., 1990). From Figure 4.53, it can be realized that after 120 min UV-C photolysis, nonylphenol and PEG also reached their peak concentration in the treated solution. From the scientific literature, there are evidences that nonylphenol and PEG could induce genotoxic effects. For instance, Frassinetti et al. (2011) have demonstrated that nonylphenol induced mutagenic effects at 12 and 25 mg L⁻¹ as evaluated by the D7 strain of *Saccharomyces cerevisiae*. In addition, PEG polymers with a molecular weight of ~ 200 have been found to have a genotoxic effect after metabolic activation as assessed by induction of chromosome aberrations in Chinese hamster epithelial liver cells in the presence of S9 (Biondi et al., 2002). Therefore, a genotoxicity increase accompanied by the generation of nonylphenol and PEG could be anticipated. On the other hand, in the present study, lower incubation factors were obtained in the presence of metabolic activation, referring to the metabolization of the weakly genotoxic transformation products being formed after 120 min UV-C photolysis to the non-genotoxic ones.

During application of the H₂O₂/UV-C process, the initial induction factor in the absence of metabolic activation significantly increased to 3.5 after 2 min photochemical treatment where 52% NP-10 and insignificant (< 5%) TOC removal was achieved, indicating that NP-10 was greatly transformed into moderately genotoxic oxidation

Table 4.24. Genotoxic effects observed at different stages of NP-10 degradation by UV-C, H₂O₂/UV-C, Fenton and photo-Fenton treatment processes.

Treatment Time (min)	Induction Factor (- S9)				Induction Factor (+ S9)			
	UV-C	H ₂ O ₂ /UV-C	Fenton	Photo-Fenton	UV-C	H ₂ O ₂ /UV-C	Fenton	Photo-Fenton
0	0.915	0.915	0.741	0.741	0.00	0.00	0.00	0.00
2	n.d.*	3.53	n.d.	1.37	n.d.	0.749	n.d.	0.701
20	n.d.	n.d.	n.d.	2.06	n.d.	n.d.	n.d.	0.391
30	1.30	2.37	4.81	2.18	0.00	1.06	2.98	0.579
60	1.35	2.11	5.08	2.14	0.00	1.01	1.99	0.455
90	0.879	2.96	6.72	n.d.	0.00	1.38	2.22	n.d.
120	2.42	1.37	1.27	1.06	1.44	0.00	0.00	0.00

*Not determined.

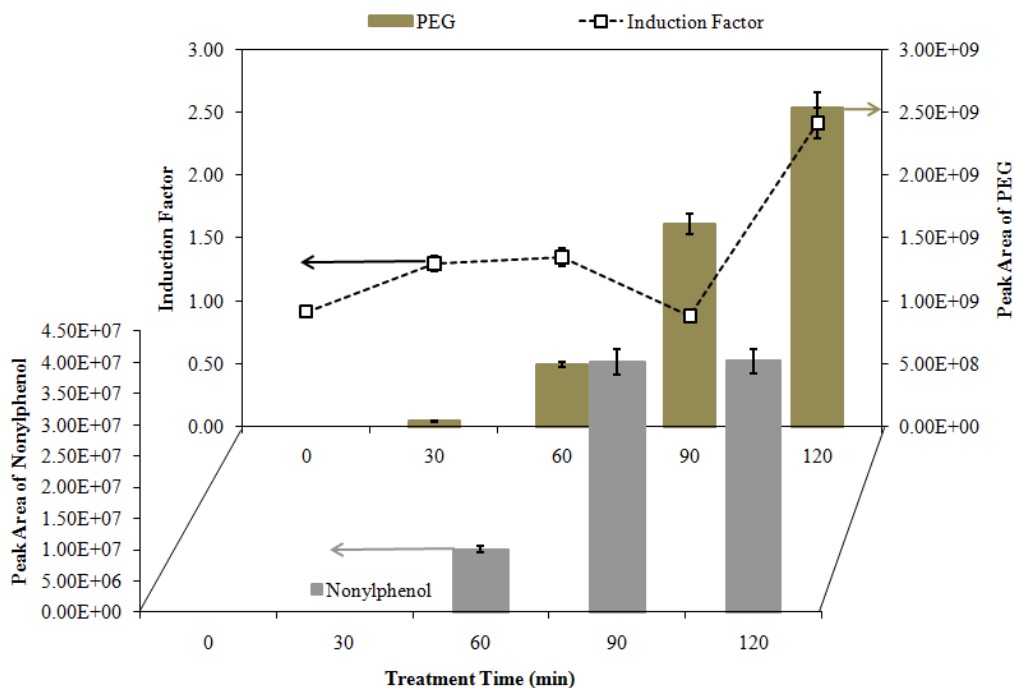


Figure 4.53. Temporal evolution of genotoxic effect without S9 mix during UV-C photolysis of NP-10 in relation with transformation products identified by GC-MS. Initial experimental conditions: NP-10 = 100 mg L⁻¹ (150 μM), pH = 7.

products at the very beginning of the H₂O₂/UV-C treatment. This initial increase in genotoxic effect was accompanied by a slight increase in acute inhibitory effect towards *V. fischeri* photobacteria from 8.9 (± 5.4)% to 21 (± 4.0)% (data not shown), suggesting that these moderately genotoxic oxidation products could exert a low acute toxicity as well. From Figure 4.54, one can realize that the genotoxic effect peaked in parallel to the appearance of PEG in the treated solution, speculating that PEG could be an important origin of the initial genotoxicity increase, as was also suggested during UV-C photolysis. In agreement with the present suggestions, the repeated exposure to high dose of PEG has been demonstrated to show genotoxic activity and histopathological changes in male mice cells (Diab et al., 2012). After 60 min H₂O₂/UV-C treatment, the induction factor decreased to 2.1 in parallel to the complete degradation of NP-10 accompanied by a significant mineralization (60%) being achieved within the same time interval. On the other hand, a slight re-increase and the subsequent decrease in genotoxic effect was observed within 60-120 min photochemical treatment following the similar trend with oxalic acid (Figure 4.54). Although no information on the genotoxicity of oxalic acid or its

salts was found in the literature, sodium oxalate has been reported to inhibit endothelial cell replication and migration (Von Burg, 1994), and this inhibitory action may be important to account for the reason of the slight genotoxicity change towards the end of the photochemical treatment in this study. It should be emphasized that, after 120 min $\text{H}_2\text{O}_2/\text{UV-C}$ treatment the treated solution did not exert any genotoxic effect. Similar to the findings obtained for UV-C photolysis of NP-10, the genotoxic effects observed after metabolic activation were lower than those achieved in the absence of metabolic activation, and induction factors corresponding to non-genotoxic levels were found for all treatment times (Table 4.24).

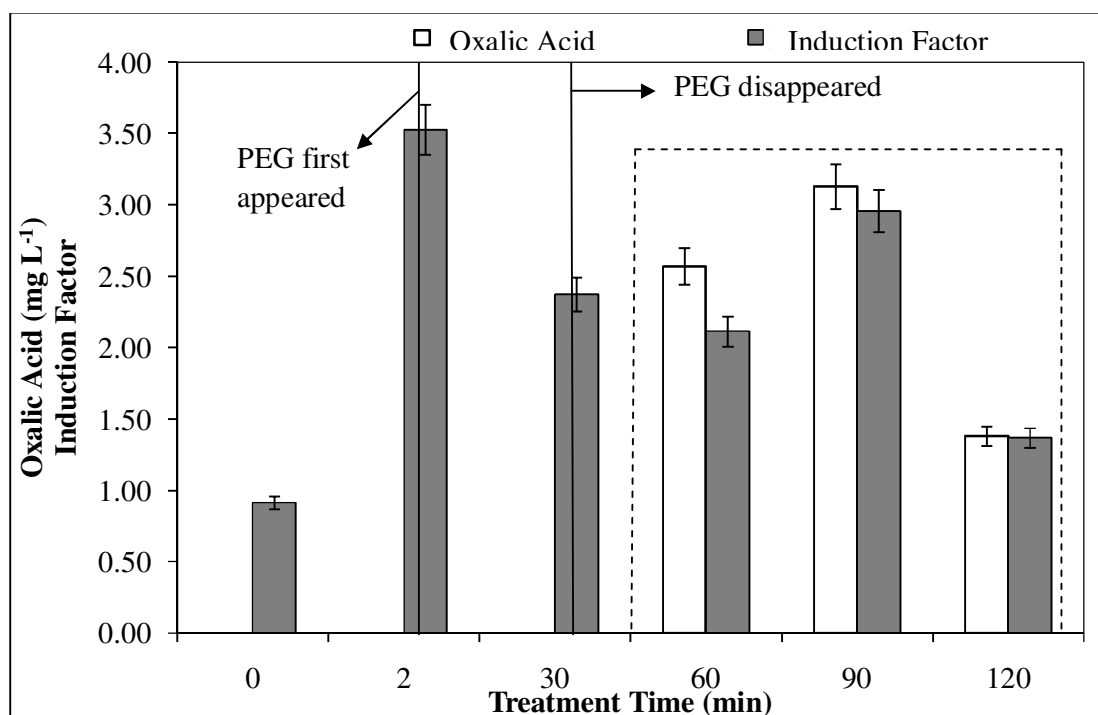


Figure 4.54. Temporal evolution of genotoxic effect without S9 mix during $\text{H}_2\text{O}_2/\text{UV-C}$ treatment of NP-10 in relation with the identified transformation products. Initial experimental conditions: NP-10 = 100 mg L^{-1} ($150 \text{ }\mu\text{M}$), H_2O_2 = 10 mM, pH = 7.

Fenton treatment of NP-10 in general resulted in higher genotoxic effects in the absence and presence of metabolic activation as compared to the other studied treatment methods (Table 4.24). In the absence of metabolic activation, induction factor initially being 0.74 gradually and significantly increased to 6.7, demonstrating that the reaction

solution became highly genotoxic after 90 min Fenton treatment. On the other hand, genotoxicity decreased sharply > 90 min Fenton treatment, and the non-genotoxic values were reached again. Considering the low NP-10 transformation and the detected relatively low amounts of carboxylic acids, PEG and aldehydes in the Fenton process, the significantly higher genotoxic effect observed in the Fenton process could not be explained by the available treatment performance and oxidation products data.

As compared to the Fenton treatment of NP-10, the photo-Fenton-treated NP-10 induced relatively low genotoxic effects particularly in the presence of metabolic activation (Table 4.24). From the presented experimental findings, it could be drawn that the genotoxic effect gradually, but slowly increased to an induction factor of 2.2 after 30 min photo-Fenton treatment where nearly complete NP-10 removal and 54% mineralization were achieved, and thereafter decreased to non-genotoxic levels again (induction factor = 1.1). Although the slight genotoxicity increase after 30 min photo-Fenton treatment and the subsequent decrease could not directly be linked to any formed oxidation intermediates, it could be concluded that photo-Fenton treatment ensured the genotoxicologically safer conditions among the studied AOP. The lower genotoxic effects found in the presence of metabolic activation as compared to the case in the absence of metabolic activation delineated that the weakly genotoxic oxidation products being formed between 20-60 min of the photo-Fenton treatment could be further transformed into non-genotoxic products under the metabolic conditions.

4.2.4. NP-10 Removal in Synthetic Freshwater

4.2.4.1. Treatment Performances and Kinetics. To evaluate the applicability of the studied treatment processes for the removal of nonylphenol polyethoxylates in real aqueous matrices, experiments aiming at assessing the treatment performances and kinetics based on the conventional monitoring parameters including parent pollutant concentration, TOC, unreacted H₂O₂ concentration and UV_{254/280} absorbances were repeated in SFW. For comparison purposes, the same operating conditions as in DW, namely 100 mg L⁻¹ (150 μM) initial NP-10 concentration, 10 mM initial H₂O₂ concentration, 200 μM initial Fe²⁺ concentration, initial pH 7.0 for UV-C and H₂O₂/UV-C and initial pH 3.0 for Fenton and photo-Fenton treatment processes, were employed. NP-10 and TOC abatements in SFW are shown in Figure 4.55a and b, respectively. NP-10 and TOC removals as well as H₂O₂ consumptions were expressed as the pseudo-first-order kinetics model, and *R*² values ≥ 0.986 were obtained in all cases. The pseudo-first-order rate coefficients and percent removal efficiencies obtained for degradation of NP-10 in SFW are given in Table 4.25 in comparison with those obtained in DW.

Table 4.25. Pseudo-first-order abatement rate coefficients and percent removal efficiencies obtained for degradation of NP-10 by UV-C, H₂O₂/UV-C, Fenton and photo-Fenton treatment processes in DW and SFW.

	<i>k</i> _{NP-10} (min ⁻¹)		NP-10 Removal (%) [*]	
	DW	SFW	DW	SFW
UV-C	0.008	0.010	92	96
H ₂ O ₂ /UV-C	0.395	0.392	100	100
Fenton	0.002	n.d.**	20	10
Photo-Fenton	0.159	0.243	100	100

^{*}After 120 min treatment.

^{**}not determined due to insignificant removal.

Comparison of NP-10 removals between the studied treatment processes in SFW (Figure 4.55a) indicated that a considerably lower NP-10 removal was obtained by applying the Fenton's reagent as compared to the other treatment processes. Although not an AOP, UV-C photolysis ensured near-complete NP-10 removal in SFW after 120 min treatment, whereas the pseudo-first-order rate coefficient for NP-10 removal obtained by

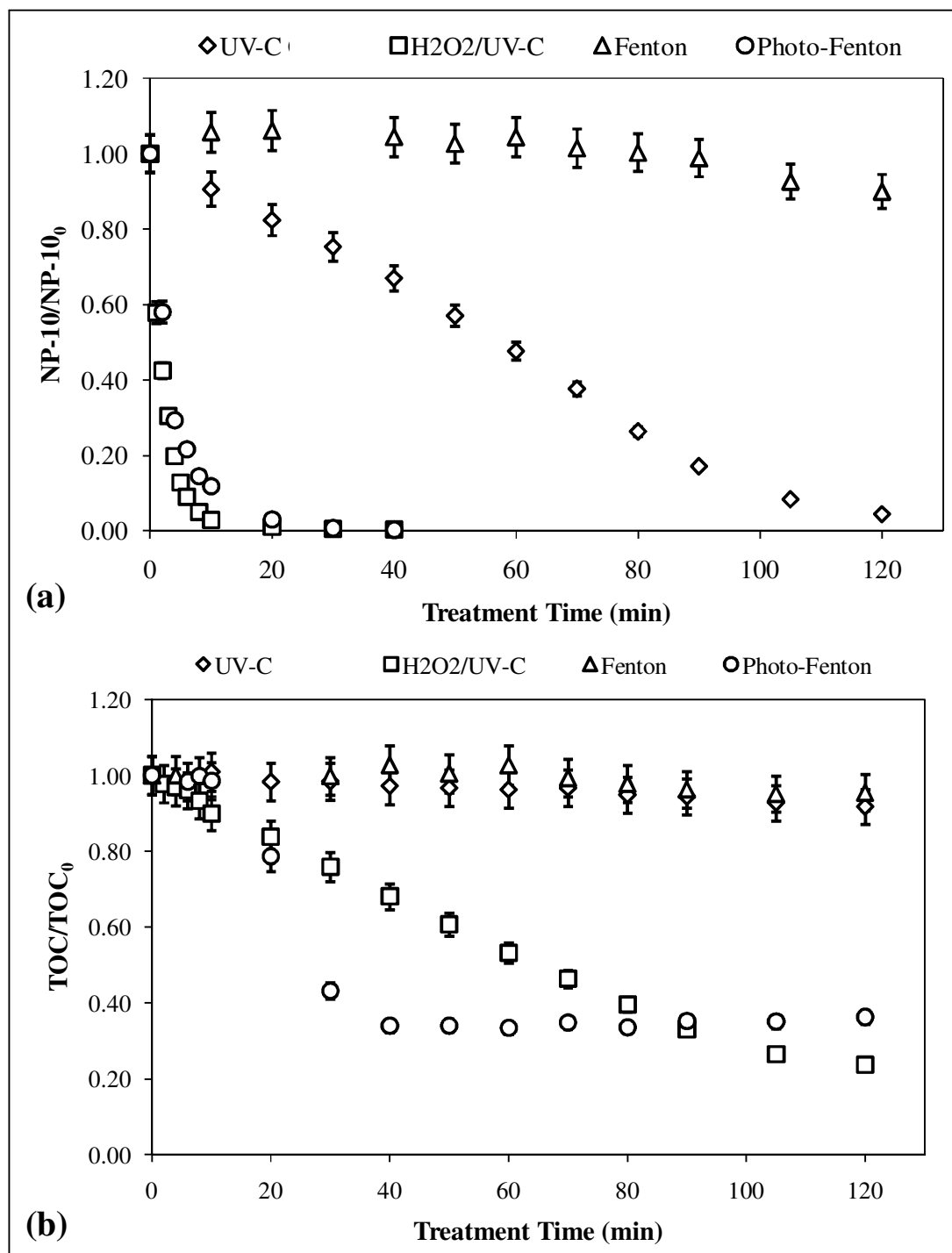


Figure 4.55. NP-10 (a) and TOC removals (b) during UV-C, H₂O₂/UV-C, Fenton and photo-Fenton treatment of NP-10 in SFW. Initial experimental conditions: NP-10 = 100 mg L⁻¹ (150 μM), H₂O₂ = 10 mM, Fe²⁺ = 200 μM, pH = 7 for UV-C and H₂O₂/UV-C and pH = 3 for Fenton and photo-Fenton treatment.

this treatment process ($k_{NP-10} = 0.010 \text{ min}^{-1}$) was more than one order of magnitude lower than those achieved via the $\text{H}_2\text{O}_2/\text{UV-C}$ and photo-Fenton processes ($k_{NP-10} = 0.39$ and 0.24 min^{-1} , respectively). NP-10 disappeared to non-detectable levels in both $\text{H}_2\text{O}_2/\text{UV-C}$ and photo-Fenton processes after 40 min treatment. An overall comparison of NP-10 removals in DW and SFW (Table 4.25) revealed that NP-10 removal efficiencies achieved in UV-C, $\text{H}_2\text{O}_2/\text{UV-C}$ and photo-Fenton treatment processes were not significantly different between DW and SFW. However, a lower NP-10 removal was obtained in SFW (10%) as compared to DW (20%) after 120 min Fenton treatment. Although this decrease could be linked to the HO^\bullet scavenging role of Cl^- and SO_4^{2-} present in SFW (Michael et al., 2012), as well as precipitation of iron by the aid of SFW matrix (Pagano et al., 2008), the reason of why the other AOP were not affected by the water matrix constituents in terms of NP-10 removal remains unknown.

Comparison of the studied treatment processes in terms of TOC removal in SFW (Figure 4.55b) revealed that UV-C photolysis and the Fenton process resulted in insignificant mineralization (< 10%) after 120 min treatment. This was an expected outcome for the Fenton process considering the insignificant NP-10 removal achieved by this AOP. On the other hand, the markedly lower TOC removal obtained by UV-C photolysis than that reached by applying $\text{H}_2\text{O}_2/\text{UV-C}$ and photo-Fenton processes (76% and 64%, respectively) despite the near-complete NP-10 removal achieved during application of UV-C photolysis clearly pointed out the inefficiency of UV-C photolysis for the degradation of transformation products being formed in SFW. The tested water matrices caused no distinct differences in TOC removal efficiency for the $\text{H}_2\text{O}_2/\text{UV-C}$ and photo-Fenton processes (Table 4.26). Both in DW and SFW, the extent of mineralization followed the order: $\text{H}_2\text{O}_2/\text{UV-C} > \text{photo-Fenton} \gg \text{UV-C} \cong \text{Fenton}$, which was in correlation with NP-10 removals. Overall, the obtained findings implied that the $\text{H}_2\text{O}_2/\text{UV-C}$ and photo-Fenton processes could be efficiently applied for the complete transformation of NP-10 and partial degradation of its oxidation products in moderately hard freshwater environments.

Table 4.26. Pseudo-first-order abatement rate coefficients and percent removal efficiencies obtained for TOC removal by UV-C, H₂O₂/UV-C, Fenton and photo-Fenton treatment processes in DW and SFW.

	$k_{TOC} \text{ (min}^{-1}\text{)}$		TOC Removal (%)*	
	DW	SFW	DW	SFW
UV-C	n.d.**	n.d.	< 10	< 10
H ₂ O ₂ /UV-C	0.011	0.010	79	76
Fenton	n.d.	n.d.	< 10	< 10
Photo-Fenton	0.032	0.032	69	64

*After 120 min treatment.

**not determined because of insignificant removal rate.

The pseudo-first-order abatement rate coefficients and percent consumptions for H₂O₂ obtained in SFW are given in Table 4.27 in comparison with those obtained in DW. H₂O₂ consumptions were not significantly different between DW and SFW which could also account for the similar levels of NP-10 and TOC removals generally achieved by applying the selected AOP, particularly the H₂O₂/UV-C and photo-Fenton processes. On the other hand, slightly lower pseudo-first-order abatement rate coefficients for H₂O₂ found in SFW as compared to DW during application of the Fenton and photo-Fenton processes could be attributed to the occurrence of complexation reactions of Fe²⁺ or Fe³⁺ by Cl⁻ or SO₄²⁻ present in the composition of SFW, leading to a decrease of the concentration of peroxo complexes and consequently of the rate of decomposition of H₂O₂ (De Laat et al., 2004).

Table 4.27. Pseudo-first-order abatement rate coefficients and percent consumptions obtained for H₂O₂ during H₂O₂/UV-C, Fenton and photo-Fenton treatment of NP-10 in DW and SFW.

	$k_{H_2O_2} \text{ (min}^{-1}\text{)}$		H ₂ O ₂ Consumption (%)*	
	DW	SFW	DW	SFW
H ₂ O ₂ /UV-C	0.021	0.024	100	99
Fenton	0.031	0.029	84	50
Photo-Fenton	0.073	0.061	100	100

*After 120 min treatment.

Treatment performances in SFW were also evaluated based on the evolution of UV absorbances being characteristic for aromaticity ($\lambda = 280$ nm; Figure 4.56a) and unsaturated carbon bonds ($\lambda = 254$ nm; Figure 4.56b). Absorbance spectra of treated and untreated NP-10 in SFW were also given in Appendix C. Characteristic peaks, related to the aromatic structure of the molecule appeared around 224 and 277 nm, in agreement with data reported for other alkylphenol ethoxylates (Ihoş et al., 2008; Kim et al., 2005). From the UV spectra, it was visible that the intensity of the peaks decreased rapidly during application of the H₂O₂/UV-C and photo-Fenton processes, suggesting the opening of aromatic groups. On the other hand, during UV-C photolysis, decrease of the intensity of those defined peaks were slower, verifying the slower NP-10 removal obtained via UV-C photolysis as compared to the H₂O₂/UV-C and photo-Fenton processes. Moreover, only partial disappearance of those peaks was apparent during the Fenton process, in agreement with the HPLC measurements of the parent compound. No additional new peaks developed for any studied treatment processes. During the H₂O₂/UV-C and photo-Fenton processes as well as UV-C photolysis, UV₂₅₄ absorbing moieties showed an initial increase and subsequent decrease, while the time and extent of this increase differed between processes (Figure 4.56b). For the UV-C photolysis, UV₂₅₄ absorbing moieties gradually increased to the point where 83% of the initial NP-10 was eliminated from the reaction solution and showed a sudden decrease thereafter. The highest increase of UV₂₅₄ absorbance was observed during application of the H₂O₂/UV-C process, where it peaked after nearly complete NP-10 transformation occurred. The extent of the initial increase in UV₂₅₄ absorbing moieties observed in the photo-Fenton process was much lower than that observed in the H₂O₂/UV-C process and was evident only until 42% NP-10 removal was achieved. The increase patterns initially observed in UV₂₅₄ absorbances were also apparent for the UV₂₈₀ absorbing moieties during the H₂O₂/UV-C process and UV-C photolysis (Figure 4.56a). Although currently not available in the scientific literature, the increases in UV_{254/280} absorbances could be attributed to the coupling of phenolic moieties via the ether linkages following the shortening of ethoxylate chains. On the other hand, for the photo-Fenton process, gradual decrease of the UV₂₈₀ absorbance closely followed the trend for the TOC removal. Comparisons of the UV absorbances obtained in DW and SFW indicated that although UV_{254/280} values in SFW were in general higher than those recorded in DW particularly for UV-C photolysis and the H₂O₂/UV-C process, the differences were not statistically significant.

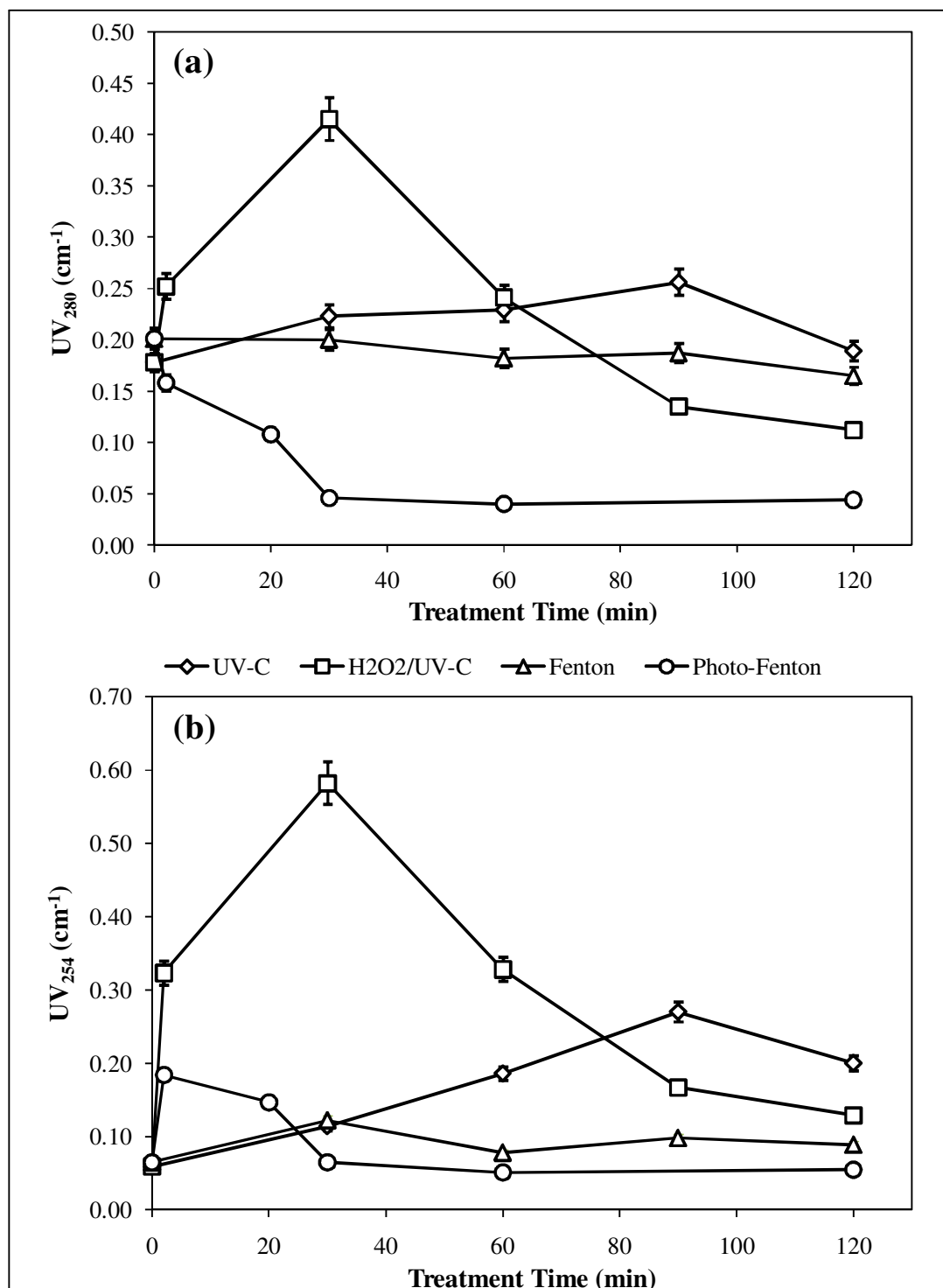


Figure 4.56. Evolution of UV₂₈₀ (a) and UV₂₅₄ (b) absorbances during H₂O₂/UV-C, Fenton and photo-Fenton treatment as well as UV-C photolysis of NP-10 in SFW. Initial experimental conditions: NP-10 = 100 mg L⁻¹ (150 μM), H₂O₂ = 10 mM, Fe²⁺ = 200 μM, pH = 7 for UV-C and H₂O₂/UV-C and pH = 3 for Fenton and photo-Fenton treatment.

4.2.4.2. Oxidation Products.

HPLC Analyses. Oxidation product analyses were performed under above-described experimental conditions to evaluate potential differences between DW and SFW. First of all, HPLC analyses targeting the monitoring of C1-C4 aliphatic carboxylic acids, namely formic, acetic, oxalic, maleic and fumaric acids, were carried out. Similar to the findings in DW, formic acid was found to be the common carboxylic acid of all studied AOP (Figure 4.57a). On the other hand, formic acid could not be detected in UV-C photolyzed SFW solutions, being unsimilar to the findings obtained in DW. Instead, relatively low concentrations of oxalic acid (up to 3.4 mg L^{-1}) and traces of maleic acid (0.14 mg L^{-1} , data not shown) were detected between 60-90 min of UV-C photolysis and disappeared thereafter (Figure 4.57c). The generation of low amounts of carboxylic acids via the UV-C photolysis was an outcome of low transformation rate (Figure 4.55a) and dearomatization (Appendix C) of NP-10 through this treatment method. Similar conclusion could also be drawn for the Fenton process where only traces of formic acid (3.3 mg L^{-1}) were detected after 105-120 min treatment. Among the studied AOP, the highest formic acid formation (41 mg L^{-1}) was observed during the photo-Fenton oxidation of NP-10 and its degradation was complete after 40 min treatment, slightly shorter than the time required for formic acid removal with the $\text{H}_2\text{O}_2/\text{UV-C}$ process. From the obtained findings, it could be concluded that in SFW, a significantly higher treatment time was needed to transform NP-10 and/or its degradation products into formic acid via the Fenton process than required in DW (≥ 10 min), similar to the lower NP-10 removal obtained in SFW as discussed in Section 4.2.4.1. Although formic acid concentrations obtained during application of the $\text{H}_2\text{O}_2/\text{UV-C}$ and photo-Fenton processes were not significantly different between DW and SFW, a major difference was observed between the results obtained in the two studied matrices. The re-increase in formic acid concentrations observed in the $\text{H}_2\text{O}_2/\text{UV-C}$ and photo-Fenton processes in DW was not apparent in SFW, and hence formic acid did not persist in SFW after 120 min treatment. The result for the $\text{H}_2\text{O}_2/\text{UV-C}$ process could in part be attributed to the rapid transformation of oxalic acid into formic acid in DW, which could be drawn from the significantly higher concentrations of oxalic acid in SFW as compared to DW observed during the $\text{H}_2\text{O}_2/\text{UV-C}$ process ($p = 0.033$).

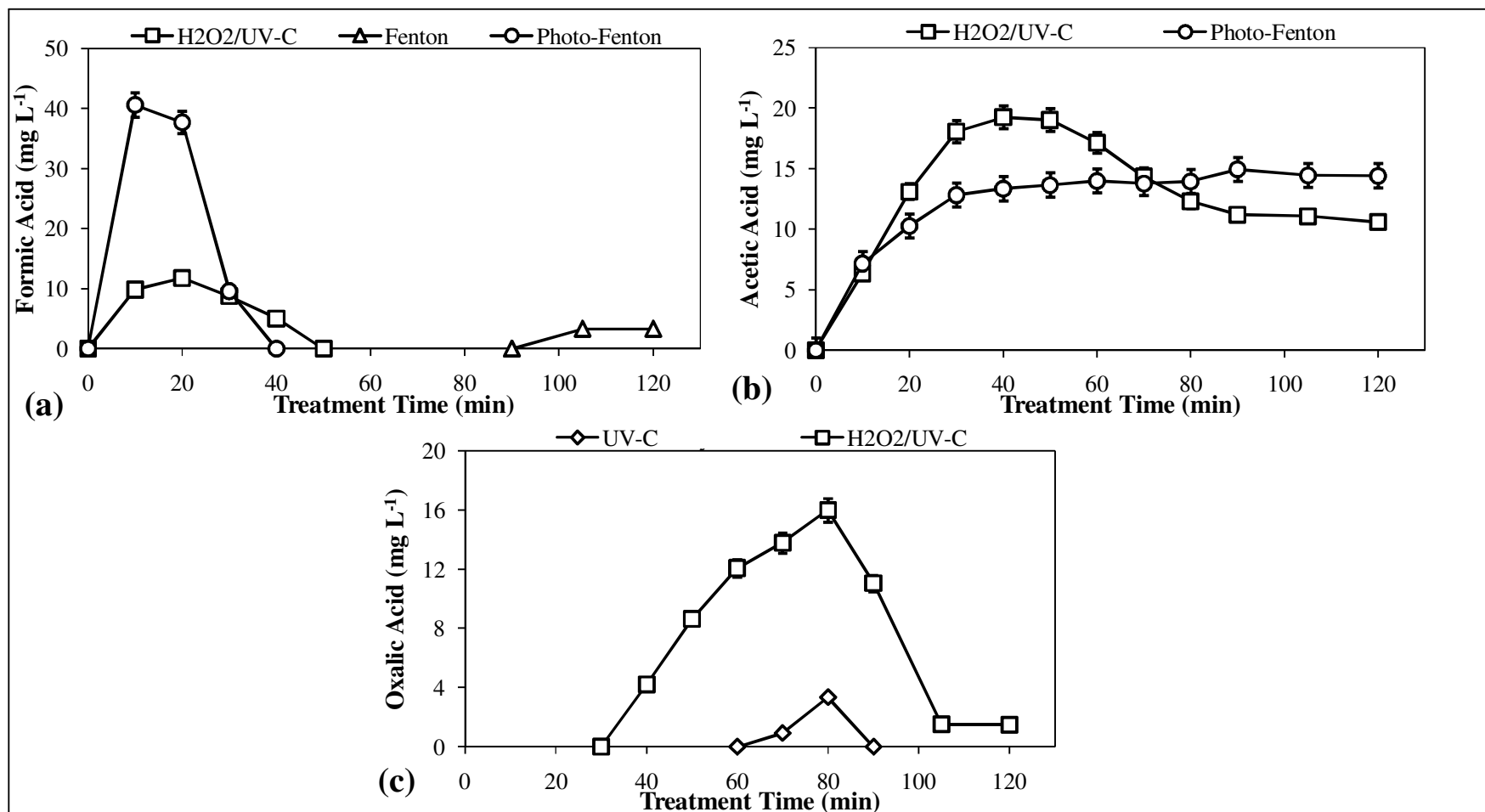


Figure 4.57. Evolution of formic acid (a), acetic acid (b) and oxalic acid (c) during H₂O₂/UV-C, Fenton and photo-Fenton treatment as well as UV-C photolysis of NP-10 in SFW. Initial experimental conditions: NP-10 = 100 mg L⁻¹ (150 μM), H₂O₂ = 10 mM, Fe²⁺ = 200 μM, pH = 7 for UV-C and H₂O₂/UV-C and pH = 3 for Fenton and photo-Fenton treatment.

In addition to formic acid, acetic acid was also detected as the common oxidation product being generated during application of the H₂O₂/UV-C and photo-Fenton processes, being similar to the results in DW. Unlike the findings obtained for formic acid, no significant difference for the acetic acid concentrations was detected between the H₂O₂/UV-C and photo-Fenton processes (Figure 4.57b). Acetic acid could not be completely eliminated from the treated SFW by applying the studied photochemical AOP. The statistical comparisons delineated that the acetic acid concentrations observed throughout the course of the H₂O₂/UV-C and photo-Fenton processes were not significantly different between DW and SFW. Maleic and fumaric acids could not be detected during application of the studied AOP, except the finding that 0.16 mg L⁻¹ maleic acid and 0.07 mg L⁻¹ fumaric acid could be quantified only after 10 min photo-Fenton treatment.

Aldehydes. During application of all treatment processes in SFW, aldehydes formation was evident, their evolution being demonstrated in Figure 4.58. As is also obvious from Figure 4.58, the highest aldehyde formations being 2.1 and 1.8 mg L⁻¹ were found during H₂O₂/UV-C and UV-C treatment of NP-10, respectively, while the lowest generation was observed during the Fenton process (0.39 mg L⁻¹). During the H₂O₂/UV-C process, aldehyde concentrations increased very rapidly during the first 2 min of the reaction, peaked after 30 min and gradually degraded until completion of the treatment, whereas they continuously accumulated in the reaction solution during application of UV-C photolysis. The similar accumulation potential was also apparent for the Fenton and photo-Fenton processes, where the aldehyde concentrations slightly increased from 0.00 and 0.37 mg L⁻¹ to 0.39 and 0.60 mg L⁻¹, respectively, between 60-120 min treatment. The finding that a relatively lower concentration of aldehydes (0.53 mg L⁻¹) was detected after 20 min photo-Fenton treatment despite the highest formic acid concentration being observed in this AOP could be an indication of that initially formed formaldehyde was rapidly oxidized to form formic acid via the photo-Fenton process. The overall findings delineated that the studied treatment processes was not able to completely transform the generated aldehydes. The comparison of the results obtained in DW and SFW indicated that although the aldehyde concentrations being formed in SFW were in general higher than those in DW, the difference was found to be statistically insignificant.

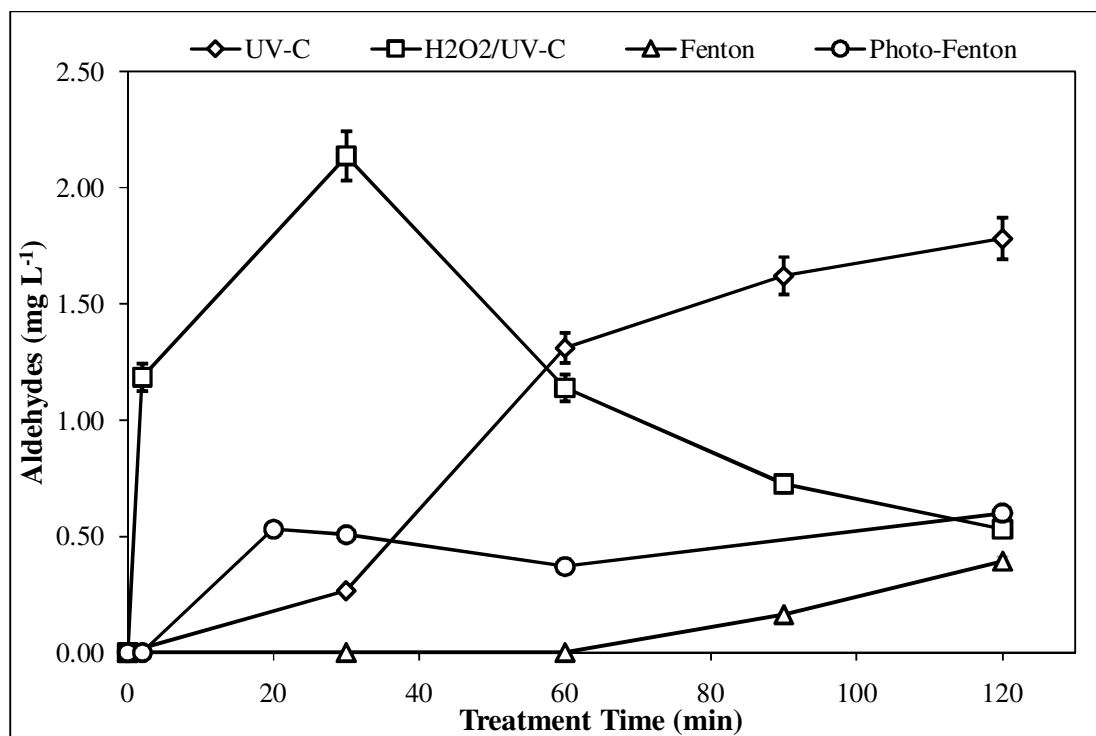


Figure 4.58. Evolution of aldehydes during H₂O₂/UV-C, Fenton and photo-Fenton treatment as well as UV-C photolysis of NP-10 in SFW. Initial experimental conditions: NP-10 = 100 mg L⁻¹ (150 μM), H₂O₂ = 10 mM, Fe²⁺ = 200 μM, pH = 7 for UV-C and H₂O₂/UV-C and pH = 3 for Fenton and photo-Fenton treatment.

GC-MS Analyses. According to the obtained GC-MS data presented in Table 4.28, PEG bearing 3-8 ethylene oxide units were identified as the common transformation products of the H₂O₂/UV-C and photo-Fenton processes as well as UV-C photolysis, being similar to the findings obtained in DW. On the other hand, formation of PEG was not observed during application of the Fenton process similar to the case for the formic acid formation being observed in the same AOP (Figure 4.61a). PEG were detected only at the initial treatment stages (2 min) of the H₂O₂/UV-C and photo-Fenton processes and disappeared thereafter due to their high reactivity with HO[•] (Buxton et al., 1988), whereas they appeared after 60 min UV-C photolysis, increased until 90 min of the treatment and decreased in the following stages. Considering these and the above carboxylic acids and aldehydes findings, one may suggest that the disappearance of NP-10 in SFW during the H₂O₂/UV-C and photo-Fenton processes as well as UV-C photolysis proceeds via a deethoxylation pathway, speculatively followed by the oxidation

Table 4.28. Transformation products identified via the GC-MS during H₂O₂/UV-C and photo-Fenton treatment as well as UV-C photolysis of NP-10 in SFW.

Structure	Name	Retention Time (min)	Major fragments (<i>m/z</i>) (Relative Abundance) (%)	Treatment Process
	PEG-3	18-19	45 (100); 31 (28-30); 89 (13-14)	UV-C; H ₂ O ₂ /UV-C; Photo-Fenton
	PEG-4	26	45 (100); 31 (21-23); 89 (21-22)	UV-C; H ₂ O ₂ /UV-C; Photo-Fenton
	PEG-5	32	45 (100); 89 (25); 43 (13-16)	UV-C; H ₂ O ₂ /UV-C; Photo-Fenton
	PEG-6	38	45 (100); 89 (26-28); 43 (13-16)	UV-C; H ₂ O ₂ /UV-C; Photo-Fenton
	PEG-7	43; 54	45 (100); 89 (28-35); 43 (13-18)	UV-C; H ₂ O ₂ /UV-C; Photo-Fenton
	PEG-8	47; 51	45 (100); 89 (29-35); 43 (16); 87 (13-15)	UV-C; Photo-Fenton
	Nonylphenol	31	135 (100); 45 (45); 107 (42)	UV-C
	Nonylphenol	31	149 (100); 107 (63); 121 (35)	UV-C

of PEG to aldehydes and carboxylic acids. Lower PEG yields obtained during the $\text{H}_2\text{O}_2/\text{UV-C}$ process (total peak area = 3.3×10^7) as compared to the photo-Fenton process (total peak area = 1.1×10^8) could indicate the rapid transformation of PEG in the former process. Although the total peak areas obtained in DW were in general one order of magnitude greater than those found in SFW, these differences were found to be statistically insignificant due to the lack of enough datapoints. In a previous study by Castillo et al. (2001), formation and degradation of PEG has been found to occur more rapidly in wastewater than in deionized water during the photodegradation, and this has been attributed to the presence of photosensitizers in wastewater. On the other hand, the same authors have demonstrated that Fe^{3+} -induced photolysis yielded higher degradation rates of PEG in deionized water than in wastewater due to the matrix interferences present in wastewater.

GC-MS analyses demonstrated that in addition to PEG, two isomers of branched chain nonylphenol were also present in the UV-C treated SFW samples (Table 4.28). These isomers produced no molecular ions without fragmentation. One isomer was evident with the spectra bearing a base peak of m/z 135 and no other major fragment ions in the region of m/z 137-219. The another isomer produced a base peak of m/z 149, major fragment ions of m/z 107 and 121 and no major fragments in the region of m/z 151-219. The first isomer with the base peak of m/z 135 was assigned an alphasdimethyl configuration. The another isomer with the base peak of m/z 149 was assigned an alpha-methyl, beta-methyl configuration as suggested by Wheeler et al. (1997). Even though these nonylphenol isomers were detected only after 90 min UV-C photolysis and could not be detected thereafter, and a lower amount of nonylphenol (total peak area = 2.3×10^7) was produced in SFW than in DW after the same treatment time, these results are of importance as far as the removal process is concerned due to the highly toxic nature of nonylphenol to aquatic fauna (Soares et al., 2008). Fortunately, this toxic compound was not produced during the applied AOP in SFW at any stage.

LC-MS Analyses. The initial attempts were made to follow the change of the individual nonylphenol polyethoxylate homologues with treatment time during chemical and photochemical reaction in SFW. For this purpose, being in general the most abundant molecular ions under positive ionization mode, sodium adducts of the individual

homologues ($[M+Na]^+$, $m/z = M+23$) were selected, and the results are illustrated in Figure 4.59a-d for UV-C, $H_2O_2/UV-C$, Fenton and photo-Fenton treatment, respectively. From Figure 4.59a, b and d it can be clearly seen that degradation of longer hydrophilic chain nonylphenol polyethoxylates (ethoxylate unit number (n) ≥ 4) was accompanied by an increase in the intensities of lower nonylphenol polyethoxylates ($n < 4$) after 30-60 min UV-C photolysis and 2 min $H_2O_2/UV-C$ and photo-Fenton processes. This finding indicated that fragmentation of the polyethoxylate chain length occurred during photochemical treatment of NP-10 in SFW, as has also been reported in the relevant studies (Pelizzetti et al., 1989; Nagarnaik and Boulanger, 2011). An exception was the gradual formation of NP-1 particularly during the course of UV-C and $H_2O_2/UV-C$ treatment which could also account for the presence of nonylphenol in UV-C-treated SFW samples (Table 4.28). For the Fenton process, increase in the peak intensities was observed for most nonylphenol polyethoxylates ($n = 2-17$) followed by a decrease (Figure 4.59c), suggesting that nonylphenol polyethoxylates of $n > 17$ whose masses were outside the upper m/z limit of 1000 in the present work were progressively transformed into lower polyethoxylate ones. This could also be the reason of that only insignificant NP-10 removal was obtained in SFW by the Fenton process as assessed by the HPLC measurements (Figure 4.55a).

Although a reasonable body of information about the biotransformation products of nonylphenol polyethoxylates already exists in the scientific literature (Di Corcia et al., 1998; Ying et al., 2002; Jahnke et al., 2004), there is still a significant data gap regarding the identities of transformation products which arise from the oxidative degradation of nonylphenol polyethoxylates during application of AOP in natural waters. Accordingly, LC-MS characterization of transformation products of NP-10 was performed under negative and positive electrospray ionization mode in order to establish the transformation routes of NP-10 via the $H_2O_2/UV-C$ and photo-Fenton processes in SFW. It should be underlined here that the LC-MS analyses deliberately focused on the determination of early-stage intermediates rather than late-stage transformation products since the former could give a better insight with respect to reaction mechanisms and pathways (Frontistis et al., 2012). As a result, the treatment time of 2 min was established considering that an average of 50% NP-10 removal with almost no mineralization was obtained after 2 min of

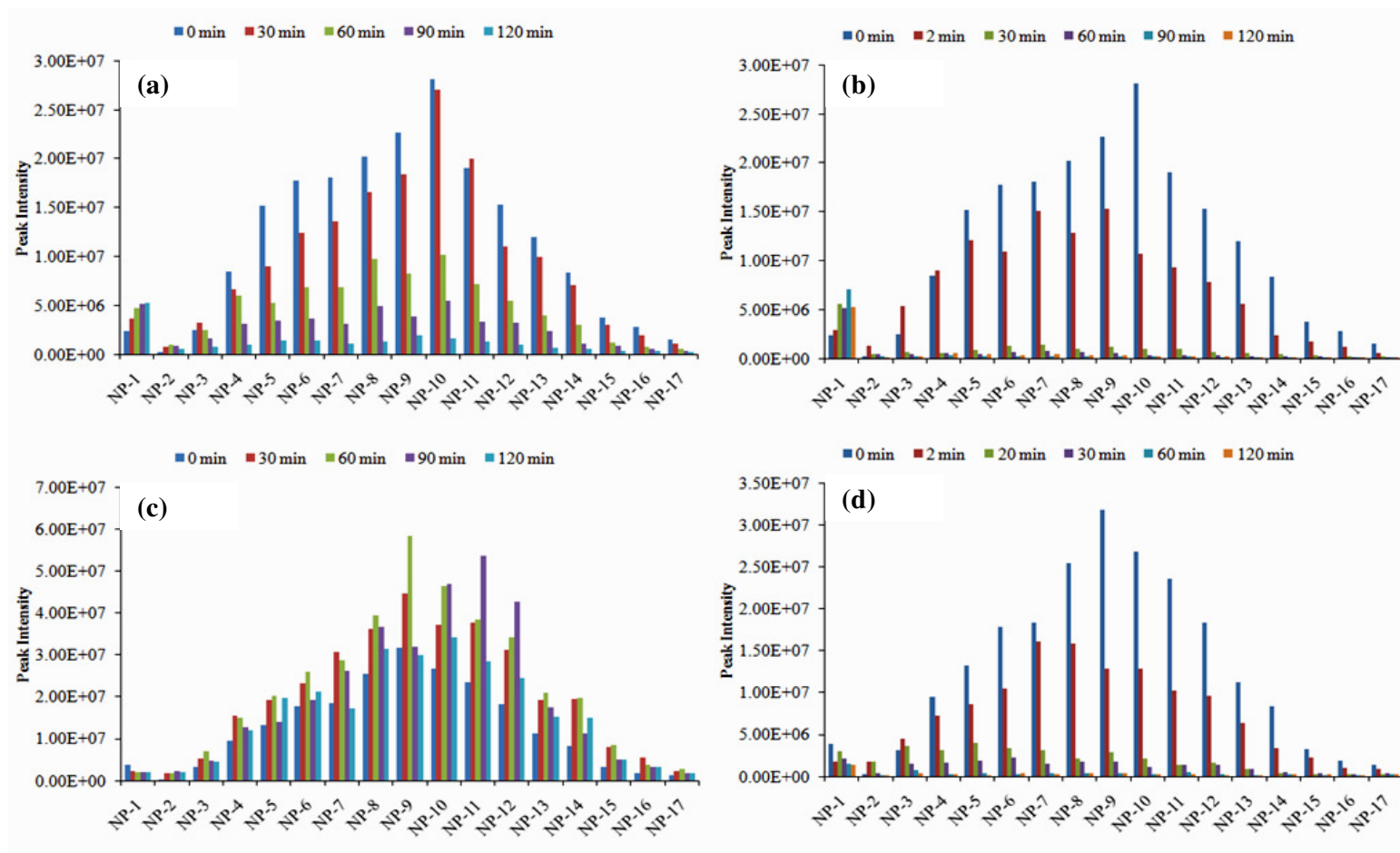


Figure 4.59. Temporal evolution of the intensities of individual nonylphenol polyethoxylate homologues during UV-C (a), H₂O₂/UV-C (b), Fenton (c) and photo-Fenton (d) treatment of NP-10 in SFW. Initial experimental conditions: NP-10 = 100 mg L⁻¹ (150 μM), H₂O₂ = 10 mM, Fe²⁺ = 200 μM, pH = 7 for UV-C and H₂O₂/UV-C and pH = 3 for Fenton and photo-Fenton treatment.

the H₂O₂/UV-C and photo-Fenton processes. The transformation product analysis performed by LC-MS under positive electrospray ionization mode first indicated that the mass spectrum obtained by applying the H₂O₂/UV-C process was more complex as compared to the photo-Fenton process, suggesting that a higher number of product was generated via the former AOP after 2 min treatment. However, additional elimination of certain types of transformation products from the aqueous phase during separation of the dissolved iron through precipitation and subsequent filtration in the photo-Fenton process could not be excluded. Despite the complexity of the obtained mass spectrum in both AOP, several classes of transformation products having molecular ions of relatively high abundance with unique clustering patterns could be differentiated upon comparison with mass spectrum of the NP-10 before photochemical treatment. In agreement with the GC-MS results, the common transformation products resulting from the photochemical degradation of NP-10 by both studied AOP were PEG, indicating that the most reactive part of the surfactant molecule is the polyethoxy chain. The Na⁺ adducts of PEG with 2-11 ethoxy subunits were evident from the series of molecular ions at m/z 129-525 separated by the difference of a single ethoxy unit, i.e. 44 m/z . The highest signal intensity within this mass cluster corresponded to tetraethylene glycol (m/z 217) for the H₂O₂/UV-C and hexaethylene glycol (m/z 305) for the photo-Fenton processes. Together with this primary cluster, another series of signals with masses of $m/z = 99 + 44n$ (m/z 495-891), which could be attributed to the Na⁺ adducts of monocarboxylated PEG with 9-18 ethoxy subunits, was identified in the H₂O₂/UV-C-treated sample. This series of signals was present in the mass spectrum of the photo-Fenton-treated sample in only minor relative abundances. Instead, a distinct series of signals at $m/z = 169 + 44n$ (m/z 389-785; $n = 5-14$) was found in the photo-Fenton-treated sample, which was not differentiated in the H₂O₂/UV-C-treated sample. This latter range of clusters could be attributed to the protonated forms of tertiary alcohols with one —OH group added to the aromatic ring, as has been previously suggested during ultrasonic irradiation of an octylphenol polyethoxylate with an average ethoxy subunits of 10 (Destailats et al., 2000). Additional analytical runs under negative ionization mode did not indicate the formation of nonylphenol during initial stages of the H₂O₂/UV-C and photo-Fenton processes.

Based on the overall experimental results, proposed degradation pathways for the transformation of NP-10 via the H₂O₂/UV-C and photo-Fenton processes are presented in

Figure 4.60. The transformation route being common for the $\text{H}_2\text{O}_2/\text{UV-C}$ and photo-Fenton processes involves the central fission of the polyethoxy chain, which brings about the generation of short-chained ethoxylates and PEG. The same mechanism has also been reported for the biological degradation of Triton X-100 (Franska et al., 2003). The formed PEG are most possibly the primary origin of the formic and acetic acids as well as aldehydes being detected in both photochemical AOP. Monocarboxylated PEG being apparent in the $\text{H}_2\text{O}_2/\text{UV-C}$ process is believed to be originated from the central fission of the polyethoxy chain of nonylphenol polyethoxycarboxylates, which could arise from the carboxylation of the terminal alcoholic group. On the other hand, nonylphenol polyethoxycarboxylates could not be identified neither in the $\text{H}_2\text{O}_2/\text{UV-C}$ nor in the photo-Fenton processes. The fragmentation and further oxidation of the monocarboxylated PEG resulted in the generation of oxalic acid in the $\text{H}_2\text{O}_2/\text{UV-C}$ process, that was otherwise not detected throughout the course of the photo-Fenton treatment. The finding that the generation of monocarboxylated PEG was of minor importance in the photo-Fenton pro-

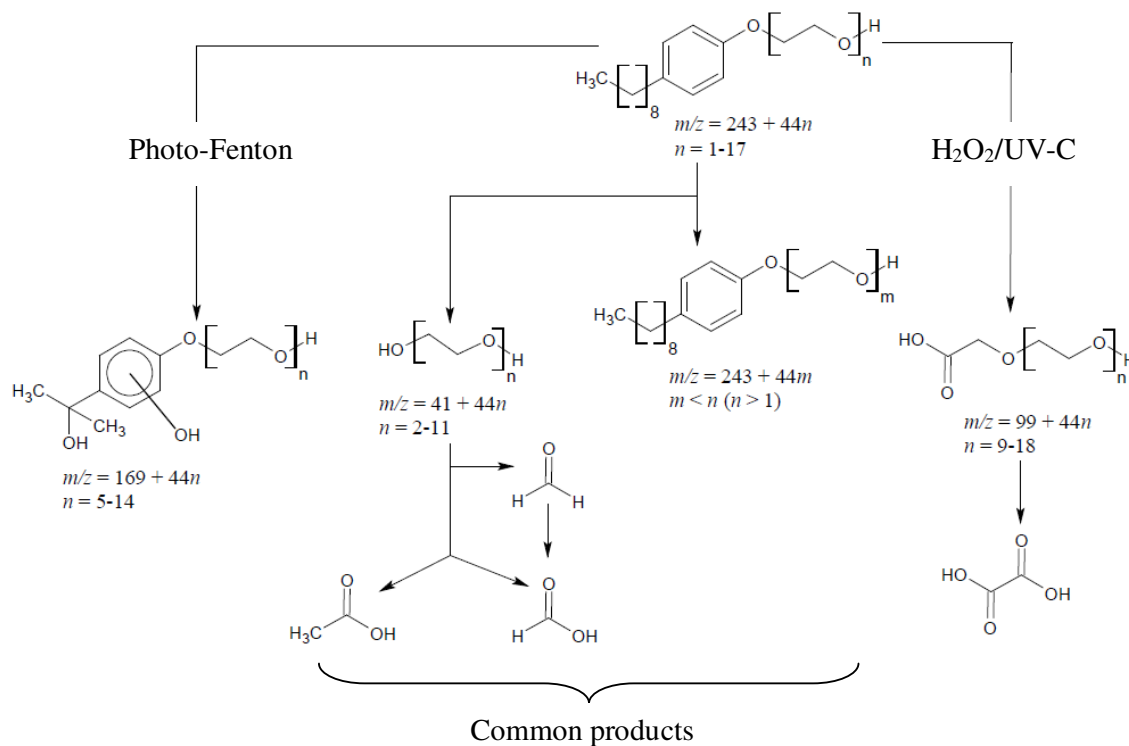


Figure 4.60. Proposed pathways for the transformation of NP-10 in SFW via the $\text{H}_2\text{O}_2/\text{UV-C}$ and photo-Fenton processes based on LC-MS results.

cess may indicate a higher susceptibility of the polyethoxy chain towards further oxidation via the H₂O₂/UV-C process. Instead, the alkyl chain and the aromatic ring were found to be relatively reactive towards the HO[•] during initial stages of the photo-Fenton treatment, as evident from the generation of the tertiary alcohols, whose chemical structures are demonstrated in Fig. 4.60.

4.2.4.3. Toxicity Evolution.

Acute Toxicity Evolution. The changes in acute toxicity towards *V. fischeri* photobacteria in terms of percent relative inhibition of the luminescence intensities during the H₂O₂/UV-C, Fenton and photo-Fenton treatment as well as UV-C photolysis of 100 mg L⁻¹ NP-10 in SFW as a function of treatment time are shown in Table 4.29.

Table 4.29. Evolution of acute inhibitory effects during the H₂O₂/UV-C, Fenton and photo-Fenton treatment as well as UV-C photolysis of NP-10 in SFW.

Treatment Time (min)	Inhibition (\pm Standard Deviation)%			
	UV-C	H ₂ O ₂ /UV-C	Fenton	Photo-Fenton
0	19 (\pm 4.4)	9.9 (\pm 0.16)	13 (\pm 3.2)	9.9 (\pm 0.16)
2	n.d.*	30 (\pm 1.3)	n.d.	19 (\pm 5.0)
20	n.d.	n.d.	n.d.	4.4 (\pm 2.9)
30	38 (\pm 4.4)	22 (\pm 5.2)	34 (\pm 0.34)	1.4 (\pm 1.5)
60	48 (\pm 2.8)	21 (\pm 2.3)	32 (\pm 0.60)	4.2 (\pm 3.5)
90	52 (\pm 0.77)	8.5 (\pm 7.7)	29 (\pm 5.6)	n.d.
120	42 (\pm 2.4)	9.0 (\pm 2.2)	33 (\pm 3.4)	1.3 (\pm 1.4)

*Not determined.

The inhibition values obtained throughout the UV-C photolysis were found to be significantly greater than those recorded during application of the H₂O₂/UV-C and photo-Fenton processes ($p < 0.010$) (Table 4.29). This finding clearly evidenced that UV-C photolysis of NP-10-contaminated natural waters presented higher risk in terms of ecotoxicological consequences as compared to the selected AOP. As can be seen from Table 4.29, during UV-C photolysis, the acute toxicity of NP-10 originally being 19 (\pm 4.4)% gradually increased, reaching 52 (\pm 0.77)% after 90 min UV-C photolysis. The

observed trend in the acute toxicity changes between 0-90 min UV-C photolysis could be attributed to the formation and accumulation of aromatic and/or unsaturated carbon-bonded oxidation intermediates being more toxic than the parent compound, as evident from the gradual increase in UV_{254/280} absorbances within the same time interval (Figure 4.50). Considering that the major difference between UV-C photolysis and the studied photochemical AOP was the lower NP-10 and TOC removal rate and efficiency achieved via the UV-C photolysis, the higher acute inhibitory effect towards *V. fischeri* being observed during UV-C photolysis was closely related to its lower treatment performance and kinetics. Since the formation of toxic nonylphenol was accompanied by high level of PEG generation in the UV-C photolysis unlike the studied AOP (Table 4.28), the significantly greater acute inhibitory effect observed during UV-C photolysis might have been contributed by *p*-nonylphenol. However, in the later stages of photolysis (> 90 min) the acute toxicity of the reaction solution slightly decreased to 42 (\pm 2.4)% and in parallel to the decrease of UV_{254/280} absorbances and disappearance of nonylphenol. Even though acute inhibitory effects observed in the UV-C-photolyzed SFW were higher than those in DW for all treatment times, the difference was found to be statistically insignificant.

Introduction of 10 mM H₂O₂ significantly decreased the acute inhibitory effects emerging after exposure to the UV-C treated SFW samples. From the patterns demonstrated in Table 4.29, it may be inferred that relatively more toxic oxidation products were formed in SFW between 0 and 90 min of the H₂O₂/UV-C treatment under the investigated experimental conditions. PEG were predominantly present in the reaction solution when the acute inhibitory effect was peaked during H₂O₂/UV-C treatment of NP-10 in SFW. On the other hand, it was speculated that the relationship between PEG and acute toxicity observed at the initial stages of the H₂O₂/UV-C process was indirectly indicative of the formation of shorter ethoxylate-chain alkylphenol ethoxylate derivatives being more acutely toxic than the original pollutant as has been also suggested in a previous related work on the ozonation of NP-10 (Ledakowicz et al., 2005). As can be followed from Table 4.29, during the H₂O₂/UV-C treatment of NP-10 in SFW, the toxicity decreased to 8.5 (\pm 7.7)% remained stagnant after 90 min treatment, which presented the major difference from that obtained in DW where a re-increase in the acute inhibitory effect from 10 (\pm 0.09)% to 24 (\pm 4.5)% was evident between 60 and 120 min of the H₂O₂/UV-C process. Considering that no re-increase in the concentration of formic acid

was observed during the H₂O₂/UV-C treatment of NP-10-contaminated SFW unlike the case in DW (Figure 4.61), the relatively lower acute inhibitory effect obtained in SFW after 120 min H₂O₂/UV-C treatment as compared to that in DW was speculated to be caused by the lack of formic acid at the end of treatment in the former aqueous matrix. On the other hand, the acute inhibitory effects observed throughout the course of the H₂O₂/UV-C treatment were not significantly different between DW and SFW.

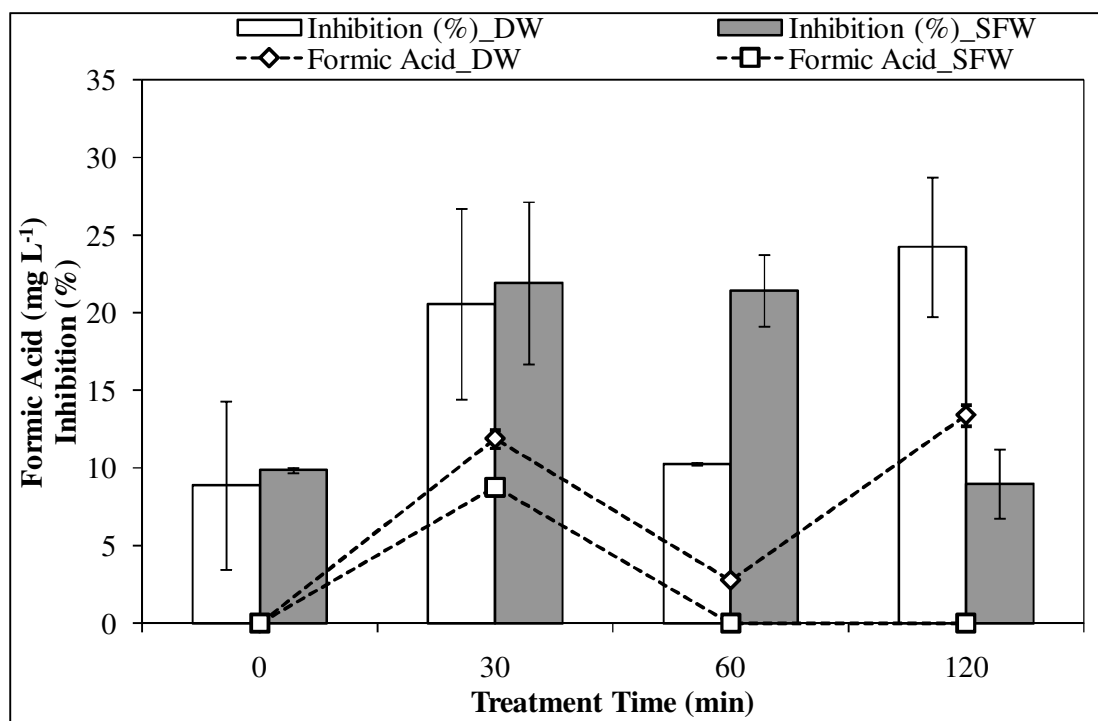


Figure 4.61. Comparative evolution of formic acid and the acute inhibitory effect during H₂O₂/UV-C treatment of NP-10 in DW and SFW. Initial experimental conditions: NP-10 = 100 mg L⁻¹ (150 μM), H₂O₂ = 10 mM, pH = 7.

As is evident from Table 4.29, the original toxicity increased abruptly already at the beginning of the Fenton process to 34 (± 0.34)% and only slightly changed thereafter. The acute toxicity evolution during application of the Fenton process followed a similar trend with the evolution of UV₂₅₄ absorbance (Figure 4.60b), hence suggesting the contribution of some aromatic species to the overall baseline toxicity. Although identity of these potentially aromatic oxidation products causing abrupt increase of the acute inhibitory effect after 30 min Fenton treatment remains unknown, the slight change of acute toxicity observed after this treatment time could be attributed to the slow kinetics of the Fenton

process. An overall comparison of the acute inhibitory effects observed during the Fenton treatment of NP-10-contaminated DW and SFW indicated that significantly greater relative inhibition values were apparent in SFW as compared to DW ($p < 0.05$) in parallel to greater formation of UV₂₅₄ absorbing moieties accompanied by slower degradation kinetics of NP-10 in SFW. Combining the acute toxicity test results in DW and SFW, one may conclude that the Fenton treatment of NP-10 in natural waters gave even worse results in terms of ecotoxicological safety due to potential interferences caused by SFW constituents.

The experimental findings delineated that the photo-Fenton treatment of NP-10-contaminated SFW resulted in significantly lower acute inhibitory effects than the other studied treatment methods ($p < 0.05$; Table 4.29). This finding rendered the photo-Fenton process ecotoxicologically safer as compared to the investigated other ones for the removal of aqueous NP-10 from natural waters. After 2 min photo-Fenton treatment where 42% NP-10 removal was achieved, a slight increase in relative inhibition to $19 (\pm 5.0)\%$ was observed which was accompanied by a sharp increase of the UV₂₅₄ absorbing moieties at the beginning of the photo-Fenton process (Figure 4.56b). On the other hand, the contribution of formic acid being rapidly generated at the beginning of the treatment to this initial acute toxicity increase should not be ruled out (Figure 4.57a). From the results presented in Table 4.29, it could be inferred that relatively less toxic oxidation products were formed after 30 min photo-Fenton treatment after which the acute inhibitory effect did not significantly change due to insignificant variation of TOC removal after this treatment time (Figure 4.55b). No re-appearance of the acute toxicity towards the end of the photo-Fenton treatment of SFW unlike the case of DW could again be explained by the complete transformation of the formed formic acid after 40 min treatment of SFW, whereas it still persisted at the end of the photo-Fenton treatment of pure aqueous solution of NP-10 (Figure 4.62). The experimental findings, on the other hand, revealed that the acute inhibitory effects throughout the course of the photo-Fenton treatment of NP-10 was not significantly affected by the SFW constituents, implying that the photo-Fenton treatment could also be safely applied for the treatment of natural waters contaminated with NP-10.

Genotoxicity Evolution. The *umu*-test was employed to estimate the genotoxic potential of NP-10-contaminated natural waters treated by the H₂O₂/UV-C, Fenton and photo-Fenton

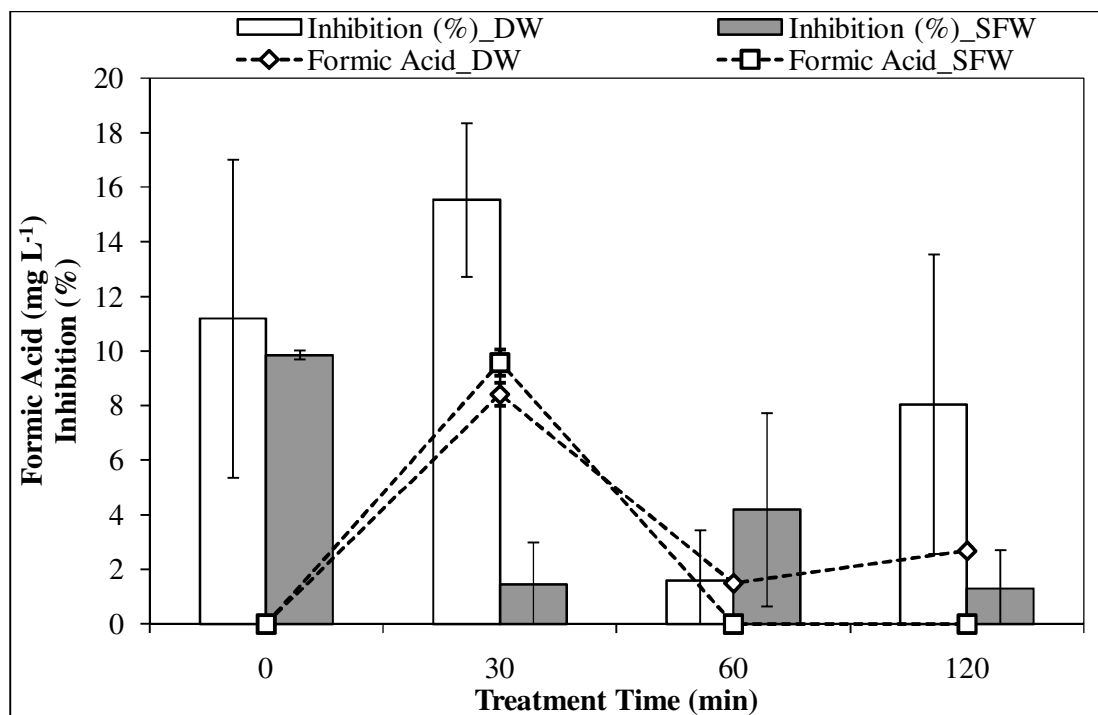


Figure 4.62. Comparative evolution of formic acid and the acute inhibitory effect during photo-Fenton treatment of NP-10 in DW and SFW. Initial experimental conditions: NP-10 = 100 mg L⁻¹ (150 μM), H₂O₂ = 10 mM, Fe²⁺ = 200 μM, pH = 3.

processes as well as UV-C photolysis. Induction factors reported in the presence and absence of metabolic activation are presented in Table 4.30. Although induction factors obtained in the absence of metabolic activation were in general greater than those found in the presence of metabolic activation, the difference was found to be statistically insignificant, demonstrating that the formation of transformation products necessitating metabolic activation for gaining genotoxic character was only of minor importance.

The *umu*-test results revealed that the overall induction factors observed throughout the experiments in general followed the order: H₂O₂/UV-C > Fenton > photo-Fenton > UV-C. UV-C photolysis was found to result in significantly lower induction factors than observed in the H₂O₂/UV-C process in the presence of metabolic activation ($p = 0.045$) (Table 4.30). It should be emphasized here that the relatively higher acute inhibitory effects obtained during application of the UV-C photolysis as compared to the studied AOP (Table 4.29) could be negatively correlated with low genotoxicity of the UV-C photolyzed SFW samples (Table 4.30), suggesting that genotoxicity could not be predicted

Table 4.30. Genotoxic effects observed at different stages of NP-10 degradation by UV-C, H₂O₂/UV-C, Fenton and photo-Fenton treatment processes in SFW.

Treatment Time (min)	Induction Factor (- S9)				Induction Factor (+ S9)			
	UV-C	H ₂ O ₂ /UV-C	Fenton	Photo-Fenton	UV-C	H ₂ O ₂ /UV-C	Fenton	Photo-Fenton
0		1.69				1.95		
2	n.d.*	2.14	n.d.	2.11	n.d.	1.49	n.d.	0.948
20	n.d.	n.d.	n.d.	1.88	n.d.	n.d.	n.d.	0.592
30	1.88	2.53	1.82	2.50	1.76	2.71	1.90	1.93
60	0.832	2.97	2.89	1.38	0.840	2.04	2.76	2.42
90	2.05	3.10	2.36	n.d.	0.868	3.18	1.50	n.d.
120	2.04	2.35	1.80	1.96	0.864	2.86	2.15	2.09

*Not determined.

from the acute toxicity data. Accordingly, Koh et al. (2004) could not find any relationship between high acute toxicity towards *V. fischeri* photobacteria and low mutagenicity during photochemical treatment of municipal leachates in their own study. In parallel, a recent study reported that anoxic-oxic treatment for municipal wastewater resulted in a complete removal of the acute inhibitory effect towards zebrafish (*Danio rerio*), but an increase in the genotoxic effect was detected by means of the micronucleus and comet assays (Zhang et al., 2013). Despite the lower genotoxic effects typically observed during UV-C photolysis as compared to the investigated AOP, induction factors generally followed an increasing trend in the absence of metabolic activation, reaching from non-genotoxic to weakly genotoxic levels (induction factor > 2) after 90-120 min UV-C photolysis. In a recent relevant work, UV-B irradiation of non-genotoxic nonylphenol ethoxylates has been reported to cause the appearance of genotoxic character by shortening of ethoxylate units (Toyooka et al., 2012). Genotoxicity, in the present study, increased with decreasing NP-10 concentration and followed a similar trend with UV_{254/280} absorbances in the absence of metabolic activation (Table 4.30), demonstrating that specific transformation products were responsible for the genotoxicity increase during UV-C photolysis. As was previously suggested for UV-C photolysis of NP-10 in DW, nonylphenol and PEG reaching their maximum concentrations after 90 min UV-C photolysis in SFW could account for this genotoxicity increase. The present experimental findings revealed, however, that no significant genotoxic activity (induction factor < 2) was observed during application of UV-C photolysis in the presence of metabolic activation, following an opposite trend with the findings obtained in the absence of metabolic activation (Table 4.30). This was in agreement with the data provided by Kubota et al. (2012) who demonstrated that the generation of γ -H2AX being a marker for DNA damage has been attenuated during UV-C irradiation of NP-10. The present findings revealed that although there was no significant difference between the induction factors in the absence of metabolic activation during UV-C photolysis of DW and SFW, the interference caused by the inorganic constituents of SFW caused the appearance of significantly higher genotoxicity in SFW as compared to DW in the presence of metabolic activation ($p = 0.034$) (Figure 4.63).

The H₂O₂/UV-C-treated SFW bearing NP-10 presented the highest genotoxic potential among the studied treatment processes (Table 4.30). As can be followed from Table 4.30, induction factors generally followed an increasing trend during the course of

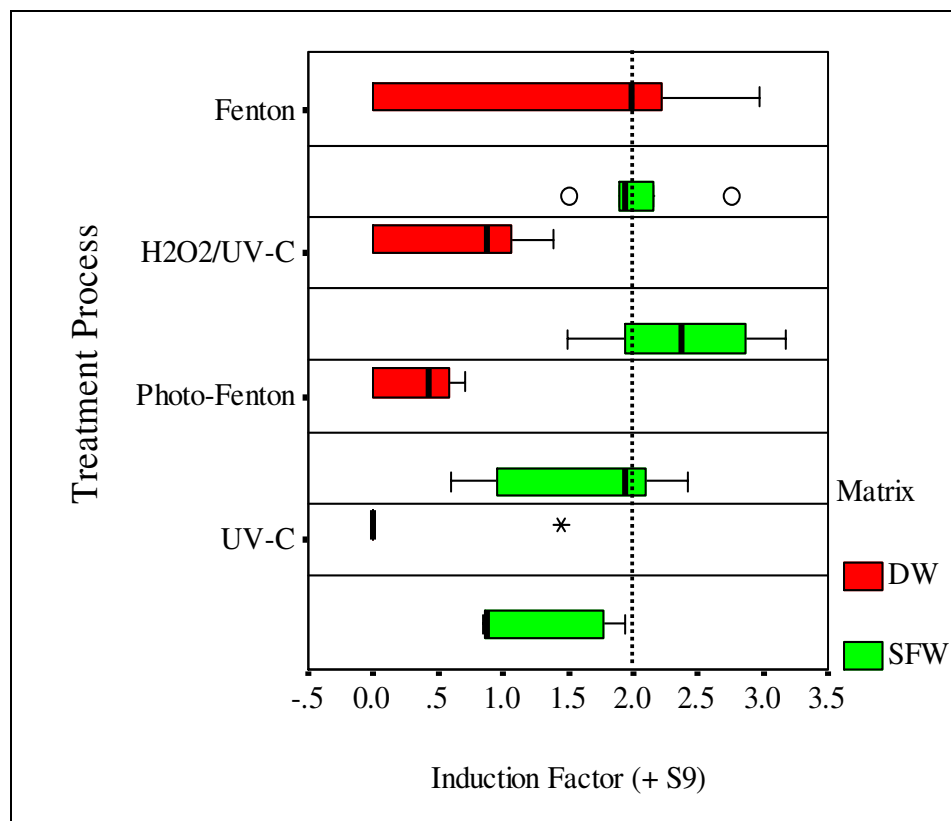


Figure 4.63. Box and whisker plots comparing genotoxic effects being observed during H₂O₂/UV-C, Fenton and photo-Fenton treatment as well as UV-C photolysis of NP-10 in DW and SFW in the presence of metabolic activation. Initial experimental conditions: NP-10 = 100 mg L⁻¹ (150 μM), H₂O₂ = 10 mM, Fe²⁺ = 200 μM, pH = 7 for UV-C and H₂O₂/UV-C and pH = 3 for Fenton and photo-Fenton treatment.

the H₂O₂/UV-C treatment, delineating that transformation products being weakly to moderately genotoxic (induction factors > 2) in the absence and presence of metabolic activation were formed with prolonged treatment time. After 90 min H₂O₂/UV-C treatment, genotoxic effect reached its peak value (induction factor > 3) both in the presence and absence of metabolic activation where 67% TOC removal and only a slight acute inhibitory effect (8.5 (± 7.7)% inhibition) were observed. Being similar to the findings obtained for the UV-C photolysis of NP-10 contaminated SFW, induction factors attained in the presence of metabolic activation during the H₂O₂/UV-C oxidation of NP-10 in SFW were significantly larger than in DW ($p = 0.001$) (Figure 4.63), rendering the H₂O₂/UV-C process genotoxicologically unsafe for the removal of NP-10 from natural waters.

As evident from Table 4.30, during Fenton treatment of NP-10 in SFW, the genotoxic effect showed an increase to weakly genotoxic levels (induction factor = 2-3) after 60 min treatment both in the absence and presence of metabolic activation and slightly decreased with prolonged treatment time in parallel to the changes observed in the acute inhibitory effects (Table 4.29). On the other hand, it should be noted that the Fenton-treated SFW still exhibited weak genotoxic potential after 120 min treatment in the presence of metabolic activation (induction factor = 2.1) (Table 4.30). According to the statistical comparisons, the induction factors obtained in DW and SFW were not significantly different in the presence and absence of metabolic activation, although the genotoxic effects observed in Fenton-treated pure aqueous solutions of NP-10 were in general higher than obtained in SFW in the absence of metabolic activation.

The photo-Fenton treatment resulted in nearly comparable genotoxic effects as found in UV-C photolysis of NP-10, particularly in the absence of metabolic activation (Table 4.30). Although some fluctuations were evident during application of the photo-Fenton process to SFW, the genotoxic effects obtained after 120 min photo-Fenton treatment were not significantly different from those of the untreated NP-10. However, it should be underlined that as the genotoxicity levels found after 120 min photo-Fenton treatment of SFW were near to weak genotoxicity level corresponding to an induction factor of 2 in the presence and absence of metabolic activation, care should be taken against potential re-appearance of genotoxic effects. In addition, it should be stressed that significantly greater genotoxic effects were recorded during photo-Fenton treatment of SFW in the presence of metabolic activation as compared to DW ($p = 0.005$) (Figure 4.63), signifying the higher potential for the formation of indirectly acting weakly genotoxic compounds during photo-Fenton treatment of NP-10 contaminated natural waters.

5. CONCLUSIONS

Biological processes are inefficient and/or ecotoxicologically unsafe for the treatment of industrially important aqueous phenol derivatives due to the toxic nature of these pollutants and/or their biotransformation products. AOP including H₂O₂/UV-C, Fenton and photo-Fenton treatment can offer efficient solutions for the partial and full degradation of phenolic compounds. However, since the risk of the formation of degradation products more toxic than the original parent compounds exists during the application of AOP, comparative evaluation of the degradation product and toxicity changes for different AOP is an important task. This experimental study primarily aimed at clarifying acute toxicity and genotoxicity patterns in light of the identified transformation products during application of the H₂O₂/UV-C, Fenton and photo-Fenton AOP for degradation of 2,4-DCP and NP-10, two phenol derivatives which deserve special focus due to toxicological concerns associated with them and/or their transformation products. The major conclusions drawn from the present study could be listed for 2,4-DCP and NP-10 individually as follows:

5.1. Studies with 2,4-DCP

Although UV-C photolysis was effective in decreasing the initial levels of 2,4-DCP, the degradation was incomplete, and insignificant TOC abatement was achieved after 90 min treatment. Rapid and complete degradation of 2,4-DCP and near-complete mineralization were observed for the H₂O₂/UV-C and photo-Fenton processes. Complete degradation of 2,4-DCP was also obtained with the Fenton's reagent, however a much lower TOC removal was evidenced than achieved by the H₂O₂/UV-C and photo-Fenton processes. The photo-Fenton process exhibited the highest pseudo-first-order 2,4-DCP and TOC abatement rate coefficients which was followed by the H₂O₂/UV-C, Fenton and UV-C treatment.

During application of the studied treatment processes, a release of Cl⁻ was evidenced, indicative of cleavage of the aromatic C – Cl bond. The rate of dechlorination was in the following decreasing order; photo-Fenton > H₂O₂/UV-C > Fenton > UV-C. The

degradation of 2,4-DCP was accompanied by the formation of chlorinated and hydroxylated aromatic intermediates as well as aliphatic late degradation products such as maleic, fumaric, oxalic, acetic and formic acids and aldehydes. Hydroquinone, chlorohydroquinone, maleic and formic acids and aldehydes were found to be the common transformation products of the studied treatment processes. UV-C photolysis brought about the steady accumulation of aliphatic aldehydes and carboxylic acids in the system. As expected, the Fenton's reagent was found to be much less efficient in removing aldehydes and carboxylic acids as compared to the H₂O₂/UV-C and photo-Fenton processes where these oxidation intermediates could be further degraded efficiently to non-detectable levels.

Ecotoxicological evaluations using *V. fischeri* as the test species revealed that although UV-C photolysis was capable of decreasing the originally high acute inhibitory effect, the time needed for a reasonable reduction of the acute toxic effect was relatively long. On the other hand, the H₂O₂/UV-C and photo-Fenton processes ensured a very fast reduction in acute inhibitory effect from 86 to $\leq 17\%$ inhibition after 30 min treatment which was highly correlated with the complete and fast 2,4-DCP abatement and the sharp Cl⁻ release, being an indicator of the rapid transformation of chlorinated oxidation intermediates. However, prolonged H₂O₂/UV-C treatment resulted in a re-increase in acute toxicity to 76% after 90 min treatment that was strongly correlated with the formation and accumulation of chloromethanediol and chlorocyclohexenedione products. The Fenton's reagent was also able to completely remove 2,4-DCP, however a relatively high toxicity was observed in the treated solution even after 90 min treatment. The poor TOC removal and accumulation of different transformation products as evidenced by the LC-MS analysis were the most likely origins of the remaining toxicity of Fenton-treated samples. Based on the genotoxicity results obtained by means of the *umu*-test, no significant genotoxic effect was evidenced for any studied AOP both with and without metabolic activation.

The H₂O₂/UV-C and photo-Fenton processes were again more effective than the Fenton's reagent in degrading and especially mineralizing 2,4-DCP when applied in synthetic freshwater. According to the genotoxicity results, degradation of 2,4-DCP in synthetic freshwater by the studied treatment processes could result in a weak to near-moderate level of genotoxic effect unlike the case in distilled water. Genotoxic effects

obtained in synthetic freshwater by applying the Fenton's reagent were higher in the presence of metabolic activation than obtained in the absence of metabolic activation, indicating that the genotoxicological risk related to Fenton treatment of freshwater contaminated with 2,4-DCP was largely due to the formation of indirectly acting transformation products.

5.2. Studies with NP-10

The H₂O₂/UV-C and photo-Fenton AOP proved to be effective treatment processes to achieve complete degradation and partial mineralization (79 and 69%, respectively) of NP-10 after 120 min treatment. On the other hand, the Fenton process resulted in only low NP-10 degradation (20%) and insignificant TOC abatement (< 10%) under comparable experimental conditions.

The aromatic oxidation products octylphenol, phenol, catechol, hydroquinone and benzoquinone were not detected in any of the studied treatment processes. On the other hand, nonylphenol formation was evidenced during UV-C and H₂O₂/UV-C treatment of NP-10. Based on the HPLC, colorimetry and GC-MS analyses, aliphatic carboxylic acids including formic, acetic and oxalic acids, aldehydes and PEG containing 2-8 ethoxy units were all identified as the degradation products of NP-10 by the studied treatment processes. The highest carboxylic acid (as the sum of concentrations recorded for formic, acetic and oxalic acids) concentration was measured in the photo-Fenton process (45 mg L⁻¹), whereas UV-C photolysis resulted in the formation of lowest concentration of carboxylic acids after 120 min treatment (4.1 mg L⁻¹). The highest aldehyde concentration was reached during UV-C and H₂O₂/UV-C treatment of NP-10 (1.2 mg L⁻¹). Low concentrations of carboxylic acids and aldehydes were produced during application of the Fenton's reagent (4.5 and 0.14 mg L⁻¹, respectively) due to rather poor NP-10 removal obtained with this treatment process. UV-C photolysis and the Fenton's reagent brought about a slow, but a steady increase in the concentrations of formic acid and aldehydes during course of treatment. These oxidation intermediates could be further degraded when the H₂O₂/UV-C and photo-Fenton treatment processes were employed, however, their complete degradation could not be achieved under the prevailing reaction conditions.

According to the acute toxicity test results, UV-C photolysis resulted in an increase in the inhibitory effect from originally 8.9% to 33% after 120 min treatment; a similar pattern seen in aldehydes and nonylphenol products. The H₂O₂/UV-C process ultimately resulted in a higher acute inhibitory effect (24 (± 4.5)% inhibition) than the original NP-10 solution. The acute inhibitory effect measured at the end of the photo-Fenton process (8.0 (± 5.5)% inhibition) was nearly at the same level as that of the untreated pollutant. Temporal evolution of the acute inhibitory effect observed during H₂O₂/UV-C and photo-Fenton treatment of NP-10 was parallel with that of carboxylic acid and aldehyde products. The lower acute inhibitory effect evidenced after 120 min photo-Fenton treatment than achieved with the H₂O₂/UV-C process was speculatively due to lower concentrations of carboxylic acids measured at the end of the photo-Fenton process.

The experimental findings obtained in synthetic freshwater delineated that the H₂O₂/UV-C and photo-Fenton processes ensured complete NP-10 removal and partial mineralization (76 and 64%, respectively). The highest concentrations of low carbon aliphatic transformation products obtained during H₂O₂/UV-C and photo-Fenton treatment of NP-10 in synthetic freshwater were measured as 12 and 41 mg L⁻¹ for formic acid, 19 and 15 mg L⁻¹ for acetic acid, 16 and 0 mg L⁻¹ for oxalic acid and 2.1 and 0.60 mg L⁻¹ for aldehydes, respectively. The acute inhibitory impact towards *V. fischeri* was in general below 10% during photo-Fenton treatment of NP-10 in synthetic freshwater, while the H₂O₂/UV-C process resulted in slightly higher acute toxic effect as compared to the photo-Fenton process with a maximum relative inhibition of 30 (± 1.3)%. According to the *umu*-test results, 120 min-H₂O₂/UV-C treatment of NP-10 in synthetic freshwater resulted in the formation of weakly genotoxic transformation products (the induction factor = 2.9) in the presence of metabolic activation. The photo-Fenton treatment results indicated that changes in the genotoxic effect levels were less pronounced, and the induction factors were in general lower than those found in the H₂O₂/UV-C process both in the absence (≤ 2.5) and presence (≤ 2.4) of metabolic activation. However, the risk of the formation of weakly genotoxic transformation products during application of the photo-Fenton process in synthetic freshwater under the applied experimental conditions should not be completely excluded.

6. RECOMMENDATIONS

Based on the achieved results, the following recommendation can be made for future research:

- Data regarding removal kinetics and efficiencies should essentially be supported with both specific and non-specific toxicity information obtained during AOP treatment of phenolic compounds in order to ensure ecotoxicologically safe conditions for the discharge into subsequent biological treatment units or direct discharge into receiving water bodies. Combination of the bioluminescence inhibition test using *V. fischeri* for acute toxicity and the *umu*-test for genotoxicity testing may prove as suitable bioanalytical tools that sufficiently represent the dynamics of transformation products formation within an AOP system.
- It should be kept in mind that in toxicity bioassays pollutants and their transformation products act more by their concentrations and interactions rather than their contribution to the biological cycle. From this point of view, some care should be taken in the characterization of the effect of AOP on the biodegradability of industrial wastewater.
- The development and validation of suitable analytical protocols seem to be the key in reliably determining the transformation products of alkylphenol polyethoxylates.
- Specific studies to be conducted on real natural waters and wastewaters may help improving the current knowledge on the effect of co-existing organics and inorganics on the generation of transformation products and evolution of the inhibitory effect.

REFERENCES

- Abe, K., Tanaka, K., 1997. Fe³⁺ and UV-enhanced ozonation of chlorophenolic compounds in aqueous medium. *Chemosphere*, 35, 2837-2847.
- Achilleos, A., Hapeshi, E., Xekoukoulotakis, N. P., Mantzavinos, D., Fatta-Kassinos, D., 2010. Factors affecting diclofenac decomposition in water by UV-A/TiO₂ photocatalysis. *Chemical Engineering Journal*, 161, 53-59.
- Adams, C. D., Cozzens, R. A., Kim, B. J., 1997. Effects of ozonation on the biodegradability of substituted phenols. *Water Research*, 31, 2655-2663.
- Ahel, M., Giger, W., Koch, M., 1994. Behaviour of alkylphenol polyethoxylate surfactants in the aquatic environment – I. Occurrence and transformation in sewage treatment. *Water Research*, 28, 1131-1142.
- Ahlborg, U. G., Thunberg, T. M., 1980. Chlorinated phenols – Occurrence, toxicity, metabolism, and environmental impact. *CRC Critical Reviews in Toxicology*, 7, 1-35.
- Al-Ekabi, H., Serpone, N., Pelizzetti, E., Minero, C., Fox, M. A., Draper, R. B., 1989. Kinetic studies in heterogeneous photocatalysis. 2. TiO₂-mediated degradation of 4-chlorophenol alone and in a three-component mixture of 4-chlorophenol, 2,4-dichlorophenol, and 2,4,5-trichlorophenol in air-equilibrated aqueous media. *Langmuir*, 5, 250-255.
- Al Momani, F., 2006. Biodegradability enhancement of 2,4-dichlorophenol aqueous solution by means of photo-Fenton reaction. *Environmental Engineering Science*, 23, 722-733.
- Al Momani, F., Sans, C., Esplugas, S., 2004. A comparative study of the advanced oxidation of 2,4-dichlorophenol. *Journal of Hazardous Materials*, B107, 123-129.

Alaton, I. A., Balcioglu, I. A., Bahnemann, D. W., 2002. Advanced oxidation of a reactive dyebath effluent. Comparison of O₃, H₂O₂/UV-C and TiO₂/UV-A processes. *Water Research*, 36, 1143-1154.

Alaton, I. A., Teksoy, S., 2007. Acid dyebath effluent pretreatment using Fenton's reagent: Process optimization, reaction kinetics and effects on acute toxicity. *Dyes and Pigments*, 73, 31-39.

Ali, M., Sreerishnan, T. R., 2001. Aquatic toxicity from pulp and paper mill effluents: A review. *Advances in Environmental Research*, 5, 175-196.

Andreozzi, R., Caprio, V., Insola, A., Marotta, R., 1999. Advanced oxidation processes (AOP) for water purification and recovery. *Catalysis Today*, 53, 51-59.

Andreu, V., Ferrer, E., Rubio, J. L., Font, G., Picó, Y., 2007. Quantitative determination of octylphenol, nonylphenol, alkylphenol ethoxylates and alcohol ethoxylates by pressurized liquid extraction, and liquid chromatography-mass spectrometry in soils treated with sewage sludges. *Science of the Total Environment*, 378, 124-129.

Androulaki, E., Hiskia, A., Dimotikali, D., Minero, C., Calza, P., Pelizzetti, E., Papaconstantinou, E., 2000. Light induced elimination of mono- and polychlorinated phenols from aqueous solutions by PW₁₂O₄₀³⁻. The case of 2,4,6-trichlorophenol. *Environmental Science and Technology*, 34, 2024-2028.

APHA/AWWA/WEF. 1998. *Standard Methods for the Examination of Water and Wastewater*. American Public Health Association, Washington DC.

Araki, H., Tatarazako, N., Kishi, K., Kuroda, K.-i., 2000. Evaluation of bioaccumulation potential of 3,4,5-trichloroguaiacol in a zooplankton (*Daphnia magna*) by pyrolysis-GC/MS in the presence of tetramethylammonium hydroxide (TMAH). *Journal of Analytical and Applied Pyrolysis*, 55, 69-80.

Arsene, D., Catrinescu, C., Drăgoi, B., Teodosiu, C., 2010. Catalytic wet hydrogen peroxide oxidation of 4-chlorophenol over iron-exchanged clays. *Environmental Engineering and Management Journal*, 9, 7-16.

Arsene, D., Musteret, C. P., Catrinescu, C., Apopei, P., Barjoveanu, G., Teodosiu, C., 2011. Combined oxidation and ultrafiltration processes for the removal of priority organic pollutants from wastewaters. *Environmental Engineering and Management Journal*, 10, 1967-1976.

Arslan-Alaton, I., 2007. Degradation of a commercial textile biocide with advanced oxidation processes and ozone. *Journal of Environmental Management*, 82, 145-154.

Arslan-Alaton, I., Akin, A., Olmez-Hanci, T., 2010. An optimization and modeling approach for H₂O₂/UV-C oxidation of a commercial nonionic textile surfactant using central composite design. *Journal of Chemical Technology and Biotechnology*, 85, 493-501.

Arslan-Alaton, I., Ayten, N., Olmez-Hanci, T., 2010. Photo-Fenton-like treatment of the commercially important H-acid: Process optimization by factorial design and effects of photocatalytic treatment on activated sludge inhibition. *Applied Catalysis B*, 96, 208-217.

Arslan-Alaton, I., Cokgor, E. U., Koban, B., 2007. Integrated photochemical and biological treatment of a commercial textile surfactant: Process optimization, process kinetics and COD fractionation. *Journal of Hazardous Materials*, 146, 453-458.

Arslan-Alaton, I., Erdinc, E., 2006. Effect of photochemical treatment on the biocompatibility of a commercial nonionic surfactant used in the textile industry. *Water Research*, 40, 3409-3418.

Arslan-Alaton, I., Gurses, F., 2004. Photo-Fenton-like and photo-fenton-like oxidation of procaine penicillin G formulation effluent. *Journal of Photochemistry and Photobiology A: Chemistry*, 165, 165-175.

Arslan-Alaton, I., GURSOY, B. H., AKYOL, A., KOBYA, M., BAYRAMOGLU, M., 2010. Modeling and optimization of acid dye manufacturing wastewater treatment with Fenton's reagent: Comparison with electrocoagulation treatment results and effects on activated sludge inhibition. *Water Science and Technology*, 62, 209-216.

Arslan-Alaton, I., Olmez-Hanci, T., Shayin, S., 2012a. H₂O₂/UV-C treatment of textile preparation wastewater: Kinetic investigation on alternative combinations of commercial textile preparation auxiliaries. *Environmental Technology*, 33, 1531-1537.

Arslan-Alaton, I., Shayin, S., Olmez-Hanci, T., 2012b. The hydroxyl radical scavenging effect of textile preparation auxiliaries on the photochemical treatment of nonylphenol ethoxylate. *Environmental Technology*, 33, 419-427.

Barbeni, M., Minero, C., Pelizzetti, E., Borgarello, E., Serpone, N., 1987. Chemical degradation of chlorophenols with Fenton's reagent (Fe²⁺ + H₂O₂). *Chemosphere*, 16, 2225-2237.

Basu, S., Wei, I. W., 1998. Advanced chemical oxidation of 2,4,6 trichlorophenol in aqueous phase by Fenton's reagent – Part I: Effects of the amounts of oxidant and catalyst on the treatment reaction. *Chemical Engineering Communications*, 164, 111-137.

Bauer, R., Waldner, G., Fallmann, H., Hager, S., Klare, M., Krutzler, T., Malato, S., Maletzky, P., 1999. The photo-Fenton reaction and the TiO₂/UV process for waste water treatment – Novel developments. *Catalysis Today*, 53, 131-144.

Bayarri, B., González, O., Maldonado, M. I., Giménez, J., Esplugas, S., 2007. Comparative study of 2,4-dichlorophenol degradation with different advanced oxidation processes. *Journal of Solar Energy Engineering*, 129, 60-67.

Bekbolet, M., Çınar, Z., Kılıç, M., Uyguner, C. S., Minero, C., Pelizzetti, E., 2009. Photocatalytic oxidation of dinitronaphthalenes: Theory and experiment. *Chemosphere*, 75, 1008-1014.

Beltrán, F. J., 2005. Ozone Reaction Kinetics for Water and Wastewater Systems, Lewis Publishers, Boca Raton.

Beltran-Heredia, J., Torregrosa, J., Dominguez, J. R., Peres, J. A., 2001. Kinetics of the oxidation of *p*-hydroxybenzoic acid by the H₂O₂/UV system. Industrial and Engineering Chemistry Research, 40, 3104-3108.

Benitez, F. J., Beltrán-Heredia, J., Acero, J. L., Rubio, F. J., 2000a. Rate constants for the reactions of ozone with chlorophenols in aqueous solutions. Journal of Hazardous Materials, B79, 271-285.

Benitez, F. J., Beltran-Heredia, J., Acero, J. L., Rubio, F. J., 2000b. Contribution of free radicals to chlorophenols decomposition by several advanced oxidation processes. Chemosphere, 41, 1271-1277.

Bermejo, M. D., Cocero, M. J., 2006. Supercritical water oxidation: A technical review. AIChE Journal, 52, 3933-3951.

Bertanza, G., Pedrazzani, R., Papa, M., Mazzoleni, G., Steimberg, N., Caimi, L., Montani, C., Dilorenzo, D., 2010. Removal of BPA and NP_nEOs from secondary effluents of municipal WWTPs by means of ozonation. Ozone: Science & Engineering, 32, 204-208.

Bertelli, M., Selli, E., 2006. Reaction paths and efficiency of photocatalysis on TiO₂ and of H₂O₂ photolysis in the degradation of 2-chlorophenol. Journal of Hazardous Materials, B138, 46-52.

Biondi, O., Motta, S., Mosesso, P., 2002. Low molecular weight polyethylene glycol induces chromosome aberrations in Chinese hamster cells cultured *in vitro*. Mutagenesis, 17, 261-264.

Bojanowska-Czajka, A., Gałęzowska, A., Marty, J.-L., Trojanowicz, M., 2010. Decomposition of pesticide chlorfenvinphos in aqueous solutions by gamma-irradiation. Journal of Radioanalytical and Nuclear Chemistry, 285, 215-221.

Boule, P., Guyon, C., Lemaire, J., 1982. Photochemistry and Environment. IV-Photochemical behaviour of monochlorophenols in dilute aqueous solution. *Chemosphere*, 11, 1179-1188.

Brand, N., Mailhot, G., Bolte, M., 1998. Degradation photoinduced by Fe(III): Method of alkylphenol ethoxylates removal in water. *Environmental Science and Technology*, 32, 2715-2720.

Brand, N., Mailhot, G., Sarakha, M., Bolte, M., 2000. Primary mechanism in the degradation of 4-octylphenol photoinduced by Fe(III) in water – acetonitrile solution. *Journal of Photochemistry and Photobiology A: Chemistry*, 135, 221-228.

Brillas, E., Calpe, J. C., Casado, J., 2000. Mineralization of 2,4-D by advanced electrochemical oxidation processes. *Water Research*, 34, 2253-2262.

Brillas, E., Sauleda, R., Casado, J., 1998. Degradation of 4-chlorophenol by anodic oxidation, electro-Fenton, photoelectro-Fenton, and peroxi-coagulation processes. *Journal of the Electrochemical Society*, 145, 759-765.

Bull, R. J., Reckhow, D. A., Li, X., Humpage, A. R., Joll, C., Hrudey, S. E., 2011. Potential carcinogenic hazards of non-regulated disinfection by-products: Haloquinones, halo-cyclopentene and cyclohexene derivatives, *N*-halamines, halonitriles, and heterocyclic amines. *Toxicology*, 286, 1-19.

Buxton, G. V., Greenstock, C. L., Helman, W. P., Ross, A. B., 1988. Critical review of data constants for reactions of hydrated electrons, hydrogen atoms and hydroxyl radicals in aqueous solutions. *Journal of Physical Chemistry Reference Data*, 17, 513-886.

Calza, P., Sakkas, V. A., Medana, C., Baiocchi, C., Dimou, A., Pelizzetti, E., Albanis, T., 2006. Photocatalytic degradation study of diclofenac over aqueous TiO₂ suspensions. *Applied Catalysis B: Environmental*, 67, 197-205.

Canonica, S., Jans, U., Stemmler, K., Hoigné, J., 1995. Transformation kinetics of phenols in water: Photosensitization by dissolved natural organic material and aromatic ketones. *Environmental Science and Technology*, 29, 1822-1831.

Castillo, M., Peñuela, G., Barceló, D., 2001. Identification of photocatalytic degradation products of non-ionic polyethoxylated surfactants in wastewaters by solid-phase extraction followed by liquid chromatography-mass spectrometric detection. *Fresenius' Journal of Analytical Chemistry*, 369, 620-628.

Catrinescu, C., Arsene, D., Teodosiu, C., 2011. Catalytic wet hydrogen peroxide oxidation of *para*-chlorophenol over Al/Fe pillared clays (AlFePILCs) prepared from different host clays. *Applied Catalysis B: Environmental*, 101, 451-460.

Céspedes, R., Lacorte, S., Ginebreda, A., Barceló, D., 2008. Occurrence and fate of alkylphenols and alkylphenol ethoxylates in sewage treatment plants and impact on receiving waters along the Ter River (Catalonia, NE Spain). *Environmental Pollution*, 153, 384-392.

Chen, L., Zhou, H. Y., Liu, L., Deng, Q. Y., 2007a. Mechanism study on UV-induced photodegradation of nonylphenol ethoxylates by intermediate products analysis. *Chinese Chemical Letters*, 18, 473-475.

Chen, L., Zhou, H. Y., Deng, Q. Y., 2007b. Photolysis of nonylphenol ethoxylates: The determination of the degradation kinetics and the intermediate products. *Chemosphere*, 68, 354-359.

Chen, R., Pignatello, J. J., 1997. Role of quinone intermediates as electron shuttles in Fenton and photoassisted Fenton oxidations of aromatic compounds. *Environmental Science and Technology*, 31, 2399-2406.

Chin, Y.-P., Miller, P. L., Zeng, L., Cawley, K., Weavers, L. K., 2004. Photosensitized degradation of bisphenol A by dissolved organic matter. *Environmental Science and Technology*, 38, 5888-5894.

Chiu, T. Y., Paterakis, N., Cartmell, E., Scrimshaw, M. D., Lester, J. N., 2010. A critical review of the formation of mono and dicarboxylated metabolic intermediates of alkylphenol polyethoxylates during wastewater treatment and their environmental significance. *Critical Reviews in Environmental Science and Technology*, 40, 199-138.

Chu, W., Kwan, C. Y., Chan, K. H., Kam, S. K., 2005. A study of kinetic modelling and reaction pathway of 2,4-dichlorophenol transformation by photo-fenton-like oxidation. *Journal of Hazardous Materials*, B121, 119-126.

Contreras, S., Rodríguez, M., Al Momani, F., Sans, C., Esplugas, S., 2003. Contribution of the ozonation pre-treatment to the biodegradation of 2,4-dichlorophenol. *Water Research*, 37, 3164-3171.

Cravotto, G., Binello, A., Di Carlo, S., Orio, L., Wu, Z.-L., Ondruschka, B., 2010. Oxidative degradation of chlorophenol derivatives promoted by microwaves or power ultrasound: A mechanism investigation. *Environmental Science and Pollution Research*, 17, 674-687.

Crittenden, J. C., Hu, S., Hand, D. W., Green, S. A., 1999. A kinetic model for H₂O₂/UV process in a completely mixed batch reactor. *Water Research*, 33, 2315-2328.

Czaplicka, M., 2004. Sources and transformations of chlorophenols in the natural environment. *Science of the Total Environment*, 322, 21-39.

Czaplicka, M., 2006. Photo-degradation of chlorophenols in the aqueous solution. *Journal of Hazardous Materials*, B134, 45-59.

Czaplicka, M., Mielżyńska, D., 2007. Influence of photodegradation on mutagenic activity of aquatic solution of chlorophenols. *Environmental Biotechnology*, 3, 30-36.

Çatalkaya, E. Ç., Bali, U., Şengül, F., 2003. Photochemical degradation and mineralization of 4-chlorophenol. *Environmental Science and Pollution Research*, 10, 113-120.

De, A. K., Chaudhuri, B., Bhattacharjee, S., Dutta, B. K., 1999. Estimation of $\cdot\text{OH}$ radical reaction rate constants for phenol and chlorinated phenols using UV/ H_2O_2 photo-oxidation. *Journal of Hazardous Materials*, 64, 91-104.

de la Fuente, L., Acosta, T., Babay, P., Curutchet, G., Candal, R., Litter, M. I., 2010. Degradation of nonylphenol ethoxylate-9 (NPE-9) by photochemical advanced oxidation technologies. *Industrial and Engineering Chemistry Research*, 49, 6909-6915.

De Laat, J., Le, G.T., Legube, B., 2004. A comparative study of the effects of chloride, sulfate and nitrate ions on the rates of decomposition of H_2O_2 and organic compounds by $\text{Fe(II)/H}_2\text{O}_2$ and $\text{Fe(III)/H}_2\text{O}_2$. *Chemosphere*, 55, 715-723.

Decision 2455/2001/EC, 2001 of the European Parliament and of the Council of November 20, establishing the list of priority substances in the field of water policy and amending Directive 2000/60/EC (L331 of 15-12-2001).

Delanghe, B., Mekras, C. I., Graham, N. J. D., 1991. Aqueous ozonation of surfactants: A review. *Ozone: Science & Engineering*, 13, 639-673.

Destailats, H., Hung, H.-M., Hoffmann, M. R., 2000. Degradation of alkylphenol ethoxylate surfactants in water with ultrasonic irradiation. *Environmental Science and Technology*, 34, 311-317.

Detomaso, A., Lopez, A., Lovecchio, G., Mascolo, G., Curci, R., 2003. Practical applications of the Fenton reaction to the removal of chlorinated aromatic pollutants. *Environmental Science and Pollution Research*, 10, 379-384.

Dhale, A. D., Mahajani, V. V., 2001. Subcritical mineralization of sodium salt of dodecyl benzene sulfonate using sonication – wet oxidation (SONIWO) technique. *Water Research*, 35, 2300-2306.

Di Corcia, A., Costantino, A., Crescenzi, C., Marinoni, E., Samperi, R., 1998. Characterization of recalcitrant intermediates from biotransformation of the branched alkyl

side chain of nonylphenol ethoxylate surfactants. *Environmental Science and Technology*, 32, 2401-2409.

Diab, K. M., El Makawy, A. I., Abd El-Moneim, O. M., Sharaf, A., 2012. Assessment of genotoxicity and histopathological changes induced by polyethylene glycol (PEG6000) in male mice. *Journal of Cytology and Histology*, 3:153, doi: 10.4172/2157-7099.1000153.

Directive 2000/60/EC, 2000 of the European Parliament and of the Council of October 23, establishing a framework for Community action in the field of water policy.

Du, Y., Zhou, M., Lei, L., 2006. Role of the intermediates in the degradation of phenolic compounds by Fenton-like process. *Journal of Hazardous Materials*, B136, 859-865.

Du, Y., Zhou, M., Lei, L., 2007. The role of oxygen in the degradation of *p*-chlorophenol by Fenton system. *Journal of Hazardous Materials*, B139, 108-115.

Duke, F. R., Haas, T. W., 1961. The homogeneous base-catalyzed decomposition of hydrogen peroxide. *The Journal of Physical Chemistry*, 65, 304-306.

Durand, A.-P. Y., Brattan, D., Brown, R. G., 1992. Mechanism of the primary photoreaction in the aqueous photochemistry of 4-chlorophenol. *Chemosphere*, 25, 783-792.

Escher, B. I., Fenner, K., 2011. Recent advances in environmental risk assessment of transformation products. *Environmental Science and Technology*, 45, 3835-3847.

Escobar, P. A., Kemper, R. A., Tarca, J., Nicolette, J., Kenyon, M., Glowienke, S., Sawant, S. G., Christensen, J., Johnson, T. E., McKnight, C., Ward, G., Galloway, S. M., Custer, L., Gocke, E., O'Donovan, M. R., Braun, K., Snyder, R. D., Mahadevan, B., 2013. Bacterial mutagenicity screening in the pharmaceutical industry. *Mutation Research/Reviews in Mutation Research*, 752, 99-118.

Essam, T., Amin, M. A., El Tayeb, O., Mattiasson, B., Guieysse, B., 2007. Sequential photochemical-biological degradation of chlorophenols. *Chemosphere*, 66, 2201-2209.

Fan, J., Yang, W., Li, A., 2011. Adsorption of phenol, bisphenol A and nonylphenol ethoxylates onto hypercrosslinked and aminated adsorbents. *Reactive & Functional Polymers*, 71, 994-1000.

Farré, M., García, M.-J., Tirapu, L., Ginebreda, A., Barceló, D., 2001. Wastewater toxicity screening of non-ionic surfactants by Toxalert[®] and Microtox[®] bioluminescence inhibition assays. *Analytica Chimica Acta*, 427, 181-189.

Fatta-Kassinos, D., Vasquez, M. I., Kümmerer, K., 2011. Transformation products of pharmaceuticals in surface waters and wastewater formed during photolysis and advanced oxidation processes – Degradation, elucidation of byproduct and assessment of their biological potency. *Chemosphere*, 85, 693-709.

Faust, B. C., Hoigne, J., 1990. Photolysis of Fe(III)-hydroxy complexes as sources of OH radicals in clouds, fog and rain. *Atmospheric Environment*, 24A, 79-89.

Fernández-Alba, A. R., Hernando, D., Agüera, A., Cáceres, J., Malato, S., 2002. Toxicity assays: A way for evaluating AOPs efficiency. *Water Research*, 36, 4255-4262.

Fox, M. A., Dulay, M. T., 1993. Heterogeneous photocatalysis. *Chemical Reviews*, 93, 341-357.

Franska, M., Franski, R., Szymanski, A., Lukaszewski, Z., 2003. A central fission pathway in alkylphenol ethoxylate biodegradation. *Water Research*, 37, 1005-1014.

Frassinetti, S., Barberio, C., Caltavuturo, L., Fava, F., Di Gioia, D., 2011. Genotoxicity of 4-nonylphenol and nonylphenol ethoxylate mixtures by the use of *Saccharomyces cerevisiae* D7 mutation assay and use of this test to evaluate the efficiency of biodegradation treatments. *Ecotoxicology and Environmental Safety*, 74, 253-258.

Frontistis, Z., Daskalaki, V. M., Hapeshi, E., Drosou, C., Fatta-Kassinou, D., Xekoukoulotakis, N. P., Mantzavinos, D., 2012. Photocatalytic (UV-A/TiO₂) degradation of 17 α -ethynylestradiol in environmental matrices: Experimental studies and artificial neural network modeling. *Journal of Photochemistry and Photobiology A: Chemistry*, 240, 33-41.

Fukushima, M., Tatsumi, K., 2001. Degradation pathways of pentachlorophenol by photo-Fenton systems in the presence of iron(III), humic acid, and hydrogen peroxide. *Environmental Science and Technology*, 35, 1771-1778.

Ghaly, M. Y., Härtel, G., Mayer, R., Haseneder, R., 2001. Photochemical oxidation of *p*-chlorophenol by UV/H₂O₂ and photo-Fenton process. A comparative study. *Waste Management*, 21, 41-47.

Gernjak, W., Maldonado, M. I., Malato, S., Cáceres, J., Krutzler, T., Glaser, A., Bauer, R., 2004. Pilot-plant treatment of olive mill wastewater (OMW) by solar TiO₂ photocatalysis and solar photo-Fenton. *Solar Energy*, 77, 567-572.

Glaze, W. H., Kang, J. W., Chapin, D. H., 1987. The chemistry of water treatment processes involving ozone, hydrogen peroxide and ultraviolet radiation. *Ozone: Science and Engineering*, 9, 335-352.

Goel, A., Müller, M. B., Sharma, M., Frimmel, F. H., 2003. Biodegradation of nonylphenol ethoxylate surfactants in biofilm reactors. *Acta Hydrochimica et Hydrobiologica*, 31, 108-119.

Gogate, P. R., Pandit, A. B., 2004. A review of imperative technologies for wastewater treatment I: Oxidation technologies at ambient conditions. *Advances in Environmental Research*, 8, 501-551.

Goi, A., Trapido, M., 2002. Hydrogen peroxide photolysis, Fenton reagent and photo-Fenton for the degradation of nitrophenols: A comparative study. *Chemosphere*, 46, 913-922.

Gómez, M., Murcia, M. D., Dams, R., Christofi, N., Gómez, E., Gómez, J. L., 2012b. Removal efficiency and toxicity reduction of 4-chlorophenol with physical, chemical and biochemical methods. *Environmental Technology*, 33, 1055-1064.

Gomez, M., Murcia, M. D., Gomez, E., Gomez, J. L., Dams, R., Christofi, N., 2010. Enhancement of 4-chlorophenol photodegradation with KrCl excimer UV lamp by adding hydrogen peroxide. *Separation Science and Technology*, 45, 1603-1609.

Gomez, M., Murcia, M. D., Gomez, J. L., Gomez, E., Maximo, M. F., Garcia, A., 2012a. A KrCl exciplex flow-through photoreactor for degrading 4-chlorophenol: Experimental and modelling. *Applied Catalysis B: Environmental*, 117-118, 194-203.

González, S., Petrovic, M., Barceló, D., 2007a. Removal of a broad range of surfactants from municipal wastewater – Comparison between membrane bioreactor and conventional activated sludge treatment. *Chemosphere*, 67, 335-343.

González, S., Petrovic, M., Barceló, D., 2007b. Advanced liquid chromatography-mass spectrometry (LC-MS) methods applied to wastewater removal and the fate of surfactants in the environment. *Trends in Analytical Chemistry*, 26, 116-124.

Goto, R., Kubota, T., Ibuki, Y., Kaji, K., Goto, A., 2004. Degradation of nonylphenol polyethoxylates by ultraviolet B irradiation and effects of their products on mammalian cultured cells. *Toxicology*, 202, 237-247.

Grebel, J., Pignatello, J. J., Mitch, W. A., 2010. Effect of halide ions and carbonates on organic contaminant degradation by hydroxyl radical-based advanced oxidation processes in saline waters. *Environmental Science and Technology*, 44, 6822-6828.

Gu, Li, Zhang, X., Lei, L., 2008. Degradation of aqueous *p*-nitrophenol by ozonation integrated with activated carbon. *Industrial and Engineering Chemistry Research*, 47, 6809-6815.

Guzzella, L., Feretti, D., Monarca, S., 2002. Advanced oxidation and adsorption technologies for organic micropollutant removal from lake water used as drinking-water supply. *Water Research*, 36, 4307-4318.

Han, J., Deming, R. L., Tao, F.-M., 2004. Theoretical study of molecular structures and properties of the complete series of chlorophenols. *The Journal of Physical Chemistry A*, 108, 7736-7743.

Hincapié, M., Maldonado, M. I., Oller, I., Gernjak, W., Sánchez-Pérez, J. A., Ballesteros, M. M., Malato, S., 2005. Solar photocatalytic degradation and detoxification of EU priority substances. *Catalysis Today*, 101, 203-210.

Hirvonen, A., Trapido, M., Hentunen, J., Tarhanen, J., 2000. Formation of hydroxylated and dimeric intermediates during oxidation of chlorinated phenols in aqueous solution. *Chemosphere*, 41, 1211-1218.

Hoffmann, M. R., Martin, S. T., Choi, W., Bahnemann, D. W., 1995. Environmental applications of semiconductor photocatalysis. *Chemical Reviews*, 95, 69-96.

Horikoshi, S., Watanabe, N., Onishi, H., Hidaka, H., Serpone, N., 2002. Photodecomposition of a nonylphenol polyethoxylate surfactant in a cylindrical photoreactor with TiO₂ immobilized fiberglass cloth. *Applied Catalysis B: Environmental*, 37, 117-129.

Horwitz, W (Eds), 1980. *Official Methods of Analysis*, Thirteenth Ed. Association of Official Analytical Chemists, Washington DC.

Hsueh, C. L., Huang, Y. H., Wang, C. C., Chen, C. Y., 2005. Decolorization of azo dyes using low iron concentration of Fenton and Fenton-like system. *Chemosphere*, 58, 1409-1414.

Hugül, M., Apak, R., Demirci, S., 2000. Modeling the kinetics of UV/hydrogen peroxide oxidation of some mono-, di-, and trichlorophenols. *Journal of Hazardous Materials*, 77, 193-208.

Huibers, P. D. T., Lobanov, V. S., Katritzky, A. R., Shah, D. O., Karelson, M., 1996. Prediction of critical micelle concentration using a quantitative structure – property relationship approach. 1. Nonionic surfactants. *Langmuir*, 12, 1462-1470.

Ihoş, M., Manea, F., Iovi, A., 2008. Removal of nonylphenol polyethoxylate by electrochemical oxidation at modified SnO₂ electrodes. *Chemical Bulletin of “Politehnica” University of Timisoara, Romania*, 53(67), 175-178.

Ikehata, K., El-Din, M. G., 2004. Degradation of recalcitrant surfactants in wastewater by ozonation and advanced oxidation processes: A review. *Ozone: Science & Engineering*, 26, 327-343.

Ikehata, K., El-Din, M. G., 2006. Aqueous pesticide degradation by hydrogen peroxide/ultraviolet irradiation and Fenton-type advanced oxidation processes: A review. *Journal of Environmental Engineering and Science*, 5, 81-135.

Jahnke, A., Gandrass, J., Ruck, W., 2004. Simultaneous determination of alkylphenol ethoxylates and their biotransformation products by liquid chromatography/electrospray ionisation tandem mass spectrometry. *Journal of Chromatography A*, 1035, 115-122.

Janex-Habibi, M.-L., Huyard, A., Esperanza, M., Bruchet, A., 2009. Reduction of endocrine disruptor emissions in the environment: The benefit of wastewater treatment, *Water Research*, 43, 1565-1576.

Jiménez, M., Oller, I., Maldonado, M. I., Malato, S., Hernández-Ramírez, A., Zapata, A., Peralta-Hernández, J. M., 2011. Solar photo-Fenton degradation of herbicides partially dissolved in water. *Catalysis Today*, 161, 214-220.

Johansson, F., Allkvist, A., Erixon, K., Malmvärn, A., Nilsson, R., Bergman, A., Helleday, T., Jenssen, D., 2004. Screening for genotoxicity using the DRAG assay: Investigation of halogenated environmental contaminants. *Mutation Research/Genetic Toxicology and Environmental Mutagenesis*, 563, 35-47.

John, D. M., House, W. A., White, G. F., 2000. Environmental fate of nonylphenol ethoxylates: Differential adsorption of homologs to components of river sediment. *Environmental Toxicology and Chemistry*, 19, 293-300.

Joseph, C. G., Li Puma, G., Bono, A., Krishnaiah, D., 2009. Sonophotocatalysis in advanced oxidation process: A short review. *Ultrasonics Sonochemistry*, 16, 583-589.

Kaiser, K. L. E., Palabrica, V. S., 1991. *Photobacterium phosphoreum* toxicity data index. *Water Pollution Research Journal of Canada*, 26, 361-431.

Kang, C., Peng, F., Guo, J., Guo, P., Xue, H., 2009. Degradation of Acetic Acid by UV/H₂O₂ Reaction. *Proceedings of the 3rd International Conference on Bioinformatics and Biomedical Engineering (ICBBE)*, Beijing, China, 11-13 June 2009, 1-4.

Kang, N., Lee, D. S., Yoon, J., 2002. Kinetic modeling of Fenton oxidation of phenol and monochlorophenols. *Chemosphere*, 47, 915-924.

Karahan, Ö., Olmez-Hanci, T., Arslan-Alaton, I., Orhon, D., 2010. Modelling biodegradation of nonylphenol ethoxylate in acclimated and non-acclimated microbial cultures. *Bioresource Technology*, 101, 8058-8066.

Karci, A., Arslan-Alaton, I., Olmez-Hanci, T., Bekbölet, M., 2012. Transformation of 2,4-dichlorophenol by H₂O₂/UV-C, Fenton and photo-Fenton processes: Oxidation products and toxicity evolution. *Journal of Photochemistry and Photobiology A: Chemistry*, 230, 65-73.

Karci, A., Arslan-Alaton, I., Olmez-Hanci, T., Bekbolet, M., 2013. Degradation and detoxification of industrially important phenol derivatives in water by direct UV-C

photolysis and H₂O₂/UV-C process: A comparative study. *Chemical Engineering Journal*, 224, 4-9.

Kasprzyk-Hordern, B., Ziólek, M., Nawrocki, J., 2003. Catalytic ozonation and methods of enhancing molecular ozone reactions in water treatment. *Applied Catalysis B: Environmental*, 46, 639-669.

Kavitha, V., Palanivelu, K., 2004. The role of ferrous ion in Fenton and photo-Fenton processes for the degradation of phenol. *Chemosphere*, 55, 1235-1243.

Kawaguchi, H., 1993. Oxidation efficiency of hydroxyl radical in the photooxidation of 2-chlorophenol using ultraviolet radiation and hydrogen peroxide. *Environmental Technology*, 14, 289-293.

Keith, L. H., Telliard, W. A., 1979. Priority pollutants. I – A perspective view. *Environmental Science and Technology*, 13, 416-423.

Kim, D. H., Mulholland, J. A., Ryu, J.-Y., 2007. Chlorinated naphthalene formation from the oxidation of dichlorophenols. *Chemosphere*, 67, S135-S143.

Kim, J., Korshin, G. V., Velichenko, A. B., 2005. Comparative study of electrochemical degradation and ozonation of nonylphenol. *Water Research*, 39, 2527-2534.

Kishino, T., Kobayashi, K., 1994. Relation between the chemical structures of chlorophenols and their dissociation constants and partition coefficients in several solvent-water systems. *Water Research*, 28, 1547-1552.

Kitis, M., Adams, C. D., Daigger, G. T., 1999. The effects of Fenton's reagent pretreatment on the biodegradability of nonionic surfactants. *Water Research*, 33, 2561-2568.

Koh, I.-O., Chen-Hamacher, X., Hicke, K., Thiemann, W., 2004. Leachate treatment by the combination of photochemical oxidation with biological process. *Journal of Photochemistry and Photobiology A: Chemistry*, 162, 261-271.

Kong, L., Lemley, A. T., 2007. Effect of nonionic surfactants on the oxidation of carbaryl by anodic Fenton treatment. *Water Research*, 41, 2794-2802.

Kralik, P., Kusic, H., Koprivanac, N., Bozic, A. L., 2010. Degradation of chlorinated hydrocarbons by UV/H₂O₂: The application of experimental design and kinetic modeling approach. *Chemical Engineering Journal*, 158, 154-166.

Krebel, M., Kusic, H., Koprivanac, N., Meixner, J., Bozic, A. L., 2011. Treatment of chlorophenols by UV-based processes: Correlation of oxidation by-products, wastewater parameters, and toxicity. *Journal of Environmental Engineering*, 137, 639-649.

Krutzler, T., Bauer, R., 1999. Optimization of a photo-Fenton prototype reactor. *Chemosphere*, 38, 2517-2532.

Kubota, T., Toyooka, T., Ibuki, Y., 2013. Nonylphenol polyethoxylates degraded by three different wavelengths of UV and their genotoxic change – detected by generation of γ -H2AX. *Photochemistry and Photobiology*, 89, 461-467.

Kucharska, M., Naumczyk, J., 2009. Degradation of selected chlorophenols by advanced oxidation processes. *Environment Protection Engineering*, 35, 47-55.

Kuo, W. G., 1992. Decolourising dye wastewater with Fenton's reagent. *Water Research*, 26, 881-886.

Lacorte, S., Latorre, A., Barceló, D., Rigol, A., Malmqvist, A., Welander, T., 2003. Organic compounds in paper-mill process waters and effluents. *Trends in Analytical Chemistry*, 22, 725-737.

Lampi, P., Vartiainen, T., Tuomisto, J., Hesso, A., 1990. Population exposure to chlorophenols, dibenzo-*p*-dioxins, and dibenzofurans after prolonged ground water pollution by chlorophenols. *Chemosphere*, 20, 625-634.

Lapertot, M., Ebrahimi, S., Oller, I., Maldonado, M. I., Gernjak, W., Malato, S., Pulgarín, C., 2008. Evaluating Microtox[®] as a tool for biodegradability assessment of partially treated solutions of pesticides using Fe³⁺ and TiO₂ solar photo-assisted processes. *Ecotoxicology and Environmental Safety*, 69, 546-555.

Latch, D. E., Packer, J. L., Stender, B. L., VanOverbeke, J., Arnold, W. A., McNeill, K., 2005. Aqueous photochemistry of triclosan: Formation of 2,4-dichlorophenol, 2,8-dichlorodibenzo-*p*-dioxin, and oligomerization products. *Environmental Toxicology and Chemistry*, 24, 517-525.

Ledakowicz, S., Perkowski, J., Bulska, A., Jamroz, T., Sencio, B., 2005. Ozonation impact on degradation and toxicity of non-ionic surfactants. *Ozone: Science and Engineering*, 27, 437-445.

Lee, S. H., Carberry, J. B., 1992. Biodegradation of PCP enhanced by chemical oxidation pretreatment. *Water Environment Research*, 64, 682-690.

Lee, Y.-J., Han, H., Kim, S.-H., Yang, J.-W., 2009. Combination of electrokinetic separation and electrochemical oxidation for acid dye removal from soil. *Separation Science and Technology*, 44, 2455-2469.

Legrini, O., Oliveros, E., Braun, A. M., 1993. Photochemical processes for water treatment. *Chemical Reviews*, 93, 671-698.

Lenz, K., Beck, V., Fuerhacker, M., 2004. Behaviour of bisphenol A (BPA), 4-nonylphenol (4-NP) and 4-nonylphenol ethoxylates (4-NP1EO, 4-NP2EO) in oxidative water treatment processes. *Water Science and Technology*, 50, 141-147.

Levec, J., Pintar, A., 2007. Catalytic wet-air oxidation processes: A review. *Catalysis Today*, 124, 172-184.

Li, X.-y., Cui, Y.-h., Feng, Y.-j., Xie, Z.-m., Gu, J.-D., 2005. Reaction pathways and mechanisms of the electrochemical degradation of phenol on different electrodes. *Water Research*, 39, 1972-1981.

Liang, C., Lin, Y.-T., Shin, W.-H., 2009. Persulfate regeneration of trichloroethylene spent activated carbon. *Journal of Hazardous Materials*, 168, 187-192.

Lindsey, M. E., Tarr, M. A., 2000. Inhibition of hydroxyl radical reaction with aromatics by dissolved natural organic matter. *Environmental Science and Technology*, 34, 444-449.

Liou, R.-M., Chen, S.-H., Hung, M.-Y., Hsu, C.-S., 2004. Catalytic oxidation of pentachlorophenol in contaminated soil suspensions by Fe^{3+} -resin/ H_2O_2 . *Chemosphere*, 55, 1271-1280.

Lipczynska-Kochany, E., Sprah, G., Harms, S., 1995. Influence of some groundwater and surface waters constituents on the degradation of 4-chlorophenol by the Fenton reaction. *Chemosphere*, 30, 9-20.

Liu, G., Zheng, S., Xing, X., Li, Y., Yin, D., Ding, Y., Pang, W., 2010. Fe(III)-oxalate complexes mediated photolysis of aqueous alkylphenol ethoxylates under simulated sunlight conditions. *Chemosphere*, 78, 402-408.

Malato, S., Blanco, J., Vidal, A., Richter, C., 2002. Photocatalysis with solar energy at a pilot-plant scale: An overview. *Applied Catalysis B: Environmental*, 37, 1-15.

Malato, S., Fernández-Ibáñez, P., Maldonado, M. I., Blanco, J., Gernjak, W., 2009. Decontamination and disinfection of water by solar photocatalysis: Recent overview and trends. *Catalysis Today*, 147, 1-59.

Maldonado, M. I., Passarinho, P. C., Oller, I., Gernjak, W., Fernández, P., Blanco, J., Malato, S., 2007. Photocatalytic degradation of EU priority substances: A comparison between TiO₂ and Fenton plus photo-Fenton in a solar pilot plant. *Journal of Photochemistry and Photobiology A: Chemistry*, 185, 354-363.

Mascolo, G., Lopez, A., Detomaso, A., Lovecchio, G., 2005. Ion chromatography-electrospray mass spectrometry for the identification of low-molecular-weight organic acids during the 2,4-dichlorophenol degradation. *Journal of Chromatography A*, 1067, 191-196.

Michael, I., Hapeshi, E., Osorio, V., Perez, S., Petrovic, M., Zapata, A., Malato, S., Barceló, D., Fatta-Kassinos, D., 2012. Solar photocatalytic treatment of trimethoprim in four environmental matrices at a pilot scale: Transformation products and ecotoxicity evaluation. *Science of the Total Environment*, 430, 167-173.

Michałowicz, J., Duda, W., Stufka-Olczyk, J., 2007. Transformation of phenol, catechol, guaiacol and syringol exposed to sodium hypochlorite. *Chemosphere*, 66, 657-663.

Micó, M. M., Chourdaki, S., Bacardit, J., Sans, C., 2010. Comparison between ozonation and photo-Fenton processes for pesticide methomyl removal in advanced greenhouses. *Ozone: Science & Engineering*, 32, 259-264.

Mills, A., Le Hunte, S., 1997. An overview of semiconductor photocatalysis. *Journal of Photochemistry and Photobiology A: Chemistry*, 108, 1-35.

Mohan, H., Mittal, J. P., 1995. Formation and reactivity of the radical-cation of bromobenzene in aqueous-solution – A pulse-radiolysis study. *Journal of Physical Chemistry*, 99, 6519-6524.

Montgomery-Brown, J., Reinhard, M., 2003. Occurrence and behavior of alkylphenol polyethoxylates in the environment. *Environmental Engineering Science*, 20, 471-486.

Morita, T., Takeda, K., Okumura, K., 1990. Evaluation of clastogenicity of formic acid, acetic acid and lactic acid on cultured mammalian cells. *Mutation Research/Genetic Toxicology*, 240, 195-202.

Moza, P. N., Fytianos, K., Samanidou, V., Korte, F., 1988. Photodecomposition of chlorophenols in aqueous medium in presence of hydrogen peroxide. *Bulletin of Environmental Contamination and Toxicology*, 41, 678-682.

Muff, J., 2010. Applications of Electrochemical Oxidation for Degradation of Aqueous Organic Pollutants, Ph.D. Thesis, Aalborg University.

Munoz, M., de Pedro, Z. M., Casas, J. A., Rodriguez, J. J., 2011. Assessment of the generation of chlorinated byproducts upon Fenton-like oxidation of chlorophenols at different conditions. *Journal of Hazardous Materials*, 190, 993-1000.

Munoz, M., de Pedro, Z. M., Casas, J. A., Rodriguez, J. J., 2012a. Triclosan breakdown by Fenton-like oxidation. *Chemical Engineering Journal*, 198-199, 275-281.

Munoz, M., de Pedro, Z. M., Pliego, G., Casas, J. A., Rodriguez, J. J., 2012b. Chlorinated byproducts from the Fenton-like oxidation of polychlorinated phenols. *Industrial & Engineering Chemistry Research*, 51, 13092-13099.

Murcia, M. D., Gomez, M., Gomez, E., Gomez, J. L., Christofi, N., 2009. Comparison of different advanced oxidation processes for degrading 4-chlorophenol. *World Academy of Science, Engineering and Technology*, 31, 245-249.

Murcia, M. D., Gómez, M., Gómez, E., Gómez, J. L., Hidalgo, A. M., Christofi, N., 2012. A new substrate and by-product kinetic model for the photodegradation of 4-chlorophenol with KrCl exciplex UV lamp and hydrogen peroxide. *Chemical Engineering Journal*, 187, 36-44.

Nagarnaik, P. M., Boulanger, B., 2011. Advanced oxidation of alkylphenol ethoxylates in aqueous systems. *Chemosphere*, 85, 854-860.

Nakamura, S., Oda, Y., Shimada, T., Oki, I., Sugimoto, K., 1987. SOS-inducing activity of chemical carcinogens and mutagens in *Salmonella typhimurium* TA 1535/pSK 1002: Examination with 151 chemicals. Mutation Research/Environmental Mutagenesis and Related Subjects, 192, 239-246.

Nash, T., 1953. The colorimetric estimation of formaldehyde by means of the Hantzsch reaction. Biochemical Journal, 55, 416-421.

Neamțu, M., Frimmel, F. H., 2006. Photodegradation of endocrine disrupting chemical nonylphenol by simulated solar UV-irradiation. Science of the Total Environment, 369, 295-306.

Neamtu, M., Yediler, A., Siminiceanu, I., Macoveanu, M., Kettrup, A., 2004. Decolorization of disperse red 354 azo dye in water by several oxidation processes – a comparative study. Dyes and Pigments, 60, 61-68.

Neyens, E., Baeyens, J., 2003. A review of classic Fenton's peroxidation as an advanced oxidation technique. Journal of Hazardous Materials, B98, 33-50.

Nicole, I., De Laat, J., Dore, M., Duguet, J. P., Bonnel, C., 1990. Use of UV-radiation in water-treatment – Measurement of photonic flux by hydrogen-peroxide actinometry. Water Research, 24, 157-168.

Ning, B., Graham, N., Zhang, Y., Nakonechny, M., El-Din, M. G., 2007. Degradation of endocrine disrupting chemicals by ozone/AOPs. Ozone: Science & Engineering, 29, 153-176.

Oda, Y., Nakamura, S., Oki, I., Kato, T., Shinagawa, H., 1985. Evaluation of the new system (*umu*-test) for the detection of environmental mutagens and carcinogens. Mutation Research/Environmental Mutagenesis and Related Subjects, 147, 219-229.

Olaniran, A. O., Igbinsola, E. O., 2011. Chlorophenols and other related derivatives of environmental concern: Properties, distribution and microbial degradation processes. *Chemosphere*, 83, 1297-1306.

Oller, I., Malato, S., Sánchez-Pérez, J. A., 2011. Combination of advanced oxidation processes and biological treatments for wastewater decontamination-a review. *Science of the Total Environment*, 409, 4141-4166.

Oller, I., Malato, S., Sánchez-Pérez, J. A., Maldonado, M. I., Gassó, R., 2007. Detoxification of wastewater containing five common pesticides by solar AOPs-biological coupled system. *Catalysis Today*, 129, 69-78.

Olmez-Hanci, T., Arslan-Alaton, I., Basar, G., 2011. Multivariate analysis of anionic, cationic and nonionic textile surfactant degradation with the $H_2O_2/UV-C$ process by using the capabilities of response surface methodology. *Journal of Hazardous Materials*, 185, 193-203.

Olmez-Hanci, T., Dalmaz, B., Arslan-Alaton, I., Kabdaşlı, I., Tünay, O., 2010. Kinetic modeling and toxicity assessment of diethyl phthalate treated by $H_2O_2/UV-C$ process. *Ozone: Science & Engineering*, 32, 238-243.

Ono, E., Tokumura, M., Kawase, Y., 2012. Photo-Fenton degradation of non-ionic surfactant and its mixture with cationic and anionic surfactant. *Journal of Environmental Science and Health, Part A: Toxic/Hazardous Substances and Environmental Engineering*, 47, 1087-1095.

Ormad, P., Cortés, S., Puig, A., Ovelleiro, J. L., 1997. Degradation of organochloride compounds by O_3 and O_3/H_2O_2 . *Water Research*, 31, 2387-2391.

Ortiz de la Plata, G. B., Alfano, O. M., Cassano, A. E., 2012. 2-Chlorophenol degradation via photo Fenton reaction employing zero valent iron nanoparticles. *Journal of Photochemistry and Photobiology A: Chemistry*, 233, 53-59.

- O'Shea, K. E., Dionysiou, D. D., 2012. Advanced oxidation processes for water treatment. *Journal of Physical Chemistry Letters*, 3, 2112-2113.
- Oturan, N., Trajkovska, S., Oturan, M. A., Couderchet, M., Aaron, J.-J., 2008. Study of the toxicity of diuron and its metabolites formed in aqueous medium during application of the electrochemical advanced oxidation process "electro-Fenton". *Chemosphere*, 73, 1550-1556.
- Özhan, G., Catalgol, B., Alpertunga, B., 2008. Assessment of the genotoxic potential of surface waters using *umu*-assay. *Fresenius Environmental Bulletin*, 17, 2071-2077.
- Pagano, M., Lopez, A., Volpe, A., Mascolo, G., Ciannarella, R., 2008. Oxidation of nonionic surfactants by Fenton and H₂O₂/UV processes. *Environmental Technology*, 29, 423-433.
- Parvez, S., Venkataraman, C., Mukherji, S., 2006. A review on advantages of implementing luminescence inhibition test (*Vibrio fischeri*) for acute toxicity prediction of chemicals. *Environment International*, 32, 265-268.
- Pekakis, P. A., Xekoukoulotakis, N. P., Mantzavinos, D., 2006. Treatment of textile dyehouse wastewater by TiO₂ photocatalysis. *Water Research*, 40, 1276-1286.
- Pelizzetti, E., Minero, C., Maurino, V., Sclafani, A., Hidaka, H., Serpone, N., 1989. Photocatalytic degradation of nonylphenol ethoxylated surfactants. *Environmental Science and Technology*, 23, 1380-1385.
- Pengyi, Z., Fuyan, L., Gang, Y., Qing, C., Wanpeng, Z., 2003. A comparative study on decomposition of gaseous toluene by O₃/UV, TiO₂/UV and O₃/TiO₂/UV. *Journal of Photochemistry and Photobiology A: Chemistry*, 156, 189-194.
- Pera-Titus, M., García-Molina, V., Baños, M. A., Giménez, J., Esplugas, S., 2004. Degradation of chlorophenols by means of advanced oxidation processes: A general review. *Applied Catalysis B: Environmental*, 47, 219-256.

Pérez-Moya, M., Graells, M., del Valle, L. J., Centelles, E., Mansilla, H. D., 2007. Fenton and photo-Fenton degradation of 2-chlorophenol: Multivariate analysis and toxicity monitoring. *Catalysis Today*, 124, 163-171.

Peternel, I., Koprivanac, N., Grcic, I., 2012. Mineralization of *p*-chlorophenol in water solution by AOPs based on UV irradiation. *Environmental Technology*, 33, 27-36.

Petrovic, M., Diaz, A., Ventura, F., Barceló, D., 2003. Occurrence and removal of estrogenic short-chain ethoxy nonylphenolic compounds and their halogenated derivatives during drinking water production. *Environmental Science and Technology*, 37, 4442-4448.

Petrovic, M., Gehringer, P., Eschweiler, H., Barceló, D., 2004. LC-MS-(MS) determination of oxidative degradation products of nonylphenol ethoxylates, carboxylates and nonylphenols in water. *Water Science and Technology*, 50, 227-234.

Petrovic, M., Gehringer, P., Eschweiler, H., Barceló, D., 2007. Radiolytic decomposition of multi-class surfactants and their biotransformation products in sewage treatment plant effluents. *Chemosphere*, 66, 114-122.

Pignatello, J. J., Oliveros, E., MacKay, A., 2006. Advanced oxidation processes for organic contaminant destruction based on the Fenton reaction and related chemistry. *Critical Reviews in Environmental Science and Technology*, 36, 1-84.

Pimentel, M., Oturan, N., Dezotti, M., Oturan, M. A., 2008. Phenol degradation by advanced electrochemical oxidation process electro-Fenton using a carbon felt cathode. *Applied Catalysis B: Environmental*, 83, 140-149.

Pintar, A., Besson, M., Gallezot, P., Gibert, J., Martin, D., 2004. Toxicity to *Daphnia magna* and *Vibrio fischeri* of Kraft bleach plant effluents treated by catalytic wet-air oxidation. *Water Research*, 38, 289-300.

Plewa, M. J., Simmons, J. E., Richardson, S. D., Wagner, E. D., 2010. Mammalian cell cytotoxicity and genotoxicity of the haloacetic acids, a major class of drinking water disinfection by-products. *Environmental and Molecular Mutagenesis*, 51, 871-878.

Poerschmann, J., Trommler, U., 2009. Pathways of advanced oxidation of phenol by Fenton's reagent – Identification of oxidative coupling intermediates by extractive acetylation. *Journal of Chromatography A*, 1216, 5570-5579.

Poerschmann, J., Trommler, U., Górecki, T., Kopinke, F.-D., 2009. Formation of chlorinated biphenyls, diphenyl ethers and benzofurans as a result of Fenton-driven oxidation of 2-chlorophenol. *Chemosphere*, 75, 772-780.

Postigo, C., Sirtori, C., Oller, I., Malato, S., Maldonado, M. I., de Alda, M. L., Barceló, D., 2011a. Solar transformation and photocatalytic treatment of cocaine in water: Kinetics, characterization of major intermediate products and toxicity evaluation. *Applied Catalysis B: Environmental*, 104, 37-48.

Postigo, C., Sirtori, C., Oller, I., Malato, S., Maldonado, M. I., de Alda, M. L., Barceló, D., 2011b. Photolytic and photocatalytic transformation of methadone in aqueous solutions under solar irradiation: Kinetics, characterization of major intermediate products and toxicity evaluation. *Water Research*, 45, 4815-4826.

Poulopoulos, S. G., Nikolaki, M., Karampetsos, D., Philippopoulos, C. J., 2008. Photochemical treatment of 2-chlorophenol aqueous solutions using ultraviolet radiation, hydrogen peroxide and photo-Fenton reaction. *Journal of Hazardous Materials*, 153, 582-587.

Radjenović, J., Petrović, M., Barceló, D., 2009. Complementary mass spectrometry and bioassays for evaluating pharmaceutical-transformation products in treatment of drinking water and wastewater. *Trends in Analytical Chemistry*, 28, 562-580.

Reungoat, J., Macova, M., Escher, B. I., Carswell, S., Mueller, J. F., Keller, J., 2010. Removal of micropollutants and reduction of biological activity in a full scale reclamation plant using ozonation and activated carbon filtration. *Water Research*, 44, 625-637.

Ricco, G., Tomei, M. C., Ramadori, R., Laera, G., 2004. Toxicity assessment of common xenobiotic compounds on municipal activated sludge: Comparison between respirometry and Microtox[®]. *Water Research*, 38, 2103-2110.

Rizzo, L., 2011. Bioassays as a tool for evaluating advanced oxidation processes in water and wastewater treatment. *Water Research*, 45, 4311-4340.

Ruppert, G., Bauer, R., Heisler, G., 1993. The photo-Fenton reaction – An effective photochemical wastewater treatment process. *Journal of Photochemistry and Photobiology A: Chemistry*, 73, 75-78.

Rutherford, L., Garron, C., Ernst, W., Kennedy, K., 2003. The aquatic environment and textile mill effluents – an ecological risk assessment. *Human and Ecological Risk Assessment*, 9, 589-606.

Samet, Y., Ayadi, M., Abdelhedi, R., 2009. Degradation of 4-chloroguaiacol by dark Fenton and solar photo-Fenton advanced oxidation processes. *Water Environment Research*, 81, 2389-2397.

Sanches, S., Crespo, M. T. B., Pereira, V. J., 2010. Drinking water treatment of priority pesticides using low pressure UV photolysis and advanced oxidation processes. *Water Research*, 44, 1809-1818.

Santiago, J., Agüera, A., Gómez-Ramos, M. M., Fernández-Alba, A. R., García-Calvo, E., Rosal, R., 2011. Oxidation by-products and ecotoxicity assessment during the photodegradation of fenofibric acid in aqueous solution with UV and UV/H₂O₂. *Journal of Hazardous Materials*, 194, 30-41.

Saritha, P., Aparna, C., Himabindu, V., Anjaneyulu, Y., 2007. Comparison of various advanced oxidation processes for the degradation of 4-chloro-2-nitrophenol. *Journal of Hazardous Materials*, 149, 609-614.

Saritha, P., Raj, D. S. S., Aparna, C., Laxmi, P. N. V., Himabindu, V., Anjaneyulu, Y., 2009. Degradative oxidation of 2,4,6 trichlorophenol using advanced oxidation processes – A comparative study. *Water, Air, & Soil Pollution*, 200, 169-179.

Schrank, S. G., José, H. J., Moreira, R. F. P. M., Schröder, H. Fr., 2004. Elucidation of the behavior of tannery wastewater under advanced oxidation conditions. *Chemosphere*, 56, 411-423.

Schrank, S. G., José, H. J., Moreira, R. F. P. M., Schröder, H. Fr., 2005. Applicability of Fenton and H₂O₂/UV-C reactions in the treatment of tannery wastewaters. *Chemosphere*, 60, 644-655.

Schröder, H. Fr., 2001. Tracing of surfactants in the biological wastewater treatment process and the identification of their metabolites by flow injection – mass spectrometry and liquid chromatography – mass spectrometry and –tandem mass spectrometry. *Journal of Chromatography A*, 926, 127-150.

Sharma, S., Mukhopadhyay, M., Murthy, Z. V. P., 2013. Treatment of chlorophenols from wastewaters by advanced oxidation processes. *Separation & Purification Reviews*, 42, 263-295.

Shemer, H., Kunukcu, Y. K., Linden, K. G., 2006. Degradation of the pharmaceutical metronidazole via UV, Fenton and photo-Fenton processes. *Chemosphere*, 63, 269-276.

Shen, Y.-S., Ku, Y., Lee, K.-C., 1995. The effect of light absorbance on the decomposition of chlorophenols by ultraviolet radiation and U.V./H₂O₂ processes. *Water Research*, 29, 907-914.

Shen, Y.-S., Ku, Y., Lee, K.-C., 1996. Decomposition of chlorophenols in aqueous solution by UV/H₂O₂ process. *Toxicological and Environmental Chemistry*, 54, 51-67.

Shimada, T., Nakamura, S., 1987. Cytochrome P-450-mediated activation of procarcinogens and promutagens to DNA-damaging products by measuring expression of *umu* gene in *Salmonella typhimurium* TA 1535/pSK 1002. *Biochemical Pharmacology*, 36, 1979-1987.

Shishida, K., Echigo, S., Kosaka, K., Tabasaki, M., Matsuda, T., Takigami, H., Yamada, H., Shimizu, Y., Matsui, S., 2000. Evaluation of advanced sewage treatment processes for reuse of wastewater using bioassays. *Environmental Technology*, 21, 553-560.

Sirtori, C., Agüera, A., Gernjak, W., Malato, S., 2010. Effect of water-matrix composition on Trimethoprim solar photodegradation kinetics and pathways. *Water Research*, 44, 2735-2744.

Sirtori, C., Zapata, A., Malato, S., Agüera, A., 2012. Formation of chlorinated by-products during photo-Fenton degradation of pyrimethanil under saline conditions. Influence on toxicity and biodegradability. *Journal of Hazardous Materials*, 217-218, 217-223.

Soares, A., Guieysse, B., Jefferson, B., Cartmell, E., Lester, J. N., 2008. Nonylphenol in the environment: A critical review on occurrence, fate, toxicity and treatment in wastewaters. *Environment International*, 34, 1033-1049.

Song-Hu, Y., Xiao-Hua, L., 2005. Comparison treatment of various chlorophenols by electro-Fenton method: Relationship between chlorine content and degradation. *Journal of Hazardous Materials*, B118, 85-92.

Spinks, J. W. T., Woods, R. J. (Eds), 1990. *An Introduction to Radiation Chemistry*, Third Ed., John Wiley & Sons, Inc., New York.

Staples, C. A., Klecka, G. M., Naylor, C. G., Losey, B. S., 2008. C8- and C9-alkylphenols and ethoxylates: I. Identity, physical characterization, and biodegradation pathways analysis. *Human and Ecological Risk Assessment*, 14, 1007-1024.

Stasinakis, A. S., 2008. Use of selected advanced oxidation processes (AOPs) for wastewater treatment – A mini review. *Global Nest Journal*, 10, 376-385.

Suarez-Ojeda, M. E., Guisasola, A., Baeza, J. A., Fabregat, A., Stüber, F., Fortuny, A., Font, J., Carrera, J., 2007. Integrated catalytic wet air oxidation and aerobic biological treatment in a municipal WWTP of a high-strength *o*-cresol wastewater. *Chemosphere*, 66, 2096-2105.

Tamer, E., Hamid, Z., Aly, A. M., Ossama, E. T., Bo, M., Benoit, G., 2006. Sequential UV – biological degradation of chlorophenols. *Chemosphere*, 63, 277-284.

Toyooka, T., Kubota, T., Ibuki, Y., 2013. UVB irradiation changes genotoxic potential of nonylphenolpolyethoxylates – remarkable generation of γ -H2AX with degradation of chemical structure. *Mutagenesis*, 28, 7-14.

Trapido, M., Hirvonen, A., Veressinina, Y., Hentunen, J., Munter, R., 1997. Ozonation, ozone/UV and UV/H₂O₂ degradation of chlorophenols. *Ozone: Science and Engineering*, 19, 75-96.

Trapido, M., Veressinina, Y., Munter, R., 1998. Advanced oxidation processes for degradation of 2,4-dichlo- and 2,4-dimethylphenol. *Journal of Environmental Engineering*, 124, 690-694.

Trovó, A. G., Nogueira, R. F. P., Agüera, A., Fernandez-Alba, A. R., Sirtori, C., Malato, S., 2009. Degradation of sulfamethoxazole in water by solar photo-Fenton. *Chemical and toxicological evaluation. Water Research*, 43, 3922-3931.

Trovó, A. G., Paterlini, W. C., Nogueira, R. F. P., 2006. Evaluation of the influences of solution path length and additives concentrations on the solar photo-Fenton degradation of

4-chlorophenol using multivariate analysis. *Journal of Hazardous Materials*, 137, 1577-1582.

Tuerk, J., Sayder, B., Boergers, A., Vitz, H., Kiffmeyer, T. K., Kabasci, S., 2010. Efficiency, costs and benefits of AOPs for removal of pharmaceuticals from the water cycle. *Water Science and Technology*, 61, 985-993.

Tureli, G., Gursoy, B. H., Olmez-Hanci, T., Arslan-Alaton, I., 2010. H₂O₂/UV-C and Fe²⁺/H₂O₂/UV-C treatment of a commercial naphthalene sulphonate (H-acid). *Desalination and Water Treatment*, 23, 66-72.

Tünay, O., Kabdaşlı, I., Arslan-Alaton, I., Ölmez-Hancı, T., 2010. Chemical oxidation applications for industrial wastewaters, IWA Publishing, London.

Ucisik, A. S., Trapp, S., 2008. Uptake, removal, accumulation, and phytotoxicity of 4-chlorophenol in willow trees. *Archives of Environmental Contamination and Toxicology*, 54, 619-627.

Vallejo, M., San Román, M.F., Irabien, A., Ortiz, I., 2013. Comparative study of the destruction of polychlorinated dibenzo-*p*-dioxins and dibenzofurans during Fenton and electrochemical oxidation of landfill leachates. *Chemosphere*, 90, 132-138.

Vega-Morales, T., Sosa-Ferrera, Z., Santana-Rodríguez, J. J., 2010. Determination of alkylphenol polyethoxylates, bisphenol-A, 17 α -ethynylestradiol and 17 β -estradiol and its metabolites in sewage samples by SPE and LC/MS/MS. *Journal of Hazardous Materials*, 183, 701-711.

Vighi, M., Migliorati, S., Monti, G. S., 2009. Toxicity on the luminescent bacterium *Vibrio fischeri* (Beijerinck). I: QSAR equation for narcotics and polar narcotics. *Ecotoxicology and Environmental Safety*, 72, 154-161.

Vinodgopal, K., Ashokkumar, M., Grieser, F., 2001. Sonochemical degradation of a polydisperse nonylphenol ethoxylate in aqueous solution. *Journal of Physical Chemistry B*, 105, 3338-3342.

Von Burg, R., 1994. Toxicology update. *Journal of Applied Toxicology*, 14, 233-237.

Walling, C., 1975. Fenton's reagent revisited. *Accounts in Chemical Research*, 8, 125-131.

Walling, C., Goosen, A., 1973. Mechanism of the ferric ion catalyzed decomposition of hydrogen peroxide. Effects of organic substrates. *Journal of American Chemical Society*, 95, 2987-2991.

Wang, J. L., Xu, L. J., 2012. Advanced oxidation processes for wastewater treatment: Formation of hydroxyl radical and application. *Critical Reviews in Environmental Science and Technology*, 42, 251-325.

Wang, X., Miao, X.-R., Li, Z.-M., Deng, W.-L., 2011. Fabrication of microporous hollow silica spheres templated by NP-10 micelles without calcinations, *Applied Surface Science*, 257, 2481-2488.

Wang, Y., Shen, Z., Chen, X., 2010a. Effects of experimental parameters on 2,4-dichlorophenol degradation over Er-chitosan-PbO₂ electrode. *Journal of Hazardous Materials*, 178, 867-874.

Wang, Y., Shen, Z., Li, Y., Niu, J., 2010b. Electrochemical properties of the erbium-chitosan-fluorine-modified PbO₂ electrode for the degradation of 2,4-dichlorophenol in aqueous solution. *Chemosphere*, 79, 987-996.

Watts, M. J., Linden, K. G., 2007. Chlorine photolysis and subsequent OH radical production during UV treatment of chlorinated water. *Water Research*, 41, 2871-2878.

Wheeler, T. F., Heim, J. R., LaTorre, M. R., Janes, A. B., 1997. Mass spectral characterization of *p*-nonylphenol isomers using high-resolution capillary GC-MS. *Journal of Chromatographic Science*, 35, 19-30.

Wong, A. S., Crosby, D. G., 1981. Photodecomposition of pentachlorophenol in water. *Journal of Agricultural and Food Chemistry*, 29, 125-130.

Wu, T., Cruz, V., Mezyk, S., Cooper, W. J., O'Shea, K. E., 2002. Gamma radiolysis of methyl *t*-butyl ether: A study of hydroxyl radical mediated reaction pathways. *Radiation Physics and Chemistry*, 65, 335-341.

Wu, Z., Zhou, M., 2001. Partial degradation of phenol by advanced electrochemical oxidation process. *Environmental Science and Technology*, 35, 2698-2703.

Xu, T., Xiao, X.-M., Liu, H.-Y., 2005. Advanced oxidation degradation of dichlorobenzene in water by the UV/H₂O₂ process. *Journal of Environmental Science and Health, Part A: Toxic/Hazardous Substances and Environmental Engineering*, 40, 751-765.

Yasunaga, K., Kiyonari, A., Oikawa, T., Abe, N., Yoshikawa, K., 2004. Evaluation of the *Salmonella umu* test with 83 NTP chemicals. *Environmental and Molecular Mutagenesis*, 44, 329-345.

Ying, G.-G., Williams, B., Kookana, R., 2002. Environmental fate of alkylphenols and alkylphenol ethoxylates – A review. *Environment International*, 28, 215-226.

Zazo, J. A., Casas, J. A., Mohedano, A. F., Gilarranz, M. A., Rodríguez, J. J., 2005. Chemical pathway and kinetics of phenol oxidation by Fenton's reagent. *Environmental Science and Technology*, 39, 9295-9302.

Zazo, J. A., Casas, J. A., Molina, C. B., Quintanilla, A., Rodríguez, J. J., 2007. Evolution of ecotoxicity upon Fenton's oxidation of phenol in water. *Environmental Science and Technology*, 41, 7164-7170.

Zhang, H., Choi, H. J., Huang, C.-P., 2005. Optimization of Fenton process for the treatment of landfill leachate. *Journal of Hazardous Materials*, B125, 166-174.

Zhang, J., Zhang, Y., Liu, W., Quan, X., Chen, S., Zhao, H., Jin, Y., Zhang, W., 2013. Evaluation of removal efficiency for acute toxicity and genotoxicity on zebrafish in anoxic-oxic process from selected municipal wastewater treatment plants. *Chemosphere*, 90, 2662-2666.

Zimbron, J. A., Reardon, K. F., 2009. Fenton's oxidation of pentachlorophenol. *Water Research*, 43, 1831-1840.

Zimbron, J. A., Reardon, K. F., 2011. Continuous combined Fenton's oxidation and biodegradation for the treatment of pentachlorophenol-contaminated water. *Water Research*, 45, 5705-5714.

APPENDIX A

CALIBRATION CURVES BEING ESTABLISHED FOR THE TARGET COMPOUNDS

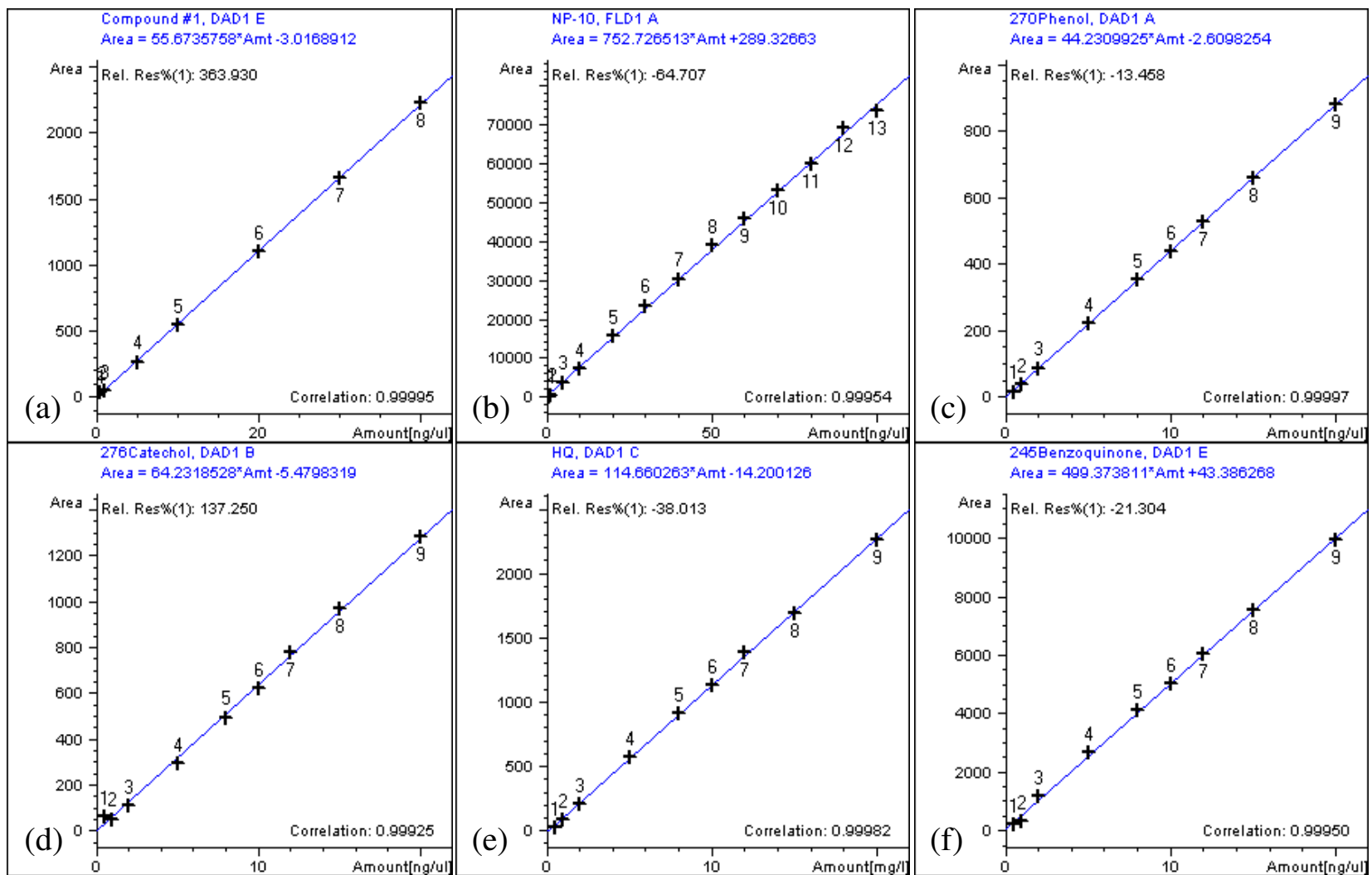


Figure A.1. HPLC calibration curves being established for 2,4-DCP (a), NP-10 (b), phenol (c), catechol (d), hydroquinone (e), *p*-benzoquinone (f), chlorohydroquinone (g), formic acid (h), acetic acid (i), oxalic acid (j), maleic acid (k) and fumaric acid (l).

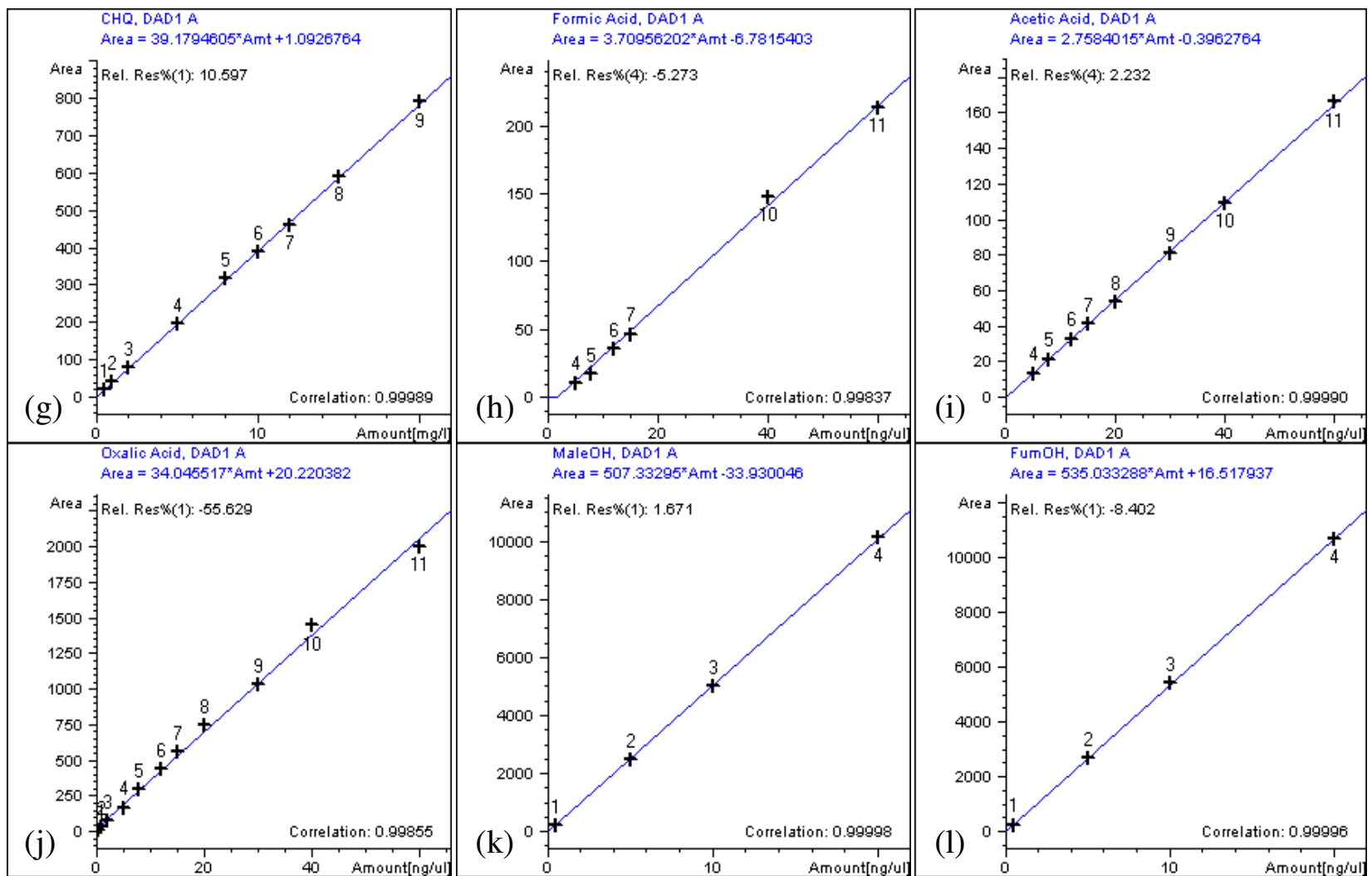


Figure A.1. (Continued)

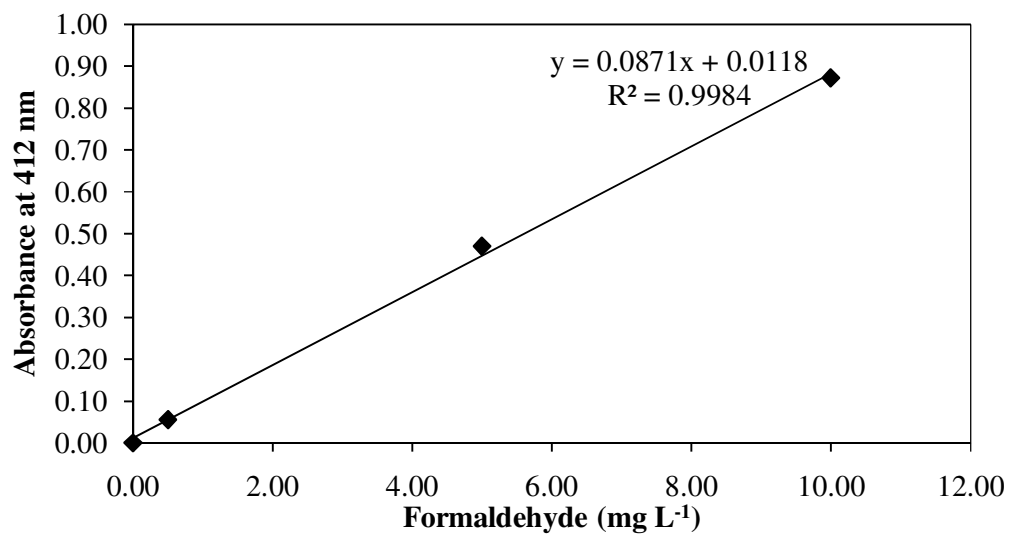


Figure A.2. The calibration curve established for aldehydes using formaldehyde as the standard.

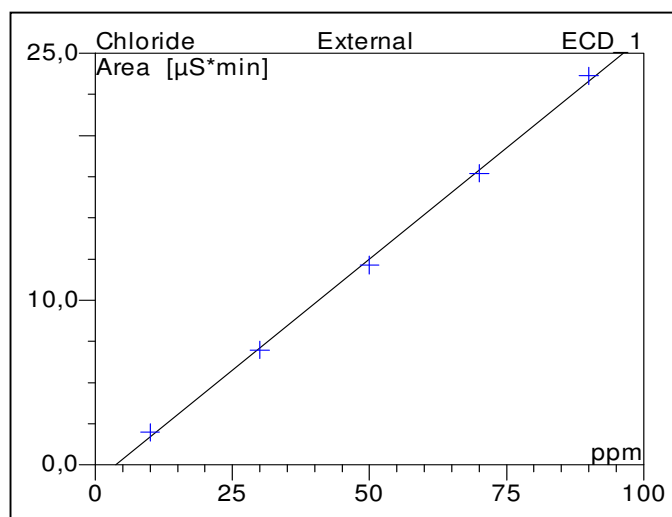


Figure A.3. IC calibration curve being established for chloride.

APPENDIX B

96-WELL MICROPLATE CONFIGURATION IN THE *umu*-TEST

	1	2	3	4	5	6	7	8	9	10	11	12
Final sample dilution	1.5x			1.5x			1.5x			1.5x		
A	S1	S1	S1	S2	S2	S2	S3	S3	S3	S4	S4	S4
B	S5	S5	S5	S6	S6	S6	S7	S7	S7	S8	S8	S8
C	S9	S9	S9	S10	S10	S10	S11	S11	S11	S12	S12	S12
D	PC	PC	PC	SC	SC	SC	NC	NC	NC	BL	BL	BL
E	S1+	S1+	S1+	S2+	S2+	S2+	S3+	S3+	S3+	S4+	S4+	S4+
F	S5+	S5+	S5+	S6+	S6+	S6+	S7+	S7+	S7+	S8+	S8+	S8+
G	S9+	S9+	S9+	S10+	S10+	S10+	S11+	S11+	S11+	S12+	S12+	S12+
H	PC+	PC+	PC+	SC+	SC+	SC+	NC+	NC+	NC+	BL+	BL+	BL+
S1-S12 Samples 1 - 12 NC Negative control PC Positive control SC Solvent control BL Blank												

APPENDIX C

UV ABSORPTION SPECTRA TAKEN DURING APPLICATION OF THE STUDIED TREATMENT PROCESSES

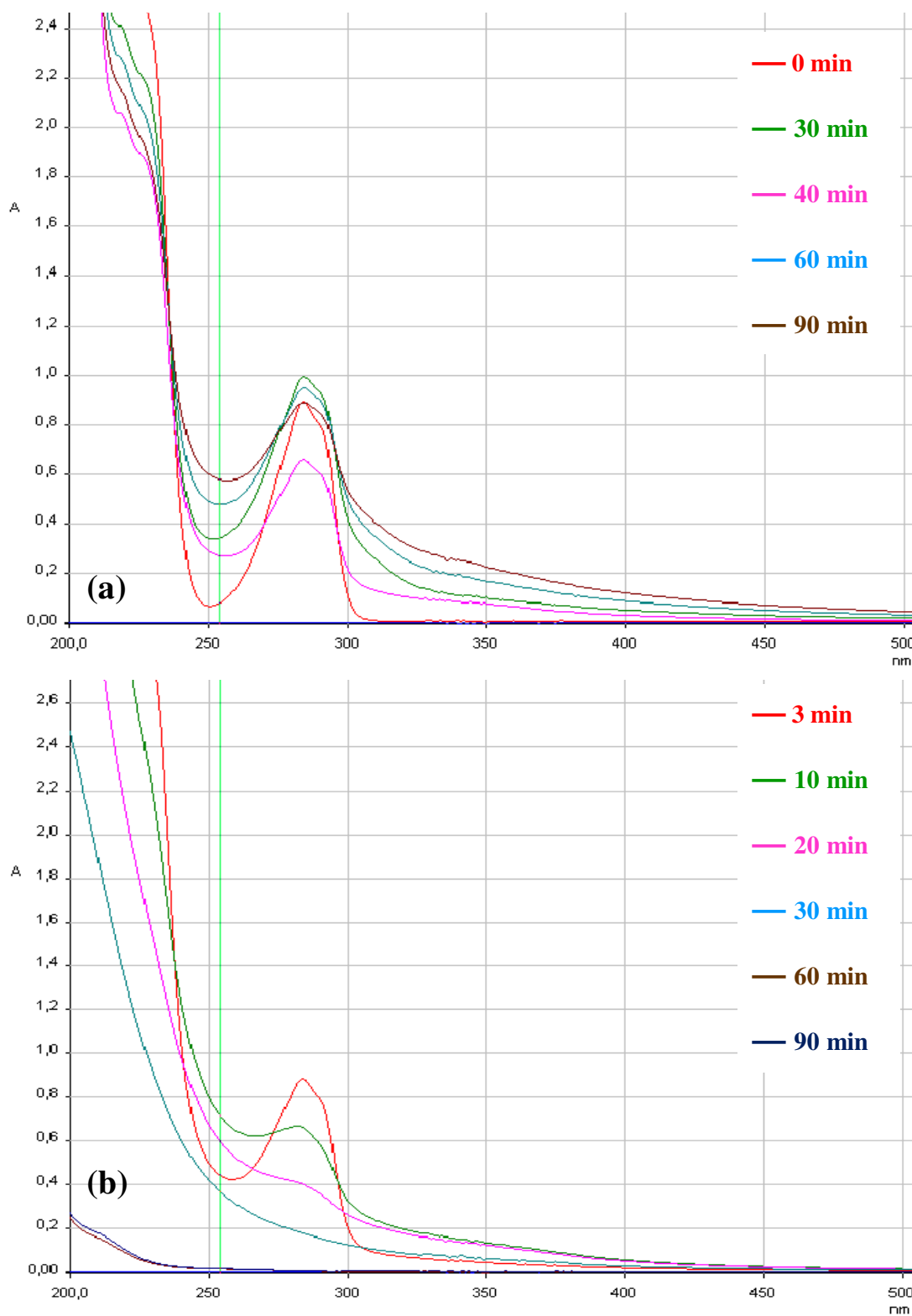


Figure C.1. Evolution of UV spectra with treatment time during UV-C photolysis (a) and H_2O_2 /UV-C treatment (b) of 2,4-DCP. Initial experimental conditions: 2,4-DCP = 75 mg L^{-1} (460 μM), H_2O_2 = 10 mM, pH = 7.

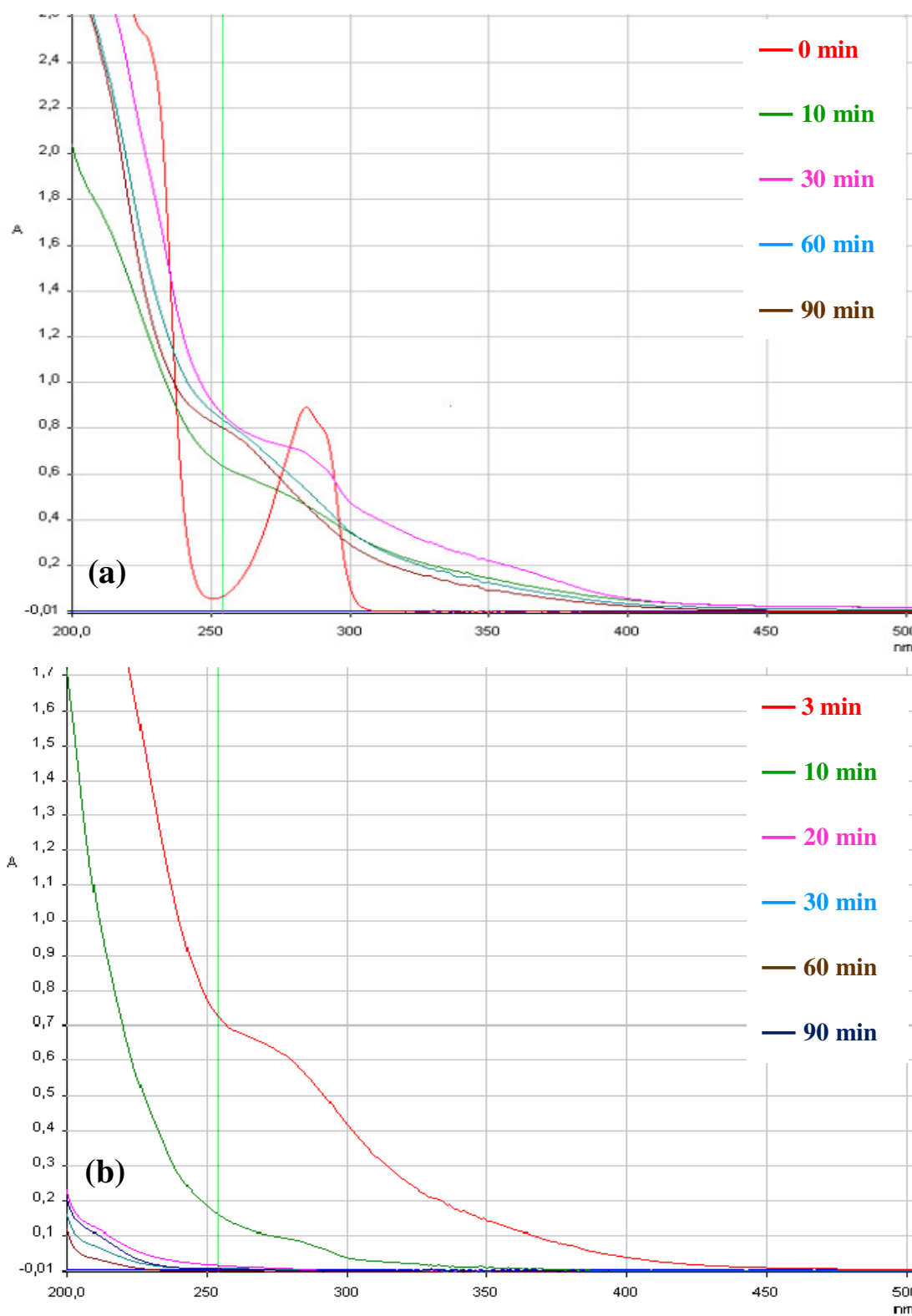


Figure C.2. Evolution of UV spectra with treatment time during Fenton (a) and photo-Fenton (b) treatment of 2,4-DCP. Initial experimental conditions: 2,4-DCP = 75 mg L⁻¹ (460 μ M), H₂O₂ = 10 mM, Fe²⁺ = 200 μ M, pH = 3.

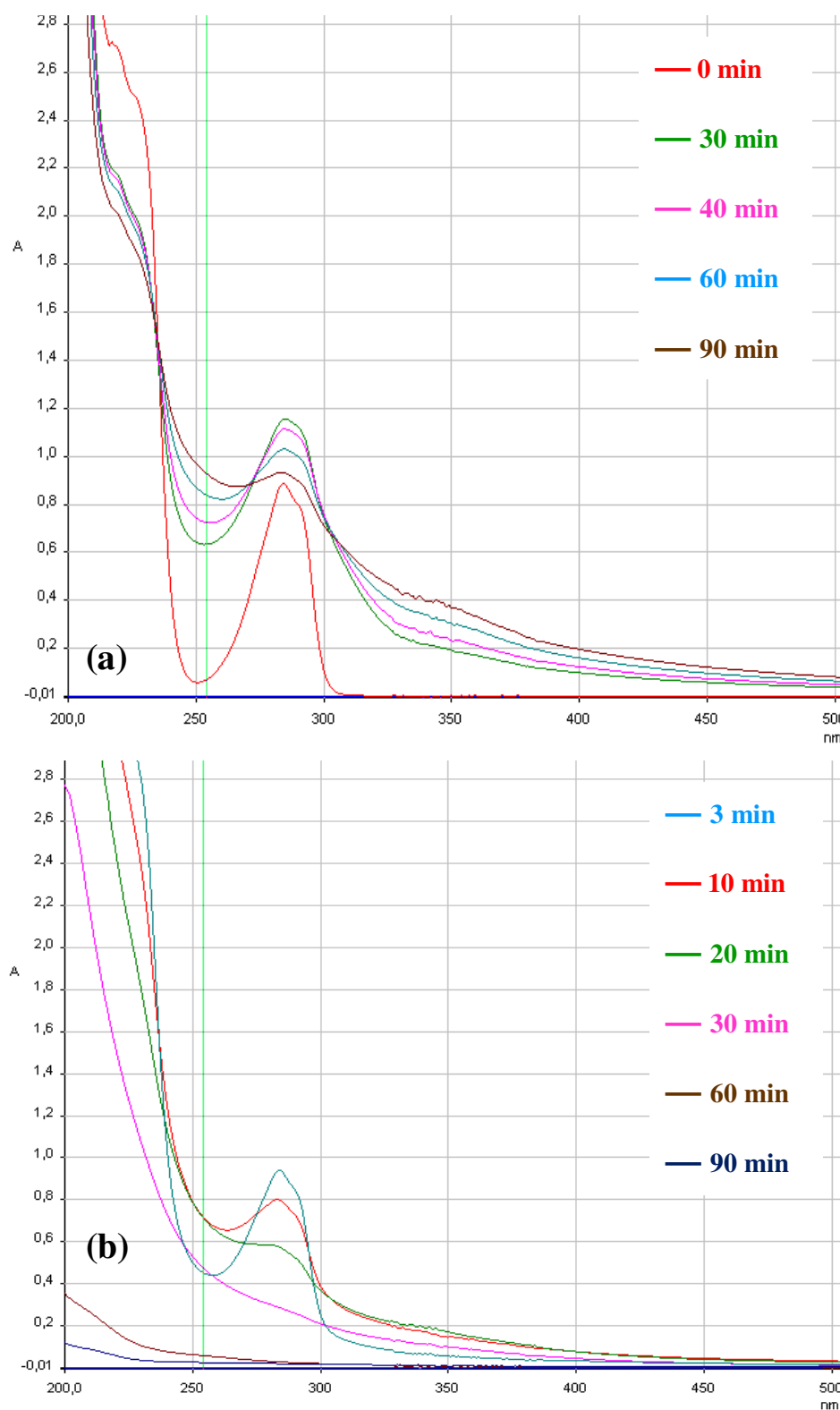


Figure C.3. Evolution of UV spectra with treatment time during UV-C photolysis (a) and the H₂O₂/UV-C treatment (b) of 2,4-DCP in SFW. Initial experimental conditions: 2,4-DCP = 75 mg L⁻¹ (460 μM), H₂O₂ = 10 mM, pH = 7.

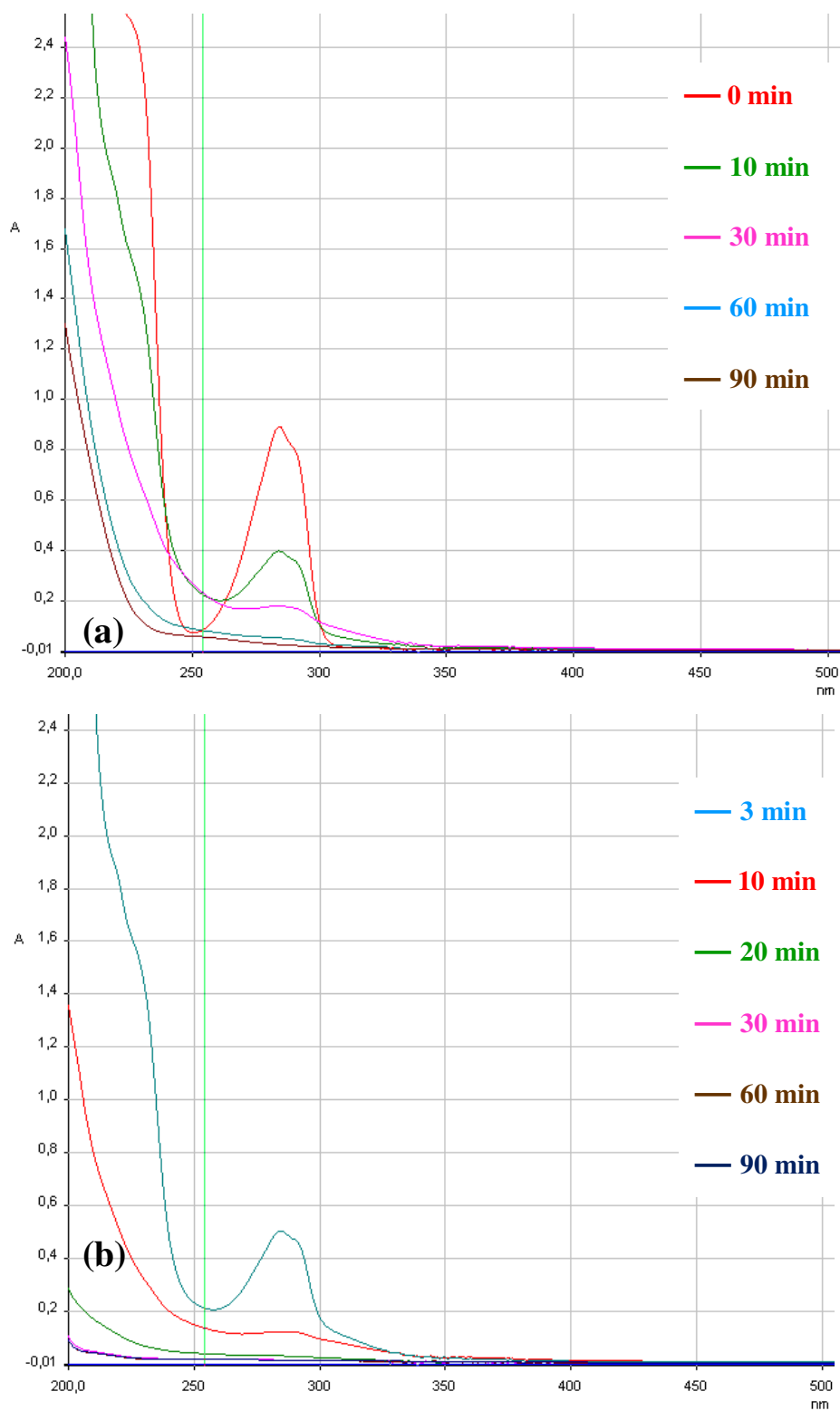


Figure C.4. Evolution of UV spectra with treatment time during the Fenton (a) and photo-Fenton (b) treatment of 2,4-DCP in SFW. Initial experimental conditions: 2,4-DCP = 75 mg L⁻¹ (460 μ M), H₂O₂ = 10 mM, Fe²⁺ = 200 μ M, pH = 3.

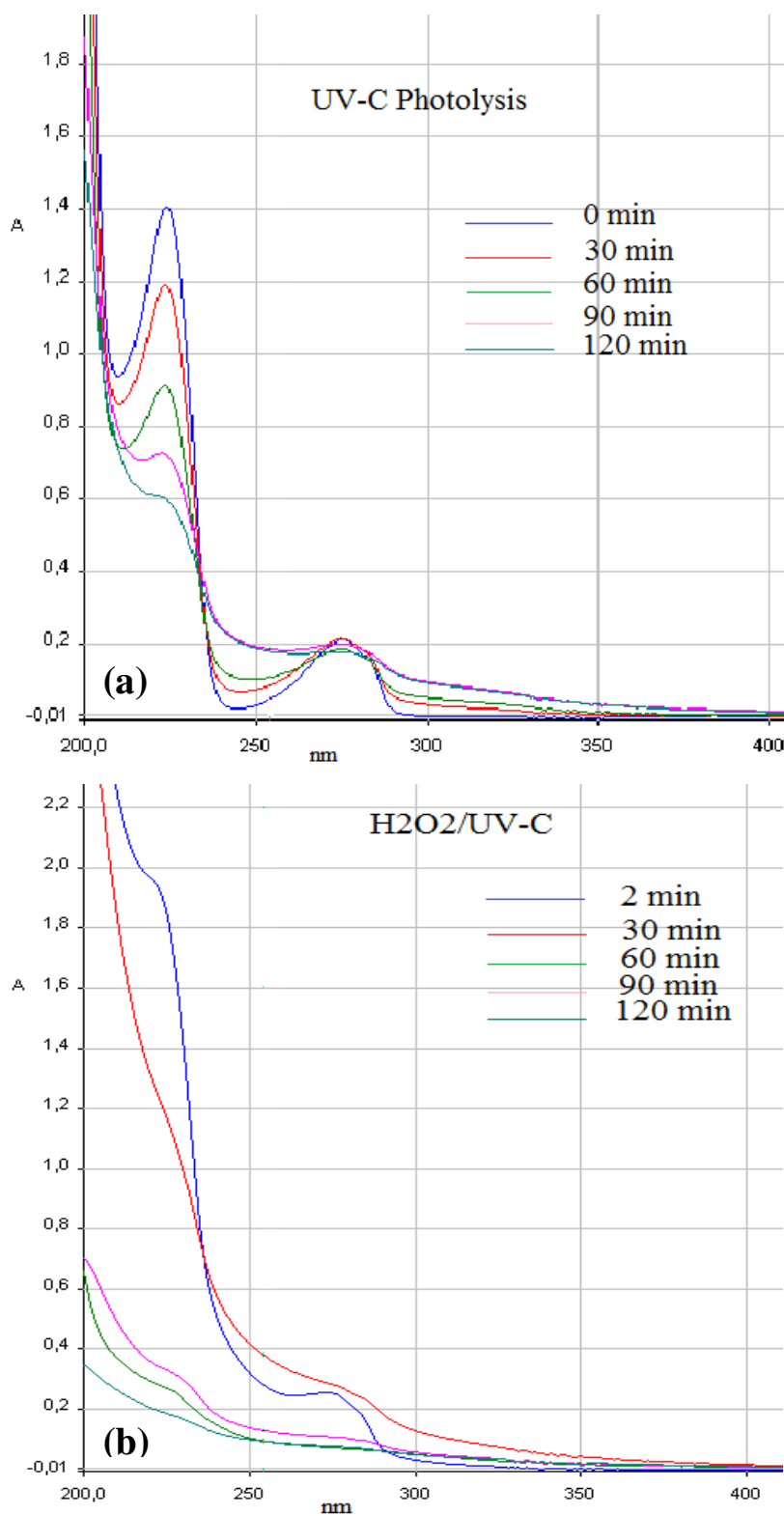


Figure C.5. Evolution of UV spectra with treatment time during UV-C (a) and H₂O₂/UV-C (b) treatment of NP-10. Initial experimental conditions: NP-10 = 100 mg L⁻¹ (150 μM), H₂O₂ = 10 mM, pH = 7.

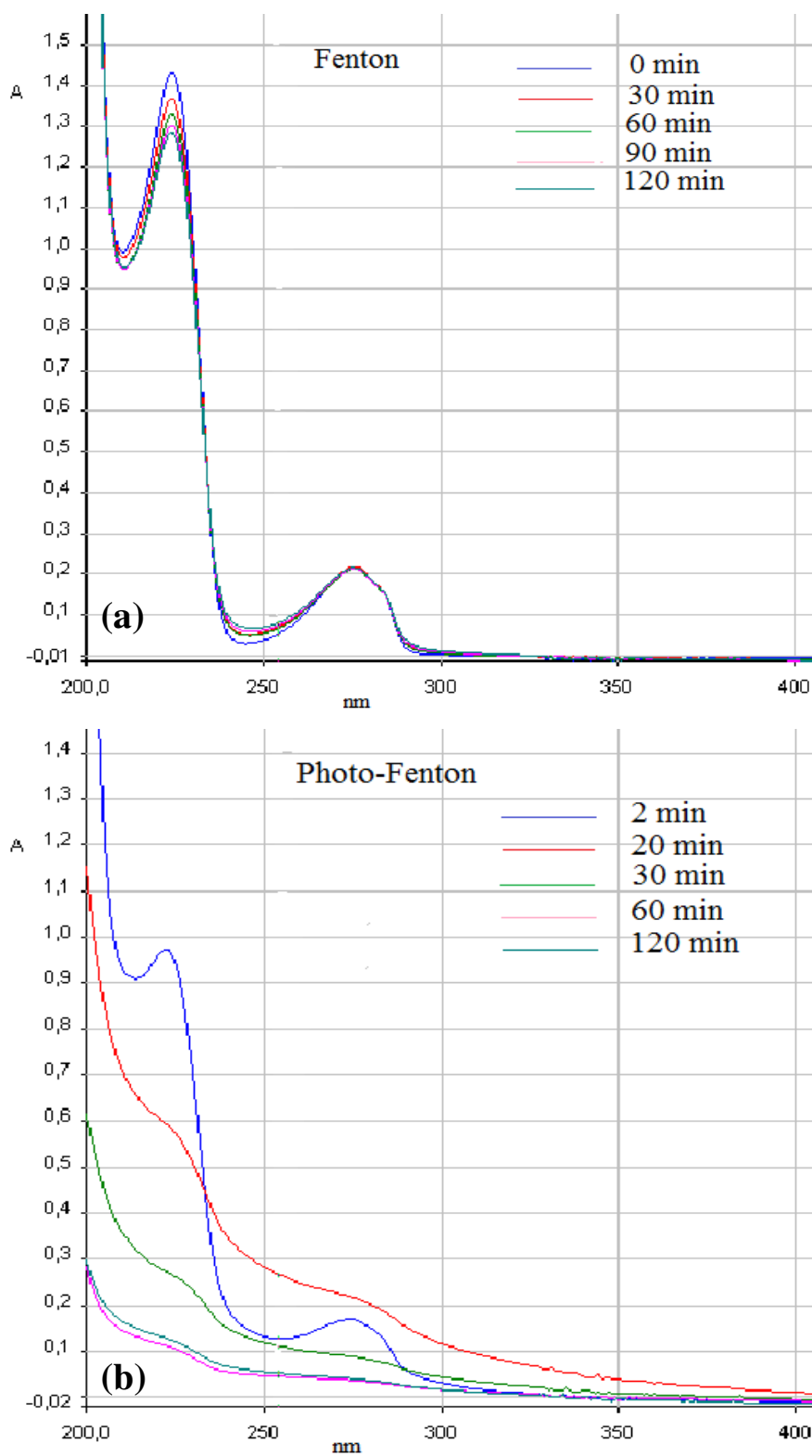


Figure C.6. Evolution of UV spectra with treatment time during Fenton (a) and photo-Fenton (b) treatment of NP-10. Initial experimental conditions: NP-10 = 100 mg L⁻¹ (150 μ M), H₂O₂ = 10 mM, Fe²⁺ = 200 μ M, pH = 3.

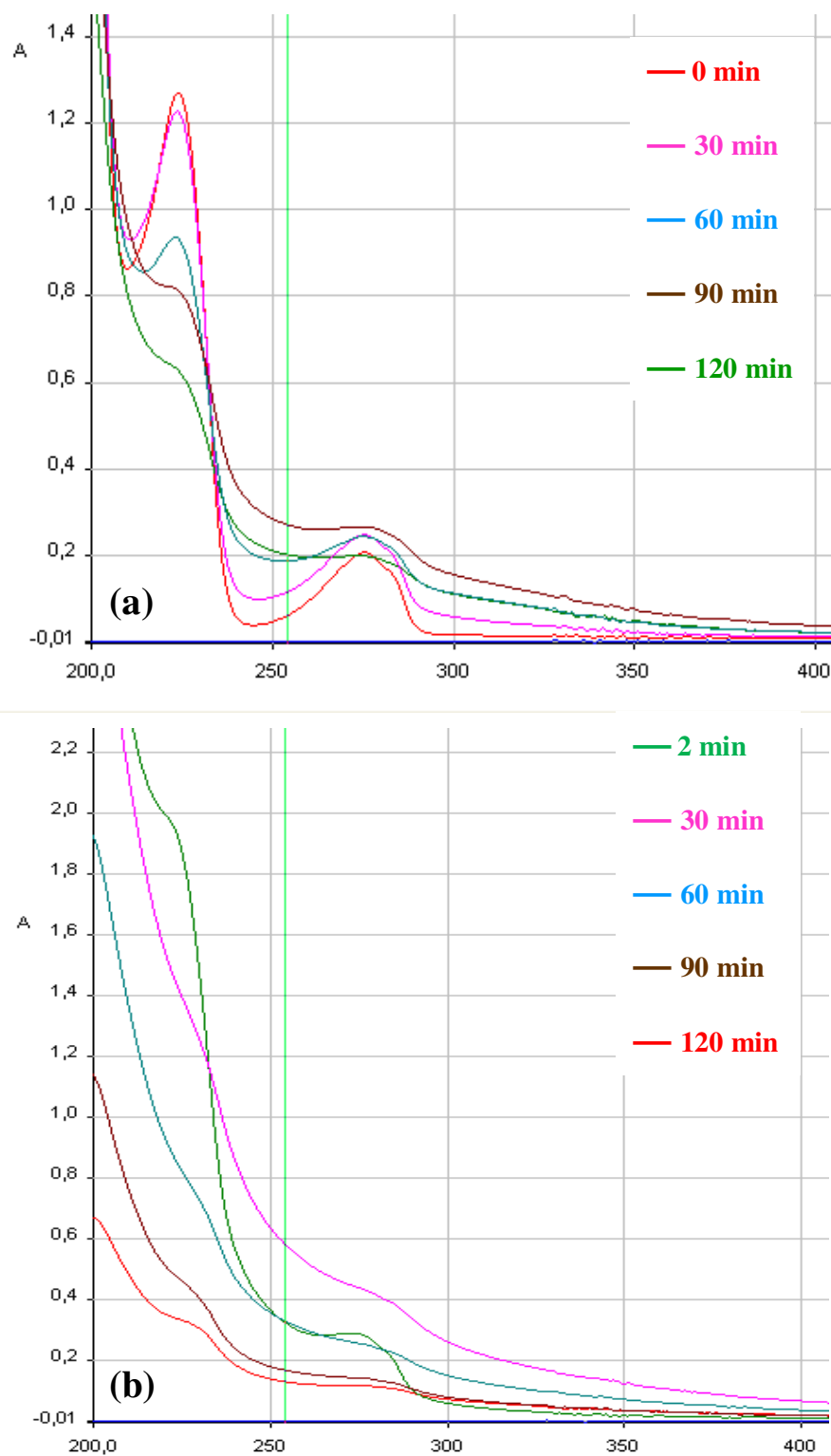


Figure C.7. Evolution of UV spectra with treatment time during UV-C (a) and H₂O₂/UV-C (b) treatment of NP-10 in SFW. Initial experimental conditions: NP-10 = 100 mg L⁻¹ (150 μM), H₂O₂ = 10 mM, pH = 7.

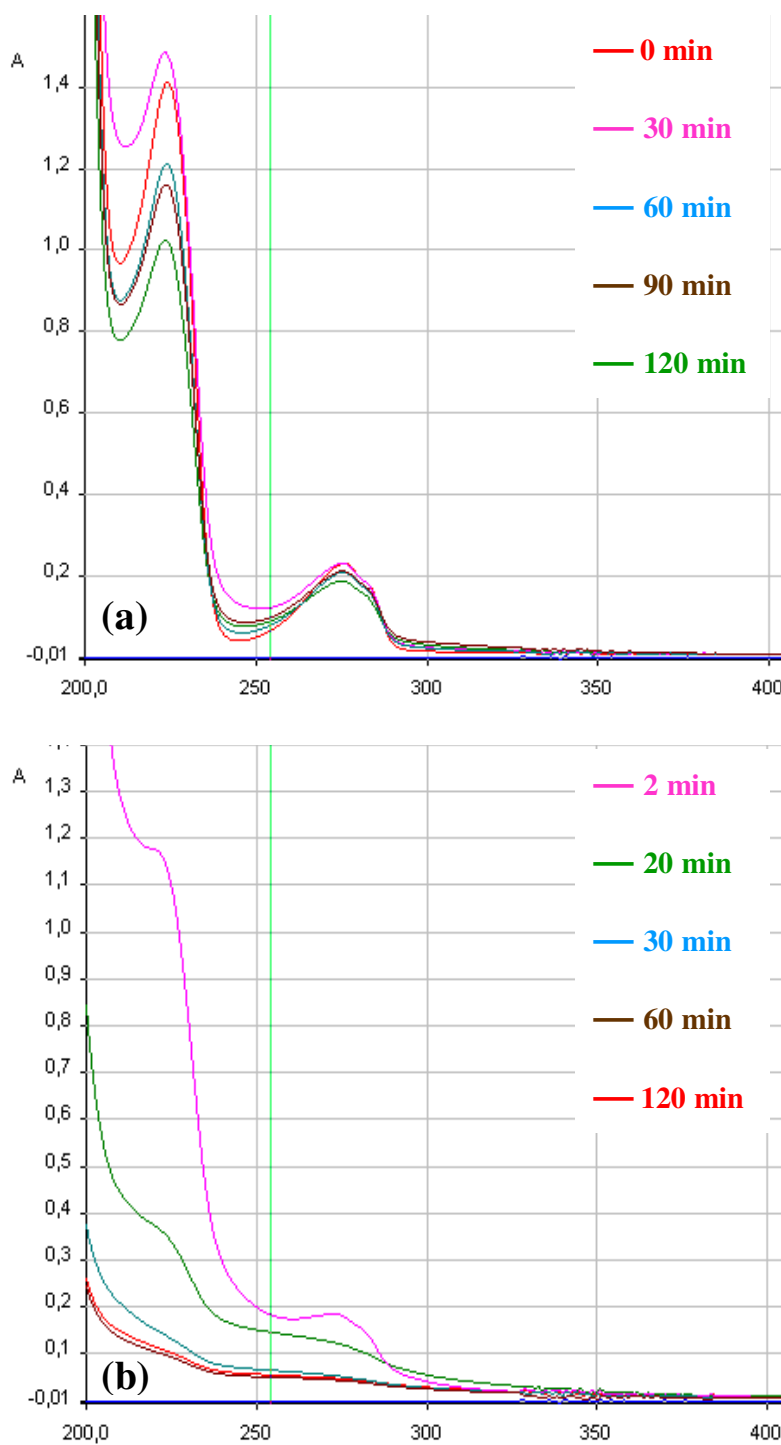


Figure C.8. Evolution of UV spectra with treatment time during Fenton (a) and photo-Fenton (b) treatment of NP-10 in SFW. Initial experimental conditions: NP-10 = 100 mg L⁻¹ (150 μ M), H₂O₂ = 10 mM, Fe²⁺ = 200 μ M, pH = 3.

APPENDIX D

**GC-MS CHROMATOGRAM AND MASS SPECTRA OF NP-10
TRANSFORMATION PRODUCTS**

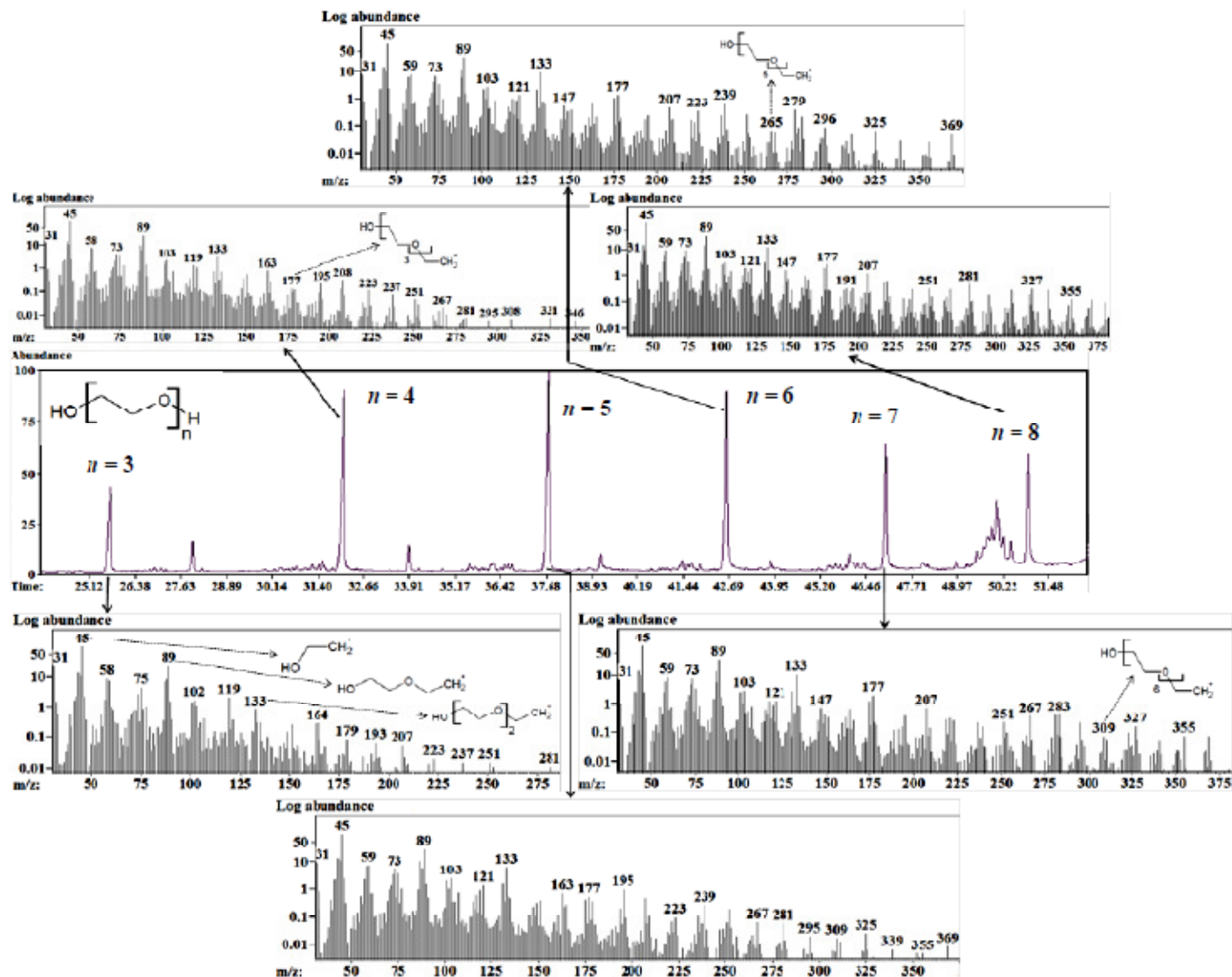


Figure D.1. Total ion chromatogram obtained after GC-MS analysis of the sample, which was subjected to the photo-Fenton treatment for 2 min, and mass spectra of the most abundant peaks in the chromatogram. Initial experimental conditions: NP-10 = 100 mg L⁻¹ (150 μM), H₂O₂ = 10 mM, Fe²⁺ = 200 μM, pH = 3.